



# Microsimulation of cyclists' behavior

*Evaluating the impacts of traffic demand and infrastructure design on cyclists' behavior*

**Master thesis**  
**Construction Management & Engineering**  
06 April 2021

Sven Thijsen  
0892983

**TU/e** EINDHOVEN  
UNIVERSITY OF  
TECHNOLOGY



# Microsimulation of cyclists' behavior

*Evaluating the impacts of traffic demand and infrastructure design on cyclists' behavior.*

06 April 2021

## Master thesis, Construction Management & Engineering

Sven Thijsen

0892983

*Department of the Built Environment*

*Eindhoven University of Technology*

## Graduation Committee

### Chair

Prof. dr. ir. Bauke de Vries

*Information Systems in the Built Environment*

*Eindhoven University of Technology*

### First supervisor

Dr. Dajuan Yang

*Information Systems in the Built Environment*

*Eindhoven University of Technology*

### Second supervisor

Milos Viktorovic

*Information Systems in the Built Environment*

*Eindhoven University of Technology*

## In cooperation with

City of Utrecht

*Stadsplateau 1*

*3500 CE Utrecht*

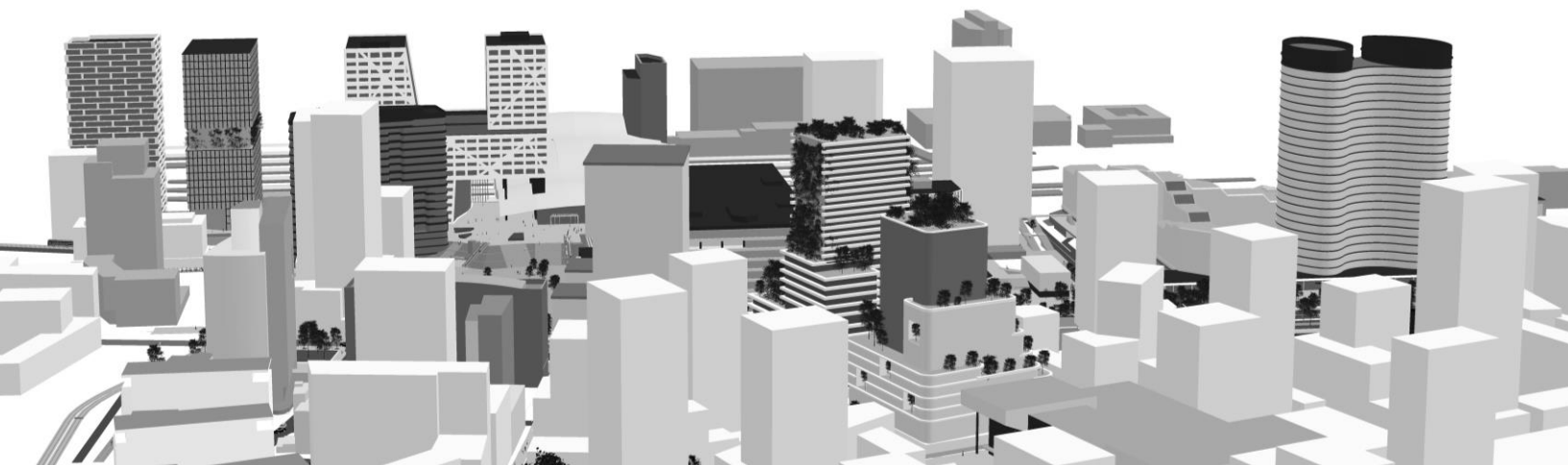


## Table of contents

Preface	VI
Abstract	VII
Summary	VIII
Samenvatting	IX
Acronyms and abbreviations	X
List of figures	XI
List of tables	XIII
<b>1. Introduction</b>	<b>1</b>
1.1. Research context	2
1.2. Research objectives	3
1.3. Research design	4
<b>2. Literature review</b>	<b>5</b>
2.1. Urban mobility	6
2.1.1. Active transportation	6
2.1.2. Urban infrastructure	7
2.2. Cyclists' behavior	11
2.2.1. Levels of behavior	11
2.2.2. Heterogeneity of cyclists	12
2.3. Behavioral model approaches	14
2.3.1. Macroscopic and microscopic modeling	14
2.3.2. Car following models	14
2.3.3. Cellular Automata models	16
2.3.4. Social force models	17
2.3.5. Microscopic modeling software	19
<b>3. Methodology</b>	<b>21</b>
3.1. Vissim and Viswalk	22
3.1.1. Vissim elements structure	22
3.1.2. Viswalk elements structure	23
3.1.3. Vissim and Viswalk interaction	25
3.2. Speed and acceleration	27
3.2.1. Desired speed	27
3.2.2. Acceleration	31
3.2.3. Relaxation time	32



<b>3.3. Calibration of behavioral models</b>	<b>35</b>
3.3.1. Lane-based behavioral model	35
3.3.2. Area-based behavioral model	39
<b>3.4. Data collection and validation</b>	<b>47</b>
3.4.1. GPS receivers	47
3.4.2. Data collection experiment	51
3.4.3. Desired speed validation	53
3.4.4. Turning speed reduction	57
3.4.5. Shared space speed reduction	59
3.4.6. Acceleration validation	61
<b>4. Case study simulations</b>	<b>65</b>
<b>4.1. Case study environment</b>	<b>66</b>
4.1.1. Urban context	66
4.1.2. Construction developments	70
4.1.3. Scenario formulation	73
4.1.4. Infrastructure modeling	75
<b>4.2. Traffic demand estimation</b>	<b>77</b>
4.2.1. Modal split	77
4.2.2. Public transport traffic	79
4.2.3. Motorized traffic	80
4.2.4. Bicycle traffic	82
4.2.5. Pedestrian traffic	85
<b>4.3. Scenario simulation results</b>	<b>87</b>
4.3.1. General simulation performance	88
4.3.2. Network evaluation	89
4.3.3. Route evaluation	95
4.3.4. Intersection evaluation	98
4.3.5. Area-specific conclusions	102
<b>5. Conclusions</b>	<b>103</b>
5.1. Conclusion	104
5.2. Scientific relevance	105
5.3. Societal relevance	106
5.4. Limitations and recommendations	107
<b>References</b>	<b>109</b>
<b>Appendices</b>	<b>120</b>
Appendix A. Speed profiles	120
Appendix B. Motorized traffic input and relative route flow	124
Appendix C. Cycling traffic input and relative route flow	126
Appendix D. Pedestrian OD Matrices	128
Appendix E. Shared space transition script	129
Appendix F. Visual data extraction script	131

## Preface

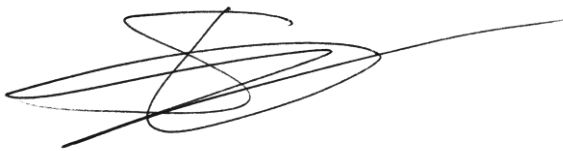
Dear reader,

This graduation thesis signifies the final part of my master Construction Management & Engineering and represents the pinnacle of my achievements at Eindhoven University of Technology. My research project aims to contribute to more sustainable mobility by stimulating cycling, I believe bicycles are the most future-proof transportation mode currently in existence. The Netherlands should share its cycling experiences as a frontrunning country with the world. Being a Dutch student at a Dutch university, this is one of the motivations to conduct this research about the microsimulation of cyclists' behavior. When I started developing the goals for this research, I did not completely know what to expect. During this project I learned many new skills in topics I never touched before.

This graduation project was primarily created from my own home due to the restrictions caused by the coronavirus pandemic. Despite only collaborating online during the entire project, I had a very pleasant collaboration with my supervisors Djujan and Milos. They provided useful feedback, offered valuable suggestions and kept me on the right track. I also had interesting discussions with Herbert and Rik from the City of Utrecht. The project was executed in collaboration with the City of Utrecht and therefore I hope they can use the outcomes in their future sustainable mobility projects.

With the completion of this graduation project I am finishing my time at Eindhoven University of Technology. I am glad my family has always supported me in my decisions that led me to this point. Studying at TU/e has been a wonderful part of my life, during which I made many new friends and memories. From the very beginning in 2014, I met my now closest friends from *Bouwkunde*. I feel like we have been walking this path together by stimulating each other to get the best out of educational and social endeavors. Also, study association *CHEOPS* has certainly brought me lots of good times as a student, from the amazing members and countless study trips, to the outstanding year we formed the 31<sup>st</sup> board. Almost my entire study time I have been part of hockey team *De Joepies*, playing and partying with them truly contributed to my awesome student life. Finally I would like to mention Tara, who kept motivating and distracting me, especially while working at home. From the people in my hometown Elst to my exchange in Taipei, I would like to thank everyone who contributed to the unforgettable moments I experienced during my life as a student.

Sven Thijsen,  
April 2021

A handwritten signature in black ink, consisting of a series of loops and a long horizontal stroke extending to the right.

## Abstract

Because of the numerous benefits of cycling as a sustainable transportation mode, governments worldwide have increasing interest in cycling. Understanding and being able to model cyclists' behavior is essential if cities want to accommodate increasing numbers of cyclists in the future. When a representative behavioral model exists, scenario evaluation can be performed to test which measures are most beneficial to implement in a certain area. However, the research and knowledge on cyclists' behavior is still limited compared to motorized traffic behavior. This research presents innovative methods to model cyclists' behavior in a multimodal environment. To validate the behavioral model, GPS data was collected by conducting an unconstrained cycling experiment. The validated behavioral model is applied to a high-density cycling area in the City of Utrecht. Various scenarios are formulated to assess the impact of traffic demand and infrastructure designs. Besides area-specific insights for the investigated network, the evaluation of scenarios showed that the microsimulation model is able to extract high resolution data. For a detailed consideration of, the impact of spatial interventions on different transportation modes or routes. This research also revealed the potential of applying multimodal microsimulation to evaluate and visualize future urban developments.

### Keywords

*Microscopic traffic simulation; cyclists' behavior modeling; cycling data collection; infrastructure planning; travel time evaluation.*

## Summary

Many governments worldwide aim to stimulate active transportation, because this contributes to a healthy lifestyle for its citizens and supports sustainability goals to reduce air pollution. Cycling presents many advantages over cars and public transportation. In terms of energy use, air and sound pollution, physical and mental health, and reliability of travel times. Cycling is also more space efficient and cheaper in terms of ownership and infrastructure than most transport modes. Compared to walking, cycling is faster and therefore offers a larger range of destinations. Investing in cycling infrastructure can support cities in their current mobility challenges. To justify these investments, cyclists' behavioral models can be of great value to cities to get a detailed insight in traffic flows or travel times.

Even though the use of bicycles and interest in cycling is increasing in cities worldwide, the research on bicycle traffic behavior still is limited compared to motorized traffic. Understanding and being able to model cyclists' behavior is essential if cities want to accommodate increasing numbers of cyclists. This research aims to evaluate the impacts of traffic demand and infrastructure design on cyclists' behavior, using microscopic traffic simulation. Both a lane-based and an area-based behavioral model are calibrated for cyclists' behavior in traffic simulation software Vissim. To ensure the compatibility of these two models, a custom script was written that allows a transition between both types of behavioral models.

To validate the behavioral models, GPS data was collected by conducting an unconstrained cycling experiment. Over 350 km of naturalistic cycling data was collected from 11 participants, of which 7 drove a 'regular' bicycle and 4 an electric bicycle. The processed data was used to validate cyclists' desired speed, acceleration and speed reduction in turns and shared space.

The validated behavioral model was applied to a case study area in the City of Utrecht. The area around *Jaarbeursplein* will be transformed into a high-density, mixed-use extension of the city center with a high presence of cyclists. Available traffic data was used to estimate the traffic demand for various scenarios. Besides a base network and a future network, spatial variations were considered to evaluate the impact of urban infrastructure design on cyclists' behavior. These variations in traffic demand and infrastructure supply yielded eleven scenarios that were simulated in Vissim.

Specifically for the case study area, the evaluation of the scenarios showed interesting results for certain locations. Explaining how the planned developments can have a dissimilar impact on different routes or transportation modes. The overall results of this research revealed the potential of microsimulation of multimodal traffic. In terms of evaluation, these modeling methods provide a very high resolution of data, with the possibility to extract detailed data units. Furthermore, three-dimensional visualizations open opportunity areas for more intuitive design and tangible citizen participation. Limitations of this research include the absence of proper traffic data and validation of interaction behavior. However, technological advancements in data collection and simulation power will increase the feasibility of large scale (cycling) traffic simulation. Cyclists' behavioral models can be used to justify investments that stimulate cycling, contributing to a more sustainable transportation system and comfortable living environment.

## Samenvatting

Wereldwijd stimuleren veel overheden actief transport, omdat dit bijdraagt aan een gezonde levensstijl voor de inwoners en helpt bij duurzaamheidsdoelen voor het verminderen van luchtvervuiling. Fietsen biedt veel voordelen ten opzichte van autovervoer en openbaar vervoer, op het gebied van energieverbruik, lucht- en geluidsvervuiling, lichamelijke en geestelijke gezondheid en betrouwbare reistijden. In eigendom en infrastructuur is fietsen ook ruimtebesparender en goedkoper dan de meeste vervoerswijzen. Vergeleken met wandelen is fietsen sneller en heeft daardoor een grotere actieradius. Investeren in fietsinfrastructuur draagt bij aan het oplossen van huidige mobiliteitsuitdagingen in steden. Om deze investeringen te onderbouwen, kunnen fietsgedragsmodellen van grote waarde zijn om inzicht te krijgen in verkeersstromen of reistijden.

Hoewel het fietsgebruik en de belangstelling voor fietsen in steden over de hele wereld toeneemt, is onderzoek naar fietsverkeer nog beperkt vergeleken met gemotoriseerd verkeer. Het begrijpen en modelleren van fietsgedrag is essentieel voor steden die te maken hebben met een toenemend aantal fietsers. Het doel van dit onderzoek is om de invloeden van de verkeersvraag en infrastructuur op het gedrag van fietsers te evalueren met behulp van microscopische verkeerssimulatie. Zowel een *lane-based* als een *area-based* gedragsmodel zijn in simulatiesoftware Vissim gekalibreerd voor fietsgedrag. Om deze modellen samen te gebruiken, is een script geschreven dat een overgang tussen beide typen gedragsmodellen mogelijk maakt.

Voor het valideren van de gedragsmodellen zijn GPS-gegevens verzameld met een onbelemmerd fietsexperiment. Ruim 350 km natuurlijke fietsdata is verzameld van 11 deelnemers, waarvan 7 op een 'gewone' fiets en 4 op een elektrische fiets. De verwerkte gegevens zijn gebruikt om de gewenste snelheid, acceleratie en snelheidsvermindering in bochten en *shared space* te valideren.

Het gevalideerde gedragsmodel is toegepast op een *casestudy* gebied in de gemeente Utrecht. Het gebied rond het *Jaarbeursplein* wordt getransformeerd als een uitbreiding van de binnenstad met hoge dichtheid, gemengde functies en een grote aanwezigheid van fietsers. De beschikbare verkeersdata is gebruikt om de verkeersvraag voor verschillende scenario's in te schatten. Naast een basisnetwerk en een toekomstig netwerk zijn ook ruimtelijke variaties meegenomen bij het evalueren van de impact van infrastructuurontwerp. Deze variaties in verkeersvraag en infrastructuur-aanbod resulteerden in elf scenario's die in Vissim zijn gesimuleerd.

Specifiek voor het *casestudy* gebied heeft de scenario evaluatie voor bepaalde locaties interessante resultaten opgeleverd. Deze maken duidelijk hoe geplande ontwikkelingen op verschillende routes of vervoerswijzen een andere impact kunnen hebben. Het onderzoeksproces laat de potentie zien van multimodale microsimulatie, deze methoden bieden een zeer hoge dataresolutie en maken het mogelijk gedetailleerde eenheden te meten. Bovendien bieden driedimensionale visualisaties kansen voor intuïtiever ontwerpen en toegankelijke burgerparticipatie. Beperkingen van dit onderzoek zijn onder meer het ontbreken van de juiste verkeersdata en de validatie van gedrag bij interacties. Door technologische vooruitgang op het gebied van dataverzameling en rekenkracht wordt grootschalige (fiets)verkeerssimulatie steeds uitvoerbaarder. De fietsgedragsmodellen kunnen worden gebruikt om fietsstimulerende investeringen te verantwoorden die bijdragen aan een duurzaam vervoerssysteem en een comfortabelere leefomgeving.

## Acronyms and abbreviations

<b>ANOVA</b>	Analysis of Variance
<b>API</b>	Application Programming Interface
<b>CA (model)</b>	Cellular Automata (model)
<b>CDF</b>	Cumulative Distribution Function
<b>COM</b>	Component Object Model
<b>COVID-19</b>	Coronavirus Disease 2019
<b>CSV</b>	Comma Separated Value (.csv)
<b>DPIA</b>	Data Protection Impact Assessment
<b>GDPR</b>	General Data Protection Regulation
<b>GIS</b>	Geographic Information System(s)
<b>GFA</b>	Gross Floor Area
<b>GPS</b>	Global Positioning System
<b>GNSS</b>	Global Navigation Satellite System
<b>GUI</b>	Graphic User Interface
<b>HOV</b>	<i>Hoogwaardig Openbaar Vervoer</i> (High quality public transport)
<b>KS-test</b>	Kolmogorov-Smirnov test
<b>MOEs</b>	Measures Of Effectiveness
<b>OD (matrix)</b>	Origin-Destination (matrix)
<b>ODiN</b>	<i>Onderweg in Nederland</i> (On the way in the Netherlands)
<b>OVIN</b>	<i>Onderzoek Verplaatsingen in Nederland</i> (Research Movements in the Netherlands)
<b>PC4</b>	Numerical 4 digit-part of Postal Code
<b>PPFM</b>	Psychological-Physical Force Model
<b>PTV</b>	<i>Planung Transport und Verkehr</i> (Planning, transportation and traffic)
<b>SFM</b>	Social Force Model
<b>Vissim</b>	<i>Verkehr In Städten – Simulationsmodell</i> (Traffic in Cities – Simulation model)
<b>WGS</b>	World Geodetic System
<b>W74/W99</b>	Wiedemann 1974/Wiedemann 1999 model
<b>XML</b>	Extensible Markup Language



## List of figures

Figure 1.1: Research design	4
Figure 2.1: Vehicle types with examples (adapted from: ANWB, 2020)	7
Figure 2.2: Common types of cycling infrastructure in the Netherlands	9
Figure 2.3: Car-following model by Wiedemann in 1974 (from: Saifuzzaman & Zheng, 2014)	15
Figure 3.1: Overview Vissim Structure	23
Figure 3.2: Overview Viswalk structure	24
Figure 3.3: Unrealistic behavior of pedestrians being stuck at the middle of the road	25
Figure 3.4: Estimated cumulative desired speed distribution of reference projects	28
Figure 3.5: Desired speed distribution in standard situations	28
Figure 3.6: Reference desired speed distribution and average measured speed (Fiets Telweek, 2016)	29
Figure 3.7: Average speeds for different types of infrastructure in Utrecht (Fiets Telweek, 2016)	30
Figure 3.8: Desired speed distributions	30
Figure 3.9: Desired (and maximum) acceleration functions (COWI, 2013)	31
Figure 3.10: Desired (and maximum) deceleration functions (COWI, 2013)	32
Figure 3.11: Acceleration test setup in Vissim network editor	32
Figure 3.12: Average speed over 30 meter for different values of relaxation time	33
Figure 3.13: Average over 15 meter for different values of relaxation time	33
Figure 3.14: Turning trajectory for different values of tau	34
Figure 3.15: Queue formation in 2D and 3D view	43
Figure 3.16: Cycling path behavior test setup	44
Figure 3.17: Transystem's GL-770 GPS receiver	47
Figure 3.18: Data comparison of speed measured and calculated with a single GPS receiver	49
Figure 3.19: Data comparison of speed measured with two separate GPS receivers	49
Figure 3.20: Example of location data for one trip measured with two GPS receivers	50
Figure 3.21: Histograms of speed frequency for bicycle and e-bicycle participants	52
Figure 3.22: Example of speed profile participant B	53
Figure 3.23: Average speed profile of all bicycle participants	54
Figure 3.24: Average speed profile of all e-bike participants	54
Figure 3.25: KS test for desired speed of cyclists	55
Figure 3.26: KS test for desired speed of e-cyclists	56
Figure 3.27: Revised distribution KS test for desired speed of e-cyclists	57
Figure 3.28: Maximal speed reduction as percentage of initial speed for different turn radii	57
Figure 3.29: Speed reduction with turn radius of: a) < 5 m, b) 5-10 m, c) 10-15 m and d) > 15 m	58
Figure 3.30: Average speed for different turn radii	59
Figure 3.31: Example of GPS data around shared space area	60
Figure 3.32: Examples of shared space speed profiles	60
Figure 3.33: Acceleration functions of all bicycle participants	62
Figure 3.34: Acceleration functions of all e-bicycle participants	62
Figure 3.35: Average measured cyclists, measured e-cyclists and reference acceleration functions	63
Figure 3.36: Acceleration functions for cyclists and e-cyclists used for simulation	63

Figure 4.1: Extension of city center to the west of the railway (adapted from: City of Utrecht, 2017)	66
Figure 4.2: Case study area borders and street names (adapted from: City of Utrecht, n.d.)	67
Figure 4.3: Planned routing for: a) cycling and b) motorized traffic (from: City of Utrecht, 2017)	68
Figure 4.4: Redesign of Westplein/Lombokplein (adapted from: City of Utrecht, 2020c)	69
Figure 4.5: Pedestrian area Forum (from: Group A, 2020)	69
Figure 4.6: Conceptual plan Jaarbeursdistrict (and Beurskwartier) (adapted from: Jaarbeurs, 2019)	72
Figure 4.7: 3D model and schematic overview of network and of: a) base and b) future network	73
Figure 4.8: Intersection spatial variations in future network (none, wider paths & shared space)	74
Figure 4.9: Case study area and PC4 area in Utrecht	77
Figure 4.10: Modal split in Netherlands, Utrecht and PC4 area 3521 (CBS, 2020)	78
Figure 4.11: Schematic overview of available car traffic data	81
Figure 4.12: Input values and relative route flow for motorized traffic in: a) base and b) future network	82
Figure 4.13: Schematic overview of available bicycle traffic data	83
Figure 4.14: Average cycling traffic over the year for several counting locations (HIG, 2019)	84
Figure 4.15: Cycling traffic over the day for several counting locations (HIG, 2019)	84
Figure 4.16: Input values and relative route flow for cycling traffic in: a) base and b) future network	85
Figure 4.17: Pedestrian density (scenario F-PMa)	88
Figure 4.18: Full network average speed in F-AMa scenario (07:35 to 07:40)	89
Figure 4.19: Average speed during simulations in future network	90
Figure 4.20: Jaarbeursplein average relative delay in F-PMa scenario (16:35 to 16:40)	90
Figure 4.21: Average relative delays during simulations in future network	91
Figure 4.22: Speed-density relation for main future scenarios	92
Figure 4.23: Speed-delay relation for main future scenarios	93
Figure 4.24: Density-delay relation for main future scenarios	93
Figure 4.25: Flow-density relation for main future scenarios	94
Figure 4.26: Routes measured for travel time evaluation	95
Figure 4.27: Average travel time for each route (average of all scenarios)	96
Figure 4.28: Average travel time per route and time of day (all scenarios)	96
Figure 4.29: Average travel time for different scenarios (all routes)	97
Figure 4.30: Average travel time all routes and scenarios in future network	98
Figure 4.31: Cyclists' flows at intersection in future network (no spatial variation)	99
Figure 4.32: Highlighted intersection relative delay in F-PMa scenario (17:30-17:35)	99
Figure 4.33: Average delay over time per approaching direction	100
Figure 4.34: Average maximal queue length for time intervals per network, origin and variation	100
Figure 4.35: Average delay for different directions for F-MXa (none) and F-MXb (wider paths)	101

## List of tables

Table 2.1: Levels of cyclists' behavior	11
Table 2.2: Thresholds of Wiedemann model (Barceló et al., 2010; Saifuzzaman & Zheng, 2014)	16
Table 3.1: Reference research projects on desired speed	27
Table 3.2: Overview of Wiedemann 74 model parameters in Vissim (PTV Group, 2020)	36
Table 3.3: Overview of W99 model parameters in Vissim (PTV Group, 2020; COWI, 2013)	37
Table 3.4: Overview of lateral driving behavior parameters in Vissim (PTV Group, 2020)	38
Table 3.5: Overview of area parameters in Viswalk (PTV Group, 2020)	41
Table 3.6: Overview of route location parameters in Viswalk (PTV Group, 2020)	41
Table 3.7: Overview of global parameters in Viswalk (PTV Group, 2020)	42
Table 3.8: Overview of calibrated walking/cycling behavior parameters (PTV Group, 2020)	45
Table 3.9: Setup of data collection experiment	51
Table 3.10: Desired speeds for different turn radii	59
Table 4.1: Completed and ongoing projects (City of Utrecht, n.d.; CU2030, 2020; Kadaster, 2021)	70
Table 4.2: Planned construction projects in case study area	71
Table 4.3: Scenario configuration for all 11 scenarios	75
Table 4.4: Composition of motorized road traffic	78
Table 4.5: Composition of bicycle traffic	79
Table 4.6: Bus line frequency through network (U-OV, 2021; OpenStreetMap, n.d.)	80
Table 4.7: Vehicle inputs per hour for all scenarios	86
Table 4.8: Overview of simulation scenarios	87
Table 4.9: Pearson's and Spearman's correlations between variables over different scenarios	92



# 1. Introduction

Traffic simulation models can be used to test and evaluate the impact of different planning measures on the traffic flow. Due to rapid urbanization and population growth, many cities are facing environmental, health and spatial challenges. Because of the numerous benefits of cycling, governments worldwide have increasing interest in cycling.

However, the research and knowledge on cyclists' behavior is still limited compared to motorized traffic behavior. Increased insight in modeling cyclists' behavior would provide a better justification for the planning of new cycling infrastructure.

This opening chapter will introduce the context and problem statement that inspired to conduct this research. Based on the observed research gap, a main research question is established and sub-questions are presented. From these sub-questions, the corresponding research phases are explained. The chapter structure will give insight into the setup of this report.

## 1.1. Research context

Many governments worldwide aim to stimulate active transportation since it contributes to a healthy lifestyle for its citizens and supports sustainability goals to reduce air pollution (Alsaleh & Sayed, 2020). Cycling presents many advantages over cars and public transportation in terms of energy use, air and sound pollution, physical and mental health, and reliability of travel times. It is also more space efficient and cheaper in terms of ownership and infrastructure than most transport modes. Compared to walking, cycling is faster and therefore offers a larger range of destinations (section 2.1.1). Investing in cycling infrastructure can support cities in their current mobility challenges. To justify these investments, microscopic cyclists' behavioral models can be of great value to cities to get more insight in traffic flows and road capacity. Scenario evaluation can be used to facilitate governments in making substantiated policy and design choices. Urban designers and traffic engineers can visualize cyclists' behavior and evaluate traffic flows prior to implementation of the measures. The models can be used in traffic modeling, safety evaluation and urban design planning (Mohammed et al., 2019). Also for short term changes in traffic flow (for example due to a road closure or an event) problem areas can be identified beforehand, to take appropriate actions.

As seen from the review of recent research (chapter 2), there lies a gap in modeling the behavior of cyclists in mixed traffic environments. Many researchers suggest the immaturity of the field is imputable to the lack of available cycling data (Alsaleh & Sayed, 2020; Gavrilidou, Wierbos, et al., 2019; Huber et al., 2019; Lee & Sener, 2020; Ma & Luo, 2016). However, researchers also point out that in recent years, many new sources of data have emerged. Cycling data traditionally relied on (manual) location counting and travel surveys, current technological advancements raise the opportunity for new data collection methods like mobile phone GPS tracking or intelligent camera systems that detect trajectories (Qu et al., 2017). For example aggregate GPS data from bicycle sharing systems (Pogodzinska et al., 2020) or commercial applications like Strava (Huber et al., 2019; Lin & Fan, 2020; Livingston et al., 2020).

Even though the use of bicycles and interest in cycling is increasing in cities worldwide, the research on bicycle traffic behavior still is limited compared to motorized traffic (Gavrilidou, Daamen, et al., 2019; Ma & Luo, 2016; Osowski & Waterson, 2017; Twaddle et al., 2014). Understanding and being able to model cyclists' behavior is essential if cities need to accommodate increasing numbers of cyclists (Yuan et al., 2019). Cyclists' behavior simulation models can be used to evaluate different future scenarios with regards to changes in the demand of trips or the supply of cycling infrastructure. Most of the currently available traffic microsimulation software tools are primarily focused on behavior of motorized vehicles (e.g. Vissim, Aimsun, SUMO, MATSim) (Krajzewicz et al., 2014; Ma & Luo, 2016; Saidallah et al., 2016). Behavioral models for pedestrians are also regularly researched (Hoogendoorn et al., 2014; Kretz et al., 2018; Lagervall & Samuelsson, 2014), often applied in the context of crowd management at transportation hubs or events (InControl, n.d.; UCrowds, n.d.).



## 1.2. Research objectives

Since the modeling of cyclists' behavior is less advanced compared to car traffic or pedestrians, special attention is given to improving these behavioral models. When a representative behavioral model exists, scenario evaluation can be performed to test which measures are most beneficial to implement in a specific area. Suitable measures to evaluate the efficiency of infrastructure are, travel time, traffic flow or delay time. This research strives to address these issues, by finding an answer to the following research question:

*How can the impacts of traffic demand and urban infrastructure designs on cyclists' behavior be evaluated with the support of microscopic traffic simulation?*

To find a comprehensive solution to this main research question, several sub-questions need to be answered as well:

- *How is cyclists' behavior modeled in existing microscopic models?*
- *Which attributes have been used to model cyclists' interaction with the built environment and other road users?*
- *How can the cyclists' behavioral model be validated with naturalistic data?*
- *How to model the influence of built environment attributes on cyclists' behavior?*
- *How to estimate traffic demand by using available data sources?*
- *What is the influence of traffic demand and infrastructure designs on travel time of cyclists?*

Cycling is embedded in the culture and built environment of the Netherlands and the share of cycling trips in the country is among the highest in the world. Hence, the Netherlands is a leading country in developing more convenient, accurate and practical cycling models. As a frontrunner country in cycling policy, infrastructure and technology, best practices from the Netherlands can be useful examples for the rest of the world. The City of Utrecht has one of the highest shares of bicycle trips in the Netherlands (Harms & Kansen, 2018) and is among the most bicycle friendly cities in the world (Copenhagenize Design Co, 2019; Coya, 2019). Utrecht is even home to the largest bicycle parking in the world, with 12500 parking spaces (Su, 2019). Cycling has a prominent role in mobility strategies of the municipality. Utrecht experiences rapid growth in total trips due to an increase of inhabitants and jobs in the city. To keep the city "attractive and accessible", more space will be made available for cycling (City of Utrecht, 2021). This makes Utrecht an ideal city to evaluate innovative cycling initiatives. A microscopic traffic simulation tool can support the municipality in development of cycling related policy, urban planning and traffic engineering.



### 1.3. Research design

To reach the research objective and answer all subquestions, six research phases will be carried out. At the end of every research phase, a research question will be answered. [Figure 1.1](#) displays the research design and how all phases and research questions are related.

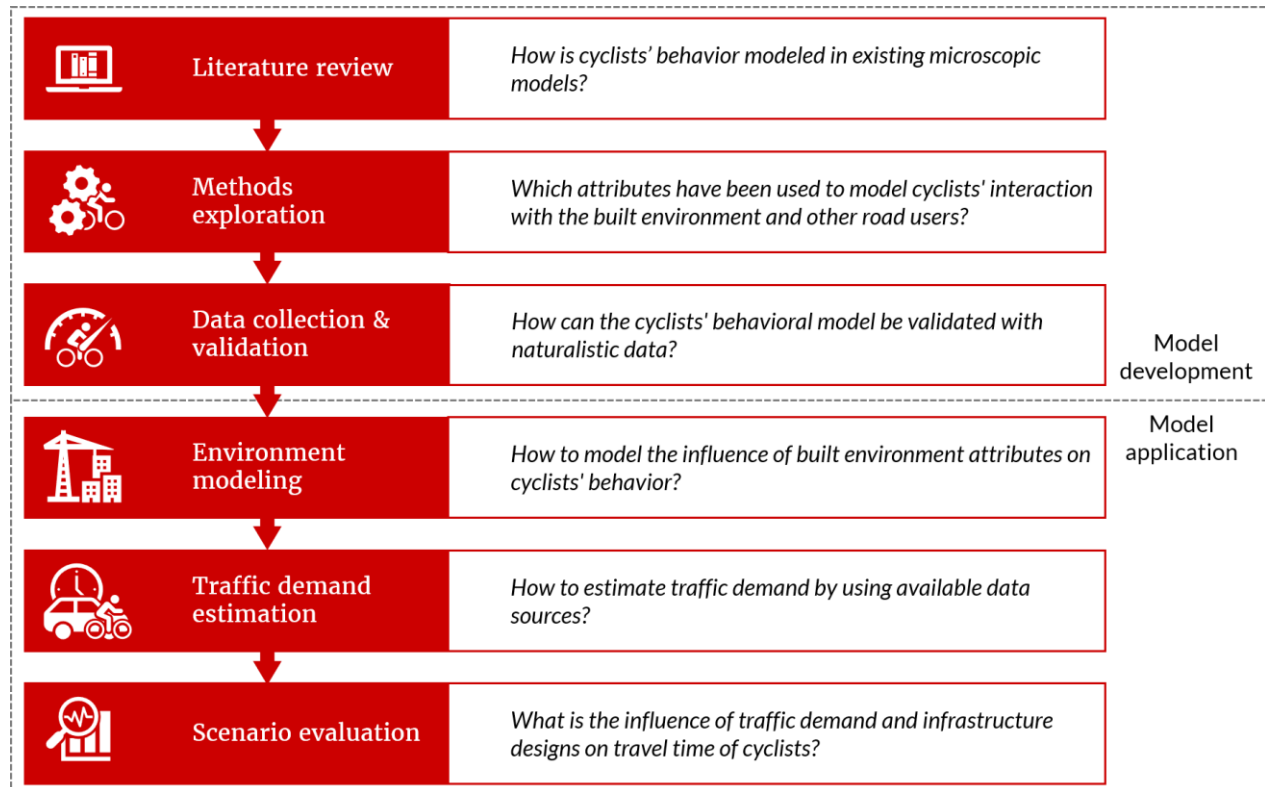


**Figure 1.1:** Research design

To explore the current practice of traffic simulation, first a literature review is conducted. The results are presented in [chapter 2](#). The research then concentrates on exploring various methods to simulate and calibrate cyclists' behavior models in the first part of [chapter 3](#). Subsequently, cycling data will be gathered by conducting a data collection experiment with cyclists in an uncontrolled environment to the behavioral models. From [chapter 4](#) the research focusses on the application of the behavioral model, according to various scenarios. By first modeling a case study environment and then estimating the traffic demand for different input scenarios. In [chapter 5](#) conclusions are drawn from the results of all research phases.



## 2. Literature review

In the literature review chapter, previously conducted studies relevant to this research are reviewed to gain information and identify possible research opportunities. Also, currently researched methods in the field of cyclists' behavior modeling are analyzed.

First the current situation and trends in urban mobility and active transportation are evaluated. After which the elements of cyclists' behavior are investigated. Cycling behavioral model approaches of other researchers are reviewed and the most suitable models and tools are selected for further application in this research.

## 2.1. Urban mobility

Many governments worldwide aim to stimulate active transportation since it contributes to a healthy lifestyle for its citizens and supports sustainability goals to reduce air pollution (Alsaleh & Sayed, 2020). Increasing the share of active transportation has high potential to achieve more sustainable transport systems. To keep cities livable, governments worldwide have increasing interest for high quality public space for walking and cycling (C40 Cities, 2019; City of Utrecht, 2020a; Transport for London, 2017).

### 2.1.1. Active transportation

The transportation sector is responsible for almost a quarter of all greenhouse gas emissions in Europe (European commission, 2016). Global climate challenges require a different approach towards urban mobility, away from fossil fuel based motorized transport. Bicycles are an exceptionally environmentally friendly mode of transportation, requiring no additional power source. Cycling is one of the most energy efficient transport modes, even 4 to 5 times more energy efficient than walking (Hermans, 2003). Compared to a car, using a bicycle can save 150 g to 250 g of CO<sub>2</sub> emissions per km (Hendriksen & Van Gijlswijk, 2010; Harms & Kansen, 2018). Electric bicycles, use about one-tenth the energy a small electric car consumes and 40 times less than a standard fossil fuel car (Fishman & Cherry, 2016). Besides being clean in terms of air pollution, cycling also produces very little sound pollution. Sound pollution is seen as the primary source of nuisance in a living environment. Currently, 48% of the Dutch population experiences sound nuisance from road traffic, of which 9% indicates this to be 'severe nuisance' (van Poll et al., 2016).

Since cycling is an active mode of transportation, a study by Nijland (2017) showed it can improve physical health in many ways. Cycling regularly decreases the probability of diseases like diabetes, cardio-vascular diseases and (forms of) cancer. Commuting by bicycle on a daily basis decreases the chance of premature death by 41% (Tour de Force, 2021). Besides physical health benefits, cycling can also have a positive effect on mental health. Because it is a flexible, calm and independent form of transportation, people experience cycling as more stress relieving than driving a car or using public transportation (Harms & Kansen, 2018). The engagement with the environment is higher and travel times are more reliable compared to public transport or car traffic. Two-thirds of adults in the Netherlands say to associate cycling with joy (Hendriksen & Van Gijlswijk, 2010).

Due to optimal routing, easy accessibility and availability, cycling is often the fastest mode of transportation for short to medium distance trips in urban areas. With an e-bicycle, the average speed is significantly faster than a standard bicycle, decreasing physical effort and travel times. The increasing adoption of e-bikes extends the acceptable range for cycling, as well as traveling faster with less physical effort (Netherlands Institute for Transport Policy Analysis [KiM], 2019). The maximum acceptable distance (defined as the distance in which 90% of all trips is taken) rises from 7.5 km to 15 km with an e-bike (Netherlands Institute for Transport Policy Analysis [KiM], 2016). The bicycle is also increasingly used for multimodal trips in combination with public transport, making it a sustainable and convenient alternative for long distance trips (Kalter & Groenendijk, 2018).

In growing cities, space becomes increasingly more scarce. Bicycles are very space efficient in terms of infrastructure and parking. A parked car takes up 10 times more space than a parked bicycle, and a moving car even need 28 times more space than a moving bicycle (Bureau Nieuwe Gracht, 2017; Harms & Kansen, 2018). This makes cycling infrastructure cheaper and more compact. The costs of infrastructure per travelled kilometer in the Netherlands is around €0.03 for cycling infrastructure, €0.10 and €0.18 for car and train infrastructure respectively. This results in annual costs per person of €33 of cycling infrastructure, €343 for car infrastructure and €133 for railways (Decisio, 2016). Parking spaces are also a lot smaller than for cars, leaving space to create more livable and attractive cities. Since parking is less of an issue than with a car, parking can be done much closer to the final destination, while also saving on parking fees.

Besides less parking costs, the ownership and operation costs of a bicycle makes it also one of the cheapest modes of transportation. In most countries (e-)bicycles do not require insurance, road taxes, or a license to ride (Hung & Lim, 2020). In the Netherlands, the annual costs (including purchase, maintenance, energy and taxes) for owning a bicycle are around €175 for a conventional bicycle and €290 for an e-bike. For cars these annual costs are somewhere between €2500 to €8500 (Hendriksen & Van Gijlswijk, 2010). These relatively low costs make the bicycle available for almost all people, thus it is a very financially accessible transportation mode.

### 2.1.2. Urban infrastructure

All advantages of cycling make governments stimulate active transportation in the form of campaigns, financial incentives and attractive infrastructure. This desired shift in mobility patterns means the urban infrastructure and public space need to adapt. Design conditions are necessary to accommodate different types of vehicles in the public space. The Dutch travelers' association ANWB has recently developed guidelines to separate transportation modes according to their maximum speed and mass (ANWB, 2020).

Vehicle family	0-10 km/h	10-20 km/h	20-30 km/h	30-40 km/h	40-50 km/h	>50 km/h
<b>A</b> "Walking" Walking	A10 Walking	A20 Running				
<b>B</b> Bicycle-like < ~ 35 kg		B20 bicycle step-scooter	B30 e-bike e-step	B40 speed pedelec racing bike		
<b>C</b> Light motorized < ~ 350 kg		C20 mobility scoo. Stint	C30 moped e-cargo bike		C50 motorscooter 'Canta'	C50+ motorcycle
<b>D</b> Car-like < ~ 3500 kg						D50+ car (delivery) van
<b>E</b> Truck-like > ~ 3500 kg						E50+ truck bus
<b>F</b> Tram-like (Conducted vehicles)						F50+ tram

Figure 2.1: Vehicle types with examples (adapted from: ANWB, 2020)

In [figure 2.1](#), vehicle families are grouped based on mass and combined with the average speed this creates vehicle types to be considered in infrastructure and public space design. Connected to each vehicle type is a domain, stating which vehicle type is determinative for the maximum speed in that domain. The infrastructure in an area consist of one or more speed domains, the combination of domains shapes the atmosphere of the public space. The biggest design tradeoff is whether to merge or separate the different vehicle types. The mass and speed differences should be minimized, suggesting a separate domain for each vehicle type. But this would drastically limit the space efficiency in the area. Based on the desired spatial quality and traffic flow, the public space is designed by dividing it into different speed domains. On a network scale, the different vehicle types can make use of different infrastructure networks across the city.

In the Netherlands, cyclists have more dedicated infrastructure than in most other countries. Not all cycling infrastructure falls under the domain of B20 (see [figure 2.1](#)), combinations with other vehicle types are made. The type of infrastructure has a large influence on the interaction with other road users and the traffic flow in a certain area. To evaluate the cycling infrastructure and use clear terminology, the different types have to be specified. Many different types of cycling infrastructure exists in the Netherlands, the most common are:

- *Cycling path*

Cycling paths are exclusively for cyclists and separated from the main road. Here there is limited to no interaction with cars or pedestrians except at intersections. A difference exists in mandatory cycling paths (sign G11) or non-mandatory cycling paths (sign G13). A variation on the mandatory cycling path is the mandatory cycling/motor scooter path (sign G12a) ([ANWB, n.d.](#); [Fietzersbond, n.d.](#)). A separated cycling path in the Netherlands should at least have a width of 2 meter, but in case of a busy path or the presence of mopeds or motor scooters a minimum width of 2.5 meter is advised ([Fietzersbond, n.d.](#)). [Wierbos et al. \(2019\)](#) researched the capacity of a cycling path by conducting a bottleneck flow experiment. They concluded that the capacity of a bicycle path has a linear relationship with the width of the path. A known phenomenon in car traffic, the capacity drop, was also observed in this cycling path experiment, which describes the sudden drop in capacity when a congested situation is reached.

- *Cycling highway*

The relatively new 'cycling highway' is a special version of the cycling path which aims to make cycling trips more convenient, fast and attractive ([Dias & Riberio, 2020](#)). Cycling highways are wider and often fully separated from motorized traffic to have a more comfortable cycling environment. Bridges, tunnels and priority at most crossings are realized to benefit the traffic flow and decrease travel times. In recent years, many of these cycling highways are constructed in the Netherlands and even more are planned to be built ([Tour de Force, 2017](#)).

- *Cycling lane*

Cycling lanes are also common in the Netherlands, the lanes are located on the main road. In contrast to cycling paths, there is no physical barrier between the cyclists and motorized traffic. A straight or dashed line indicates whether cars are allowed to drive onto the cycling lane. In both cases, cars are not allowed to stop or park on the cycling lane ([BSA, 2017](#); [Fietzersbond, n.d.](#)). No official laws govern the width of cycling lanes, however a minimum



width of 1.70 m is advised (Fietzersbond, n.d.). If cars are allowed to drive on the cycling lane, they often have to drive over the opposing car lane to overtake cyclists. Cyclists on the other hand often have to drive onto the car lane if they want to overtake cyclists driving on the cycling lane. This switching of lanes can cause delays in the traffic flow when the road is busy.

- **Cycling suggestion lane**

This type has a similar appearance as the cycling lane but offers no legal protection for the cyclist (BSA, 2017; Fietzersbond, n.d.). Making it essentially part of the main road, only with a visual indication where cyclists could be present, creating more awareness among motorists and a higher perceived safety for cyclists.

- **Cycling street**

The essence of shared space is that the space is designed without clear segregations so all road users are aware of each other and move with caution. In a shared space of cyclists with motorized traffic, often the same rules as on a regular urban road apply but the idea is that cars adjust their speed to the cyclists' speed. More and more car oriented streets are transformed into bicycle priority streets (*fietsstraat*) in the Netherlands (Boggelen & Hulshof, 2019).

- **Shared space**

A shared space of cyclists with pedestrians has less characteristics of a road and often functions more like a square. Pedestrians and cyclists can freely move through the space, road users try to maneuver around by avoiding collisions with each other, traffic rules are undefined. A complete merge of all traffic modes can occur as well, in the Netherlands these spaces are usually identified as a *Woonerf* (sign G5), for all road users a maximum speed of 15 km/h applies (ANWB, n.d.) Later the concept of the *Woonerf* has been adopted in other countries as well (Anvari et al., 2015). Shared space is also common in city centers, where cars have restricted access and only service and delivery vehicles can enter the zone.

In figure 2.2 an overview of these types of cycling infrastructure is visualized in their typical width and common traffic signs.

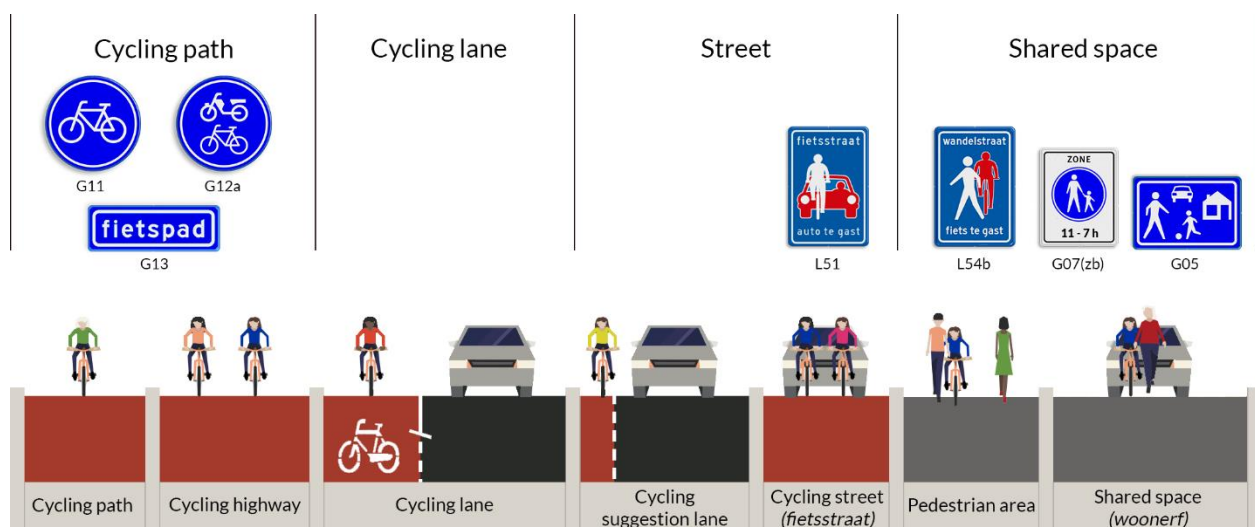


**Figure 2.2:** Common types of cycling infrastructure in the Netherlands



The bicycle gets a more prominent role in governmental policy making and infrastructural developments. In the Netherlands, these measures have their effect the increase of cycling, from 2010 till 2017, cycling (in distance) has risen with 4%, especially in cities ([Netherlands Institute for Transport Policy Analysis \[KiM\], 2019](#)). Also other countries in Europe and Asia) see an increase in cycling ([Huber et al., 2019](#); [Liang et al., 2018](#); [Liu, Sun et al., 2020](#); [Qu et al., 2017](#)). Besides the conventional bicycle, the fast growth of e-bicycle adoption has the potential of replacing more car trips, especially in countries that do not already have a strong cycling culture ([Sun et al., 2020](#)). Due to improvements in power and battery technology, the e-bike market is growing rapidly, between 2020 and 2023, more than 130 million e-bikes are expected to be sold worldwide, which is around a 50% increase from the current number of e-bikes on the road ([Sallomi et al., 2020](#)).

From this section it can be concluded that active transportation, cycling in particular, has proven advantages over other transportation modes in numerous areas. The advantages of cycling help solving the challenges many cities are currently facing, which has increased the interest and popularity of cycling. The Netherlands has many infrastructure solutions to accommodate cyclists, but the rising diversity of vehicles on the road produces new design challenges and policy considerations.

## 2.2. Cyclists' behavior

The behavior of cyclists' can be explained in many ways. This subchapter looks into behavioral aspects that need to be considered when aiming to model cyclists' behavior. Certain levels in cyclists' behavior exist, as well as differences in the behavior of cyclists.

### 2.2.1. Levels of behavior

Three bicycle behavioral levels are distinguished in literature (table 2.1). The strategic level, relating to departure times, route choice and activity pattern choices. The tactical level represents controlled action patterns like: interactions with other road users, favored speed and infrastructure selection (cycling on the bicycle lane, sidewalk, street, etc.). In the operational level cyclists make split-second decisions to execute the behavior determined at the tactical level. These are operations like turning, accelerating, decelerating, yielding and stopping (Gavrilidou, Daamen, et al., 2019; Ma & Luo, 2016; Twaddle et al., 2014; Twaddle, 2018).

**Table 2.1:** Levels of cyclists' behavior

Level	Behavior	Examples
<b>Strategic level</b>	Route & planning	Departure times, route choice, activity pattern.
<b>Tactical level</b>	Trajectory/maneuver	Interactions with other road users, favored speed, infrastructure selection.
<b>Operational level</b>	Control	Accelerating, decelerating, turning, positioning.

Many researchers have investigated the strategic behavioral level of cyclists, mainly in the context of route choice. The strategic behavioral level deals with large scale networks consisting of links and nodes. Travel distance or travel time are primary used to determine the route choice through the network. Besides the travel distance or time, additional properties of a link or intersection can influence the route choice of a cyclist. The combination of properties that influence route choice is defined as the utility or travel cost of a link (Mauttone et al., 2017). Ziemke et al. (2017) used a utility model to determine route choice on a cycling network. Taking into account the travel time, as well as slope, continuity and pavement conditions of the cycling infrastructure. A research by Winters & Teschke (2010) revealed cyclists prefer off-street cycling infrastructure when planning their route. Other findings from this research were the negative effects of parked cars and the absence of road markings on the preference of a route. No preference differences were found between frequent, occasional or potential cyclists (Winters & Teschke, 2010). Broach et al. (2012) found cyclists are also sensitive to turn frequency, signalized intersections and separated cycling paths. More characteristics like environmental attractiveness (e.g.: greenery or lamps), environmental diversity or weather also influence the utility of the route and thus the route choice behavior (Dane et al., 2020; Kalter & Groenendijk, 2018; Liu, Yang et al., 2020). Strategic behavior choices are not part of

the goal for this research, since it focusses on a smaller area, not the whole network. Environmental characteristics are often considered in strategic behavior level for route choice of cyclists, but little to no research is available that considers specific environmental characteristics in tactical or operational behavior.

The tactical behavior includes conscious decisions on a time horizon of seconds to minutes. Tactical decisions are made with regards to, for example: infrastructure selection, deciding whether to overtake other road users to satisfy desired speed, driving on the opposite side of the road and violating red lights or priority rules (Twaddle, 2018). Tactical decisions of cyclists can be complex since they differ greatly for each cyclist, but also in each traffic situation. The route of the cyclist is determined in the strategic level, the path or trajectory choice is decided in the tactical level. The trajectory states how the cyclists move through the environment and which infrastructure they prefer. Flexibility of infrastructure selection for cyclists is higher than for other modes of transportation, meaning they can choose to drive on a cycling path, the street, the sidewalk, over a strip of grass, or for example through a shared space area that has no clear segregation between road users. Especially in shared space environments, the trajectory is primarily based on the movements of other road users. Despite the emerging popularity of these kind of spaces, the insight in efficiency, capacity and safety is limited (Krajewicz et al., 2014; Alsaleh & Sayed, 2020).

The operational behavior level deals with split-second actions to operate the bicycle, these are the actions needed to accomplish the goals set in the tactical level and react to immediate situations. These include basic operations like accelerating, decelerating (braking) and turning (steering) but also positioning operations like yielding, overtaking and keeping distance to other road users. The distinction between constrained and unconstrained behavior is often found in previous research. Unconstrained behavior is more straightforward, since cyclists have the freedom to perform their desired actions without constraints from other road users. The headway is defined as the difference between the time a preceding vehicle passes a reference point and the time a following vehicle passes the same point (Yuan et al., 2019). Constrained headways indicate the longitudinal distance where cyclists are following each other or want to overtake. Positioning the bicycle when following or overtaking other road users consists of operational decisions, however, choosing to overtake or keep following is considered a tactical decision. Mohammed et al. (2019) used video data to evaluate the threshold for unconstrained and constrained cycling behavior. A longitudinal distance of 25 m (5 sec headway time at 5 m/s speed) and lateral distance of 1 m were found to be the thresholds for unconstrained cycling behavior. Hoogendoorn & Daamen (2016) found the constrained headway value to be 4 to 5 sec.

### 2.2.2. Heterogeneity of cyclists

In comparison to modeling car traffic, a lot of heterogeneity among cyclists exists (Hoogendoorn & Daamen, 2016; Liu, Sun et al, 2020). Differences in equipment (bicycle type) and physical fitness can limit cyclists from reaching high speeds (Paulsen et al., 2019). Different types of bicycles vary in average speeds and associated behavior, for example the: regular (city) bicycle, touring bicycle, racing bicycle, e-bike, (electronic) cargo bike, speed pedelec, or even other forms of micro mobility making use of bicycle infrastructure like the: (electronic) motor scooter, (electronic) kick scooter, Segway, etc. (Diepens et al., 2020). These developments cause a change in the composition of road users in terms of speed, size and weight and all these (novel) types of vehicles need to be accommodated in the urban infrastructure (Diepens et al., 2020). Figure 2.1 shows many different

vehicle types, most of which make up only a small share of the total road users. The regular bicycle and electric bicycle will be the focus points for this research, because these have a high presence on Dutch roads. Regarding the dimensions, Dutch guidelines indicate that the handlebars of a bicycle should be less than 0.75 m in width. Also the length of 95% of all bicycles is less than 1.9 m (Hoogendoorn & Daamen, 2016). E-bicycles often have an electric motor which in the EU has a maximum power of 250 W and can support speeds up to 25 km/h (Dozza et al., 2015; Fietsenwinkel, 2018; Hung & Lim, 2020).

Paulsen et al. (2019) pointed out that studies around the world all revealed a large difference in average speeds of cyclists, from 9.61 km/h in China to 21.67 km/h in Denmark. Eriksson et al. (2019) set up a large experiment to measure speed differences at different areas by looking at the time of week and types of bicycles, they found a speed distribution needs to be set for each location. To account for the variance in speed, Ma & Luo (2016) assigned random agility numbers to each cyclists. A cyclist with higher agility choses a higher desired speed, depending on the free-flow speed at each link. Higher speed cyclists approaching lower speed cyclists can probabilistically choose to overtake and continue in higher speed or follow the leading cyclist based on the headway distance. Kalter & Groenendijk (2018) identified five types of cyclists in the Netherlands with specific traits by using a latent class analysis. The findings suggested the most common types were the 'recreational cyclist' (30%) and the 'functional cyclist' (23%), others were identified as 'relaxed, frequent cyclist', 'hurried millennial' and 'senior cycling fanatic'. Cyclists can also consist of social groups. Mohammed et al. (2019) stress the importance of research in cyclists' group following behavior to reveal further behavioral characteristics. When estimating modeling parameters, it should be acknowledged that cycling behavior can substantially vary in different regions.

This section presented different levels of cyclists' behavior, the tactical and operational behavior level will be considered in the modeling process. Strategic behavior deals with a larger scale in space and time and hence falls outside of the scope of this research. The heterogeneity of cyclists was also acknowledged, which will be important for the calibration of behavioral parameters.

## 2.3. Behavioral model approaches

This section will look at the most common approaches for microsimulation of traffic. First of all, macroscopic and microscopic modeling are shortly discussed, after which various modeling approaches to cyclists' behavior simulation are distinguished, which each have different origins and applications. The software tools to apply these behavioral models are evaluated in this subchapter as well.

### 2.3.1. Macroscopic and microscopic modeling

Existing approaches to model traffic behavior can be classified into macro and micro simulation methods. Macrosimulation describes traffic flow using aggregated quantities such as volume, density and speed (Barceló et al., 2010). Whereas in microscopic models, the movement and interaction of each individual road user is modeled. Macroscopic models often use an equilibrium known from the fundamental diagram of traffic flow, assuming a linear relationship between speed and density (Barceló et al., 2010):

$$q(x, t) = k(x, t)u(x, t) \quad [2.1]$$

In equation [2.1], flow  $q$  (veh/h) is a function of density  $k$  (veh/km) and speed  $u$  (km/h). This equation holds up only in equilibrium conditions, making it hard to model mixed traffic flows. Examples of macroscopic models are network models, using graph theory approaches. Or continuum models, where crowds are treated as particles of flow (Hoogendoorn et al., 2014). To simulate mixed traffic flows, macrosimulation models generally assign different Passenger Car Equivalent (PCE) values to other modes, based on their impact on the traffic flow. Wierbos et al. (2020) use mode specific speed functions to include cyclists in the macroscopic model, describing the speeds of cars and cyclists based on the spacing of both modes separately. Macroscopic models are suitable for fast and large scale simulations that not necessarily need to be highly accurate (Hoogendoorn et al., 2014). Less computational power is required than for microscopic models and thus the macroscopic approach is mostly used for large scale infrastructure networks.

Microscopic modeling of traffic flows is based on the motion and actions of each vehicle individually (Barceló et al., 2010). Microscopic models are more suitable for high resolution simulation of a smaller area with mixed traffic flows (Huang et al., 2012). Recent improvements in computational power suggest microscopic approaches will become increasingly more feasible for large scale implementation. Since bicycles often interact in mixed traffic flows, a more detailed representation of road user behavior is required, therefore microsimulation is seen as a more valuable approach to model tactical and operational cyclists' behavior.

### 2.3.2. Car following models

Most traffic simulation software tools use a longitudinally continuous approach, in which two model components are used to independently model the longitudinal and lateral movement of vehicles (Ma & Luo, 2016). The longitudinal movement looks at the movement and interaction of vehicles within

a traffic lane. This behavior is typically modeled with car following models (Twaddle et al., 2014). The car following models use a leading vehicle to determine the behavior of the following vehicles in the lane. Car following models are generally classified into three different classes based on the utilized logic (Olstam, & Tapani, 2004; Twaddle et al., 2014):

- *Gazis-Herman-Rorhery (GHR) models*  
Models where the following vehicle's acceleration is proportional to the current speed, speed difference between the follower and leader and the headway space (Olstam & Tapani 2004). This model is relatively simple and therefore makes several strong assumptions that makes it less complementary to actual traffic phenomena (Saifuzzaman & Zheng, 2014).
- *Safety-distance models*  
Based on the assumption that the following vehicle keeps a 'safe' distance to the vehicle in front. A safe distance can be calculated as the distance that is necessary to avoid a collision if the leading vehicle rapidly decelerates (Saifuzzaman & Zheng, 2014).
- *Psycho-physical car following models*  
To incorporate more human factors, psycho-physical models use thresholds for action points where the driver changes behavior. These models state that slight changes in the environment will not trigger a change in behavior by the driver. An often used psycho-physical model was first proposed by Wiedemann (1974) and uses thresholds of speed and distance differences to determine the behavior type (Barceló et al., 2010).

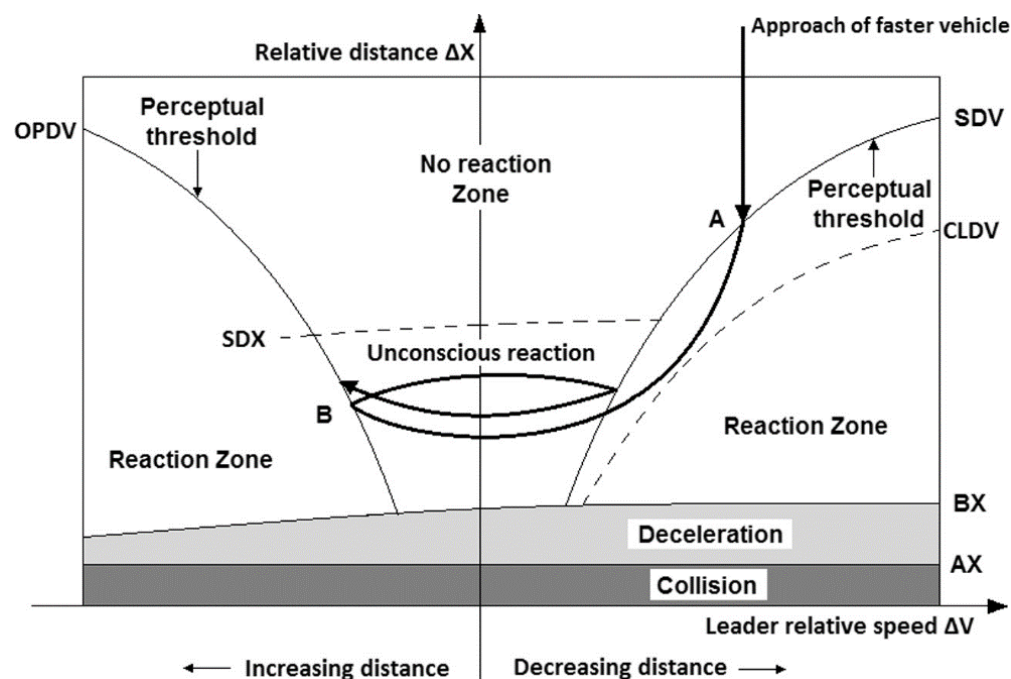


**Figure 2.3:** Car-following model by Wiedemann in 1974 (from: Saifuzzaman & Zheng, 2014)

The Wiedemann model states that while following a leading vehicle, an oscillating process between different stages can be observed (see [figure 2.3](#)). At first, the difference in distance between the faster vehicle that is approaching and the leader vehicle is still large, therefore no reaction is needed



and the driver will try to reach his desired speed. Until reaching the perceptual threshold for deceleration (*SDV*), then the vehicle enters the reaction zone. In this zone the driver tries to decelerate to the speed of the leading vehicle. When reaching the perceptual threshold for acceleration (*OPDV*), the driver will again speed up to match the leading vehicle's speed. This process continues in the unconscious reaction zone. Table 2.2 shows an overview of the thresholds visualized in figure 2.3.

**Table 2.2:** Thresholds of Wiedemann model (Barceló et al., 2010; Saifuzzaman & Zheng, 2014)

Threshold	Description
<i>AX</i>	The desired distance between the front sides of two vehicles in a standing queue.
<i>BX</i>	The desired minimum following distance, a function of <i>AX</i> , the safety distance, and speed.
<i>SDV</i>	The action point where a driver consciously observes a slower leading vehicle; <i>SDV</i> increases with increasing speed difference.
<i>CLDV</i>	Closing delta velocity ( <i>CLDV</i> ) is an additional threshold that accounts for additional deceleration by the application of brakes.
<i>OPDV</i>	The action point where the driver notices that he is slower than the leading vehicle and starts to accelerate again.
<i>SDX</i>	A perception threshold to model the maximum following distance, which is approximately 1.5–2.5 times <i>BX</i> .

The lateral movement model considers the changing of lanes, taking into consideration the position and speeds of other vehicles (Liang et al., 2018). Logical test are performed to check for a better interaction situation in other traffic lanes (Barceló et al., 2010).

In contrast to cars, cyclists are much less bounded by lanes and vehicles in front of them. Overtaking can be done more easily and no concrete lanes are set on a bicycle path (Mohammed et al., 2019). Various possibilities to use the car following model for cycling simulation have been proposed, for example dividing the lane in smaller strips/pseudo-lanes (Paulsen et al., 2019) or using a continuous lateral axis (Mathew et al., 2015).

### 2.3.3. Cellular Automata models

An early stream of microscopic models were Cellular Automata (CA) models (Hoogendoorn et al., 2014). Nagel & Schreckenberg (1992) introduced this model approach, where space is divided into discrete cells and predefined rules for movement are followed by the road users. Interaction between road users occurs when multiple road users have the same target cell (Anvari et al., 2015). By making the cells size smaller, more types of road users can be included in the model. The cells are sized in accordance with the dimensions of the smallest road user (Twaddle et al., 2014).

Both the longitudinally continuous and the CA models have deficiencies in modeling cyclist movement since they assume lane-based behavior that models longitudinal and lateral movement separately (Liang et al., 2018). Using a two-dimensional plane would be more suitable for modeling tactical behavior of cyclists (Twaddle et al., 2014). Since cyclists can use the infrastructure in a more flexible way and often take part in shared space environments, a two-dimensional approach is preferred at these locations.

### 2.3.4. Social force models

The most common two-dimensional approach is the Social Force Model (SFM), which is not bound to the longitudinal and lateral axis, this approach models behavior in a two-dimensional plane using forces based on Newton's second law of dynamics. This model was originally created to model pedestrian behavior, first introduced by Helbing & Molnár (1995). They used three different force terms to describe the behavior:

- The primary driving force is the acceleration to a desired speed in the desired direction of the shortest path towards the goal.
- Repulsive forces are terms reflecting pedestrians keeping their distance from borders, obstacles and other road users.
- Attractive forces are terms to model attractive effects like social groups or objects.

The latter two are forces that make the road user deviate from the path towards the goal. These forces describe a pedestrian's motivation to act in a certain way (Helbing & Molnár, 1995). The trajectory of the agents is often based on collision avoidance or clearance towards obstacles (Liang et al, 2012; Rosman, 2015). Each pedestrian is assigned with a goal area, the shortest path towards this goal area in each point in time determines the desired direction  $\vec{e}_\alpha(t)$ . Helbing & Molnár (1995) present this desired direction as:

$$\vec{e}_\alpha(t) := \frac{\vec{r}_\alpha^k - \vec{r}_\alpha(t)}{\|\vec{r}_\alpha^k - \vec{r}_\alpha(t)\|} \quad [2.2]$$

Where in equation [2.2],  $\vec{r}_\alpha(t)$  denotes the actual position of pedestrian  $\alpha$  at time  $t$ . For each time unit  $t$ , the pedestrian will steer to the nearest point of the goal area  $\vec{r}_\alpha^k(t)$ . If pedestrians (or cyclists) are not disturbed, they will move in the desired direction  $\vec{e}_\alpha(t)$  with a certain desired speed  $v_\alpha^0$ , leading to the desired velocity  $\vec{v}_\alpha^0(t) := v_\alpha^0 \vec{e}_\alpha(t)$  (directional speed). When due to disturbance by other forces, a deviation from the actual velocity  $\vec{v}_\alpha(t)$  occurs, the desired velocity is approached again within a certain relaxation time  $\tau_\alpha$ . Relaxation time can also be explained as the time a cyclists needs to recover from its current speed to desired speed without any disturbance (Huang et al., 2017). Equation [2.3] explains that a low relaxation time implies high acceleration towards the desired velocity. Therefore the main acceleration term towards the goal is described as:

$$\vec{F}_\alpha^0(\vec{v}_\alpha, v_\alpha^0 \vec{e}_\alpha) := \frac{v_\alpha^0 \vec{e}_\alpha - \vec{v}_\alpha}{\tau_\alpha} \quad [2.3]$$

Equation [2.3] determines the driving force of the SFM. In unconstrained behavior, this is the only active force. The full model for a pedestrian's total motivation  $\vec{F}_\alpha(t)$ , is given by the sum of all effects. Including the repulsive and attractive effects, will result in equation [2.4]:

$$\begin{aligned} \vec{F}_\alpha(t) := & \vec{F}_\alpha^0(\vec{v}_\alpha, v_\alpha^0 \vec{e}_\alpha) + \sum_{\beta} \vec{F}_{\alpha\beta}(\vec{e}_\alpha, \vec{r}_\alpha - \vec{r}_\beta) \\ & + \sum_B \vec{F}_{\alpha B}(\vec{e}_\alpha, \vec{r}_\alpha - \vec{r}_B^\alpha) + \sum_i \vec{F}_{\alpha i}(\vec{e}_\alpha, \vec{r}_\alpha - \vec{r}_i, t) \end{aligned} \quad [2.4]$$

The three summation terms in equation [2.4] represent the: repulsive effects of other pedestrians  $\beta$ , repulsive effects of borders  $B$  and the attractive effects of people or objects  $i$ . These effects have underlying equations that include the private sphere and the effective angle of sight of the pedestrian (Helbing & Molnár, 1995). The implications of these additional effects will be further explored in the methodology chapter. In addition to the total motivation, the complete SFM includes random variations in the behavior described as fluctuations. Fluctuations cause deviation from the usual rules of motion, which can be useful when alternatives are equivalent, for example choosing to pass an obstacle on the left or right side (Helbing & Molnár, 1995).

Many different extensions to the original SFM are developed. Schönauer et al. (2012) and Anvari et al. (2015) both proposed models based on this SFM, to model traffic interactions in a shared space, but did not develop a specific cyclists' behavioral model. Huang et al. (2012) also proposed a car extension to the original SFM, excluding the attractive force from the original model because cars are not socially attracted to each other. An additional dynamic model component is integrated to obtain realistic vehicle response with respect to yaw rate, front/rear axles and vehicle mass (Huang et al., 2012).

A cyclists' extension to the SFM was developed by Liang et al. (2012), where a range of psychological and physical forces determine the motion of a cyclist, the so-called psychological-physical force model (PPFM). The psychological forces are similar to the original model, when the density is high ( $0.25 \text{ bicycles/m}^2$ ), the physical forces start acting on the individual at near physical contact with another cyclist. The physical forces are considered to be contact force and sliding friction force. In addition, a 'trajectories choice model' can determine which direction the cyclist wants to move on a more tactical level (Liang et al., 2012). The same research group (Liang et al., 2018) later extended this SFM, introducing the concepts of a reactive range and perceptive range in the form of ellipses. The obstacles and density in the reactive range and perceptive range determine the direction a cyclist moves towards. A collision avoidance force is triggered when an object or another cyclist is entering the reactive range. In this research, various parameters like longitudinal and lateral response coefficients, relaxation time and collision-avoidance strength are estimated by conducting an experiment (Liang et al., 2018).

Dias et al. (2018) used a SFM to model shared space interactions of pedestrians, Segway riders and cyclists. The model used for pedestrians was used to model cyclists as well, only the boundary forces component is removed, since "cyclists do not directly interact with boundaries".

Huang et al. (2017) put more emphasis on the path planning of cyclists at intersections, considering expected conflict zones. When evading conflict zones generated by other vehicles, directness, comfort and efficiency are evaluated to determine the path through the intersection.

In a model developed by Rinke et al. (2017), interaction behavior of pedestrians, cyclists and cars in a shared space is modeled in a multi-layer approach to the SFM. A free-flow layer calculates the path towards the goal, a conflict layer is used to compute appropriate reactions to possible conflicts with other road users. The main contribution of this model is the implementation of a long range conflict avoidance method for cyclists. Cyclists choose a trajectory to avoid the conflict, with minimal breaking and centripetal acceleration (Rinke et al., 2017).

Qu et al. (2017) proposed an extension to the original SFM, specifically aimed at modeling e-bicycle lane changing behavior. They also included principles from the car-following model to account for following characteristics of the cyclists. Also the concept of virtual boundaries is introduced, which

are the lane boundaries of the bicycle lane that can be crossed in crowded conditions. When certain conditions apply, the lane generates a lane changing force to overcome the repulsive force of the virtual boundary, without collision with cars (Qu et al., 2017). The risk of collision between cars and cyclists is also researched by Li et al. (2011), they considered a SFM where cyclists were able to switch from the bicycle lane to the car lane, based on the density in both lanes.

### 2.3.5. Microscopic modeling software

To develop a simulation model, three software options are possible. When using a commercially available simulation software, the initial development time is short but the limitations of the software impose some restrictions. Additionally, a license to the software is needed. When using an open source simulation software, the source codes can be modified, offering more flexibility within the framework of the software. Since it is open source, the software is freely available online. The third option is to create an independent simulation environment, for which the most modeling effort is required but the flexibility is highest (Twaddle et al., 2016).

Many software tools have been developed for the microsimulation of traffic. However, most of these tools are primarily focused on behavior of motorized vehicles or crowds simulation of pedestrians (Krajzewicz et al., 2014; Ma & Luo, 2016). For this project, the commercial software Vissim with the add-on Viswalk will be used, but to assess their functionality other software tools are explored as well.

- *Vissim*

The traffic simulation software Vissim created by the German company PTV Group offers many possibilities for microscopic simulation of multimodal transportation. The main components of Vissim make use of car-following methods based on the Wiedemann model (PTV Group, 2020). As discussed earlier, this modeling approach considers longitudinal and lateral movements separately. Within this framework, it is possible to simulate all kinds of transportation modes, including cyclists and pedestrians. Since this lane behavior does not apply for all situations, the integrated add-on Viswalk is provided within Vissim. This add-on is specially focused on pedestrian behavior and uses a different underlying modeling method based on the Social Force Model by Helbing & Molnár (1995). Vissim offers many options to change parameters of the default settings and the option to create user defined attributes. Vissim offers the opportunity of realistically visualizing the environment and customize vehicles, display types and 3D models.

- *Aimsun*

Aimsun (Advanced Interactive Microscopic Simulator for Urban and Non-Urban Networks) is also a commercial traffic simulation software tool developed by the Polytechnic University of Catalunya (Gao, 2008). It has the capability of modeling the traffic network and vehicles in detail, for example by being able to model roadway types, traffic detectors and the impact of incidents (Ejercito et al., 2017). Heavy coding is required to build the road network in Aimsun (Saidallah et al., 2016). Just as Vissim, Aimsun provides three-dimensional graphic representation of the simulations, but visualizations are considered less realistic than in Vissim (Ejercito et al., 2017).

- **MATsim**  
MATSim is an agent-based open source transport simulation software implemented in Java. Frameworks for demand modeling, traffic flow simulation, re-planning and analysis methods are offered. It is designed to analyze large-scale networks, making computations efficient but less specific in vehicle behavior (Horni et al, 2016). In contrast to Vissim and Aimsun, MATSim does not offer three-dimensional graphic visualization of the simulations (Saidallah et al., 2016).
- **SUMO**  
SUMO is an acronym of 'Simulation of Urban MObility' and is developed by the German Aerospace Center. SUMO is an open source application that is continuously evolving with new projects since the source code is openly available and gives the capability of extending the software using own algorithms (Krajewicz et al., 2014). Still, the width of lanes or types of vehicles are fixed in SUMO (Saidallah et al., 2016). The traffic network should be manually written in an XML file or imported from other simulation packages (Ejercito et al., 2017).

Since this research will primarily focus on the application of the model to evaluate different scenarios in the case study area, it is preferred to choose an already existing simulation software. This way more effort can be put into location specific applications and possibly a larger area can be evaluated than when using more labor intensive modeling software. This offers more valuable and complete results to support the municipality of Utrecht in their decisions regarding cycling policy and developments.

In conclusion it can be stated that there are multiple ways to simulate cyclists on a microscopic level. Based on the environment and road users, different model approaches can be useful. An existing software is selected to perform the simulations, Vissim offers detailed and ready-to use functionalities, while also keeping flexibility in changing behavioral parameters. Furthermore it offers the best graphical representation in terms of network building and three-dimensional visualizations.





### 3. Methodology

In the literature review chapter, currently used models and methods for cyclists' behavior modeling were investigated. The traffic simulation software Vissim was selected to perform the simulation of scenarios. This chapter explores how this software tool can be used to reach the established research goals. The software is explored to evaluate how cyclists' behavior is most realistically simulated. Previous research efforts are used to calibrate parameters of the models.

After initial calibration, a data collection experiment is set up to obtain relevant data for the verification of the behavior model. This experiment is executed by evaluating naturalistic cycling data in unconstrained environment. After processing this collected data it is used to check if it matches the calibrated parameters, validating the behavioral model.



## 3.1. Vissim and Viswalk

As discussed in [section 2.3.5](#), the software Vissim created by PTV Group will be used in this project. The thesis license versions of Vissim 2020 and Vissim 2021 are used. The main Vissim module, which uses lane based models, provides bicycles as a calibrated vehicle type. The integrated add-on Viswalk is developed to model pedestrian behavior. In the default settings, the parameters of this model are calibrated for pedestrian behavior but can be changed and used to reflect cyclists' behavior as well. For some locations, the two-dimensional approach of the SFM is preferred over the lane-based approach. Depending on whether cyclists interact more with pedestrians or with cars. This determines the choice if cyclists are simulated as vehicles or as pedestrians. At some locations a transition between the two models is needed to combine the two types of behaviors.

The both models are calibrated to check how cyclists' behavior is best reflected in different situations. Especially the SFM will need extensive calibration. Besides changing the speed distribution, size and appearance of the agents, calibration of parameters is essential in order to reflect cyclists' behavior instead of pedestrian behavior. When mentioning functions of the Vissim or Viswalk software, many terms are related to 'vehicles' or 'pedestrians' since these are the conventional terms. For this project, terms like vehicle types or pedestrian classes can also relate to cyclists.

### 3.1.1. Vissim elements structure

To clarify terminology used in the research, the structure of Vissim will be explained in this section and for Viswalk in [section 3.1.2](#). Vissim uses connected network objects that have attributes, which can be objects, distributions, functions or parameters values. [Figure 3.1](#) shows the most important objects, settings and relations of the main behavioral model.

The structure can be divided in input dependent and settings which are link or area dependent. The upper part of [figure 3.1](#) shows all settings related to the input in the network. Vehicle inputs are set on a link and consist of a certain vehicle composition and volumes (vehicles/hour). The vehicle compositions are made up of relative flows of vehicle types. At vehicle compositions the desired speed distribution can also be set. Vehicle classes also consist of vehicle types, which are used to group vehicle types for visualization, evaluation and application of various class dependent behavioral decisions. At vehicle types, the desired and maximum acceleration and deceleration functions can be set. Furthermore the vehicle type settings can regulate the dimensions and visual appearance of the vehicles.

On the other side there are the network objects that form the infrastructure. Links form the main roads and are connected by connectors, which mostly have the same properties as links. Links consist of one or more lanes. For links as well as for individual lanes, a link behavior type can be specified. The link behavior type consists of a default driving behavior, or driving behaviors that apply only to certain vehicle classes. In the settings for driving behaviors, almost all behavioral parameters can be set, including following, car following model, lane change, lateral and signal control parameters.

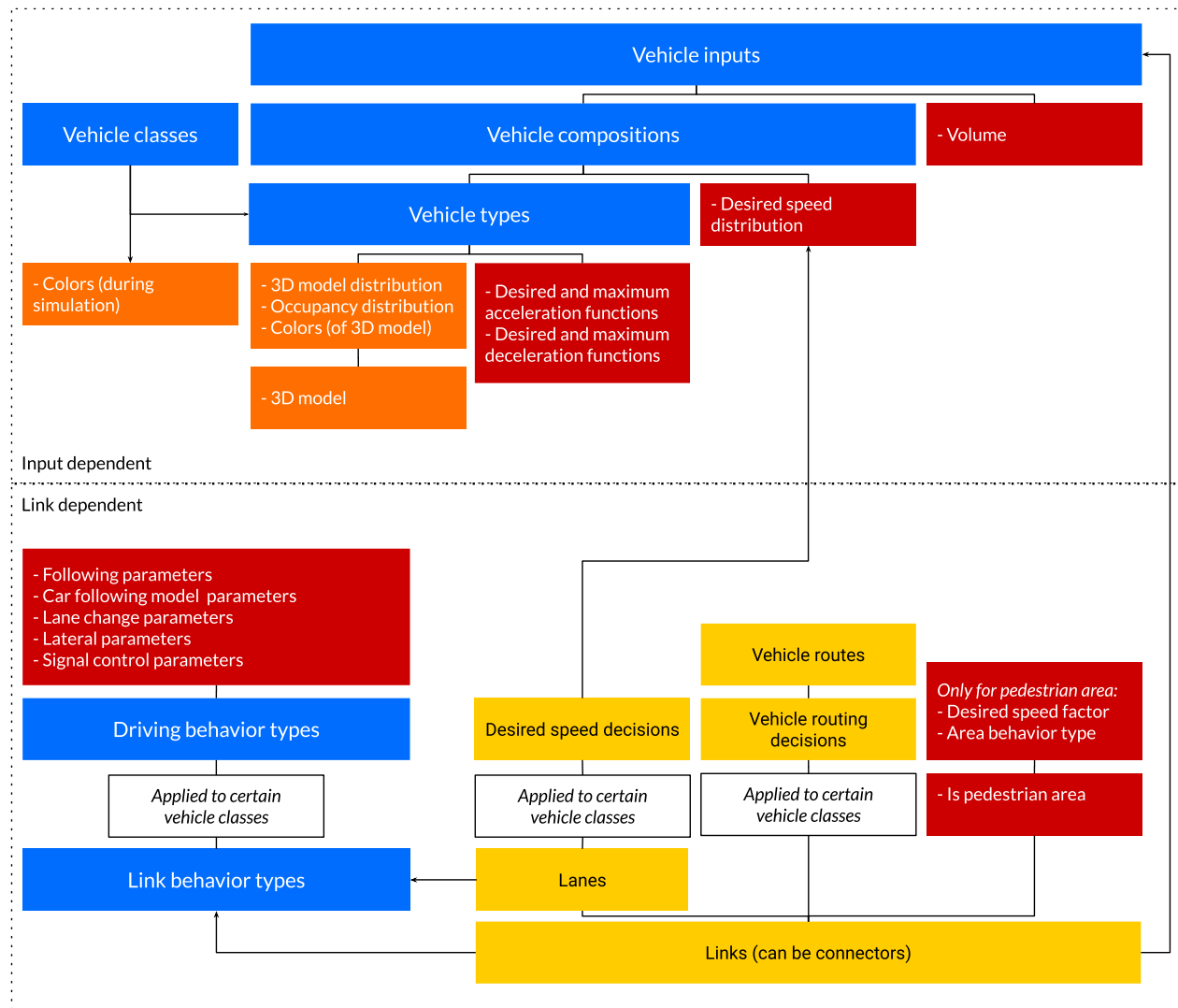


**Figure 3.1:** Overview Vissim Structure

At a specific location on a lane, a desired speed decision can be placed, linking to a desired speed distribution on that lane. Similar to this, vehicle routing decisions can be placed on links, which makes vehicles (of a certain class) decide on a route. Lastly, a link can be classified as a pedestrian area. When using this, most properties of the link, such as vehicle input or link behavior, can no longer be accessed. The link now functions as an area object of the Viswalk module type that pedestrians can use.

### 3.1.2. Viswalk elements structure

In section 3.1.1 the most important elements of the main Vissim module were described. Even though Viswalk is integrated in the same software, it uses other network objects and works slightly different. The most important objects and parameters of Viswalk are visualized in figure 3.2. Some parameters can only be defined as global parameters (that apply to the whole network). Some parameters can be influenced in multiple ways, for example as a global parameter and as an attribute value of a network object.

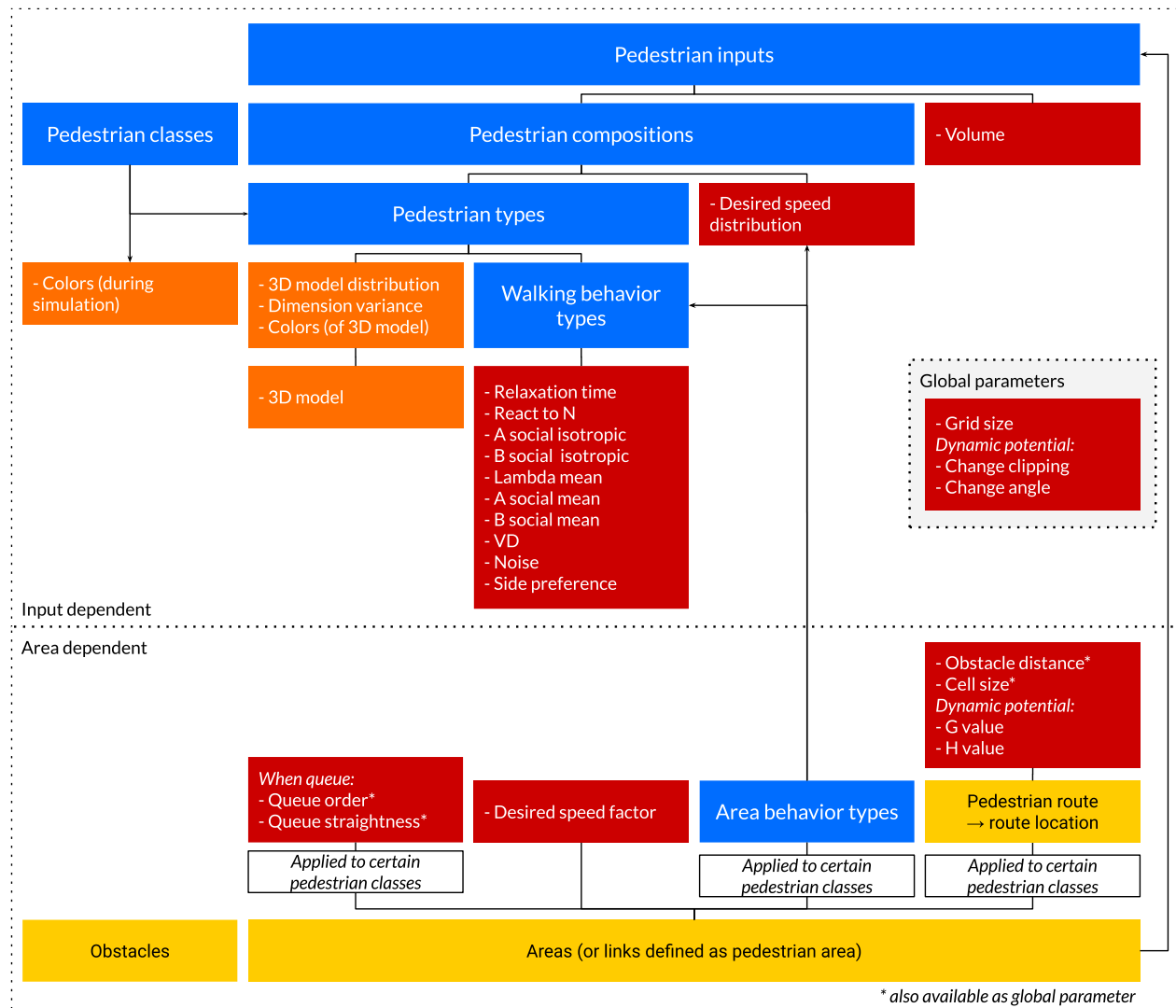


**Figure 3.2:** Overview Viswalk structure

The infrastructure of the model is created with areas, as said earlier, links can also be classified as pedestrian areas. To generate traffic, pedestrian inputs have to be created on an existing area. Pedestrian inputs consist of a volume parameter (pedestrians/hour) and a certain pedestrian composition. A pedestrian composition is a set of relative flows of pedestrian types. As an attribute of the pedestrian composition, the desired speed distribution for this composition can be set as well. Pedestrian types have the attributes: 3D model distribution, dimension variance, colors and walking behavior type. The 3D model distribution consists of a set of 3D models that make up this pedestrian type, these settings are purely visual and do not influence the results of the simulation. The walking behavior type consists of ten parameters, which are further explained in [section 3.3.2](#). Pedestrian classes function similar to vehicle classes.

Besides being used as a pedestrian input, areas have many attributes, most notably the pedestrian route decision. Here the origin and destination of the pedestrians is set. The route decisions/locations have many different settings, including certain parameters that can be applied to the pedestrian classes following this route. For example, obstacle distance or cell size.

An area can also have an area behavior type for certain pedestrian classes. The area behavior types then consist of a walking behavior type and desired speed distribution. When applied in the area behavior type, the parameters set in the upper part of the diagram in [figure 3.2](#) are overwritten by the area behavior type. Furthermore an area can be set as a queue area, here two parameters can be adjusted for each pedestrian class as well. Another parameter of an area independent of the pedestrian class, is the desired speed factor, which can decrease or increase the desired speed of all pedestrians in the area by a certain percentage factor. All the parameters all further explained in [section 3.3.2](#).

### 3.1.3. Vissim and Viswalk interaction

Since the two modules of Vissim (lane-based and area-based) use different behavioral models and infrastructure objects, their interaction is limited. In the standard Graphic User Interface (GUI) of Vissim, the only possibility for interaction between the two models is at an intersection of two links, where one link is classified as pedestrian area. At the crossing of two links, a conflict area is identified by the software. For each conflict area, the link that has right-of-way and the link that has to yield can be set. Pedestrians or vehicles that enter the detector area attached to the conflict area are taken under consideration for conflict area rules. The parameters *Front gap* and *Rear gap* determine the minimum gap for yielding vehicles to move through the conflict area.

In addition to conflict areas, priority rules can be placed, consisting of a stop line and conflict marker. These priority rules can also be set for multiple links for one stop line. This prevents pedestrians crossing one link without considering traffic from the opposite direction, which might result in pedestrians being stuck on the middle of the road, blocking the other link (see [figure 3.3](#)). Pedestrians blocking the road like this quickly cause a traffic jam across the entire network. In the setting for priority rules, two main parameters can be adjusted. Firstly, the *Minimum gap time*, the minimum time in which the right-of-way vehicle reaches the conflict marker. Secondly, the *Minimum clearance*, stating its minimal distance from the previous vehicle ([Dahlberg & Segernäs, 2017](#)).



**Figure 3.3:** Unrealistic behavior of pedestrians being stuck at the middle of the road

Vissim implements Microsoft's Component Object Model (COM) as an Application Programming Interface (API). By using the COM Interface, Vissim offers the possibility to access objects from external applications or scripts. By using this module, scripts can be used to go beyond the standard operations of the software. External script files in the languages of Visual Basic, Javascript and Python are supported (PTV Group, 2020). For this project, Python 3.7 is installed and linked with the COM Interface. Custom scripts are developed in PyScripter, an Integrated Development Environment for Python, this way coding and debugging is made easier. The script file (in a .py file format) is loaded into Vissim and is executed for every time step. [Appendix E](#) shows the full script for one transition zone.

The script is created in two separate functions, one for the transition from a link (vehicle) to an area (pedestrian) and one function from area to link. The coding differs slightly because of the different attributes for vehicles and pedestrians but in general, both functions operate similarly. Cyclists on the exit link/area are accessed and if a cyclist is within one meter of the end of the link/area, a new cyclist is generated on the enter link/area. The entering cyclists has the same desired speed as the exiting cyclist, optionally this desired speed can be adjusted for shared space areas. When this new cyclist enters the network, the exiting cyclist is simultaneously removed from the network. The generation of a new cyclist differs for cyclists modeled as vehicles or as pedestrians:

- *Cyclists as vehicles*  
The transition from areas to links removes a pedestrian and adds a vehicle to the network. The generation of a vehicle is done with the *AddVehicleAtLinkPosition* method. This method allows to set the vehicle type, link number, lane number, distance from start of the link and desired speed. The lateral position within the lane is set according to the driving behavior in the enter link. The speed when entering is set according to the current traffic situation and the desired speed (PTV Group, 2020). Consequently, this can cause a rapid change in speed and/or lateral position at the transition point.
- *Cyclists as pedestrians*  
Adding a pedestrian to the network is done with the *AddPedestrianOnAreaAtCoordinate* method. For this method, the pedestrian type, area number, relative position, orientation, desired speed and enter speed can be specified. In contrast to the vehicle generation, this method does allow the speed to be set according to the speed of the vehicle when exiting the network, creating a fluent transition. Furthermore, the exact location and orientation of entering can be specified. However, for environments that are not right angled it will be hard to translate the position of the vehicle to the position of the pedestrian. Since the vehicle position is specified as longitudinal and lateral position within the link and the pedestrian entering position is specified as the x and y distance (in meters) from the center of the entering area. The orientation can be specified with an x and y component of the viewing direction vector, which should be aligned with the angle of the exit link relative to the north.

For each transition of link to area (or reverse), the script must specify the exact link, lane and area numbers, as well as the right position and orientation corresponding to that transition zone. This makes this method rather labor-intensive. It also disables the ability to track one cyclist in their complete journey, since a new cyclist is generated at every transition. This method does make it possible to use the advantages of both models in an integrated environment.

## 3.2. Speed and acceleration

Since two behavioral models will be used, both have to be calibrated separately. However, in both behavioral models, speed is modeled by using individual desired speeds. Acceleration towards this desired speed is either modeled as a function of speed (in lane-based model) or indirectly with the relaxation time (in area-based model).

### 3.2.1. Desired speed

Desired speed is a clearly measurable parameter that is set according to a probability distribution which applies to both models. To clarify, the desired speed is the speed a cyclist aims to reach when not disturbed by external factors. In motorized traffic simulation, the desired speed is often modeled by taking the speed limit of the road. For the simulation of cyclists, the desired speed often depends on the personal preferences or physical capabilities of the cyclist, as well as external factors like the type and quality of the infrastructure and the presence of other road users (Twaddle & Grigoropoulos, 2016). The differences in personal characteristics are incorporated through the probability distribution. Differences in desired speeds caused by the environment can be modeled locally for specific types of infrastructure. This can be achieved by creating a separate desired speed distribution that applies to a specific area.

Since local desired speed data is not available, reference values are used to estimate the desired speed distribution. In table 3.1, five different reference research projects are displayed with the corresponding average desired speed, standard deviation and city where the research was conducted.

**Table 3.1:** Reference research projects on desired speed

Average desired speed	Researchers	Location
22.6 km/h ( $\sigma$ of 3.99)	Paulsen et al. (2019)	Copenhagen (Denmark)
18.9 km/h ( $\sigma$ of 3.16)	Bernardi & Rupi (2015)	Bologna (Italy)
18.8 km/h ( $\sigma$ of 4.50)	Twaddle & Grigoropoulos (2016)	Munich (Germany)
18.4 km/h ( $\sigma$ of 6.2)	Boufous et al. (2018)	Sydney (Australia)
17.4 km/h ( $\sigma$ of 5.4)	Huang et al. (2017)	Beijing, Guangzhou (China)

With the aid of a normal distribution number generator, sets of numbers with these average desired speed and standard deviation are generated, leading to the cumulative distribution functions (CDF), visualized in figure 3.4. By taking average points of these five reference projects, the standard desired speed distribution in figure 3.5 is yielded. Resulting in an average desired speed of 19.43 km/h, with a standard deviation of 4.37.



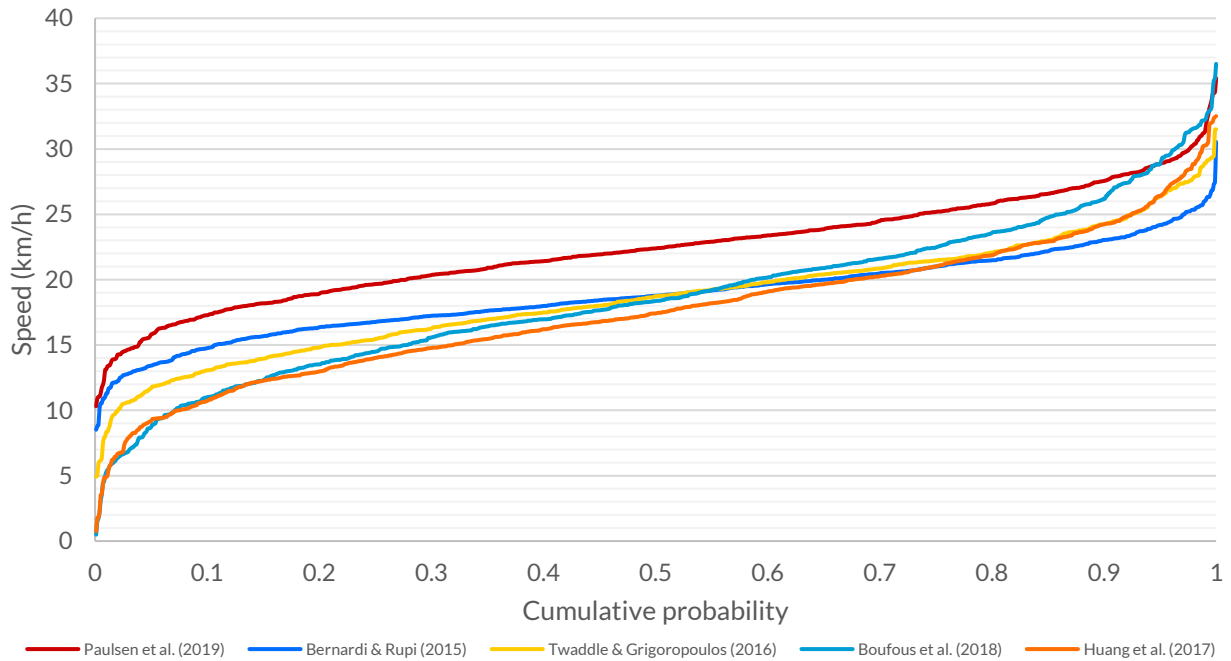


**Figure 3.4:** Estimated cumulative desired speed distribution of reference projects

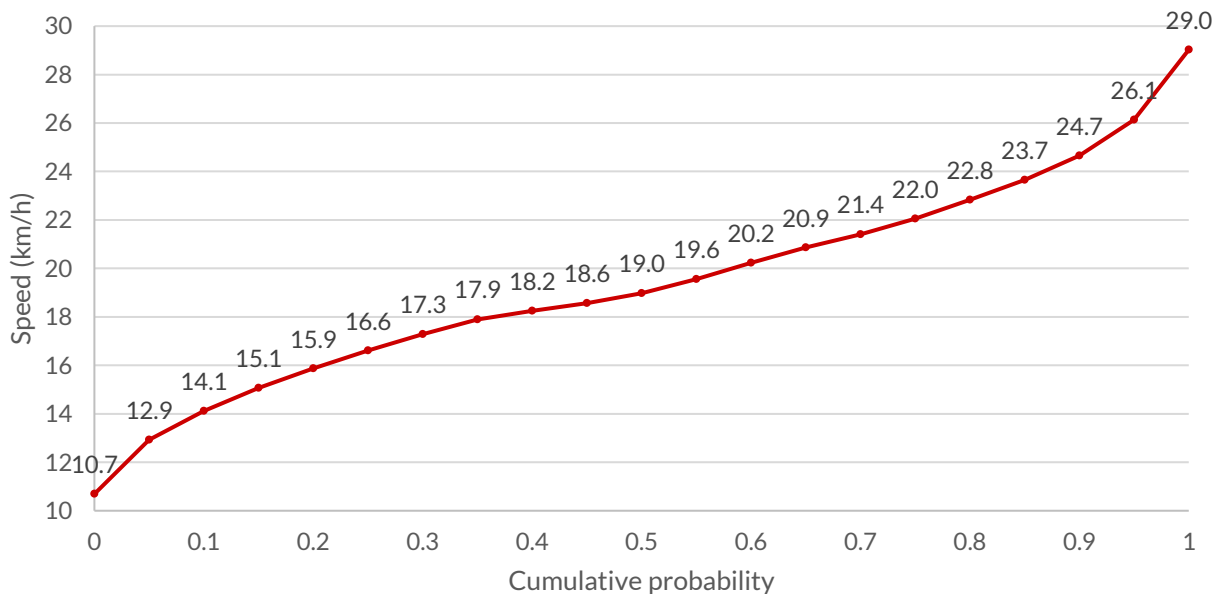


**Figure 3.5:** Desired speed distribution in standard situations

Also data from the *National Cyclists counting week* is considered, which is an annual national data collection project in the Netherlands. In the total research, the GPS location and speed of more than 40,000 participants was measured and aggregated per road section (Fietstelweek, 2016). A portion of data from the 2016 edition was obtained for analysis. This dataset contains the average measured cycling speed at 28,629 roads in the city of Utrecht. To clean this dataset, a total of 2889 data entries with values above 35 km/h and with a value of 0 are removed, leaving 25,740 entries. The measured average speed is compared to the desired speed from this dataset in figure 3.6. The observed speeds

are lower than the desired speed, which can be explained by hinderance from other road users to reach the individual desired speed. Besides being around 2 km/h slower, [figure 3.6](#) shows similar patterns in probability and range of speed values, confirming the desired speed estimated according to reference projects.

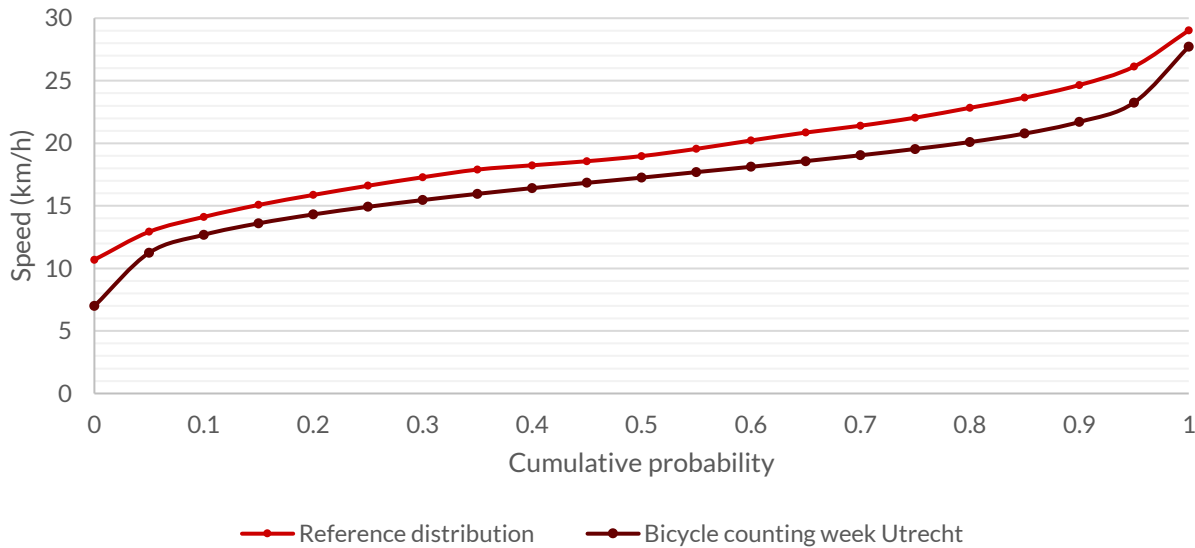


**Figure 3.6:** Reference desired speed distribution and average measured speed (*Fiets Telweek, 2016*)

Since e-bicyclists have a considerably higher desired speed, a separate speed distribution has to be created. The electric motor of typical e-bicycles supports speeds up to 25 km/h ([Dozza et al., 2015](#)), therefore the assumption is made the desired speed for most e-cyclists is around this 25 km/h. [COWI \(2013\)](#) used cycling measurements in Copenhagen for the calibration of a microsimulation model for cyclists, which is also provided as a separate file in the Vissim installation. In this research, a desired speed distribution ranging from 22 km/h to 30 km/h is used for e-cyclists, which is around 20% higher than the desired speed distribution used for regular cyclists in this research. By increasing the estimated desired speed distribution with 20%, a desired speed distribution for e-cyclists is yielded ([figure 3.8](#)).

Even though in the Netherlands this is less of an issue, the slope of the road has a large impact on the speed of cyclists. A research by [Eriksson et al. \(2019\)](#) found that the average speed uphill was about 14 km/h compared to 26 km/h when riding downhill. Since the height differences are negligible in the case study area, slopes will not be further considered.

It is assumed the desired speed of cyclists when taking turns is lower than when cycling at a straight part of road. Unfortunately, very limited data on turning speed is available. For a riding speed of 20 km/h, the minimum radius is 7 m ([Gavriilidou, Wierbos, et al., 2019](#)). More data collection is needed to implement a turning speed reduction in the model.

[Figure 3.5](#) shows the desired speed distribution that applies to cyclists in standard situations. A separate environment-dependent speed distribution is created for shared space with pedestrians. [Boufous et al. \(2018\)](#) found an average reduction of 14% in desired speed on paths that were used by pedestrians as well. [Bernardi & Rupi \(2015\)](#) found that cyclists speed reduces on average 17% at infrastructure shared with pedestrians.

The dataset from Fiets Telweek (2016) can also be used to evaluate the speed difference for different infrastructure types. Figure 3.7 shows the average speed of cyclists on various types of infrastructure, which is not necessarily their desired speed. The average speed for infrastructure type 'pedestrian' is around 18% lower than the average speed of all other infrastructure types. Based on these observed changes in average speed from various sources, the standard speed distribution is lowered by 17% for shared space areas (figure 3.8).

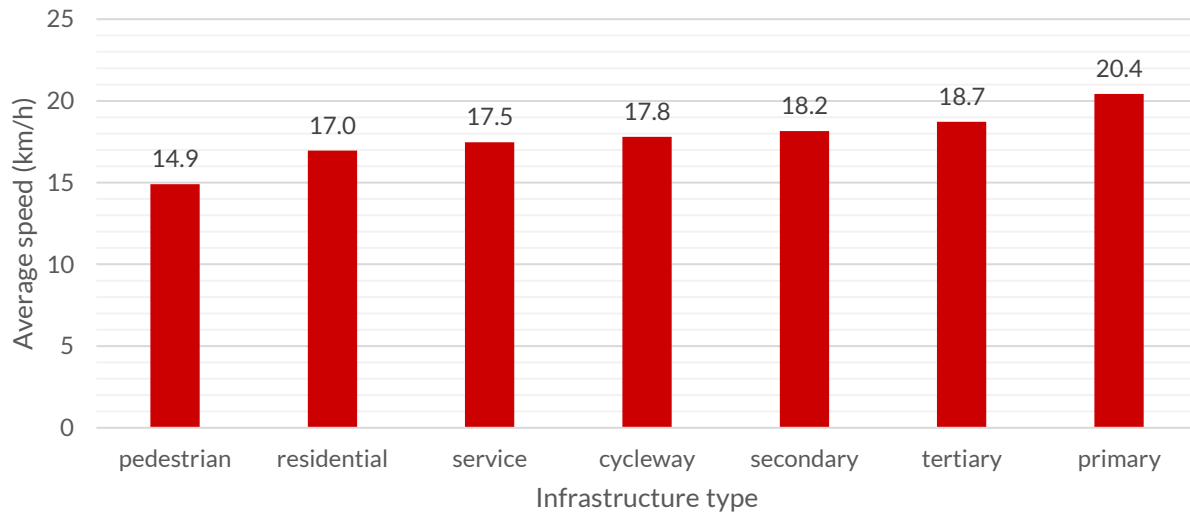


**Figure 3.7:** Average speeds for different types of infrastructure in Utrecht (Fiets Telweek, 2016)

To summarize, three different desired speed distributions are estimated based on reference projects and theoretical theories. The research by COWI (2013) is used as a reference for the desired speed distribution for e-bicyclists. A shared space speed distribution applies to areas that are shared with pedestrians. The desired speed distribution for e-bikes applies to the input of cyclists, but will be overwritten by the area dependent distribution when an e-cyclists enters a shared space. All speed distributions are visualized in figure 3.8.

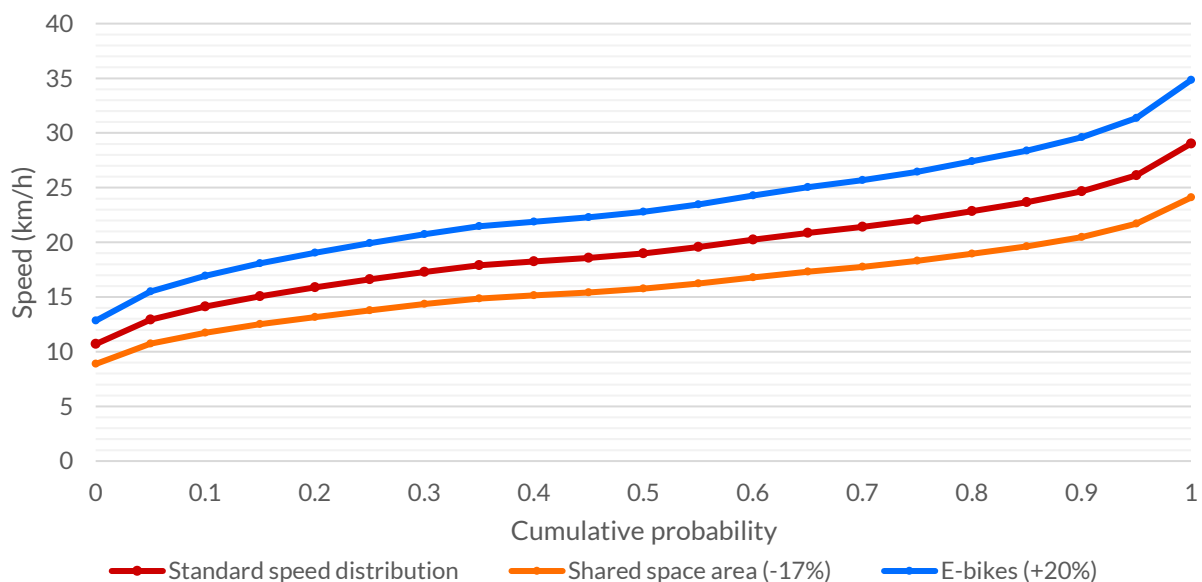


**Figure 3.8:** Desired speed distributions

### 3.2.2. Acceleration

The desired acceleration and deceleration are modeled as a function of speed in the lane-based model. The maximum acceleration function quantifies the maximum acceleration that is technically possible and is not relevant for cyclists in most situations. The desired acceleration function applies in all situations where the a maximum acceleration is not required (PTV Group, 2020). The maximum acceleration is mainly used for behavior on slopes, which are not present in the case study environment.

For the default 'bicycle' vehicle type in Vissim, the same acceleration function as for cars is used (PTV Group, 2020), which seems improbable. Limited research mentioning acceleration for cyclists is conducted, Twaddle & Grigoropoulos (2016) found that cyclists reach their maximum acceleration when their current speed is at 40% of their desired speed. The observed average maximum acceleration was  $0.7 \text{ m/s}^2$ . Figliozzi et al. (2013) found maximum acceleration values between  $1 \text{ m/s}^2$  and  $2 \text{ m/s}^2$ , with an average around  $1.6 \text{ m/s}^2$ . Ma & Luo (2016) found maximum acceleration values between  $0.5 \text{ m/s}^2$  and  $2 \text{ m/s}^2$ . In the research by COWI (2013), the desired acceleration and maximum acceleration functions are identical for all cyclist types, this function will also be used to model the acceleration of cyclists in this project (see figure 3.9). Besides the median value, also a minimum and a maximum function are presented that describe the stochastic distribution (PTV Group, 2020). At very high speeds ( $>30 \text{ km/h}$ ) still a (low) desired acceleration is visible to prevent irregular behavior at high speeds. It is assumed e-cyclists have a higher acceleration since they are electronically assisted. However, very limited previous research is available on this topic. Therefore also data collection on this topic is performed (see section 3.4).

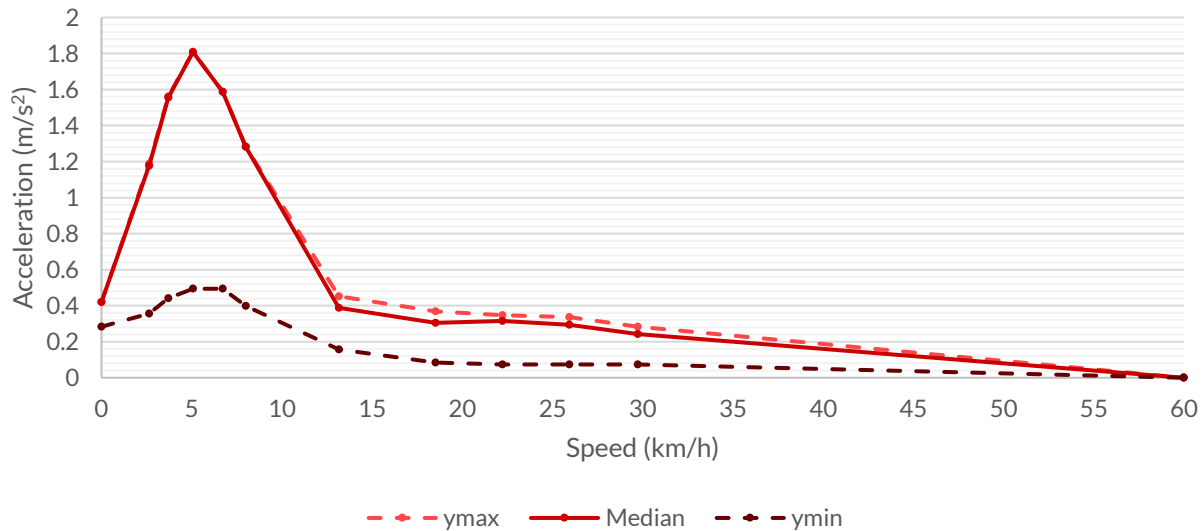


**Figure 3.9:** Desired (and maximum) acceleration functions (COWI, 2013)

The modeling of deceleration is similar to acceleration, with a maximum and desired function, again the desired deceleration function is also set as maximum deceleration function. Ma & Luo (2016) found a maximum average deceleration (reverse acceleration) around  $-0.9 \text{ m/s}^2$ . Deceleration of cyclists was also researched by COWI (2013), figure 3.10 shows this function of desired deceleration. This desired deceleration function will be used for the lane-based cycling behavioral model.

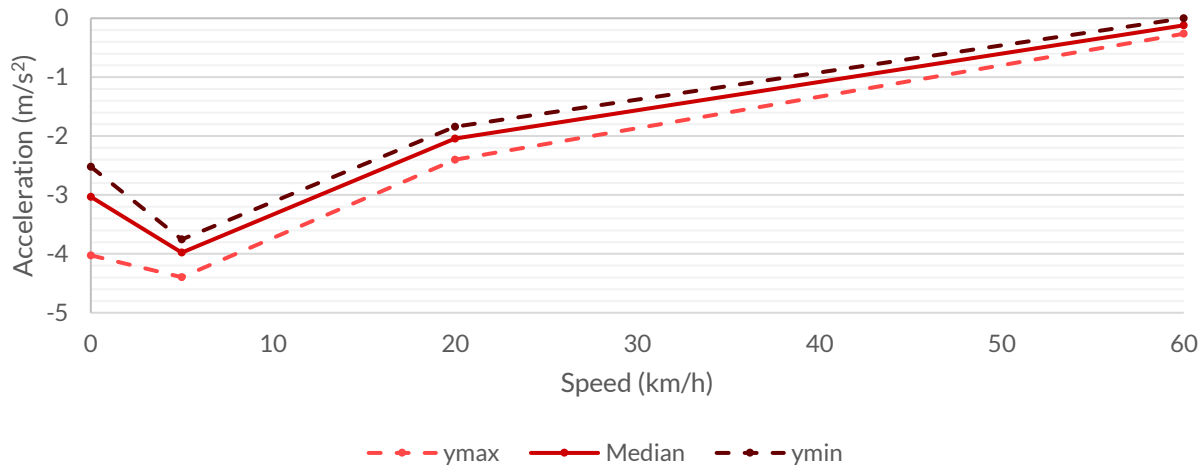


**Figure 3.10:** Desired (and maximum) deceleration functions (COWI, 2013)

### 3.2.3. Relaxation time

In the SFM, acceleration is primarily modeled through relaxation time  $\tau$  (also see [section 2.3.4](#)). When increasing the relaxation time, the acceleration will decrease since the cyclist will take longer to reach his desired speed. Besides influencing the acceleration, a large relaxation time also increases the radius of taking turns around corners. The cyclist will drift outwards when making turns. Thirdly, the relaxation time also influences the extent of evasive behavior in SFM. With a higher  $\tau$ , cyclists or pedestrians will evade each other more and thus the density around bottle necks becomes less. (Johansson et al., 2014; PTV Group, 2020). The relaxation time will be calibrated so the time a cyclist needs to change speed and change direction both show realistic values.

Compared to the default value of the relaxation time which is calibrated for pedestrians at 0.4 s, this parameter should increase. To test which value is realistic, a digital acceleration test is created with the aforementioned speed distribution ([section 3.2.1](#)). A test environment is created where each meter, the average speed is calculated for 30 meter ([figure 3.11](#)). To make sure the cyclists show unconstrained behavior, an input of 100 cyclists/hour is generated. The average value of 10 simulations of 60 min is taken for each  $\tau$  value.



**Figure 3.11:** Acceleration test setup in Vissim network editor

The average speed for different values of the relaxation time is shown in [figure 3.12](#). Since the desired speed distribution is identical for all values of  $\tau$ , cyclists aim to reach a similar average end speed. However, the average speed at 30 meter gradually decreases for higher tau values. This occurs because cyclists take longer to reach their desired speed, but also because for the highest values of  $\tau$ , cyclists cannot adjust their direction quickly enough and are conflicting with the edges of the 4 meter wide path.

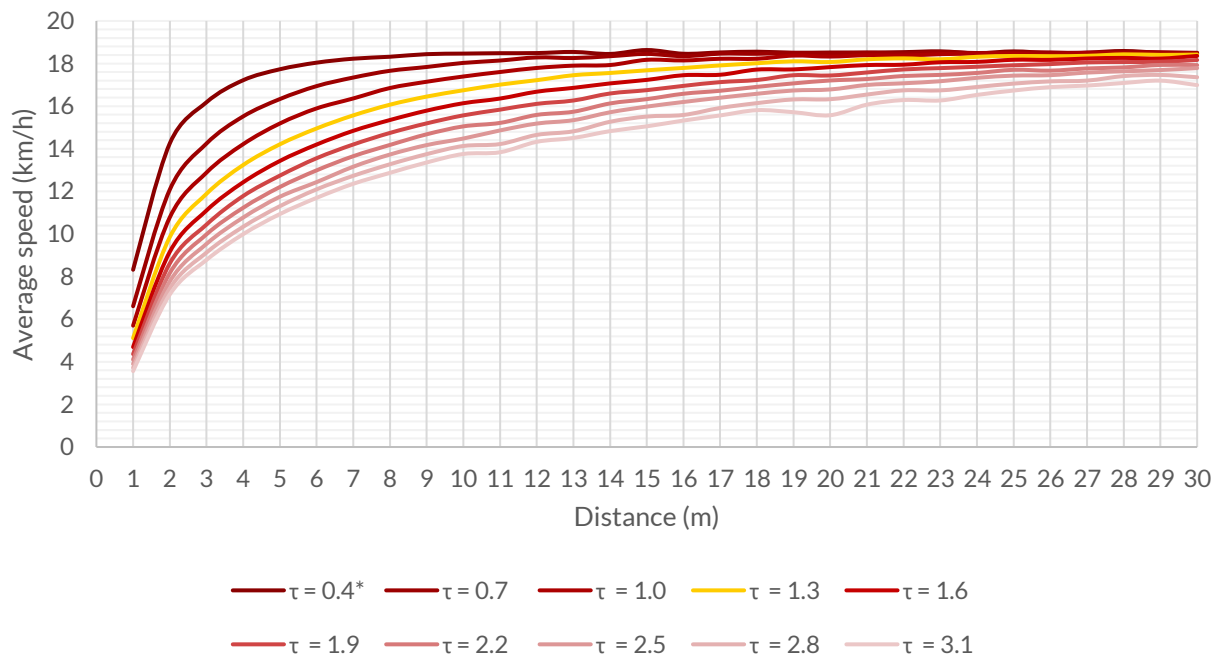


**Figure 3.12:** Average speed over 30 meter for different values of relaxation time

From figure 3.12 it can be observed that low values for relaxation time see a high acceleration. To assess this more clearly, the average acceleration for the first 15 meter is graphed in figure 3.13. What can be noticed is the highest average acceleration occurs in the second meter. The lower values of  $\tau$  show acceleration values that are more like the values presented in figure 3.9. Based on figure 3.13, a  $\tau$  value of 3.1 would best match the acceleration function set for lane-based behavior.

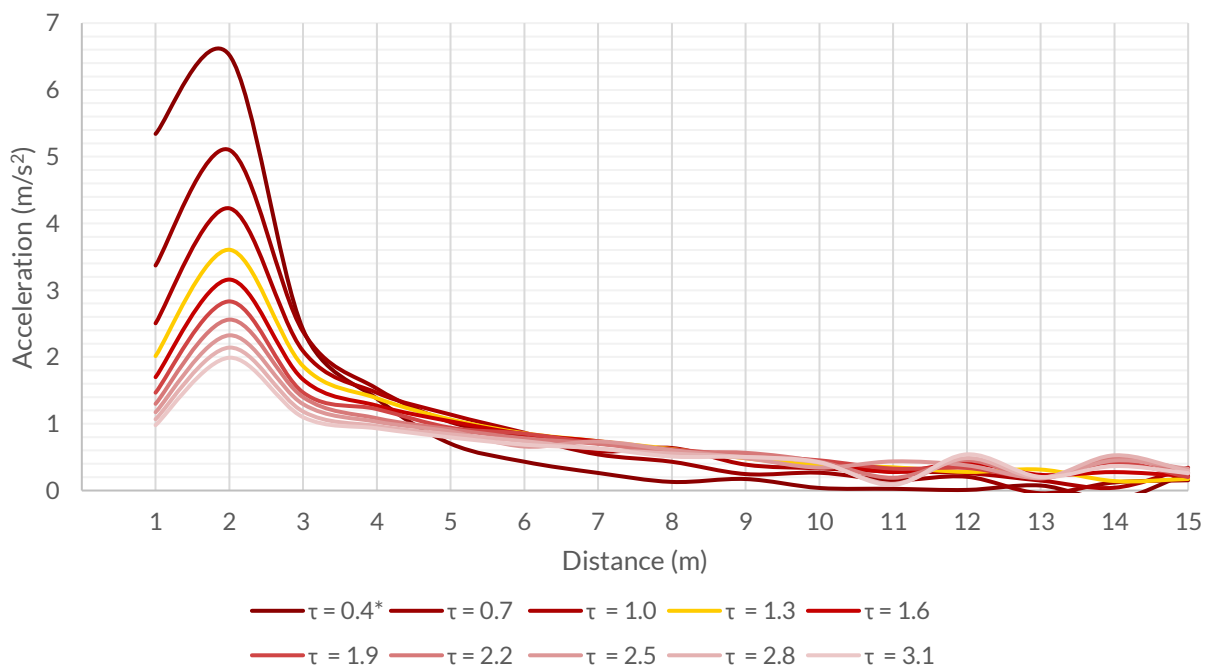


**Figure 3.13:** Average over 15 meter for different values of relaxation time



To test another unconstrained property of the relaxation time parameter, a different digital test is set up where a cyclist rides for 25 meter alongside an obstacle before making a right turn towards the goal area of 3x3m (see figure 3.14). The relaxation time is changed and the trajectories are evaluated by visualizing the average density on grid cells of 0.5 m. Figure 3.14 shows a trend where higher  $\tau$  values of make cyclists take a wider turn around the corner. For  $\tau$  values higher than 2.2, the cyclists sometimes even drive past the goal area in an irregular spinning movement. This occurs because the relaxation time not only influences the time needed to change speed (figure 3.12), but also the time needed to change direction. For the higher  $\tau$  values, the cyclists take too long to adjust direction therefore the turning radius becomes wider, even though their speed while making the turn is lower.

These two tests (acceleration and turning) show contradicting results as to which value of  $\tau$  suits best. In terms of acceleration, a higher relaxation time would be more realistic. However, in the analysis of turning trajectories (figure 3.14), a lower relaxation time seems more logical because cyclists otherwise pass the goal area. For low  $\tau$  values, a larger deceleration and sharper turns are observed.

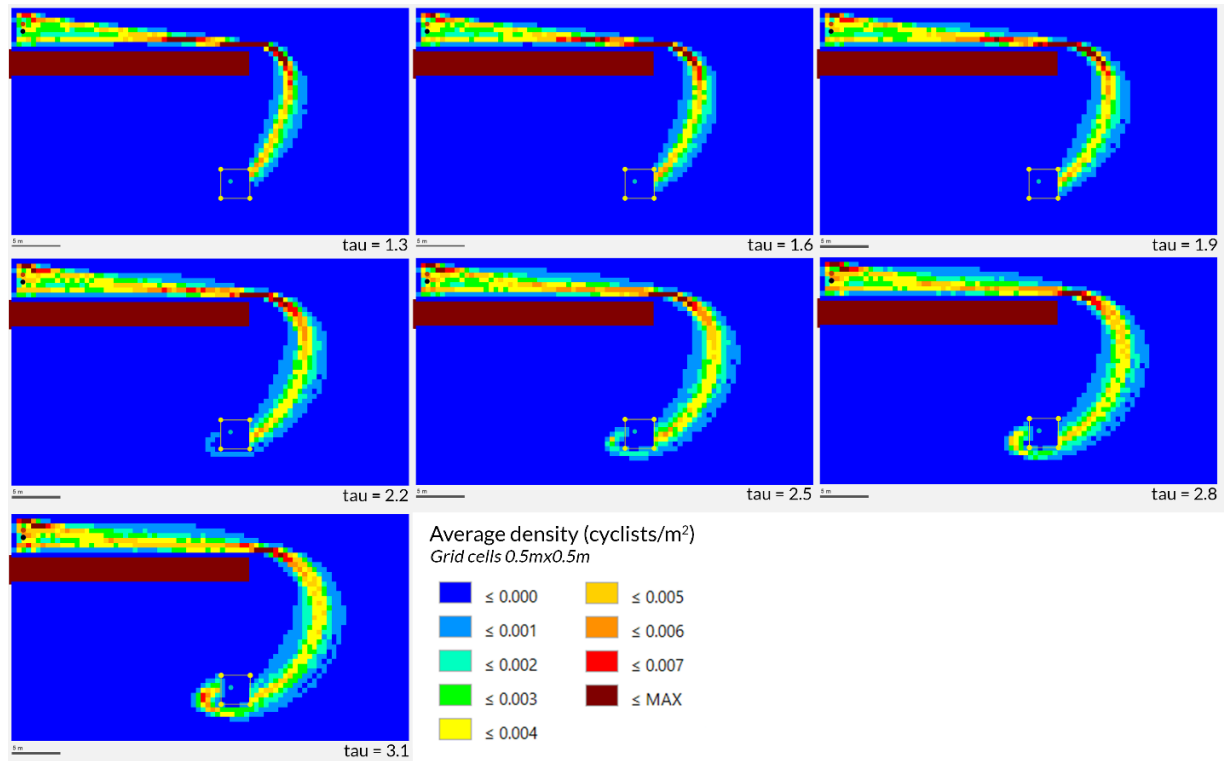


**Figure 3.14:** Turning trajectory for different values of  $\tau$

Various other researchers aimed to calibrate the relaxation time for cyclists in a SFM. A research by Liang et al. (2012) used a relaxation time of 1.22 s. Huang et al. (2017) suggest 1.61 s is the right value, Dias et al. (2018) found this value to be 1.67 s. Based on the two simulation tests and relaxation times found by other researchers, 1.3 seconds is found to be the most suitable value for the relaxation time. This results in a high maximum acceleration of 3.6 m/s<sup>2</sup> at the second meter, but other acceleration values remain below 2 m/s<sup>2</sup>. This  $\tau$  value ensures cyclists can adapt their direction and speed within sufficient time. Otherwise irrational behavior is observed near edges of the infrastructure and other road users.

### 3.3. Calibration of behavioral models

In the lane-based model, following behavior is largely regulated with the Wiedemann 99 car following model. For the lane-based model, more extensive built-in calibration efforts for cyclists are available. For most parameters, either the default parameter values for the cycle-track behavior type or the values calibrated by COWI (2013) are used. Other research on headway or lateral distance distributions of cyclists is rare (Yuan et al., 2019) and the combination of both calibration efforts (PTV Group, 2020; COWI, 2013) offers sufficient accuracy for this research project.

The SFM will be used to model cyclists' behavior in spaces with a two-dimensional character. The parameters calibrated for pedestrian behavior have to be adjusted to reflect cyclists' behavior. This is challenging since most of the parameters cannot be measured directly and often a single parameter has an impact on many aspects of behavior (Kretz et al., 2018).

#### 3.3.1. Lane-based behavioral model

The main model component to represent vehicle movement in Vissim is the psycho-physical perception model originally developed by Wiedemann (1974). The model uses four different vehicle states to determine acceleration and deceleration behavior. The states are classified as: free driving, approaching, following and braking. In each stage, the acceleration/deceleration is described as a result of driver and vehicle characteristics, current speed, speed difference and distance to the preceding vehicle (PTV Group, 2020). Driving behavior types can be created based on the infrastructure type. Driving behavior type has many different attributes and parameters, which can vary for each vehicle class. The attributes and parameters of driving behavior in Vissim are divided in different parameter sets.

In the *Following* parameter set, the minimum and maximum *Look ahead distance* and *Look back distance* can be quantified, which are important to determine the extent of vehicle interaction. Also the *Number of interaction objects* and *Number of interaction vehicles* parameters can limit the number of objects or vehicles the driver is aware of and will interact with. Especially in situations with a cycling lane or shared road, this number should be higher than the default of 2 in order for drivers to interact with all surrounding objects. Therefore this parameter is increased to 10. In addition, the *Standstill distance for static obstacles* can be set (PTV Group, 2020).

The longitudinal behavior is primarily calculated with car following models. The car following model parameter set has three options (PTV Group, 2020):

- *No interaction*  
Here drivers do not recognize any other vehicles. This can be useful for the simulation of pedestrians in lanes.
- *Wiedemann 74 (W74) model*  
In the W74 model, the desired safety distance increases with the square root of the speed.
- *Wiedemann 99 (W99) model.*  
The desired safety distance increases linearly with the speed in the W99. This makes the W99 model more suitable for freeway traffic.

A major difference between the two car following models is that the W99 model has much more editable parameters than the W74 model in Vissim (PTV Group, 2020). The parameter overview for both of these models is visible in table 3.2 and table 3.3.

**Table 3.2:** Overview of Wiedemann 74 model parameters in Vissim (PTV Group, 2020)

Name	Function	Default value
<b>Average standstill distance (AX)</b>	Average distance between two vehicles (rear to front), has a standard deviation of 0.3 m. Desired distance is calculated as: $d = AX + BX$ .	2.0 m
<b>Additive part of safety distance (<math>BX_{add}</math>)</b>	BX is calculated as: $BX = (BX_{add} + BX_{mult} * z) * \sqrt{v}$ . Where z is a range from 0 to 1 normally distributed around 0.5 with a standard deviation of 0.15. And v is vehicle speed in m/s.	2.0 m
<b>Multiplicative part of safety distance (<math>BX_{mult}</math>)</b>	Used to calculate BX, where a greater value of $BX_{mult}$ yields a higher distribution of safety distance.	3.0 m

In the W74 model, the thresholds from the original model (also see figure 2.3 and table 2.2) are directly quantified. In the W99 model, the first seven of the ten parameters (CC0-CC6) are used to determine the thresholds established in the original model. The AX threshold is defined by parameter CC0 in equation [3.1], with the addition of the vehicle length of the lead vehicle:

$$AX = L + CC0 \quad [3.1]$$

The time distribution of the speed dependent part of the desired safety distance CC1, is used together with AX to determine BX in equation [3.2]:

$$BX = AX + CC1 * v \quad [3.2]$$

Where  $v$  is the speed of the following vehicle if lower than the leading vehicle, otherwise  $v$  is equal to the lead vehicle's speed with some random errors. These errors are calculated by multiplying the speed difference by a random number between -0.5 and 0.5 (Aghabayk et al., 2013). The perception threshold SDX is calculated by equation [3.3]:

$$SDX = BX + CC2 \quad [3.3]$$

Where CC2 represents the longitudinal oscillation. The perceptual threshold for deceleration is calculated by equation [3.4]. Where CC3 defines the threshold for entering following (in seconds) and CC4 the negative speed difference between both vehicles:

$$SDV = -\frac{\Delta x - SDX}{CC3} - CC4 \quad [3.4]$$

In equation [3.4], the space headway between the two vehicles (from front to front) is represented by  $\Delta x$ . Equation [3.5] and [3.6] calculate the thresholds for deceleration and acceleration:

$$CLDV = \frac{CC6}{17000} * (\Delta x - L)^2 - CC4 \quad [3.5]$$

$$OPDV = \frac{CC6}{17000} * (\Delta x - L)^2 - \delta CC5 \quad [3.6]$$

Where CC4 and CC5 are the negative and positive speed difference between the vehicles and CC6 regulates the influence of distance on speed oscillation. Larger values lead to greater speed oscillation for larger distances. Dummy variable  $\delta$  is equal to 1 when the following vehicle speed is greater than CC5, otherwise it is set to 0 (Aghabayk et al., 2013; PTV Group, 2020).

**Table 3.3:** Overview of W99 model parameters in Vissim (PTV Group, 2020; COWI, 2013)

Name	Function	Default value (cycle-track)	Used value (COWI, 2013)
<b>Standstill distance (CC0)</b>	Desired standstill distance between two vehicles (front to rear).	0.50 m	0.20 m
<b>Following distance (CC1)</b>	The speed dependent part of desired safety distance. This parameter can also be set as a normal or empirical time distribution.	0.5 s	0.5 s
<b>Longitudinal oscillation (CC2)</b>	Is restricting the distance difference the driver allows before intentionally moving closer to the leading vehicle. the additional safety distance ranges between 0 and CC2.	0.00 m	2.00 m
<b>Perception threshold for following (CC3)</b>	Defines the beginning of the deceleration process, at this stage the driver recognizes a preceding slower vehicle.	-8.00 s	-20.00
<b>Negative speed difference (CC4)</b>	Negative speed difference during the following process, low values result in a more sensitive reaction of the following driver.	-0.35 m/s	-0.25 m/s
<b>Positive speed difference (CC5)</b>	Positive speed difference during the following process, corresponds to the negative value of CC4.	0.35 m/s	0.25 m/s
<b>Influence of distance on speed oscillation (CC6)</b>	Distance dependency of speed oscillation, for a value of 0, the distance has no influence on speed oscillation.	11.44 1/(m*s)	1.00 1/(m*s)
<b>Oscillation acceleration (CC7)</b>	The minimum value of acceleration or deceleration when following.	0.25 m/s <sup>2</sup>	0.25 m/s <sup>2</sup>
<b>Acceleration form standstill (CC8)</b>	Desired acceleration when starting from stationary position (limited by acceleration function).	3.50 m/s <sup>2</sup>	1.80 m/s <sup>2</sup>
<b>Acceleration at 80 km/h (CC9)</b>	Desired acceleration at a speed of 80 km/h (limited by acceleration function).	1.50 m/s <sup>2</sup>	0.01 m/s <sup>2</sup>

Parameter CC7, the oscillation acceleration is the minimum value for absolute acceleration or deceleration when following. The parameters CC8 and CC9 determine the desired acceleration from standstill or at 80 km/h respectively. These values are limited by the vehicle acceleration functions defined for each vehicle type. Many of these parameter values are similar for all driving behavior types the default settings of Vissim. Parameter CC1, the gap time distribution, has the highest impact on the capacity (COWI, 2013).

Both W74 and W99 can be used to simulate cyclists' behavior. Since the W99 offers more flexibility in changing parameters and COWI (2013) did an extensive calibration process for the W99 model to simulate cyclists' behavior, this version is preferred. The results of this research provide suitable calibrated values for the Wiedemann 99 model.

For the changing of lanes, Vissim distinguishes between necessary lanes changes to follow the right route and free lane changes to have more space to drive at the desired speed. Safety distances are considered when deciding to perform a lane change. At cycling paths, these lane changing parameters are less important than at highways or motorized streets. However, in two-directional cycling paths, cyclists may be able to overtake using the opposite lane. This can be modeled in Vissim by adding an additional lane to one direction, marked as *Overtaking lane* overlaying the opposing lane.

Overtaking of cyclists mostly happens on the same lane, this is modeled at the lateral behavior parameter set. The parameter explanation and values of this parameter set are presented in table 3.4. Again the values of COWI (2013) are used, with the exception of *Observe Adjacent Lane*, which is activated since these lanes have to be considered when using overtaking lanes.

Another driving parameter set is signal control, which specifies how vehicles respond to red, amber and green signals. Here also a reduced safety distance can be set. Additionally, driving behavior parameter sets are available for autonomous driving, mesoscopic simulation and driver errors. Of which the latter can take into account temporary loss of attention or distraction of the driver. These three parameter sets are inactive by default.

**Table 3.4:** Overview of lateral driving behavior parameters in Vissim (PTV Group, 2020)

Name	Function	Default value (cycle-track)	Used value (COWI, 2013)
<b><i>Desired position at free flow</i></b>	Here the <i>Desired position at free flow</i> can be set, where vehicles can prefer the right or left side, the middle of the lane or have no preference.	Right	Right
<b><i>Observe adjacent lane(s)</i></b>	When using the option <i>Observe adjacent lanes</i> , vehicles also consider other lanes to adjust their lateral orientation to comply to the <i>Minimum lateral distance</i> .	Not activated	Activated (not COWI value)
<b><i>Diamond queuing</i></b>	The option <i>Diamond Queuing</i> results in more realistic queues for vehicles like bicycles, since they are not represented as a rectangle but as a diamond.	Activated	Activated

<b>Consider next turn</b>	To consider the lateral position for upcoming turns, the option <i>Consider next turn</i> can be activated. In addition to vehicles moving to the preferred side of the road for their next turning direction, approaching vehicles also do not try to overtake vehicles that, for example, already move to the left for their next turn. This option overwrites the desired lateral position.	Not activated	Activated
<b>Collision time gain</b>	The minimum value of collision time gain so that a change of lateral position on the lane is worthwhile and will be performed. More lateral movement is observed for lower values of this parameter.	2.00 s	2.00 s
<b>Minimum longitudinal speed</b>	The minimum speed which allows for lateral movements.	3.60 km/h	3.60 km/h
<b>Time between direction changes</b>	Minimum time that must pass between the start of a lateral movement in one direction and the start of a lateral movement in the reverse direction.	0 s	5.00 s
<b>Overtake on the same lane</b>	Allows vehicle classes to overtake within a lane to the right, left or both.	Left and right	Left and right
<b>Minimum lateral distance</b>	Minimum lateral distance between vehicles at standstill (0 km/h) and driving (50 km/h).	0.10 m at 0 km/h 0.30 m at 50 km/h	0.20 m at 0 km/h 0.75 m at 50 km/h

### 3.3.2. Area-based behavioral model

The SFM used to model pedestrian behavior in Viswalk works similar to the model first presented by Helbing & Molnár (1995) (see 2.3.4 Social force models). The main acceleration force towards the goal is described identical to the original model in Viswalk:

$$\vec{F}_\alpha^0(\vec{v}_\alpha, v_\alpha^0 \vec{e}_\alpha) := \frac{v_\alpha^0 \vec{e}_\alpha - \vec{v}_\alpha}{\tau_\alpha} \quad [3.7]$$

The desired direction  $\vec{e}_\alpha$  is determined by equation [2.2] and depends on the set goal area, the desired speed  $v_\alpha^0$  can be set according to the desired speed distribution. The speed distribution can be set to either a pedestrian composition or area behavior type. Combined the desired direction and desired speed form the desired velocity  $v_\alpha^0 \vec{e}_\alpha$ . The value of the relaxation time  $\tau_\alpha$  can be easily changed as a parameter of the walking behavior in Viswalk. Equation [3.7] explains that a low relaxation time implies high acceleration towards the desired velocity.



The repulsive effects are represented in Viswalk as a summation of two equations that form the repulsive forces between two pedestrians (Lagervall & Samuelsson, 2014; PTV Group, 2020). These are equations [3.8] and [3.10]. Equation [3.8] is more focused on the territorial sphere of a pedestrian and is also active while stationary and equation [3.10] deals with the forces in movement. The sum of these equations determines the total force between two pedestrians:

$$\vec{F}_1 = A_i w(\lambda_m) \exp^{-d/B_i} n \quad [3.8]$$

Where  $d$  represents the distance between the two pedestrians and  $n$  is the unit vector pointing from one pedestrian to the other. The other terms  $A_i$ ,  $B_i$  and  $\lambda_m$  are parameters that can be modified in the walking behaviors. Where  $A$  Social Isotropic  $A_i$  determines the interaction strength,  $B$  Social Isotropic  $B_i$  determines the interaction range (Lopez, 2019; PTV Group, 2020).

The parameter  $\lambda_m$  is used to adjust the amount of anisotropy of forces. Pedestrians are influenced more by pedestrians and objects in their field of view than pedestrians and objects behind them. This anisotropy is represented by the weight  $w(\lambda_m)$  in equation [3.8]. The modifiable parameter *Lambda Mean* can have a value between 0 and 1 and is part of equation [3.9]:

$$w(\lambda) = \lambda + (1 - \lambda) \frac{1 + \cos \varphi_{\alpha\beta}}{2} \quad [3.9]$$

Where  $\varphi_{\alpha\beta}$  is the angle (in degrees) between current desired direction of pedestrian  $\alpha$  (the field of vision) and the direction of pedestrian  $\beta$ . If pedestrian  $\beta$  is right in front of pedestrian  $\alpha$ , the angle  $\varphi_{\alpha\beta}$  is  $0^\circ$ , always yielding a  $w(\lambda)$  of 1. With a  $\lambda$  of 1, forces from pedestrians in all directions have equal weight and the  $w(\lambda)$  will always yield 1.

The other repulsive force is calculated if the influencing pedestrian is in front of the pedestrian being influenced and thus angle between the two  $\varphi$  is between  $90^\circ$  and  $-90^\circ$ , otherwise it is zero (PTV Group, 2020). Equation [3.10] for this second repulsive force is defined as:

$$\vec{F}_2 = A_m w(\lambda_m) \exp^{-d_m/B_m} n \quad [3.10]$$

This force can be modified by changing parameters *A Social Mean*  $A_m$ , *B Social Mean*  $B_m$  and *VD* (part of equation [3.11]), where  $A_m$  decides the strength and  $B_m$  decides the range of the social forces.  $n$  again is the unit vector pointing from one pedestrian to the other, and  $d_m$  is calculated (Lagervall & Samuelsson, 2014) according to:

$$d_m = \frac{1}{2} \sqrt{((d + |d - (v_1 - v_0)VD|)^2 - |(v_1 - v_0)VD|^2)} \quad [3.11]$$

In equation [3.11],  $v_0$  is the velocity of the influenced pedestrian and  $v_1$  the velocity of the influencing pedestrian. The relative velocities of the pedestrians are considered if  $VD > 0$ , a higher  $VD$  makes pedestrians evade each other more (PTV Group, 2020). This also implies that in a cycling path, cyclists will overtake more with a higher value of this parameter.

The parameter *Noise* in Viswalk can also be modified in the walking behavior section. This parameter is described as fluctuations in the original SFM (Helbing & Molnár, 1995) and adds a random component to the calculated forces. *Noise* makes pedestrians move more randomly, which can be useful to prevent stable deadlock situations (PTV Group, 2020).

The parameter *React to N*, regulates the number of closest pedestrians that are taken into account for calculation. The preference of using the left or right side to pass opposing pedestrians can be set with parameter *Side Preference* (PTV Group, 2020). An overview of all calibrated parameters for walking behavior types is visible in table 3.8.

As stated in section 3.1.2, areas can have attributes with parameters as well. Table 3.5 shows the parameters that can be specified for areas. The desired speed factor applies to all pedestrian types. The *Queue straightness* and *Queue order* are only available for modeling queue behavior with a delay time, meant to model counters or cash desks for pedestrians. Not queues that form when waiting for a traffic light or priority road.

**Table 3.5:** Overview of area parameters in Viswalk (PTV Group, 2020)

Name	Function	Default value
<b>Area behavior type</b>	Not a parameter, area behavior types consist of: - Desired speed distribution - Walking behavior (see table 3.8)	-
<b>Desired speed factor</b>	Factor to change desired speed of all pedestrians in the area (range from 10% to 300%).	100%
<b>Queue straightness*</b>	Degree of straightness of a queue.	0.60
<b>Queue order*</b>	Degree of orderliness of a queue.	0.70

\* Also available as global parameter

Parameters of a route can be set in the route location network object (table 3.6). For example the cell size for a route can be set, which defines the distance between data points when calculating the route towards the goal area. The *Obstacle distance* is the distance up to which edges and obstacles have an impact on the distance potential.

Dynamic potential is a method where pedestrians do not consider choosing the shortest path but the fastest path. They will avoid crowded places and search for a quicker path towards their goal. When using dynamic potential the computation time will be much higher since many other pedestrians influence each other. The dynamic potential parameters of route location are the g-value and h-value, which impact the strength and direction of the dynamic potential respectively.

**Table 3.6:** Overview of route location parameters in Viswalk (PTV Group, 2020)

Name	Function	Default value
<b>Cell size*</b>	Defines the distances between fixed data points used for calculation of path to destination.	0.15 m
<b>Obstacle distance*</b>	The general distance pedestrians keep from obstacles (not considered in the dynamic potential).	0.50 m
<b>Use dynamic potential</b>	Whether dynamic potential is considered or not.	Not activated
<b>Dynamic potential g</b>	General strength, how the delay of an occupied grid cell is estimated in relation to an unoccupied one.	1.500
<b>Dynamic potential h</b>	Direction impact, influence of speed on the estimated travel time of a cell.	0.700

\* Also available as global parameter

Besides the parameters that can be set specifically, Viswalk also considers some global parameters that apply to all pedestrians in all areas of the simulated environment. These parameters are included in the global parameter overview in [table 3.7](#). The *Grid size* is setting the maximum distance pedestrians can have affect each other. The grid is measured as a square where the pedestrian is located in the center, the parameter specifies the length of an edge of this square. This parameter is mainly useful to shorten calculation times, since no pedestrians outside this square have to be considered.

**Table 3.7:** Overview of global parameters in Viswalk (PTV Group, 2020)

Name	Function	Default value
<b>Grid size</b>	The length of one size of the grid that determines the maximum distance at which pedestrians have an effect upon each other.	5.00 m
<b>Direction change clipping</b>	Whether the angle between the fastest and shortest route can increase at any speed.	-
<b>Direction change angle</b>	Maximum permitted angle by which the angle between quickest and shortest path can increase.	4.0°

Relaxation time is a separate parameter with observable, unconstrained behavior changes. The other 'walking behavior' parameters (see [table 3.8](#)) are much harder to quantify since these influence the interaction of cyclists and often do not have direct measurable effects (Kretz et al., 2018). To calibrate these parameters in a structured way, first the behavior in queues is observed. This way the effect of the parameters *A social mean* and *B social mean* can be calibrated separately from the others since this force term (equation [3.8]) mostly deals with the territorial sphere around cyclists.

A straight cycling path with a width of 2 m is created in a digital environment, at some point the path is crossing a very busy road with cars where the cyclists constantly have to yield. This causes all cyclists to join the end of the queue (see [figure 3.15](#)). Changes have to be made in comparison to the default settings of walking behavior (with the adjusted relaxation time and speed distribution), the parameters should be calibrated to achieve the following queuing behavior:

- **Distance**  
Cyclists are too close to each other, the 3D models intermingle. Their lateral and longitudinal distance to each other should be reasonable, especially in the queue. Gavrilidou, Daamen et al. (2019) used cells of 2 meter length and 0.7 meter width to fit cyclists in a queue, corresponding to a longitudinal and lateral distance around 0.1 meter. The settings for the lane-based model uses a standstill distance (CC0) of 0.2 m and a lateral distance of 0.2 m at 0 km/h (see [section 3.3.1](#)).
- **Movement**  
In the default settings, cyclists constantly keep moving and pushing others away while in the queue. They should remain stationary when in the queue.
- **Queueing**  
Cyclists approaching the queue are going too fast and crash into queue. After the crash (being too close to the cyclist in front) the approaching cyclist is pushed backwards by the

social force. Sometimes a rapidly approaching cyclist even 'overtakes' cyclists already in the queue, who are then pushed backwards by the approaching cyclist. This should not occur because cyclists should not be able to overtake cyclists already in the queue.

It is challenging to find out how modifying different parameter values can lead to this desired behavior. Many simulations are run with different combinations of parameter values to test which configuration matches the behavioral goals best. The assumption is made that parameter *React to N* can remain the same. and the parameter *Side Preference* is set to 'right', meaning cyclists prefer keeping right when opposing another road user. The parameter *Noise* is assumed to be 0. The parameter  $\lambda_m$  describes that cyclists are not influenced by cyclists directly behind them. By setting this parameter to 0, a weighing factor of 0.5 is given to forces from cyclists at exactly 90 degrees in their field of vision (see equation [3.9]). In a queue, the parameter *VD* is also set to 0, since this causes cyclists to crash into the queue and overtake cyclists already in the queue. Consequently, the overtaken cyclists are pushed backwards. This behavior is not observed with a *VD* of 0.

The distance cyclists keep from each other while in the queue is mostly determined by  $A_i$  and  $B_i$ . Parameter values of respectively 5.0 and 0.4 make the cyclists keep a reasonable distance to each other in the queue. When increasing the  $B_i$ , cyclists keep more distance from each other and when increasing the  $A_i$  parameter, approaching cyclists drive into the territorial sphere before being forced backwards.

High values of  $A_m$  and  $B_m$  cause cyclists to adapt their speed more in advance and not crash into the queue with a high speed. However, especially a large  $B_m$  also makes cyclists behave move nervously and keep moving while in the queue. To find a balance between these two behaviors, the more favorable setting is where the cyclists in the queue are static. The best value for  $A_m$  is found to be 3.0 and for  $B_m$  the value is set at 1.1. How the cyclists form the queue is visualized in figure 3.15, an overview of the parameter values is presented in table 3.8.

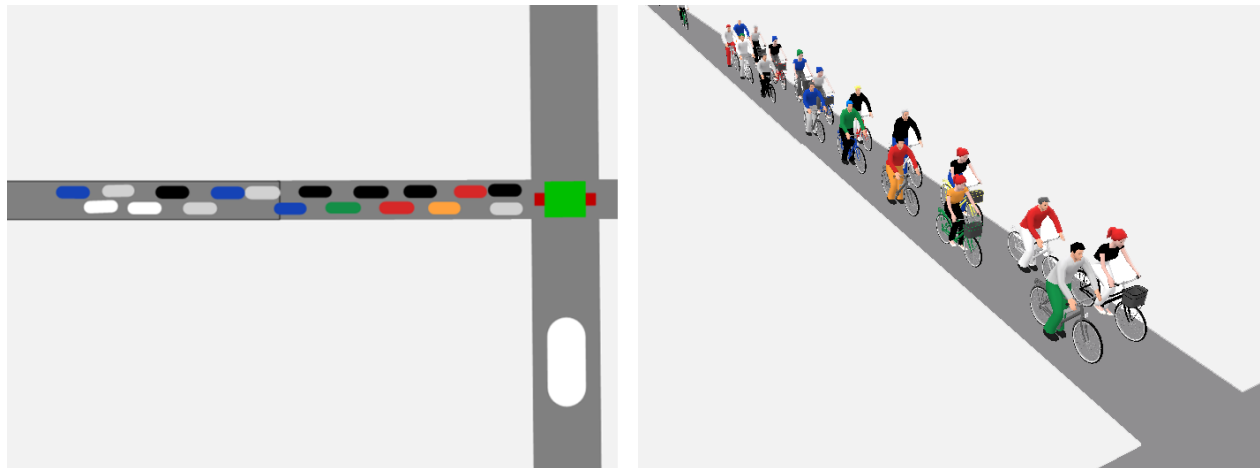


**Figure 3.15:** Queue formation in 2D and 3D view

The results are similar for a cycling paths of different widths. When lowering the desired speed factor at the area behavior type, cyclists drive slower when approaching the queue. A linear relationship exists between the surface area and number of cyclists in the queue, the area a cyclists uses is independent of the length of the queue. Around 0.44 cyclists per square meter can fit into the queue (DTV Consultants, 2016). This empirically found value corresponds to the calibrated model simulation.

To attempt using the SFM for cyclists driving on a cycling path, the parameter values calibrated for the queuing behavior are used as a basis. By visually assessing the behavior of the cyclists in the simulation, the parameters are calibrated to match behavior on cycling paths. Similar to the calibration of the queuing behavior, many simulations are run with different combinations of parameter values to assess the most suitable values. The cyclists' behavior should match a couple of goals:

- **Overtaking**  
Cyclists with a high desired speed should be able to overtake slower cyclists at cycling path widths over 2.5 m. Preferably on the left side of the path.
- **Following**  
When cyclists decide not to overtake, their following behavior should be calm and without too much lateral movement. The following distance should not be too small, sufficient longitudinal distance should remain between the cyclists.
- **Positioning and evasion**  
In two directional paths, cyclists should mostly keep to the right side of the path. To prevent collisions with the opposing traffic.

A test environment with multiple areas is set up with dimensions and traffic volumes based on cycling paths around the case study area in Utrecht (NDC, 2018). As a reference, the cycling paths at *Vleutenseweg* and *Leidseweg* are used. At *Leidseweg* a one-way cycling path of 2.5 m in width is located, where cyclists should be able to overtake each other when having a large difference in desired speed. Secondly, a little more spacious, 3 m wide cycling path is modeled. In which cyclists should be able to overtake more easily. Thirdly, based on the cycling path at *Leidseweg*, a two-directional cycling path without segregation is modeled. Here cyclists should be able to use the opposing lane to overtake without causing irregular behavior or gridlocks. The cycling traffic volume of these paths is based on average bicycle traffic counts at the most busy hour of the day (08:00 – 09:00) counted for a period of two weeks. For the *Leidseweg* cycling path, this can be up to 1252 cyclist/hour in one direction (NDC, 2018). The setup of this test is shown in figure 3.16.

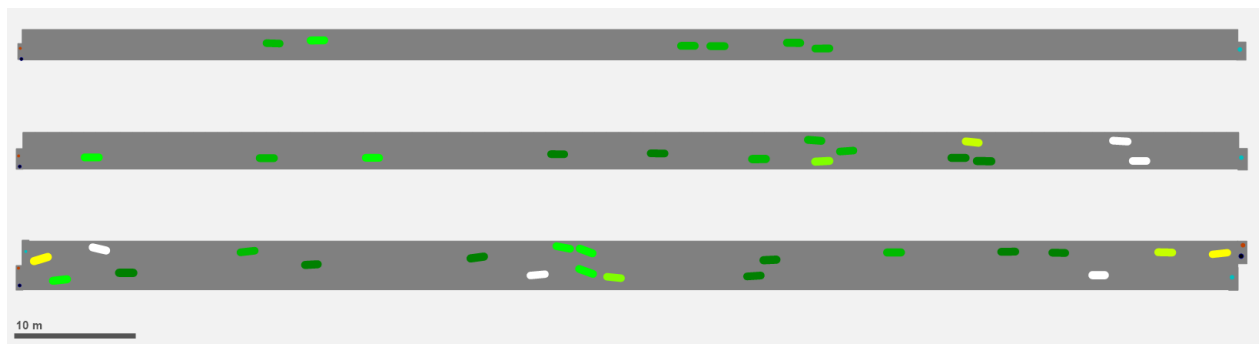


**Figure 3.16:** Cycling path behavior test setup

The values of parameters  $A_i$  and  $B_i$  remain the same as in the queuing situation, since the territorial sphere should be similar. The parameters  $\lambda_m$ , *Noise* and *Side preference* also have the same value as in the queue behavior settings. A high value of parameter  $A_m$  makes cyclists aggressively steer from left to right when following behind a slower cyclist. When lowering this value cyclists behave more calmly. To make cyclists keep more distance from each other, the parameter  $B_m$  should increase.

However, when this value becomes too large, it is impossible to overtake. This is one of the main issues with the SFM in Viswalk, there is limited distinction between longitudinal and lateral distance. Therefore, a balance has to be found between the following distance and possibility to overtake. When desired speeds of two cyclists are further apart, the possibility of overtaking becomes larger. Another way to increase overtaking is with a large value of  $VD$ . However, this also makes cyclists ride more aggressive and therefore should not be too large. In the case of small flow volumes on the two-way cycling path, collisions with the other side are limited. But with a large traffic flow from both sides, many collisions are observed. Collisions can only be avoided by modeling a separation of lanes in the middle, which completely limits cyclists to cross to the other side. Taking all these aspects into account the best configuration seems to have a low value of  $A_m$ , namely 0.8. A relatively high value of 5.0 for  $B_m$  and a value of 15 for parameter  $VD$ .

With this configuration of parameter values (also see [table 3.8](#)), cyclists are still able to overtake, keep some distance and behave relatively calm when following the cyclist in front. When following, the longitudinal distance between cyclists is much smaller than in reality, but being able to overtake is considered to be more important. Busier two-directional cycling paths (>500 cyclists/hour per direction) should be modeled as two separate one-way paths, since otherwise too much collisions take place when cyclists try to overtake by using the opposing lane. This can be justified since in reality cyclists also cannot use the opposing lane in situations with a high traffic flow.

Considering all resulting behavior, the conclusion can be drawn that not enough distinction can be made between longitudinal and lateral distance, therefore unrealistic behavior is observed especially in cycling paths. Based on this calibration process, it was decided to use the SFM only for shared space areas with pedestrians and the lane-based model for cycling paths. To make the parameter values more suitable for shared space areas instead of cycling paths, the value of  $A_m$  is doubled to 1.6, to better avoid pedestrians. Also the right side preference is removed to make better use of the two-dimensional space and not always evade pedestrians to the right side. Table 3.8 shows an overview of the parameter values for the different types of cyclists' behaviors.

**Table 3.8:** Overview of calibrated walking/cycling behavior parameters (PTV Group, 2020)

Name	Function	Default value	Queue area	Shared space
<b>Relaxation time (<math>\tau</math>)</b>	Tau represents the relaxation/response time needed to accelerate to the desired velocity.	0.4 s	1.3 s	1.3 s
<b>React to N</b>	Number of closest pedestrians that are taken into account for calculation	8	8	8
<b>A social isotropic (<math>A_i</math>)</b>	A social (isotropic) governs the amplitude of private sphere force between pedestrians.	2.720	5.0	5.0
<b>B social isotropic (<math>B_i</math>)</b>	B social (isotropic) governs the range of private sphere force between pedestrians.	0.200	0.4	0.4
<b>Lambda mean (<math>\lambda_m</math>)</b>	This parameter sets the degree of anisotropy of the forces.	0.176	0.0	0.0



<b><i>A social mean</i></b> <b><i>(<math>A_m</math>)</i></b>	Represents the strength of the social force between two pedestrians required in movement.	0.400	3.0	1.6
<b><i>B social mean</i></b> <b><i>(<math>B_m</math>)</i></b>	Represents the range of the social force between two pedestrians required in movement.	2.800	1.1	5.0
<b><i>VD</i></b>	The parameter determining degree of evasion, used to calculate $d_m$ .	3.000	0.0	15
<b><i>Noise</i></b>	Noise adds a random force to the total calculated forces.	1.200	0.0	0.0
<b><i>Side preference</i></b>	Opposing pedestrians prefer the left or right side when passing each other.	None	Right	None

## 3.4. Data collection and validation

To examine if the estimated parameters and values correspond to reality, the behavioral model should be validated. Collecting trajectory data is cumbersome since robust, accurate and comprehensive trajectories from various traffic situations are needed, thus typically video footage with automatic annotation is recorded (Seer et al., 2014). Crowdsourced GPS data can be used to visualize traffic flows, traffic volume, speed on links, waiting times at intersections and O-D locations. However, limitations exist in the representativeness of this data, the routes and speed of fitness app users might be different from the total population (Huber et al., 2019; McArthur & Hong, 2019). Roy et al. (2019) also acknowledged this issue and developed a generalized method to correct the bias in crowdsourced cycling data. When handled well, currently available methods for the collection of higher quality data can improve calibration of model parameters (Ma & Luo, 2016; Paulsen et al., 2019; Lee & Sener, 2020). These techniques are not available and fall outside of the scope of this research. Furthermore, travel restrictions due to the COVID-19 pandemic lead to unrepresentative traffic situations. In this research, individual naturalistic cycling data from an uncontrolled data collection experiment is used for validation of the previously estimated distributions and functions. This section presents the setup of the data collection experiment as well as various validation tests using this cycling data.

### 3.4.1. GPS receivers

The device used to collect data from the validation experiments is the GL-770 from Transystem (figure 3.17). It has a GNSS (Global Navigation Satellite System) receiver, meaning it has worldwide coverage and supports satellite systems such as GPS (USA) and GLONASS (Russia) (Transystem, n.d.). For convenience, this device will henceforth be called a GPS receiver. The output data of the receiver has a maximum frequency of 5 Hz, one data point for every 0.2 seconds. The location points are saved in a latitude and longitude format in decimal degrees, with an accuracy of six decimals. In addition to the time and location, also height, speed, distance travelled and heading (orientation in degrees, clockwise from north) are saved for each data point.



**Figure 3.17:** Transystem's GL-770 GPS receiver

To test the accuracy of the GPS receivers, some preparation experiments are conducted. First, the consistency for a single GPS receiver is measured by calculating the speed using three different data outputs:

- *Direct speed*

The speed average speed (in km/h) for the last time interval is measured and outputted directly by the GPS receiver for each 0.2 seconds.

- *Calculated by distance*

The distance traveled in one interval is outputted for each data point. By dividing this distance with 0.2 s (the time interval) and multiply by 3.6 (to convert m/s to km/h), the speed is calculated (equation [3.12]):

$$v = \frac{d}{0.2} * 3.6 \quad [3.12]$$

- *Calculated by coordinates*

Since the coordinates are given in degrees, the spherical distance between the points can be calculated with the haversine formula (Basyir et al., 2017). This formula uses the radius of the earth in combination with the central angle to calculate the distance ( $d$ ) between two coordinate points:

$$d = r_e * 2 \arcsin \sqrt{\sin^2 \left( \frac{\phi_2 - \phi_1}{2} \right) + \cos(\phi_1) \cos(\phi_2) \sin^2 \left( \frac{\psi_2 - \psi_1}{2} \right)} \quad [3.13]$$

Where  $r_e$  is the radius of the earth, which in WGS 84 is set to 6378137.298 m (Maptiler, n.d.).  $\phi$  is the latitude coordinate and  $\psi$  is the longitude coordinate, the degrees must be converted to radians as well. For small distances, measurement errors or rounding errors can cause bigger fluctuations when using this method. By using equation [3.12] again, the speed can be calculated.

From a test experiment with a regular bicycle, one minute of data is extracted where the cyclist is accelerating from a complete stop at a traffic light. The speed is calculated and graphed for all three methods in figure 3.18. All three methods follow the same trend line, the directly outputted speed however shows less fluctuations in speed. Where the two other methods show much more fluctuations around the directly measured speed. This may be due to the inaccuracy of the GPS receiver itself and rounding errors of the distance calculation. Since the speed calculated with the distance and coordinate points is very much similar, it is likely that the GPS receiver uses a similar equation as [3.13] to determine the distance traveled. Since the direct speed output seems more realistic and gives a more fluent result, this method is preferred to calculate the other variables. Besides the differences, the consistency proves to be sufficient for speed and acceleration measurements.

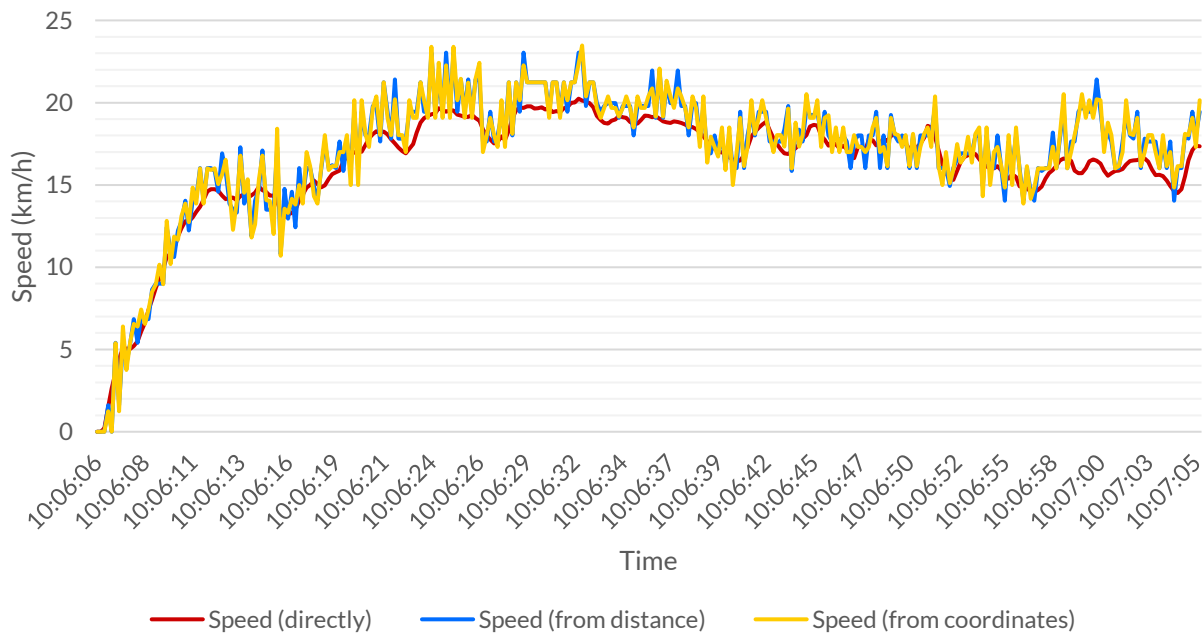


**Figure 3.18:** Data comparison of speed measured and calculated with a single GPS receiver

To evaluate the accuracy of the GPS receivers in another way, also tests are conducted by measuring the same cycling trip with two separate receivers. In total, five identical GPS receivers are available for this project. To distinguish them, they are identified by the last three digits of the serial number (e.g. 330 or 351). The same minute of data displayed in figure 3.18, is also graphed in figure 3.19, but the speed measured with another GPS receiver is also added. When comparing the speed of both receivers, some inconsistencies can be observed, but generally the same speed pattern is observed. Therefore the GPS receivers are considered to have sufficient accuracy to be used for speed and acceleration analysis.

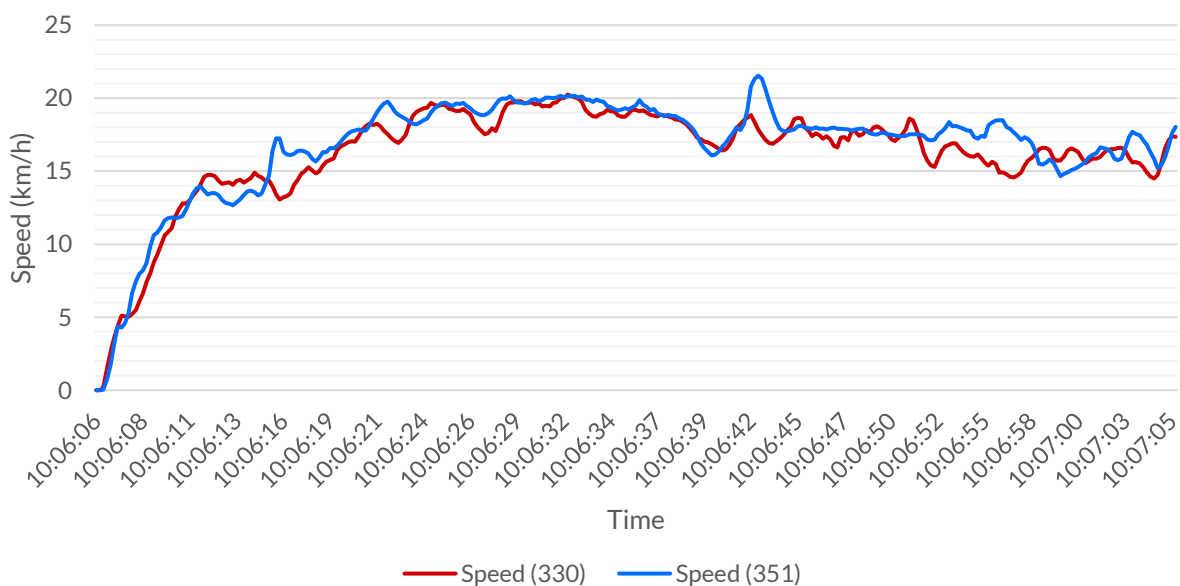


**Figure 3.19:** Data comparison of speed measured with two separate GPS receivers

The accuracy of the location data is also analyzed by measuring the same trip with two GPS receivers. With a Geographic Information System (GIS), the location data can be visualized on a map. For all GIS related activities in this project, the open source software QGIS is used, maintained by the non-profit organization OSGeo ([OSGeo, n.d.](#)). [Figure 3.20](#) shows the data points of an example route measured with two GPS receivers simultaneously, a standard OpenStreetMap (OSM) map is placed in the background ([OpenStreetMap, n.d.](#)). What becomes clear is that the two data sets do not follow the same route and do not follow the exact roads. Inaccuracies in the coordinate values may be caused by bad weather, high buildings, trees or tunnels ([Transystem, n.d.](#)). After multiple tests have been conducted, still many errors like the example visible in [figure 3.20](#) were observed. Because of these geographic inaccuracies, the GPS receivers cannot be used for validation of distance parameters like following headway or lateral distance. However, the location data will be used to evaluate the change in average speed for different types of infrastructure.

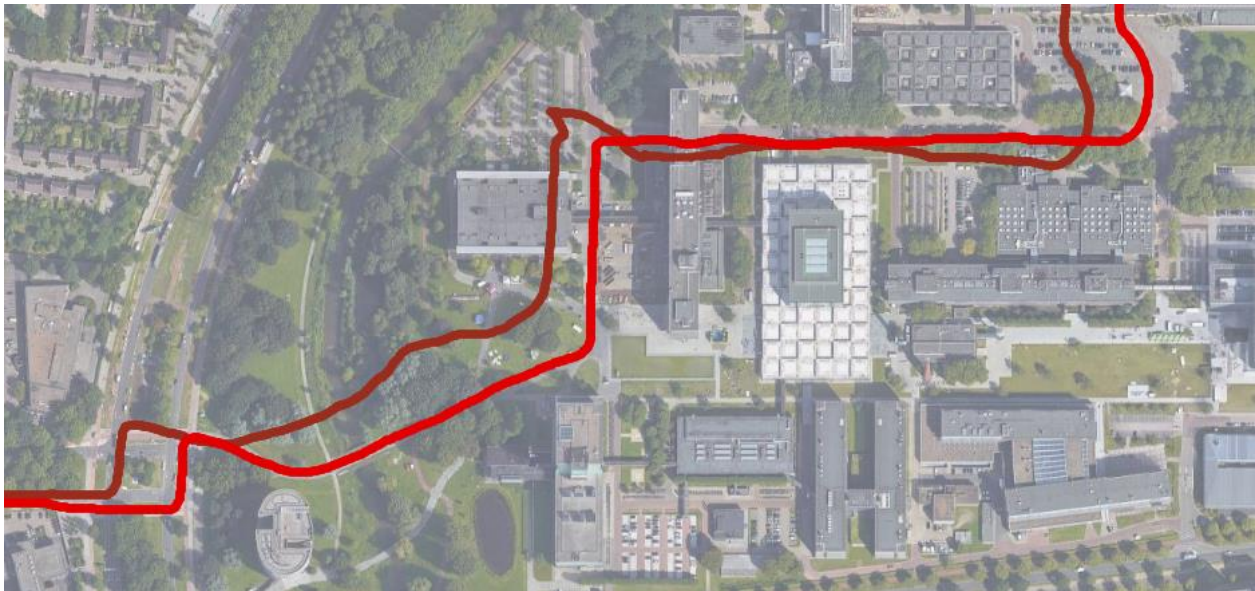


**Figure 3.20:** Example of location data for one trip measured with two GPS receivers

### 3.4.2. Data collection experiment

The GPS receivers discussed in [section 3.4.1](#) are used to collect speed and acceleration data that can be used for the validation of the behavioral model. The participants were asked to carry a GPS receiver while cycling their regular routes for a couple of days. A total of 11 cyclists participated in the experiment of which four participants drove an e-bicycle. The participants are given an anonymous identification to comply with the General Data Protection Regulation (GDPR) ([European Parliament, 2016](#)). The data can no longer be attributed to a specific person and a Data Protection Impact Assessment (DPIA) is not mandatory ([Dutch Data Protection Authority, n.d.; TU/e, 2019](#)). The identification codes of participants that rode an e-bicycle are preceded with an 'E'. An overview of the data collection is shown in [table 3.9](#).

**Table 3.9:** Setup of data collection experiment

	Participant ID	Number of trips	Total distance cycled (km)	(GPS receiver ID)
Bicycle	A	9	23.72	330
	B	11	30.59	355
	C	12	22.14	354
	D	12	28.20	353
	E	12	29.50	351
	F	9	38.32	330
	G	8	29.51	355
E-bicycle	EH	4	58.97	330
	EI	1	6.92	330
	EJ	5	40.02	354
	EK	3	48.13	353
Total		86	356.02	-

Data of 86 trips, covering 356 km was collected with this experiment. Most of the experiment data was collected in and around Eindhoven (Netherlands). Ideally, data from more participants would have been collected to be more representative for the entire population, but unfortunately this was not possible due to the COVID-19 pandemic and limitations on measurement equipment. Still these participants generated a sufficient amount of data to obtain representative results.



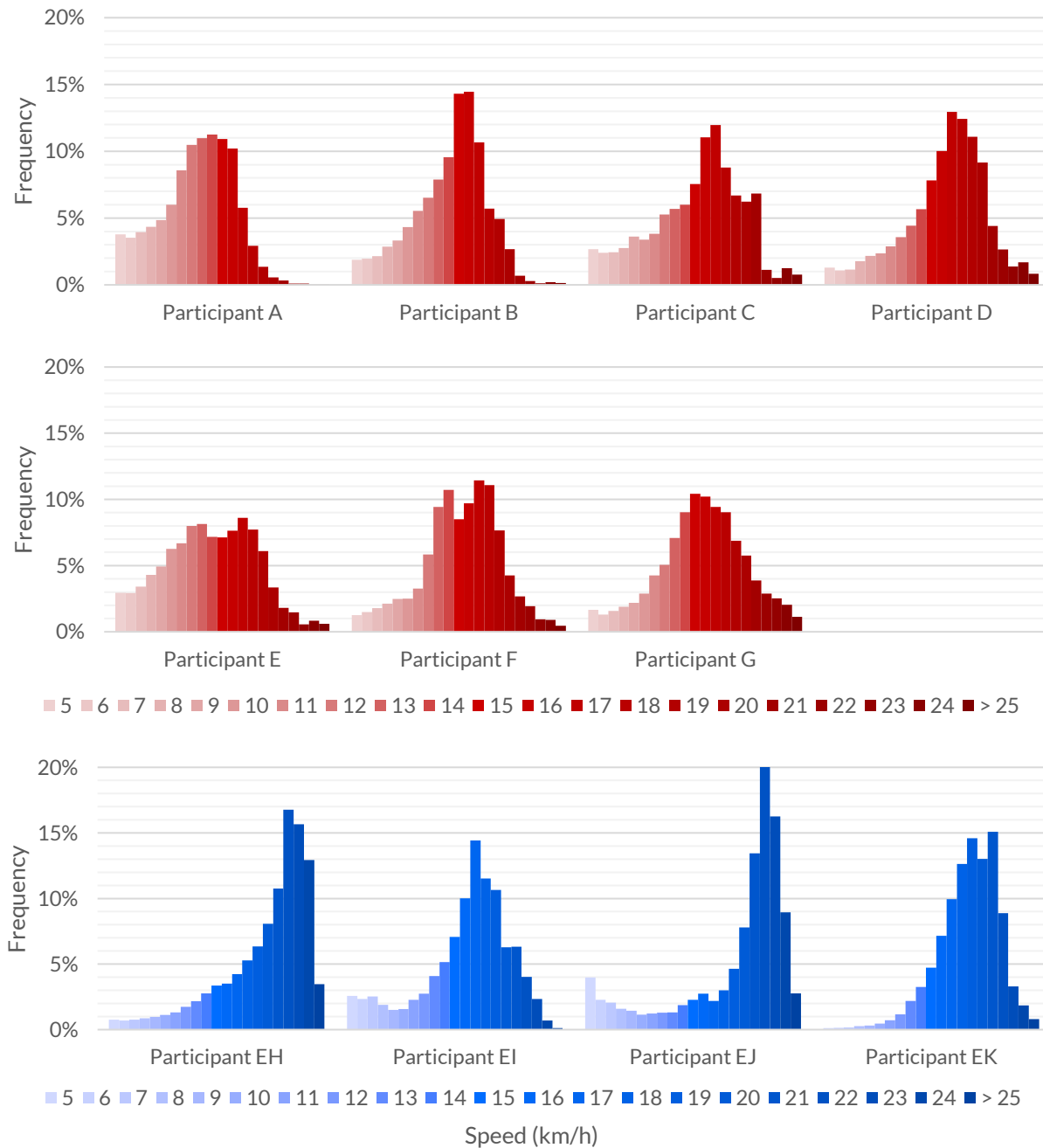


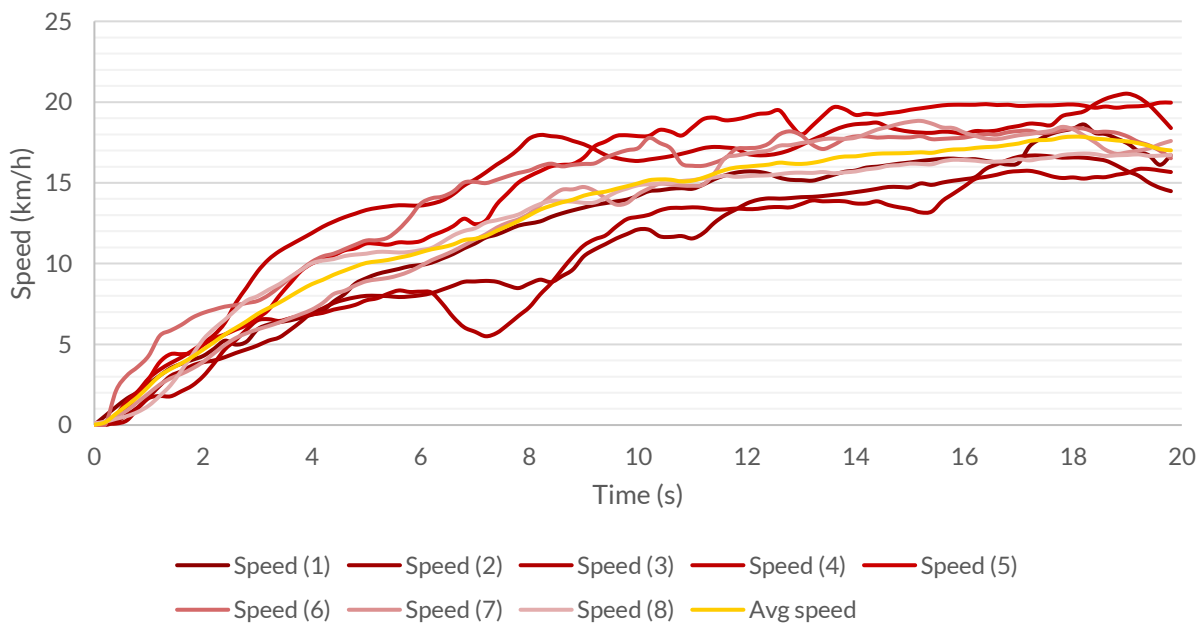
**Figure 3.21:** Histograms of speed frequency for bicycle and e-bicycle participants

The overall frequency of different values of speed gives some insight in the preferred speed of a cyclist. The GPS receivers measured speed every 0.2 s, collecting a total of over 440,000 data points from all 11 participants. Since each participant cycled for a different period of time, with different standstill periods, the absolute frequency of speed cannot be compared between participants. For each participant, figure 3.21 shows histograms for speed frequency in percentage, with bins of 1 km/h. Values above 25 km/h are group together and values below 5 km/h are not included in the calculation of percentage. The shape of each histogram does give some insight in the speed

difference between individuals. Also the difference between bicyclists and e-bicyclists can be observed. These differences are also largely influenced by the environment and the type of trip.

### 3.4.3. Desired speed validation

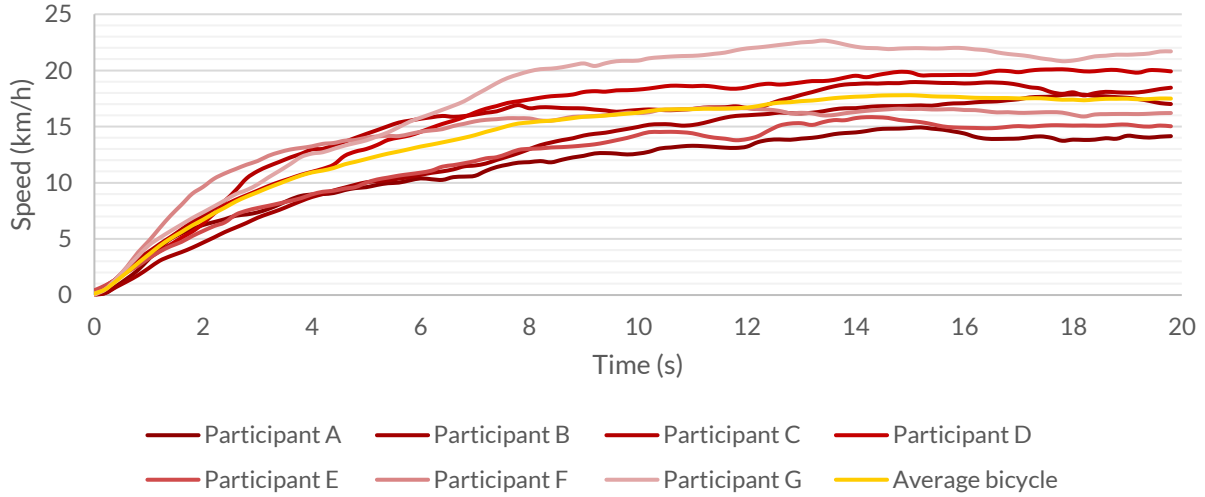
Since the raw collected data contains a lot of noise or measurement errors, calculating the overall average speed of participants is not very insightful. Specific parts of data are extracted and used for desired speed validation analysis. For all participants, eight 20-second segments of representative acceleration from standstill are extracted. The aim is to retrieve unconstrained accelerations in order to obtain a realistic desired speed, so to avoid selecting outlining data points. When using the 0 km/h data point as the start of all segments, the average speed profile can be calculated for each participant.



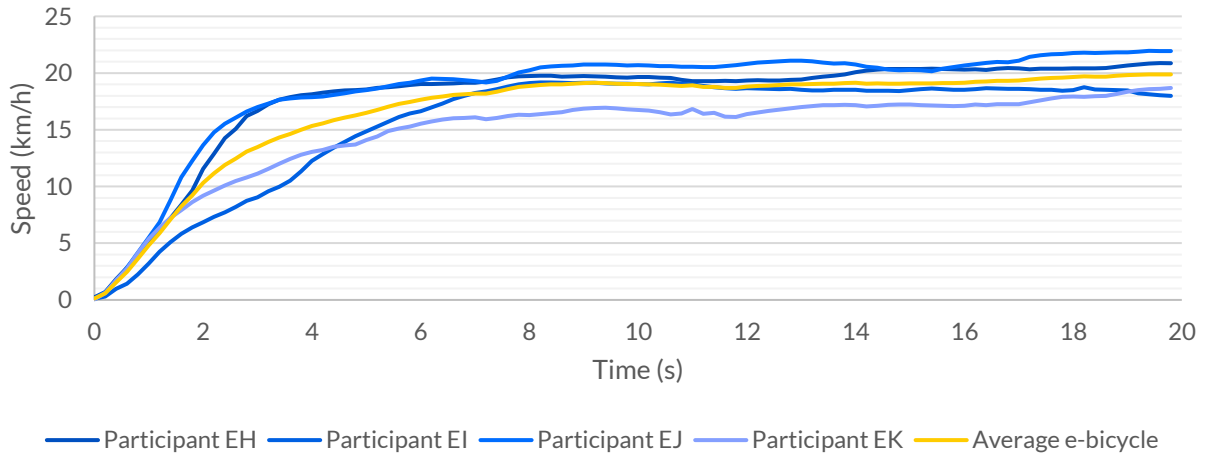
**Figure 3.22:** Example of speed profile participant B

Figure 3.22 shows eight typical acceleration segments of participant B, similar data is used for all other participants to determine the average speed of an unconstrained acceleration. Appendix A shows the speed profiles for all participants. The average speed profiles of all 'regular' bicycle participants are visualized in figure 3.23 and for e-bicycle participants in figure 3.24. The difference between the cyclists and e-cyclists is most recognizable by a higher speed. The e-cyclists also take much less time to reach their desired speed. Furthermore it is observed that the speed profiles of e-cyclists are more alike than for normal cyclists.

It is observed that after about 15 seconds (10 seconds for e-cyclists), their speed is stabilizing (figure 3.23 and figure 3.24). This stable speed at the end of the average unconstrained accelerations is assumed to be the desired speed of each participant. By taking the average speed from 15 to 20 seconds of these reference segments, the desired speed for each participant is approximated.



**Figure 3.23:** Average speed profile of all bicycle participants



**Figure 3.24:** Average speed profile of all e-bike participants

To test whether these observed desired speeds correspond to the theoretical desired speed distribution found in [section 3.2.1](#), an independent samples t-test can be used (equation [3.14]). The t-test is used to compare means of two samples ([Nigam, 2018](#)), in this case the observed sample values are compared to the values found in other literature sources. Since the desired speed distribution is estimated using various reference normal distributions the theoretical desired speed distribution can be regarded as a normally distributed sample.

$$t = \frac{\bar{x}_{theoretical} - \bar{x}_{observed}}{\sqrt{\frac{SD_{theoretical}^2}{n_{theoretical}} + \frac{SD_{observed}^2}{n_{observed}}}} \quad [3.14]$$

The results of this test:  $t(18) = 1.318$ ,  $p = .204$ , show that the difference between the estimated values and the observed values is not statistically significant (p-value higher than 0.05). Hence, the conclusion can be drawn that the observed desired speed values correspond to the range of values in the estimated speed distribution.

The desired speed distribution for e-cyclists was estimated by increasing the distribution of bicyclists with 20%. The same t-test is executed with the sample of e-cyclists' desired speed ( $n = 4$ ). Resulting in a statistically significant difference between both samples,  $t(17) = 2.606$ ,  $p = .018$ . Meaning that the theoretically determined speed distribution for e-cyclists does not correspond to the observed values. Not only is there a mean difference of almost 4 km/h, also the range of values differs greatly between the theoretical and observed distribution. Where the theoretical desired speed distribution ranges from 12.82 km/h to 34.83 km/h, only values between 17.70 km/h and 21.27 km/h are observed. This may be due to the small sample size of the observations.

The independent samples t-test assumes normal distribution, which is not necessarily the case with a distribution. In addition to the independent samples t-test, also the Kolmogorov-Smirnov (KS) test is executed. Here the observed sample can be compared with the theoretical desired speed distributions (Kawwa, 2020). For the KS test, the following procedure is executed:

- The observations are sorted in ascending order.
- The cumulative probability of observations are calculated.
- Cumulative probability of observed speed in the theoretical speed distribution is calculated. In other words, the cumulative probability that the same speed occurs in both samples.
- Absolute differences between cumulative probabilities for each observed speed point are calculated (visualized in figure 3.25).
- The statistical 95% critical value is calculated according to:  $1.36/\sqrt{n}$ . (Kawwa, 2020). Therefore the critical value for the cyclists is 0.514 (7 observations) and 0.680 for e-cyclists (4 observations).

The maximal absolute difference for the cyclists desired speed (at the speed point of 21.5 km/h) is 0.292, which is lower than the critical value (0.514). Therefore the conclusion is drawn that the samples of desired speed come from the theoretically estimated speed distribution, these results are visualized in figure 3.25. Based on the statistical tests, the estimated desired speed distribution ( $M = 19.43$ ,  $SD = 4.37$ ) is validated and used in the simulation.

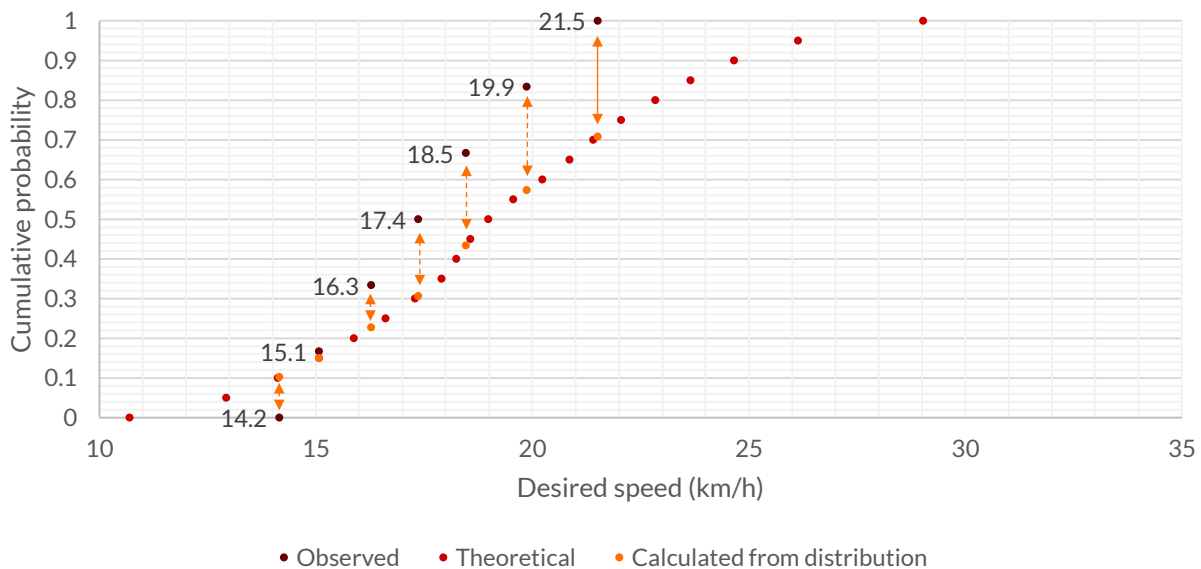


**Figure 3.25:** KS test for desired speed of cyclists

The same procedure is executed for the desired speed observations of e-cyclists. Here the maximal absolute difference is found to be 0.664, which is only slightly lower than the critical value of 0.680. This large difference is found because the fastest observed desired speed for e-cyclists is 21.27 km/h, in the theoretical desired speed distribution, more than half of all individuals will have a desired speed higher than this value. This large difference might be partly due to the small sample size of observations, nonetheless the conclusion is drawn to adjust the desired speed distribution for e-cyclists.

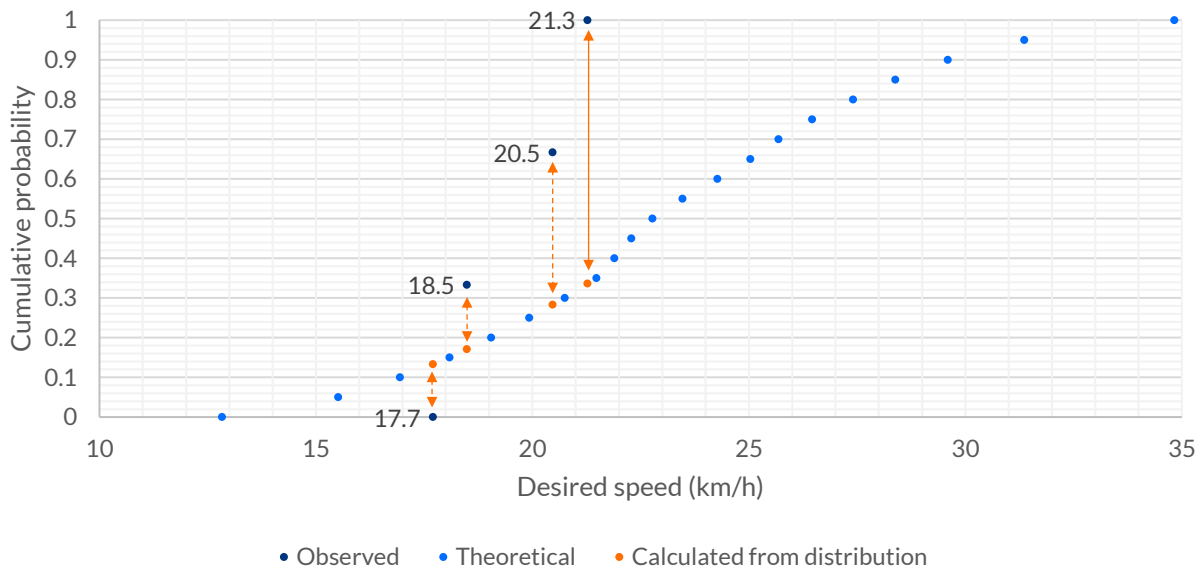


**Figure 3.26:** KS test for desired speed of e-cyclists

Adjusting the set speed distribution is tricky, since there is no additional data to base the new distribution on. However, based on the observed values and some common sense, the assumption is made that for e-cyclists, the desired speed values have a much lower variance. Since e-bicycles are equipped with an electronic motor, much of the variance in physical strength to pedal is dismissed. Because of this electronic motor, also a lower percentage of people wants to cycle faster than what the motor supports. The previously estimated speed distribution values have a mean of 23.2 km/h and a standard deviation of 5.39. Based on the observed values ( $M = 19.5$  km/h,  $SD = 1.67$ ) the mean and standard deviation should be lower. Taken into consideration these values, a new desired speed distribution is generated, with a mean of 21.5 km/h and standard deviation of 3.47. Figure 3.27 shows that this new distribution better matches the observed values, and prevents small and large outliers. The independent samples t-test shows more promising results,  $t(17) = 1.831$ ,  $p = .100$ . Also the KS test offers a more suitable result, the maximal difference in probability (0.512) is less than with the previously estimated speed distribution and further removed from the critical value of 0.680. The revised desired speed distribution corresponds better to the observed values, as can be seen in figure 3.27).

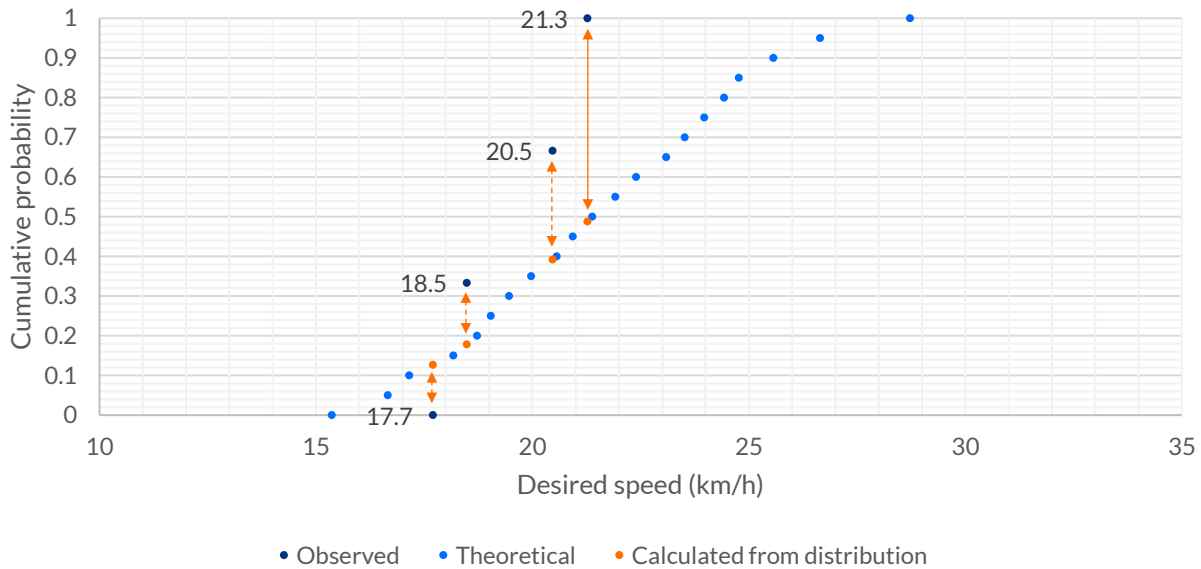


**Figure 3.27:** Revised distribution KS test for desired speed of e-cyclists

### 3.4.4. Turning speed reduction

It is assumed that cyclists reduce their (desired) speed when making turns and the amount of speed reduction depends on the radius of the turn. From the data collection experiment, data segments where a cyclist is turning and does not come to a complete stop are extracted (cyclists and e-cyclists are considered). The maximal speed reduction, regardless of the duration of the turn is visualized in figure 3.28 for each of the extracted turn segments. A trend can be observed from the graph, which is confirmed by performing a Pearson correlation test ( $r(26) = 0.767$ ,  $p < .001$ ). This verifies that there is an influence of turn radius on cyclists' speed.

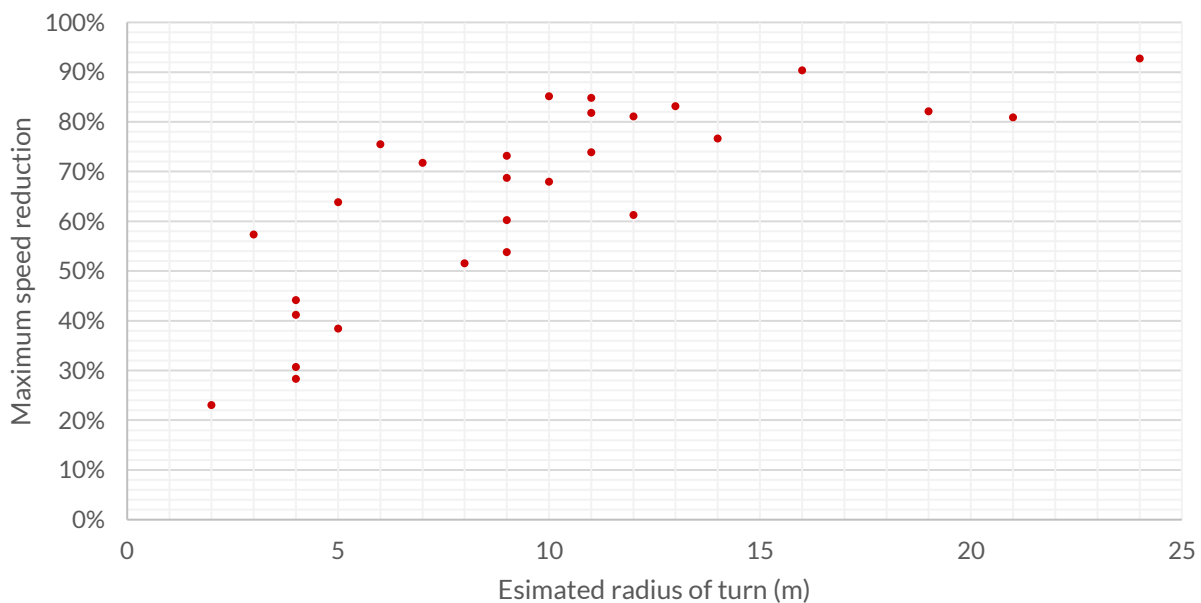


**Figure 3.28:** Maximal speed reduction as percentage of initial speed for different turn radii



Turns are categorized into four categories by estimating the turn radius from the trajectory visualized in QGIS: smaller than 5 m, 5 to 10 m, 10 to 15 m and larger than 15 m. Multiple turning segments are compared by aligning the start of the turn, which is defined as the data point where the heading (in degrees) is deviating from the initial heading. In figure 3.29, various turning segments are visualized by aligning the turning point at the 6 second mark. The speed in figure 3.29 is presented as a percentage of the initial speed, defined as the average speed in the first 3 seconds of the extracted segment.

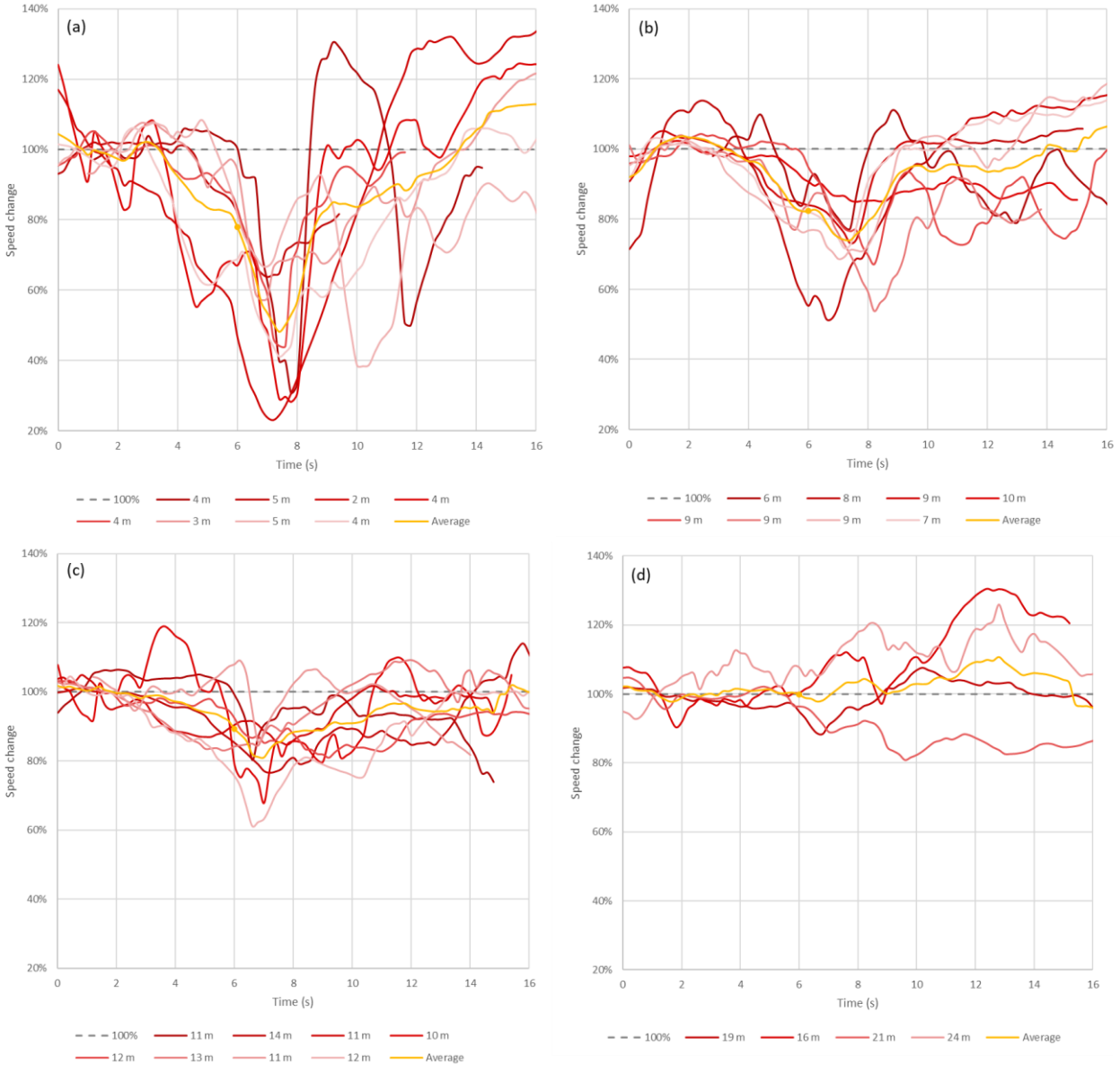


**Figure 3.29:** Speed reduction with turn radius of: a) < 5 m, b) 5-10 m, c) 10-15 m and d) > 15 m

Categorizing the turning segments according to estimated turn radius, confirms the general assumption that speed is decreasing more with a smaller turn radius. For the largest turn radius category, with turn radii larger than 15 m, almost no speed reduction is observed. For the other three categories, a trend is observed where cyclists start decelerating about 3 seconds prior to

changing their heading. Figure 3.29 also shows the average speed reduction per category, in figure 3.30 the average speed for each turn radius category is visualized. Figure 3.30 shows that before making the turn, cyclists already decelerate and reach their maximal speed reduction about 1 to 1.5 seconds after starting the turn, before accelerating again.

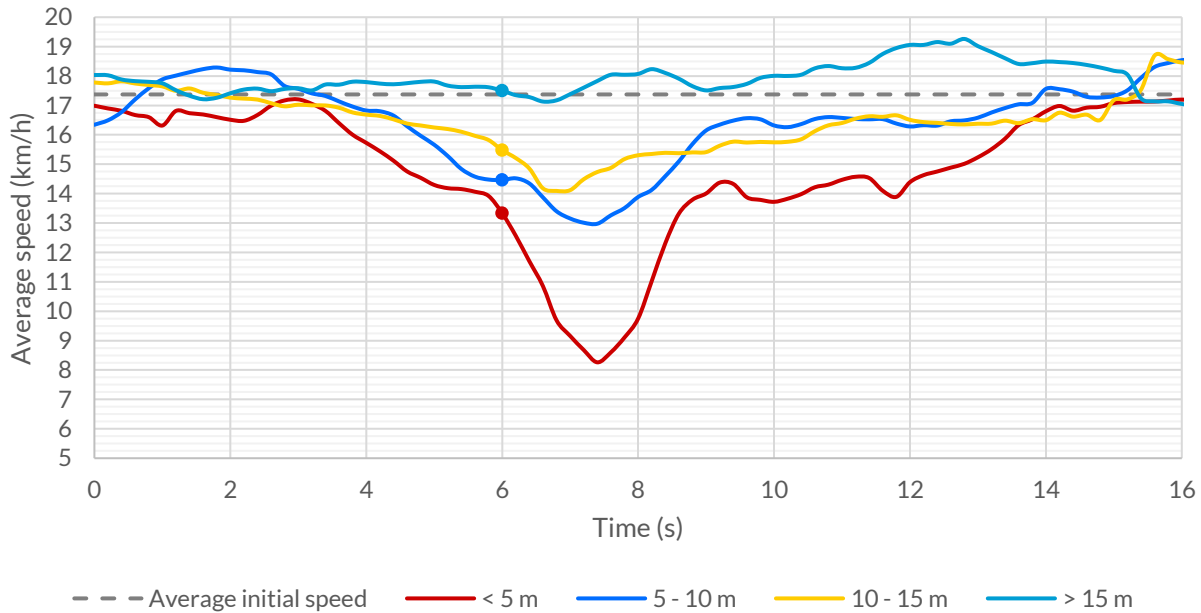


**Figure 3.30:** Average speed for different turn radii

Figure 3.30 shows the average speed over time for four different turn radii categories. Based on these average observed values, a reduced speed area is modeled for the three turn categories where speed reduction was observed (less than 5 m, 5 – 10 m and 10 – 15 m). This is achieved by applying a separate speed distribution to the area where cyclists take the turn. A continuous uniform distribution between two values is created, based on the values from the GPS data collection (table 3.10).

**Table 3.10:** Desired speeds for different turn radii

Turn radius	Speed distribution
Less than 5 m	6 km/h to 10 km/h
5 to 10 m	8 km/h to 12 km/h
10 to 15 m	12 km/h to 16 km/h
More than 15 m	No reduction (keep desired speed)

### 3.4.5. Shared space speed reduction

It is assumed that in a shared space with pedestrians, cyclists have a lower desired speed than at regular cycling paths. In section 3.2.1, this assumption was confirmed by local data from Fiets Telweek (2016). The reduced speed in shared space assumption is also tested by analyzing the collected cycling data. Even though pedestrian spaces can be easily queried using GIS software, it is hard to automatically distinct shared space from non-shared space speed data. Firstly because of

the accuracy of the GPS receivers and secondly because including all data leads to a lot of noise. Thus, shared space trajectories have to be extracted manually. To achieve this, data segments around a shared space are extracted from participants that ride through such an area (example in figure 3.31).

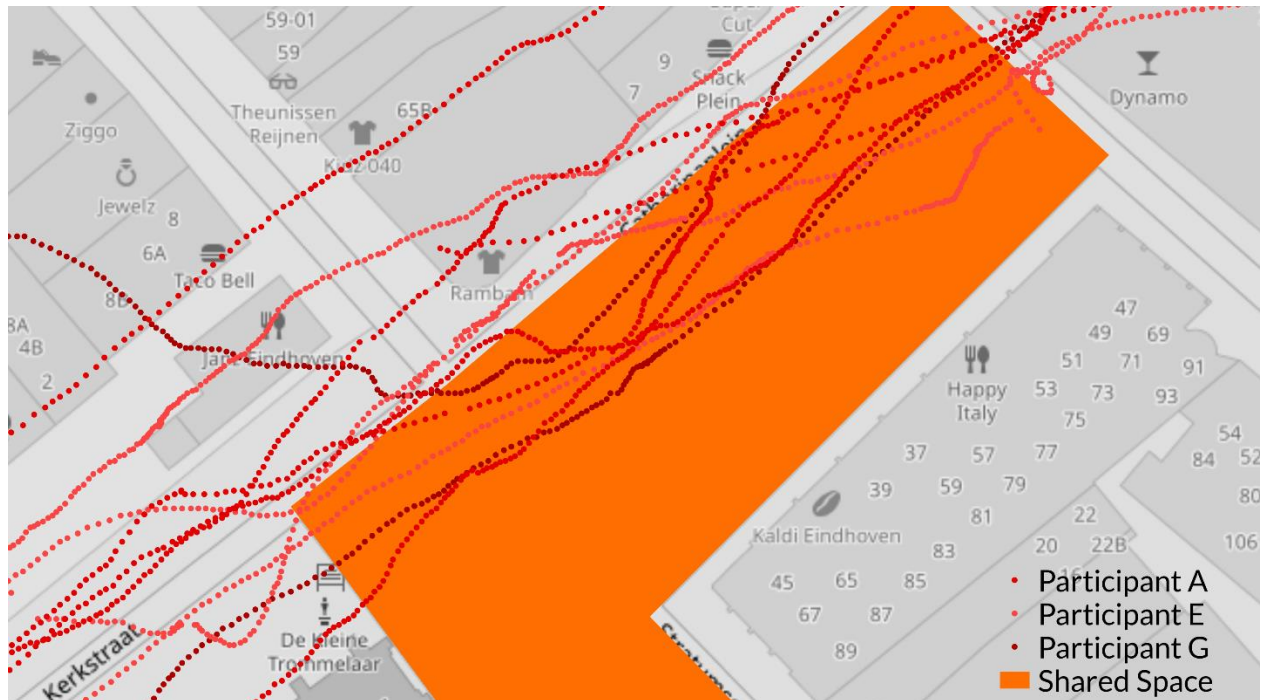


**Figure 3.31:** Example of GPS data around shared space area

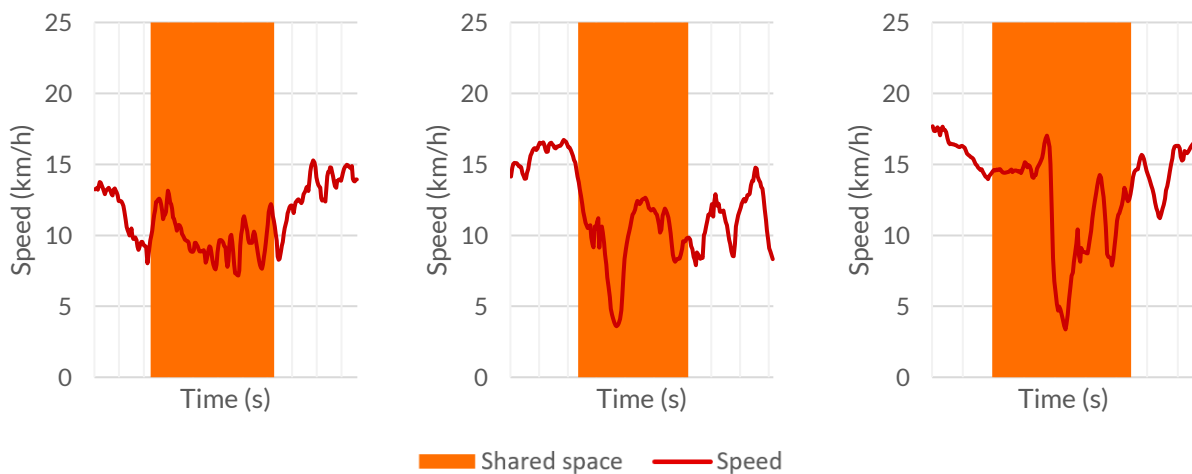


**Figure 3.32:** Examples of shared space speed profiles

Figure 3.32 shows three examples of observed speed in and around a shared space area. By looking at many speed profiles around four different shared spaces in Eindhoven, often a speed reduction is observed. Not in all extracted segments, a decrease in speed is clearly visible. Of all the extracted data around shared spaces, a t-test comparison is conducted between the speed values in the shared space and around the shared space. This test shows a statistically significant difference in speed between the two samples,  $t(1842) = 30.47, p < .001$ . With an observed mean of 10.21 km/h within

the boundaries of the shared spaces and 14.02 km/h around the spaces. Noteworthy is the relatively low average value of both samples compared to the desired speed averages. Raising the question if speed around shared spaces is lower in general, since these are often located in busier areas. Because the simulation models speed through desired speed, this question is not further investigated.

The script presented in [section 3.1.3](#), which models the transition of cyclists from roads to areas and vice-versa, will be used to adjust the desired speed when in a shared space area. By choosing to model the speed reduction this way, individual cyclists maintain their desired speed value even though new cyclist are constantly generated. So cyclists that have a high desired speed, will keep a high desired speed. When entering a shared space, their desired speed is decreased with a certain percentage. When exiting the shared space, this adjusted desired speed will reset to their initial desired speed. The collected data shows an average decrease of more than 27% when comparing the speed around shared spaces to the speed within the shared space. The speed reduction at shared spaces was initially estimated at 17%, based on local data ([Fiets Telweek, 2016](#)) and research projects by Bernardi & Rupi (2015) and Boufous et al. (2018). Considering all these results, the shared space reduction factor is set at 20%, to better match the observed values.

### 3.4.6. Acceleration validation

By using the speed profile segments for the collected GPS data, also the acceleration of cyclists and e-cyclists can be validated. Acceleration is specified as a function of speed in the simulation model so should be independent of time. To achieve this, the acceleration for each data point is simply calculated with equation [3.15] before matching it to the speed each data point.

$$a = \frac{\Delta v / 3.6}{0.2} \quad [3.15]$$

Then for every interval value of speed (for example between 4 and 5 km/h) the mean acceleration value is calculated over all data segments of each participant. This yields an average acceleration function for each participant. [Figure 3.33](#) and [figure 3.34](#) show the acceleration functions of all participants, including an average function for cyclists and e-cyclists. Cyclists reach their maximum acceleration when cycling around 3 km/h, after which their acceleration gradually drops to 0 m/s<sup>2</sup>. E-cyclists seem to not only have a higher acceleration, also they keep a large acceleration value at higher speeds. From 0 km/h to 3 km/h the acceleration function is similar, but where the acceleration for cyclists gradually drops, e-cyclists keep a relatively stable acceleration value. Faster than 13 km/h, their acceleration begins decreasing to zero.

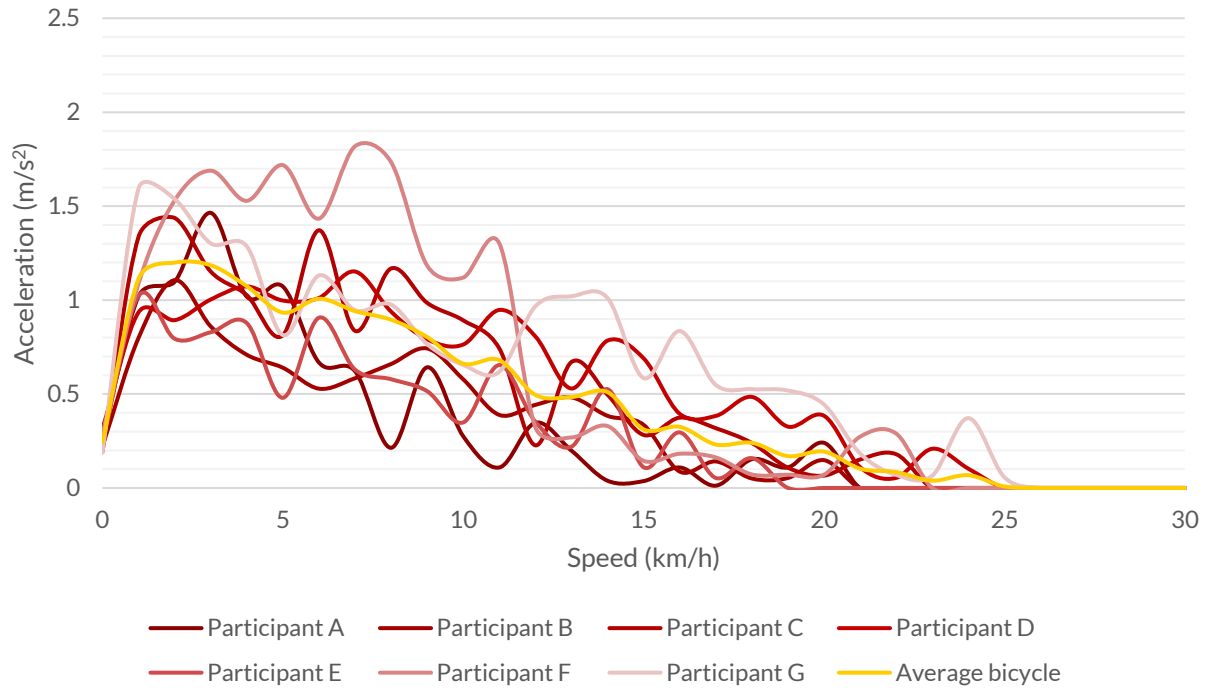


**Figure 3.33:** Acceleration functions of all bicycle participants

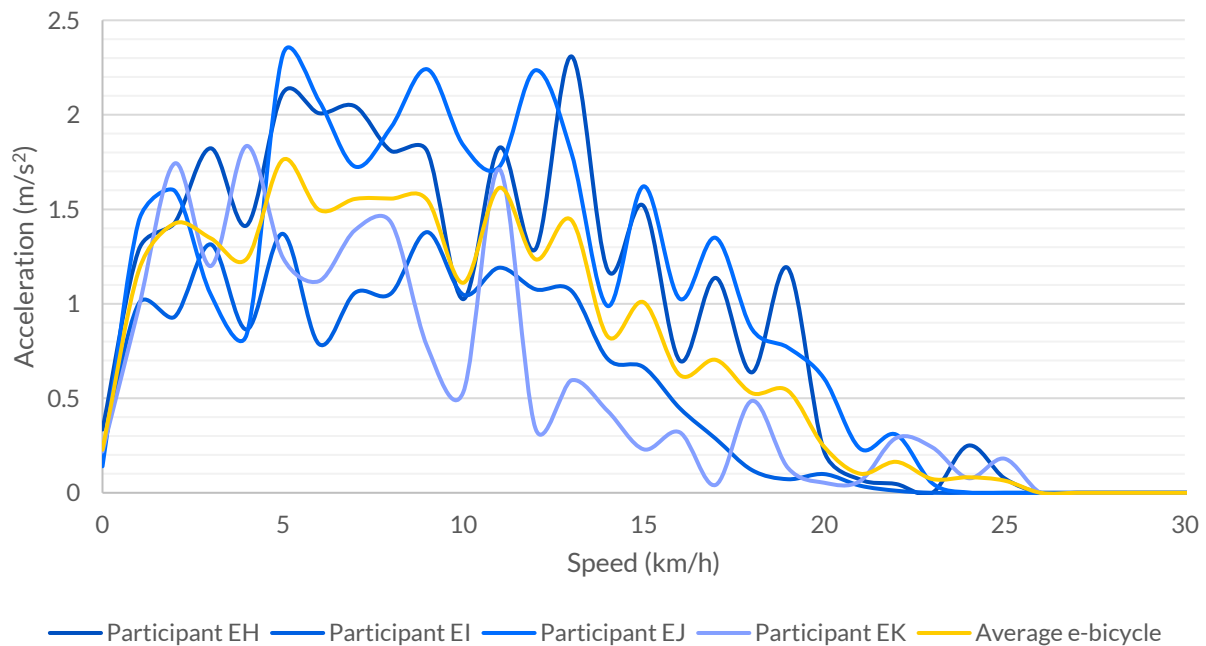


**Figure 3.34:** Acceleration functions of all e-bicycle participants

The observed acceleration behavior is compared to the median reference acceleration function by COWI (2013). Figure 3.35 shows the average observed functions do not show the same pattern as the reference function. For cyclists, the maximum acceleration value seems too large and specified at a too high speed. E-cyclists can reach accelerations of  $1.8 \text{ m/s}^2$ , but here the reference function is decreasing acceleration too fast. To realistically simulate the differences in cyclists and e-cyclists,

two separate acceleration functions are proposed. A simplified form of the average observed acceleration serves as the median acceleration function. Since Vissim offers the possibility to add a maximum and minimum function, these are added as well within some range of the median. Both proposed functions including the maximum and minimum range are visible in figure 3.36.

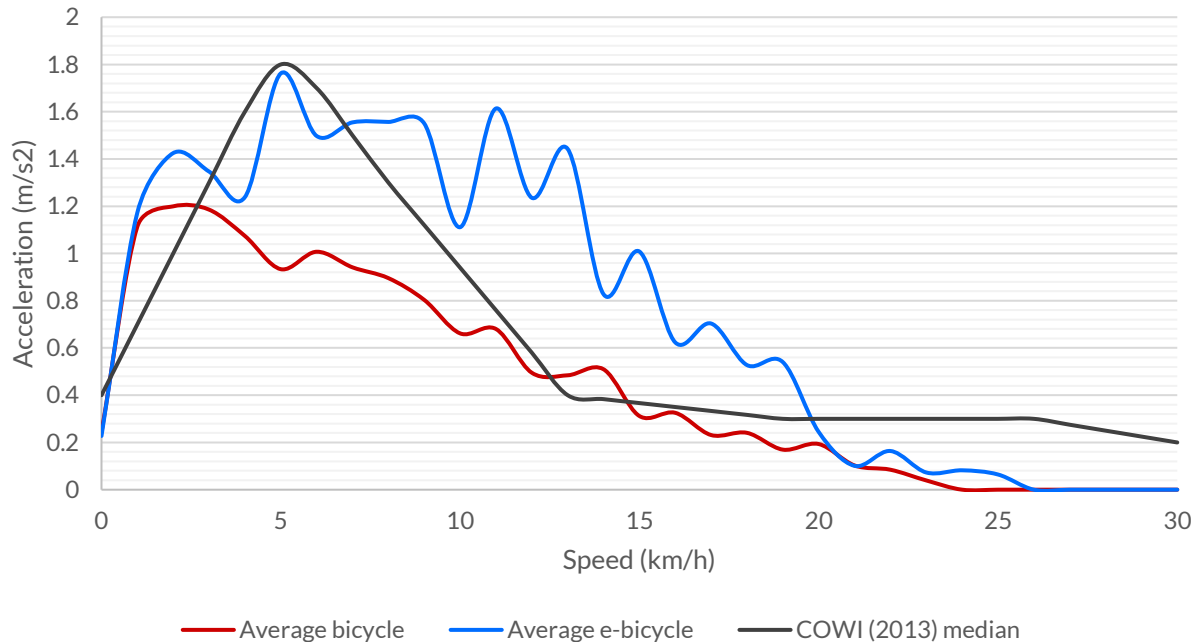


**Figure 3.35:** Average measured cyclists, measured e-cyclists and reference acceleration functions

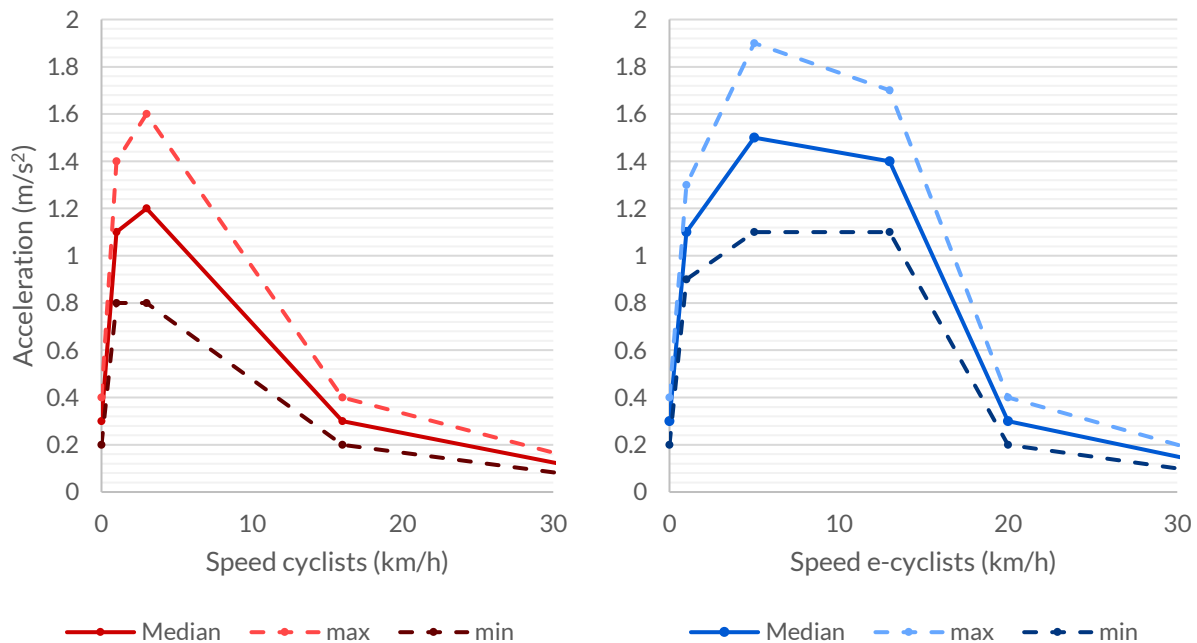


**Figure 3.36:** Acceleration functions for cyclists and e-cyclists used for simulation

Also noteworthy is both observed acceleration functions drop to 0 m/s<sup>2</sup> at speeds higher than 25 km/h, while the reference function is slowly decreasing from 0.3 m/s<sup>2</sup>, reaching zero at 60 km/h



(figure 3.35). The participants in the data collection experiment rarely reached speeds over 25 km/h in the extracted segments. However, when adopting this behavior in the model, cyclists with a desired speed higher than 25 km/h would never be able to reach their desired speed. To prevent this, a low acceleration from 0.3 m/s<sup>2</sup> to 0 m/s<sup>2</sup> is assigned to high speeds up to 40 km/h.

The reference functions for deceleration are not validated using the observed data, since deceleration is assumed to have less influence on capacity and traffic flow. People rarely break in a way the maximum deceleration is reached, but only when really necessary. Deceleration also is less constrained by individual physical differences between (e-)cyclists. For these reasons, the deceleration function presented in section 3.2.2 is used in the model for both cyclists and e-cyclists.



## 4. Case study simulations

After validation of the behavioral model, it can be applied to simulate traffic in a certain area. The improved behavioral model is used to regulate the traffic input within a simulation environment.

The City of Utrecht is one of the fastest growing cities in the Netherlands and expects an increase of 100,000 inhabitants in the coming 20 years, this will raise the number of trips by around 35% (City of Utrecht, 2021). To reach their goals of a healthy, social, sustainable, accessible and livable city within the financial constraints (City of Utrecht, 2020d), Utrecht is taking countless measures to stimulate cycling. The City of Utrecht is one of the global hotspots for cycling innovation and therefore the perfect place to select a case study area.

This chapter first establishes and explores the environment that will be used for the case study simulations and presents how this environment is modeled digitally for different network scenarios.

Secondly, traffic volume data of various transportation modes is collected to make future estimations that will function as inputs in the network. Three different input scenarios are used to evaluate different traffic situations.

The results of the performed simulations are presented in the final section of this chapter. Here the general conclusions are drawn as well as comparisons of the various scenarios.

## 4.1. Case study environment

In Utrecht a case study environment for the simulations is selected by looking at locations that will be transformed into high density areas where many cyclists are expected. Section 4.1.1 introduces the area of *Beurskwartier* and the borders for the scope of the simulations. A timeline of all construction developments is presented to explore the area and formulate scenarios for different simulation networks. The procedure used to model all elements of the network is also shown in this section.

### 4.1.1. Urban context

Despite the expected population growth in the City of Utrecht, the municipality is embracing the 10-minute-city concept. Where people are able to reach all their activity locations (work, school, leisure, sport, public transport, etc.) within ten minutes of their home (City of Utrecht, 2021). To reach this goal, many of the development plans consist of high density, mixed-use buildings with an emphasis on active and public transportation. A mode shift is desired that makes the bicycle more popular than the car for trips in and around Utrecht (City of Utrecht, 2020a). The city expects the population growth together with this mode shift will raise the number of bicycle trips by 32% from 2015 to 2030 (Jousma et al., 2018).

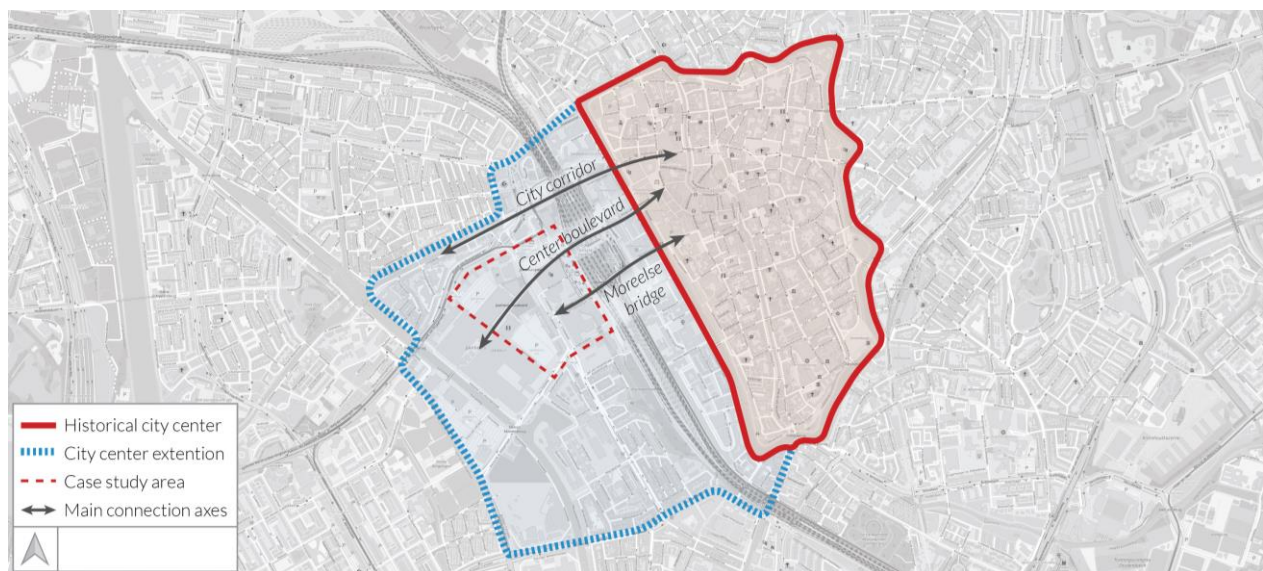


**Figure 4.1:** Extension of city center to the west of the railway (adapted from: City of Utrecht, 2017)

The case study area is located on west side of the railway (figure 4.1) and is one of the locations in Utrecht that will be redeveloped to accommodate the city's estimated growth. Utrecht is home to the busiest train station in the country. The central train station, *Utrecht Centraal*, processes almost 200,000 railway travelers on a daily basis and also is an important hub for bus and tram transportation (NS, 2019). On the east side of the train station and railway, the historical city center is located (figure 4.1). Over the years, the area west of the railway has developed into a large scale office, business and leisure area. The most prominent landowner in the area is the *Jaarbeurs*, a 100,000 m<sup>2</sup> event and exhibition center with 11 event halls and 4 large car parks (Jaarbeurs, 2019).



The aim of the municipality of Utrecht is to integrate the area west of the railway as a lively extension of the city center. This is achieved by many redevelopment projects in the area and enhancement of the main axes that connect the east and west (figure 4.1). The 'City corridor' *Leidseweg-Vredenburg* is an important connection for bicycle traffic. The emphasis on this connection includes restoring the historic canal *Leidsche Rijn*. Just like the canal *Catharijnesingel*, it was transformed into a motorway in the 1970s but was recently restored, completing the encirclement of canals around the historic city center (Boffey, 2020). The pedestrian focused 'Center boulevard' connects the *Jaarbeurs*, through *Utrecht Centraal* and shopping center *Hoog Catharijne*, to *Vredenburg* square. The *Moreelse* bridge (constructed in 2016) is a footbridge crossing the railway, this bridge has stairs and elevators on both sides that allow for bicycles to be taken across.

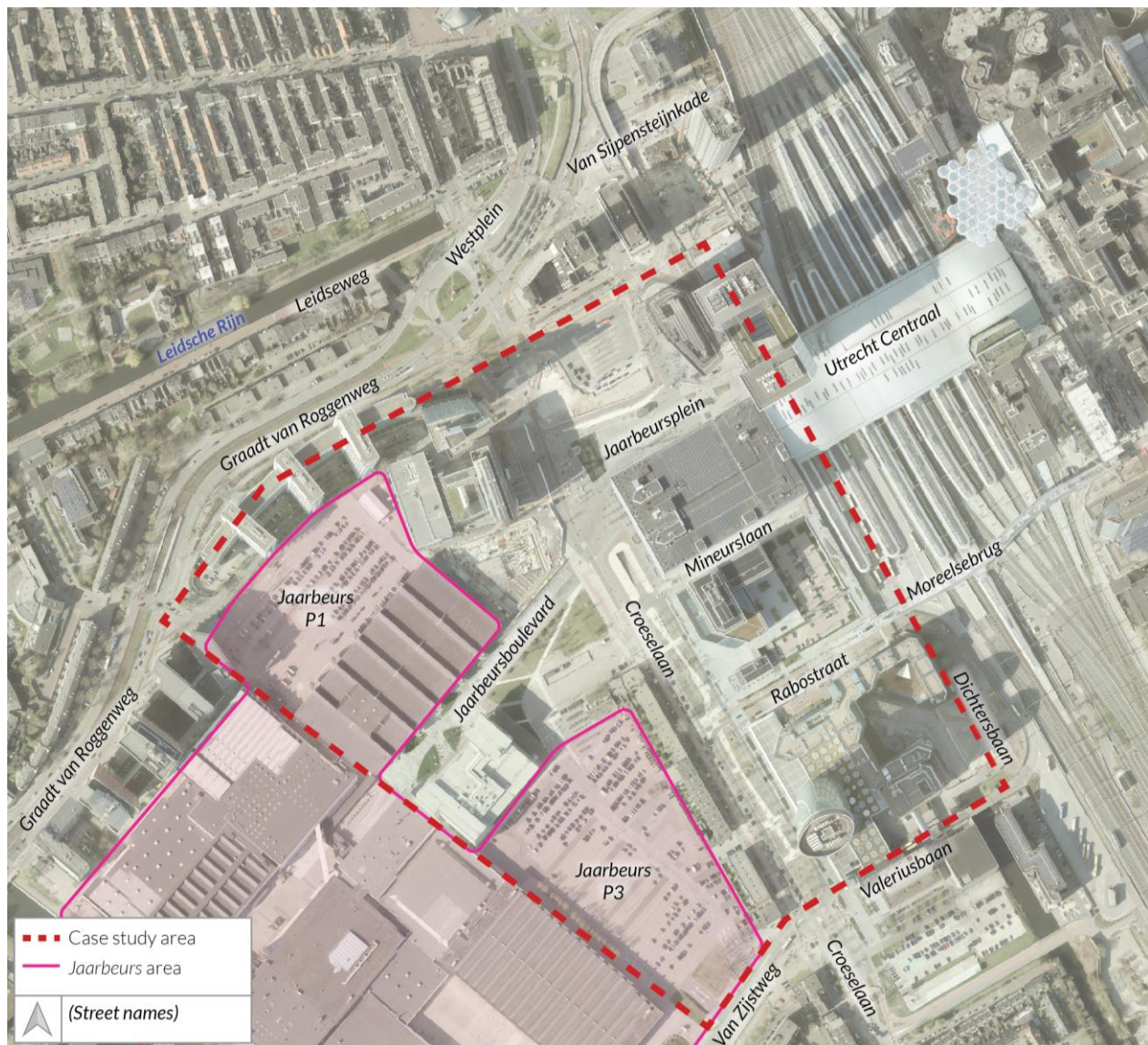


**Figure 4.2:** Case study area borders and street names (adapted from: *City of Utrecht, n.d.*)

Due to these visions for the west side of the *Utrecht Centraal*, the area will see a huge increase in residents and visitors during the coming years. The overarching project of revitalizing the area around the central station of Utrecht has been initiated many years ago, which in 2003 led to a

masterplan for the entire area (City of Utrecht, 2003). Even though this masterplan has changed over the years, the main concepts are still applicable. The city center extension on the west side of the central station is planned to have a much larger building scale than the historic city center. With a standard building height of 45 meter and added towers of 70 m to 90 m with a large diversity of functions.

Investigating the infrastructure layout is key to the modeling the network for simulation. The edges of the network are presented in a recent satellite image in figure 4.2. The borders are defined by: the railway and station in the east, *Valeriusbaan* and *Van Zijlsweg* in the south, the boundary of the *Jaarbeurs* in the west, the northern edge of the network is marked by the tram rail and *Graadt van Roggenweg*. These edges and their associated intersections are not included in the network, to save computation time and have a less complex model. For example, only cyclists and cars going north on the *Croeselaan* from the *Croeselaan-Van Zijlsweg* intersection are considered in the model. The same applies to the large intersection north of the network (*Westplein*), only road users that cross the tram rail to enter *Jaarbeursplein* are inputted. A large masterplan called *Beurskwartier* takes up the majority of the to be developed area and also outlines the new urban structure. The northeast *Jaarbeurs* grounds, mainly exists of parking places *P1* and *P3*, will be transferred to the municipality in 2023 (figure 4.2). After which the construction on the majority of the area will start, the southwest halls of *Jaarbeurs* will be transformed into *Jaarbeursdistrict*, to also accommodate dwellings and other functions (Jaarbeurs, 2019). A cycling street (*fietsstraat*) is planned on the edge separating *Beurskwartier* and *Jaarbeursdistrict* (Wolbertus, 2020).

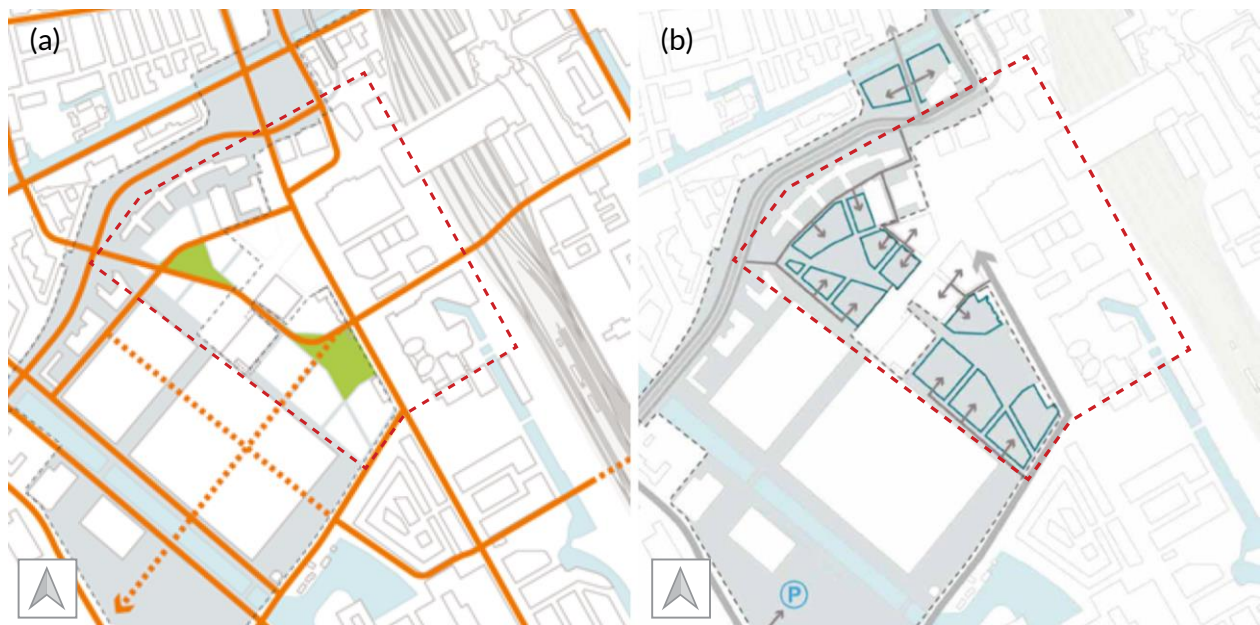


**Figure 4.3:** Planned routing for: a) cycling and b) motorized traffic (from: City of Utrecht, 2017)

Figure 4.3 displays the planned network for cycling and motorized traffic. The aim of the cycling network is to connect green spaces and parks to provide a pleasant and healthy route (City of Utrecht, 2017). Two new parks are planned, bordering the *Croeselaan* is the *Croesepark* and the *Oranjepark* on the west side. Figure 4.3 also shows some potential cycling connections, like an additional tunnel crossing the railway in the south. The planned access routes reveal that cars are mostly kept from the center of the area.



The traffic square *Westplein* will also see a large redevelopment, the *Graadt van Roggenweg* is redirected south of the *NH Hotel*, following the direction of the tram (figure 4.4). This creates a lot of additional space for buildings, green public space and the continuation of *Leidsche Rijn* canal. The access road to *Jaarbeursplein* will be made into a cycling street, where cyclists share the road with cars but have priority.

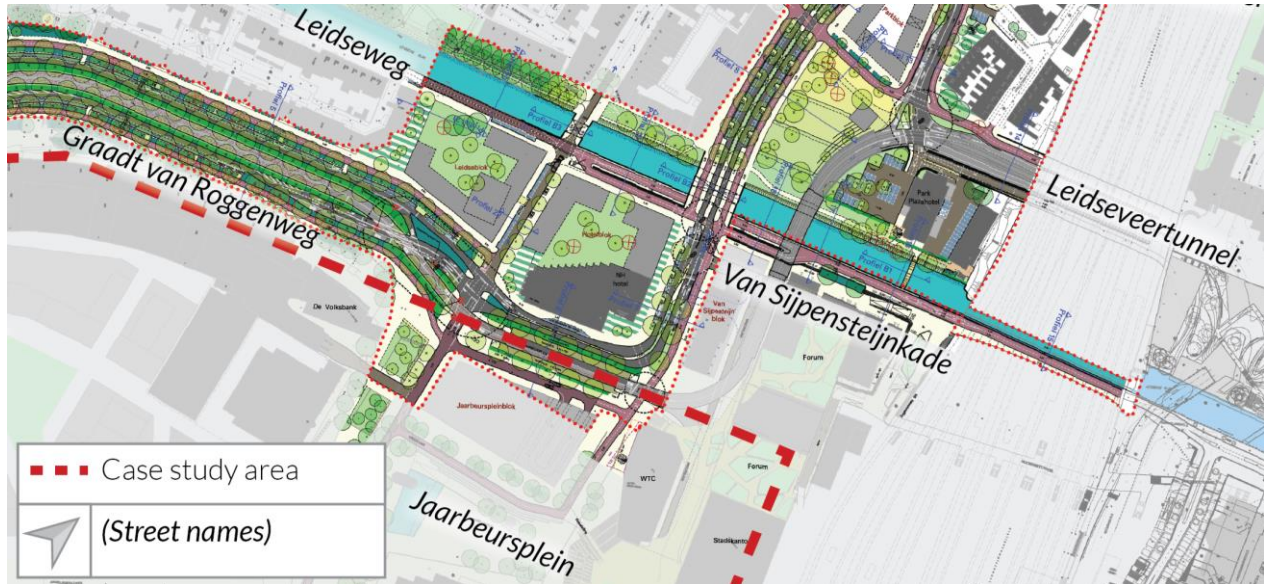


**Figure 4.4:** Redesign of Westplein/Lombokplein (adapted from: *City of Utrecht, 2020c*)

Regarding pedestrian traffic in the area, an important infrastructural development is *Forum*. Which is an elevated pedestrian area at 7.5 m above ground level, stretching from the *Van Sijpesteijnkade* in the north to the *Moreelse bridge* in the south. Many of the new developments are located along this pedestrian zone parallel to the railway. The 450 m long *Forum* is elevated to have out-of-sight space for loading and unloading at the *Mineurslaan* (CU2030, 2020; Group A, 2020).

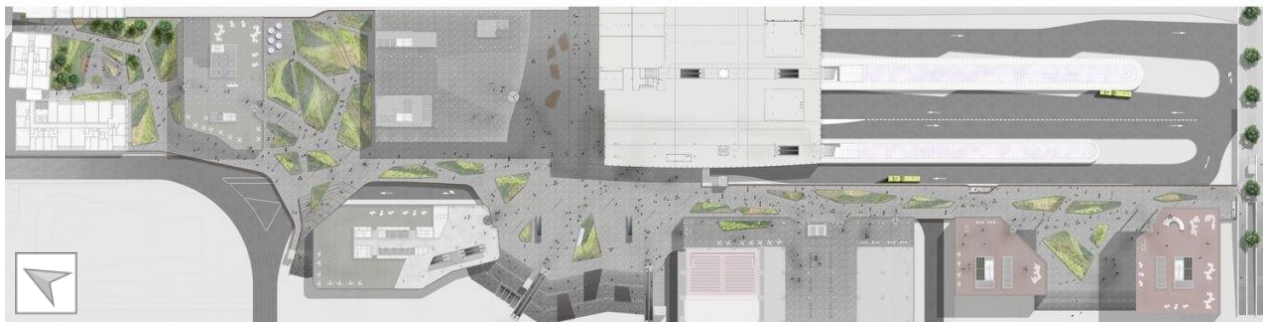


**Figure 4.5:** Pedestrian area Forum (from: *Group A, 2020*)

This section presented the urban and infrastructural context around the case study area. The infrastructure will form the basis of the simulation networks. Individual construction projects will be discussed in section 4.1.2.



### 4.1.2. Construction developments

By looking at a timeline of all construction projects in the case study area, the time frame of the scenarios can be specified. After establishing the outlines and structure of the case study area in [section 4.1.1](#), this section presents an overview of all relevant construction developments in the case study area. Almost all buildings and plots in the area will be, or are already, redeveloped in roughly the period from 2014 to 2030. Large buildings already existing before this period are the offices *Rabobank*, *Sypsteyn and Hojel city center 1 and 2*, the *NH hotel tower* and the centrally located *Beatrix Theater*. A timeline of all recently completed and ongoing building or infrastructural construction projects is presented in [table 4.1](#), starting with the completion of the new city hall (*Stadskantoor*) in 2014 ([CU2030, 2021](#)).

**Table 4.1:** Completed and ongoing projects (*City of Utrecht, n.d.; CU2030, 2020; Kadaster, 2021*)

Project	Type	(Expected) completion	Description
<b>City hall Utrecht (Stadskantoor)</b>	Public office	2014	2500 work places, built to centralize other municipal offices.
<b>Bicycle parking Jaarbeursplein</b>	Bicycle parking	2014	4200 bicycle parking spaces, has a shared space entrance at <i>Jaarbeursplein</i> .
<b>Utrecht Centraal (Train station)</b>	Public transport, retail	2016	Busiest train station in the Netherlands with 194,385 travelers per day (NS, 2019).
<b>Moreelsebrug</b>	Bridge	2016	Footbridge over the rail tracks with option to take bicycle, the bridge has stairs and elevators on both sides.
<b>Kinepolis</b>	Cinema	2017	Large cinema with 14 screens.
<b>De Knoop</b>	Office	2018	1070 work places, with a large car parking. Including temporary pavilion planned for around 15 years.
<b>Bicycle parking Knoop</b>	Bicycle parking	2018	3000 parking spaces, part of elevated pedestrian space <i>Forum</i> is situated on the roof.
<b>Car parking Croeselaan</b>	Car parking	2018	Car parking garage with 778 parking spaces, below the <i>Jaarbeurs</i> square. Only accessible from the south.
<b>WTC Utrecht</b>	Office	2018	Office with around 2000 work places.
<b>Croeselaan redesign</b>	Public space	2019	Redesigned from <i>Jaarbeursplein</i> until <i>Van Zijstweg</i> to have more space for pedestrians, cyclists and green spaces. The maximum speed is lowered from 50 km/h to 30 km/h.
<b>Tram and bus station</b>	Public transport	2019	Completion of bus station at east side of replaces temporal bus station at <i>Jaarbeursplein</i> .

<b>Central Park</b>	Office	2021	Office tower of 90 m with an indoor 'park' at 45 m. 28500 m <sup>2</sup> GFA office space. Includes 370 car and 1100 bicycle parking spaces (Bouwinvest, 2021).
<b>Van Sijpensteijn kade (De Syb)</b>	Residential	2019/2022	Residential tower <i>De Syb</i> , with 266 apartments, was completed in 2019, rest of project to be constructed.
<b>Forum</b>	Public space	2022	Elevated pedestrian space from <i>Van Sijpensteijnkade</i> to <i>Moreelse</i> bridge. The south part is complete, the north part is expected to be completed together with <i>Van Sijpensteijnkade</i> .
<b>Galaxy tower</b>	Hotel, residential	2021	92 m tower with 260 hotel rooms at first 7 floors, above 317 apartments,.
<b>Wonderwoods</b>	Residential, office	2023	Two towers (105 m, 73 m) with 420 apartments, 15000 m <sup>2</sup> office space, 7500 m <sup>2</sup> commercial functions, 160 car parking and 1900 bicycle parking spaces.

Table 4.1 shows projects that are completed in recent years as well as ongoing projects in the case study area. The projects planned for the future are displayed in table 4.2, some may be divided into smaller construction projects in a later stage. All projects in table 4.2 are still in a conceptual design phase.

**Table 4.2:** Planned construction projects in case study area

Building	Type	Expected completion	Description
<b>Jaarbeursplein building</b>	Office	2026	No design yet, but expected 47200 m <sup>2</sup> office space, 3300 m <sup>2</sup> retail and commercial functions.
<b>Westplein/ Lombokplein</b>	Mixed	2030	Redesign of infrastructure and public space, restoring of Leidse Rijn, 350 residential units, office and commercial functions, parks,
<b>Beurskwartier</b>	Mixed	2030	Masterplan of 3000 dwellings, 65000 m <sup>2</sup> office/working space. Transfer of ground in 2023.
<b>Jaarbeurs</b>	Mixed	2030	Masterplan of neighborhood with 117,00 m <sup>2</sup> <i>Jaarbeurs</i> at its core. Total program of 600,000 m <sup>2</sup> , with 40%-60% residential. Also leisure, commercial, offices and green spaces.
<b>Office towers Knoop</b>	Office	Unknown	Two office towers next to 'De Knoop', estimated 40000 m <sup>2</sup> GFA.

The *Westplein/Lombokplein* (figure 4.4) is located just outside of the edges of the case study area, but it will shape the way people are entering *Jaarbeursplein* from the north. Also some additional traffic is expected from the 500 residential dwellings and commercial developments.

The *Beurskwartier* masterplan exists of around 12 building blocks mostly constructed on the current parking grounds of *Jaarbeurs* (figure 4.6). The directive is to design enclosed building blocks, with a diversity of functions and building heights. The inside of the building blocks can be used for logistic activities (Bureau Nieuwe Gracht, 2018). The total project program contains around 3000 residential units, 65000 m<sup>2</sup> office/working space and 15000 m<sup>2</sup> of other facilities, among which a primary school and supermarket. The dwellings at *Croeselaan* will be partly demolished for the park, and partly integrated into the building blocks. At ground floor or -1 level there will be indoor bicycle parking available to stimulate cycling (City of Utrecht, 2017).

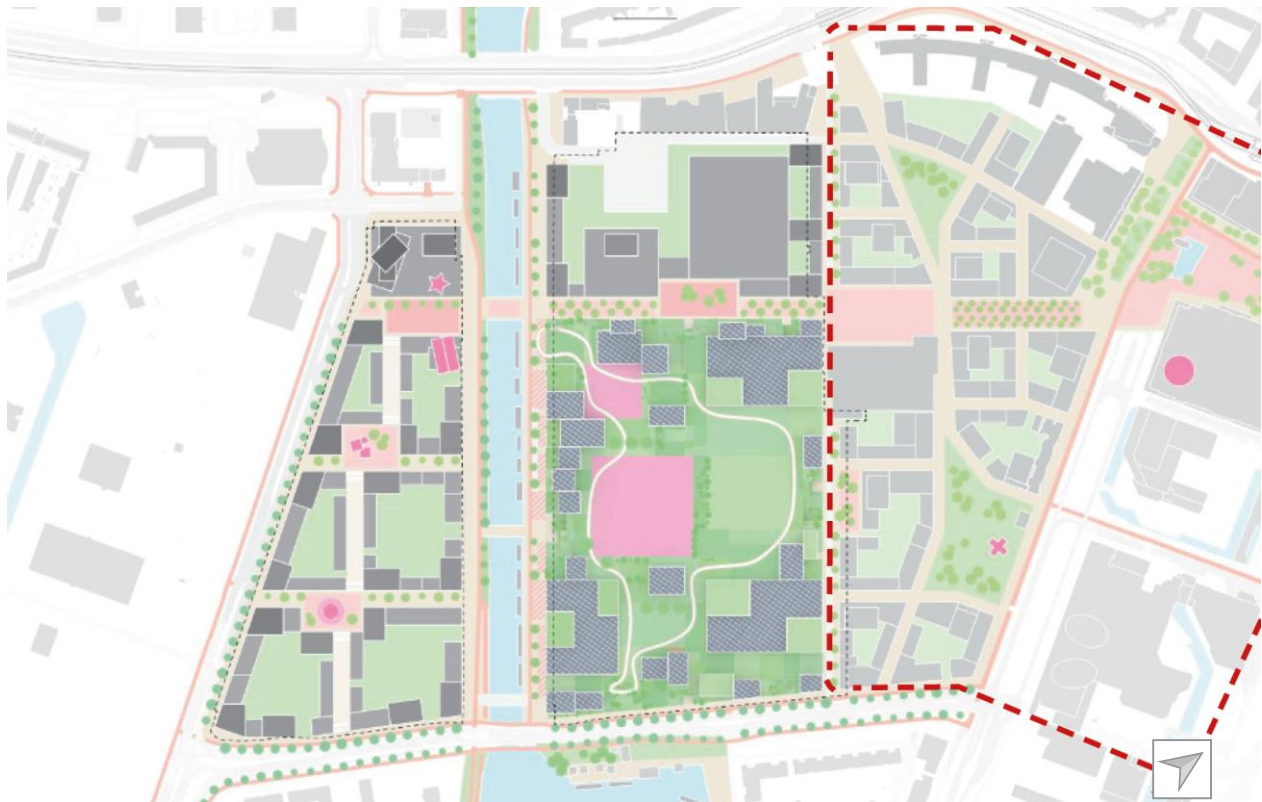


**Figure 4.6:** Conceptual plan Jaarbeursdistrict (and Beurskwartier) (adapted from: *Jaarbeurs*, 2019)

An even larger masterplan is made by the *Jaarbeurs*, which is outside the scope of the network but is expected to also generate a lot of additional traffic. Figure 4.6 shows the conceptual plan to incorporate the *Jaarbeurs* event venue in a complete neighborhood. It will include 240,000 m<sup>2</sup> to 360,000 m<sup>2</sup> of residential space and 123,00 m<sup>2</sup> to 243,000 m<sup>2</sup> of office, commercial and leisure space. *Jaarbeurs* also plans for a public park on top of the new event halls, at around 15 m above ground level (Jaarbeurs, 2019). According to all presented plans, a base and future infrastructure network are modeled.

### 4.1.3. Scenario formulation

New construction projects influence the infrastructure network and traffic volumes in the area. Based on the projects timeline presented in section 4.1.2, two separate networks are built in Vissim:

- **Base network**  
The base network includes all infrastructure and buildings that are already finished and are currently (2021) under construction (see table 4.1). These projects are planned to be delivered in the coming years, thus the time scope of this network is 2022/2023 (figure 4.7a)
- **Future network**  
All currently planned construction projects are included in the future network table 4.2. The completion date for this entire masterplan is unclear, but the future network roughly represents the situation in 2030 (figure 4.7b).



**Figure 4.7:** 3D model and schematic overview of network and of: a) base and b) future network



The infrastructure network can be regarded as the mobility supply, the mobility demand is regulated with vehicle, cyclists and pedestrian inputs. Combinations of supply and demand configurations are considered to be a scenario. The primary distinction of scenarios is made by the base and future network.

Besides the spatial differences between both networks, also the traffic inputs vary. Typically the busiest times of the day are when people travel to their work and back home at weekdays, therefore these peak hours are considered the most interesting periods to simulate. For both the base network and the future network, a scenario of the morning peak hours (AM) and the afternoon/evening peak hours (PM) is simulated. In agreement with many traffic counting datasets, the morning peak is considered to be a two-hour period between 07:00 and 09:00, whereas 16:00 to 18:00 is considered the afternoon peak. In addition to these two inputs, a third input configuration with irregularly large traffic flows is estimated for the future network, representing an event or other situation with a maximal traffic flow in the area. The purpose of simulating this fifth scenario is to discover bottlenecks in an unusually busy situation. The sources and input values for each scenario are presented in [section 4.2](#). The combinations of networks and inputs yield five different scenarios.

One cycling path intersection is selected to conduct additional analysis. For the future network, two spatial variations in the intersection are designed, resulting in six additional scenarios ([table 4.3](#)). These additional scenarios are simulated to analyze the influence on the traffic flow and travel times around this intersection. The selected intersection is located where the main cycling connection from north to south (*Croeselaan*) intersects with the route to the *Moreelse* bridge and *Knoop* bicycle parking (*Rabostraat*). In the future network, the route towards the west (through the parks) is connecting to this intersection as well.



**Figure 4.8:** Intersection spatial variations in future network (none, wider paths & shared space)

The first variation is to widen the paths on all sides of the intersection ([figure 4.8](#)). In the original network, the north-south paths are 2.3 m wide and the east-west paths are 2.0 m wide (per direction). For this spatial variation, the paths are widened to 2.5 m in all directions. This increase in width is made to evaluate if this increases the traffic flow through the intersection. As a second variation, the intersection is transformed into a shared space area together with the surrounding pedestrian paths ([figure 4.8](#)). Cyclists and pedestrians can freely move over this 30mx20m area using informal traffic rules, without having to wait in a queue.

Since the scope of these spatial variation scenarios is much smaller, more extensive analysis can be performed at intersection level. An overview of all scenarios that will be simulated can be seen in [table 4.3](#). To clarify, the inputs in the base network are not identical to the future network but have higher input values as well as additional input links.

**Table 4.3:** Scenario configuration for all 11 scenarios

Network	Variation	Morning peak (AM)	Afternoon peak (PM)	Maximal input (MX)
Base	None	B-AM Scenario	B-PM Scenario	-
Future	None	F-AMa Scenario	F-PMa Scenario	F-MXa Scenario
Future	Wider paths	F-AMb Scenario	F-PMb Scenario	F-MXb Scenario
Future	Shared space	F-AMc Scenario	F-PMc Scenario	F-MXc Scenario

#### 4.1.4. Infrastructure modeling

The majority of network objects is modeled in the Vissim GUI, with the exception of the buildings. In Vissim these are inserted as a *Static 3D model* and thus have no influence on the simulated behavior. Models of buildings in the base and future network are created in Sketchup Pro 2021 ([Trimble, n.d.](#)). The plans and designs presented in [section 4.1.2](#) are used as guidelines to create the buildings, but since for some projects no actual design is available, often illustrative volumes are used for future developments. All other network objects are modeled with Vissim.

The primarily cycling paths and roads for motorized traffic are modeled by links. The motorized links all have the default link behavior type *Urban (motorized)*, the behavior type of cycling paths is calibrated using the findings of [chapter 3](#). In the northern part of the future network, a cycling street is planned ([figure 4.4](#)), for which a separate link behavior type is made. Cyclists behave similar to the cycling paths behavior type. Car behavior is similar to the *Urban (motorized)* behavior type, with some additional rules that allow cars to overtake cyclists on the left. Vehicle inputs are modeled for busses, motorized traffic and cyclists (see [section 4.2](#)). The routes of vehicles and cyclists are modeled with a relative route flow per intersection. In all directions the relative share of vehicles or cyclists is estimated, and remain identical in all scenarios [figure 4.12](#) and [figure 4.16](#)). Motorized traffic has a desired speed distribution of 30 km/h, with the exception of vehicles exiting or entering a parking space zone, there a desired speed decision is modeled that sets their desired speed to 5 km/h or back to 30 km/h. The desired speed distributions for cyclists and e-cyclists presented in [section 3.4.3](#) apply at all links, with the exception of temporal reduced speed areas in turns. To model this the turning speed reduction for different turn radii determined in [section 3.4.4](#) are used.

The walkable area for pedestrians is modeled by areas and links defined as pedestrian area. Obstacles are the areas that cannot be accessed by pedestrians and are often visualized with a 'display type' of bushes, benches or grass. For pedestrians three levels are modeled: the ground level, the *Forum* (at 7.5 m) and a level in between (at 3.5 m) only used around the *Knoop* and *Rabobank* offices. Pedestrians are able to access the different levels by means of stairs and escalators. Since Vissim does not support non-straight stairs, the large stairs at *Jaarbeursplein* are modeled using



straight stairs, surrounded by a static 3D model for representation. Slightly different from reality is the absence of elevators, which are not modeled to decrease computation time and model complexity. The routes of pedestrians are modeled by an Origin-Destination (OD) matrix. The matrix displays all origin and destination areas in the rows and columns each cell then specifies the number of trips going from each origin to each destination (Ordinez et al., 2018). The matrix does not include the route. Pedestrians are assigned the shortest route from their origin to their destination. In the base network, 9 areas are modeled where pedestrians enter or exit the network. In addition, 16 buildings or building blocks are used as pedestrian ODs. In the future network, these are 11 network entry areas and 28 buildings or building blocks. Appendix D shows the complete pedestrian OD matrices.

At most pedestrian areas, the default area behavior type applies. However, if cyclists (modeled as pedestrians) also make use of the area, a shared space area behavior type is modeled. The behavior of pedestrians walking on these areas is still the default. Since the exits of the bicycle parking *Jaarbeursplein* and *Knoop* are both located in a shared space area, these cyclists' inputs are modeled as a pedestrians input. The transition between links and areas for pedestrians is modeled by the script presented in section 3.1.3. Cyclists in the area-based model are kept outside the pedestrian OD matrix and are modeled with routes specific for the shared space area. In the case of the 'shared space' spatial variation, the pedestrian routing decisions are equal to the relative route flows in the original intersection.

The interaction of vehicles, cyclists and pedestrians at intersections is mostly modeled by means of conflict areas and occasionally with priority rules (section 3.1.3). All intersections except the tram crossing are unsignalized. Instead of a regular vehicle input, the trams are modeled with the 'Public transport line' function, where the schedule and occupation can be set (see section 4.2.2). The tram stops, platform edges and waiting areas are modeled to connect to the public transport line, so pedestrians with the tram stop as their destination wait at the platform and board the tram when it arrives. The traffic lights are constantly green for cars, cyclists and pedestrians, except when a tram or bus is arriving. The traffic lights are connected to 'detectors' that signal the arrival of a tram or bus. Then the traffic light turns green for the public transport line and red for the other road users, when the tram drives over the other detector, the signal is set to green again. 3D traffic signals are modeled to connect to the correct signal group. At certain locations 3D traffic signals are added for the visualization of traffic signs, furthermore 3D trees are added for realistic representation of the environment, both have no influence on the behavioral models.

In addition to all network objects for the simulation, also some objects for evaluation are added. Travel time measurement pairs are added to evaluate travel times at certain routes (section 4.3.3). At the intersection used for the spatial variations, a 'node' is specified. Additional analysis on this intersection can be performed because the 'node' registers volumes, queue lengths and delay times in all directions.

The complete network consists of many network objects with their own attributes. Besides the correct placement of all network objects, time had to be spend on fixing errors the simulation showed. For example the parameter settings of crossings and intersections, which in some cases were changed to prevent traffic jams already at low traffic volumes.

## 4.2. Traffic demand estimation

In this section the input values for each scenario are estimated by studying available data for each transportation mode. The general modal split in the region will be evaluated to account for different types of vehicles within one of five transportation modes: tram, bus, private motorized traffic (primarily cars), cyclists and pedestrians. Subsequently the input values of these four transport modes are presented for the various scenarios. Input scenarios were formulated for the morning peak hour (07:00-09:00) and afternoon peak hour (16:00-18:00).

### 4.2.1. Modal split

To estimate the modal split and possible origin and destination of all trips, the 2019 edition of the annual national mobility survey ODiN (*Onderweg in Nederland*) is used. This survey is known as OViN before 2018 (CBS, 2020). A representative sample of the Dutch population of around 53,000 participants is surveyed on the trips they make, including individual, household and trip characteristics. Each trip is assigned a weighing factor based on the participant characteristics. By applying the participant-depended weighing factor to each trip, yearly statistics on the trips of the total population can be calculated. The highest accuracy level for the origin and destination of each trip is the numerical part of the postal code, also known as PC4. As visible in figure 4.9, the case study area is part of the PC4 area '3521',

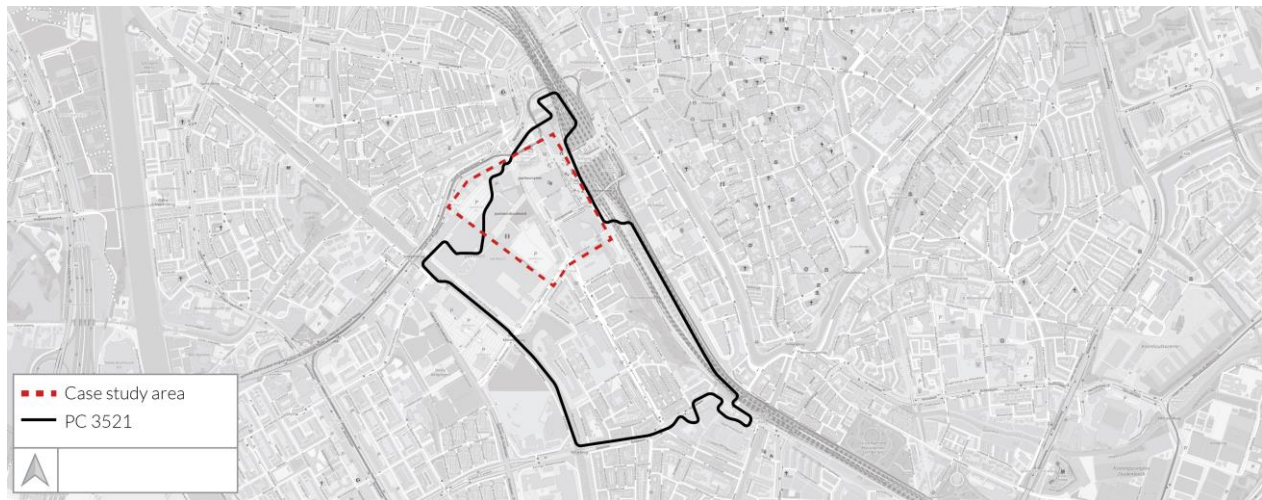


**Figure 4.9:** Case study area and PC4 area in Utrecht

The representativeness of the survey becomes less when analyzing with a higher aggregation level, for example analyzing the e-bicycle use in only one PC4 area yields unreliable results (CBS, 2020). Therefore also the modal split in the complete dataset and the city of Utrecht was analyzed. From the total data file (.csv), trips are extracted by location and transport mode using MS Excel formulas. Trips with origin or destination in Utrecht and PC4 area 3521 are considered, each trip is multiplied with its weighing factor to calculate the total number of trips in a year. Grouping the number of trips in categories results in the graph presented in figure 4.10.

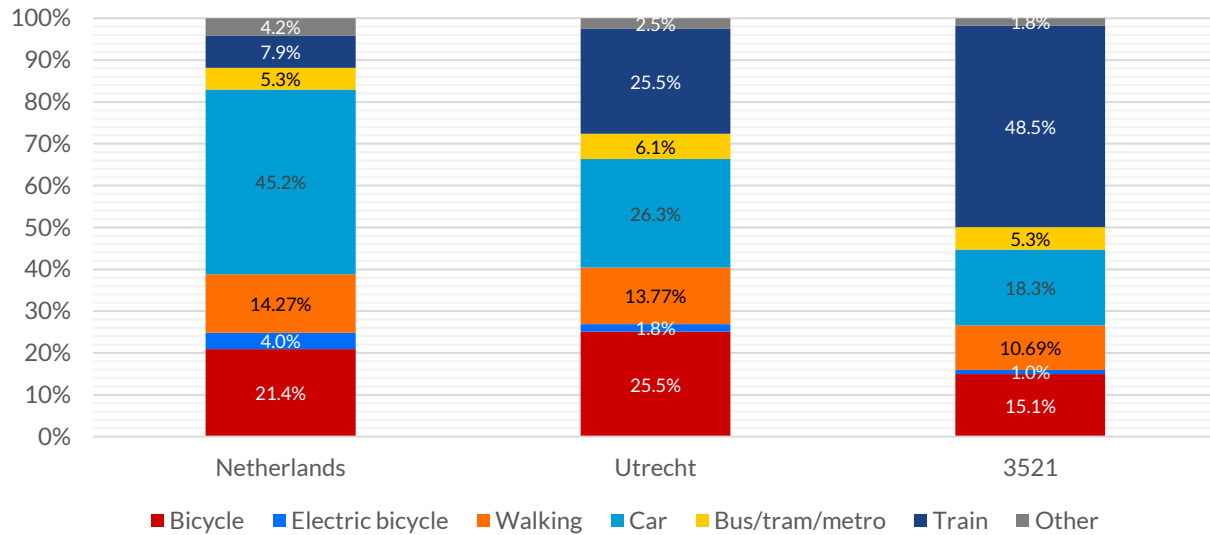


**Figure 4.10:** Modal split in Netherlands, Utrecht and PC4 area 3521 (CBS, 2020)

Vehicle types that show a relatively low share in the total trips are grouped in the category 'other', for example: campers, taxis, tractors, mobility scooters, skates, etc. From figure 4.10, it is observed that the percentage of car trips is much higher in the rest of the Netherlands than in Utrecht. The share of train trips is especially high in the investigated PC4 area. The lower percentage of cyclists in the PC4 area is probably due to the high number of train trips. Statistics from the ODiN trip data show a large majority of motorized road traffic trips is made with a car, but some other vehicle types that are also considered in the simulation model. In figure 4.10, the mode 'car' contains various other vehicle types. To create a more heterogeneous traffic composition, trucks, vans and motorcycles are also included in the vehicle inputs for cars (table 4.4). Important to note is that work-related trips with trucks (almost all freight transport) are not considered in the ODiN survey, making trucks underrepresented in the total traffic composition (CBS, 2020). The share of trucks is measured by considering traffic counting data from loop detectors at 72 locations in Utrecht (HIG, 2015). On weekdays, these locations on average showed 2.8% of trucks (medium heavy and heavy transport). Table 4.4 shows the composition of vehicle types from different sources, the rounded percentages used in simulation are calculated by taking the average and adjust to a sum of 100%. Vans use the same behavioral model as cars and default Vissim behavioral models are used to simulate the behavior of trucks and motorcycles. For purely visual purposes, a color distribution for the car input is created according to Oostvogels (2018).

**Table 4.4:** Composition of motorized road traffic

	Vissim default (PTV Group, 2020)	ODiN, Utrecht (CBS, 2020)	Utrecht traffic counting (HIG, 2015)	Used in simulation
<b>Cars</b>	98%	94.6%	96.6%**	<b>93.0%</b>
<b>Vans</b>	-	3.7%		<b>3.5%</b>
<b>Trucks</b>	2%	0.5%*	2.8%	<b>2.5%</b>
<b>Motorcycles</b>	-	1.3%	0.6%	<b>1.0%</b>

\* Excluding professional transport

\*\* Cars and light vans

Regarding the composition of bicycles, the ratio between regular bicycles and e-bicycles, a lower percentage of e-bicycle trips is observed in Utrecht compared to the rest of the country (CBS, 2020). This can be explained by the higher popularity of e-bicycles in rural areas. E-bicycles are also more vulnerable to damage and theft when parking on-street in a large city like Utrecht. Unfortunately, little to no traffic counting data was found on the percentage of different cyclists types. A dataset of bicycle counting on 7 locations in Utrecht (Het Verkeershuis, 2014) distinguished between cyclists, race cyclists, e-cyclists and cargo cyclists. However, the single day of measurement in September 2014 showed unrealistically low values for the other types of cyclists. Furthermore, all measurement locations fall outside of the case study area. To estimate the ratio used for simulation, a weighted average is calculated by considering the country ratio for 50%. Resulting in a rounded ratio where one in ten bicycles is an e-bicycle (table 4.5).

**Table 4.5:** Composition of bicycle traffic

	ODiN, Netherlands (CBS, 2020)	ODiN, Utrecht (CBS, 2020)	Used in simulation
<b>Cyclists</b>	84.1%	93.4%	<b>90%</b>
<b>E-cyclists</b>	15.9%	6.6%	<b>10%</b>

Initially it was believed the ODiN data could also be used to estimate traffic in different directions. However, only 371 trips originate or end in PC4 area 3521, which is not a sufficient amount to analyze the direction of trips for different transport modes, thus other sources were used for the estimation of traffic flows.

#### 4.2.2. Public transport traffic

The tram station *Jaarbeursplein* is part of a southbound tram service to the town Nieuwegein. The tram station *Jaarbeursplein* is recently connected to the tram station on the west side of the train tracks, now the terminal station of this tram service as well as the tram to *Utrecht Science Park* (Line 22). These two tram lines are connected by a public transport bridge identified as the *HOV bridge*, High quality Public Transport (*Hoogwaardig Openbaar Vervoer*) (City of Utrecht, 2020c). The tram service 60/61 is a shared line until *Nieuwegein Stadscentrum*, where the line splits. Line 60 continues to *Nieuwegein Zuid* and line 61 splits of to *IJsselstein*. In the morning and afternoon peak hour, both of these lines have an operation frequency of 4 trams per hour, resulting in 8 trams per hour in the direction of Nieuwegein and 8 trams per hour in the direction of the city center via the *HOV bridge* (Province of Utrecht, 2020; U-OV, n.d.).

The input from the *HOV bridge* and the *Graadt van Roggenweg* is therefore 8 trams per hour. The trams currently in operation are the 41.2 m *Urbos100* trams, with a total capacity of 277 passengers per tram (CAF, 2020). The assumption is made that a considerable share of passengers is alighting when the tram is originating from *Nieuwegein* (100 passengers) and only a small portion of the total capacity alights when the tram is originating from the starting station on the west side of the tracks (20 passengers).

The *HOV track* also is an important route for busses, since it is one of three roads leading to the main bus station of Utrecht, integrated in *Utrecht Centraal*. From here, busses arrive and leave in the direction of the *HOV bridge* (north and east), *Graadt van Roggenweg* (west) and *Dichtersbaan/Valeriusbaan* (south). [Table 4.6](#) presents an overview of the direction and frequency of all bus lines traversing through the network area. Some lines terminate at the central bus station, others make a stop and then continue.

**Table 4.6:** Bus line frequency through network (*U-OV, 2021; OpenStreetMap, n.d.*)

	6 times/hour	4 times/hour	2 times/hour	Total/hour
<b>Graadt van Roggenweg – Utrecht Centraal</b>	Line 387	-	Lines 5,400, 401	12
<b>Graadt van Roggenweg – Utrecht Centraal - HOV bridge</b>	Line 7	Line 4	-	10
<b>HOV bridge – Utrecht Centraal</b>	Line 50	Line 38	Lines 12, 55, 120	16
<b>HOV bridge – Utrecht Centraal – HOV bridge</b>	Line 73	-	-	6
<b>HOV bridge – Utrecht Centraal – Dichtersbaan/Valeriusbaan</b>	Lines 1, 8, 74, 77	Line 6	-	28

The bus line frequencies shown in [table 4.6](#) are used to determine the volume of bus traffic on various routes. In practice, all busses stop at the central bus station therefore the route *Graadt van Roggenweg – HOV bridge* is only used by trams. Adding up the line frequencies yields a total of 22 busses/hour from *Graadt van Roggenweg* to *Utrecht Centraal*, 66 busses/hour from *HOV bridge* to *Utrecht Centraal*. Resulting in 88 busses/hour from *Utrecht Centraal*, of which three quarters leave via the *HOV bridge* (66/h) and the remaining quarter (22/h) over the *Graadt van Roggenweg*. The boarding and alighting volumes of bus passengers are irrelevant since no bus stops are located in the network.

### 4.2.3. Motorized traffic

To quantify the inputs and routes of motorized traffic, traffic data from the City of Utrecht and other commercial parties was collected. Traffic data from week 2 until week 11 of 2020 was collected from induction loops of traffic control installations ([City of Utrecht, 2020b](#)). This was just before the travel restrictions imposed as a result of the COVID-19 pandemic. From these ten weeks, the average counting value at weekdays (Monday to Friday) from 07:00 to 09:00 for AM input and 16:00 – 18:00 for PM input was calculated. [Figure 4.11](#) shows the locations where data was collected, the reliability of this data is 10%-30% according to City of Utrecht ([2020b](#)).

Another primary source of motorized traffic data provided an estimation of traffic flows in 2030. This research was performed based on a 'capacity tool' by which the future traffic flow in the south of the case study area was predicted ([Royal HaskoningDHV, 2018](#)). Since 2030 is also the time scope of the future network scenarios, this is particularly insightful data. This research provided the hourly flow of vehicles during the morning and afternoon peak hours. This data is included in the schematic overview in [figure 4.11](#).

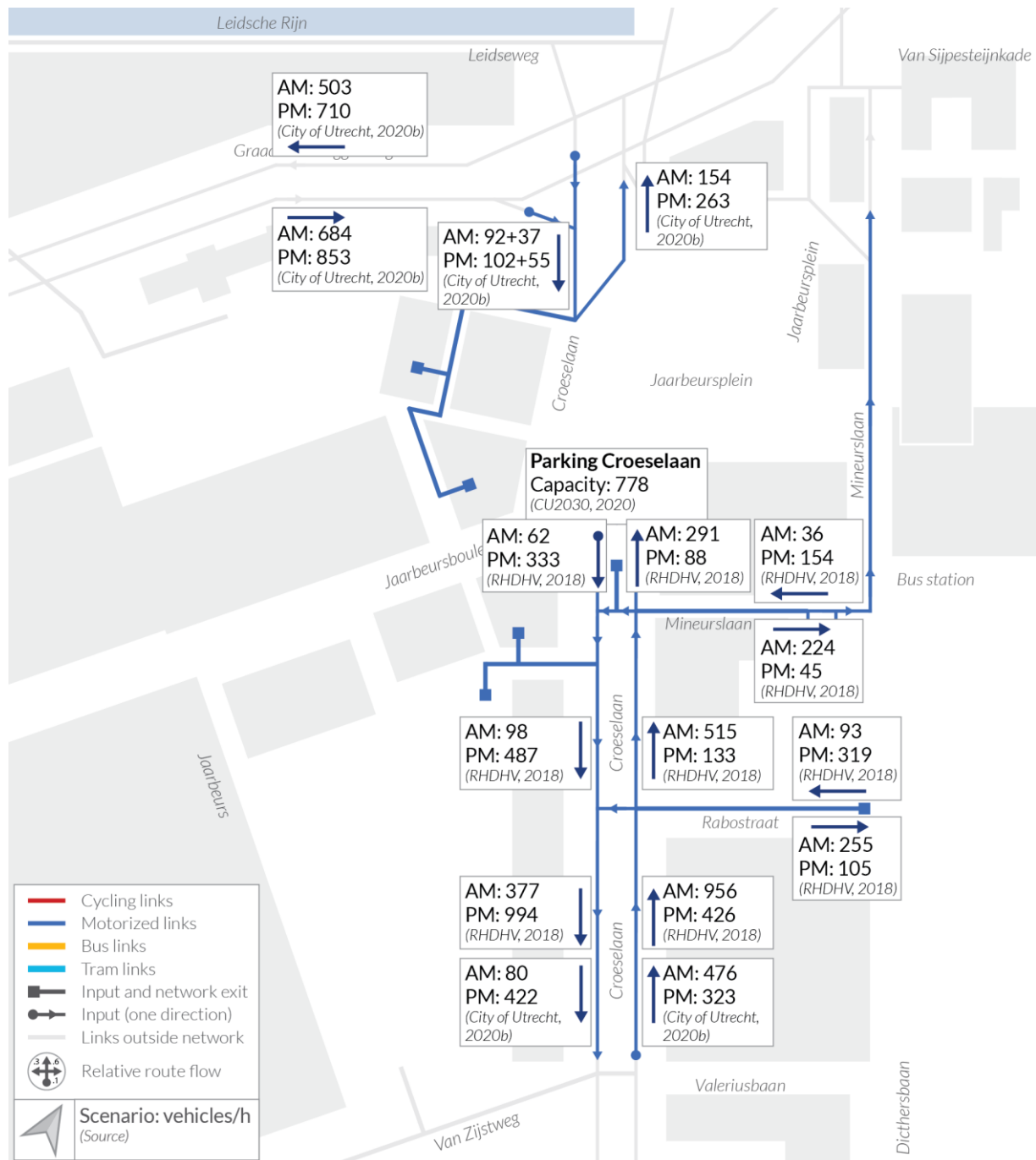


**Figure 4.11:** Schematic overview of available car traffic data

Based on figure 4.11, the traffic inputs and relative route flows for the base and future network are estimated. During this process, many assumptions had to be made but the outcomes sufficiently reflect motorized traffic in the morning and afternoon peak hours. For the maximal (MX) input, the maximal of either the AM or PM was used. The purpose of this is to leave the motorized inputs approximately the same, so more conclusions can be drawn on the cyclist input changes. Figure 4.12 shows how the collected data is translated into inputs and relative route flows for AM/PM inputs in the base network and AM, PM and MX inputs for the future network. Appendix B shows enlarged versions of these overviews.



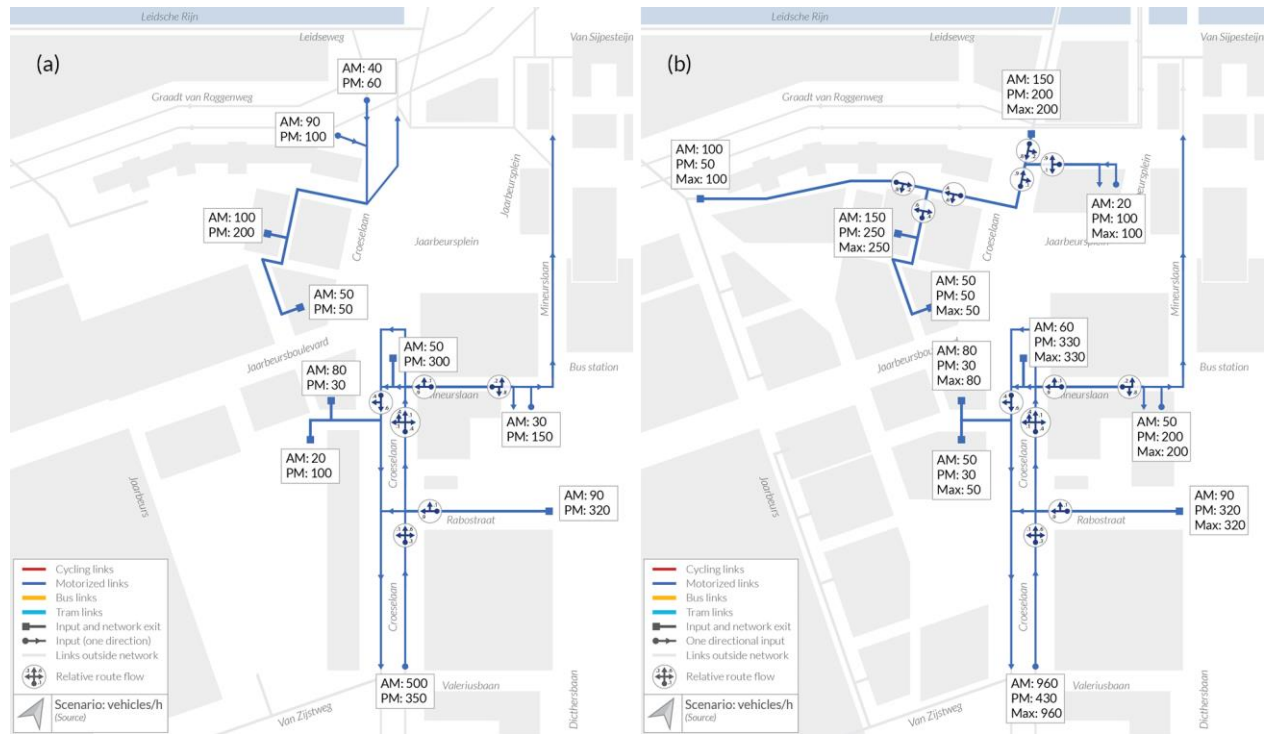


**Figure 4.12:** Input values and relative route flow for motorized traffic in: a) base and b) future network

#### 4.2.4. Bicycle traffic

For the data collection of bicycle traffic, the primary source is derived from bicycle counting around *Westplein* in 2018 (NDC, 2018). Over the course of two weeks in September 2018, temporary counting tubes were installed to count in both directions at four useful locations in the case study area. The average flows at working days from 07:00 to 09:00 and 16:00 to 18:00 are shown in figure 4.13. The same research also involved visual counting at one useful location (*Jaarbeursplein northeast*) during morning and afternoon peak hours (NDC, 2018). From this data, the average of two counting days (11 and 13 September 2018) is included in the available traffic data overview in figure 4.13.

The source using permanent counting for motorized traffic also showed one location of cyclists counting inside the case study area (City of Utrecht, 2020b). From this data, the same period (week 2 to week 11) in 2020 was used to calculate the average during work day peak hours (figure 4.13).

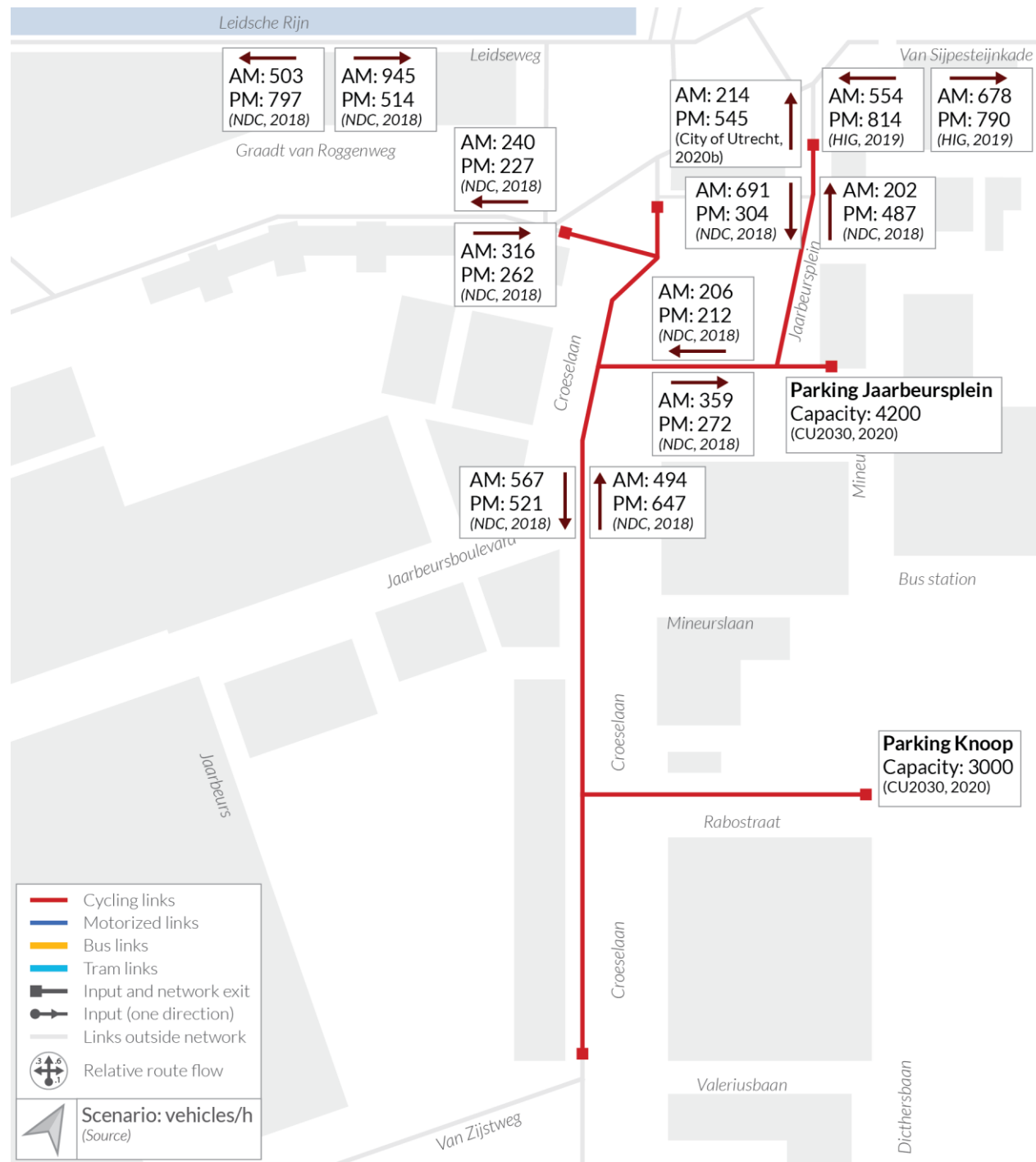


**Figure 4.13:** Schematic overview of available bicycle traffic data

Data from 2019 at a couple of permanent bicycle counting locations in Utrecht was also collected (HIG, 2019). These measurements unfortunately were not executed the case study area. For reference, the average flow for the counting location *Van Sijpesteijnkade* is added to the overview in [figure 4.13](#). However, this counting data proved to have some insightful information on the daily and yearly variation of cyclists in Utrecht (HIG, 2019). [Figure 4.14](#) shows the cyclist flow in both directions over the year at several locations in Utrecht. From these values the conclusion can be

drawn that February, March and November represent the yearly average. During peak of winter (January), an average 10% decrease from the average is observed. The spring and summer show a 5%-10% increase from the average, with the exception of July and August when holidays cause the flow to be around 10% below average. These insights can be useful when comparing datasets from different seasons. Figure 4.15 visualizes the average flow in both directions during one day for the same locations in Utrecht. This data illustrates that from the total daily traffic flow, 19% is observed during the morning peak (07:00-09:00) and 20% during the afternoon peak (16:00-18:00). From this observation, the conclusion is drawn that 10% of a daily flow is the hourly flow during a peak hour.

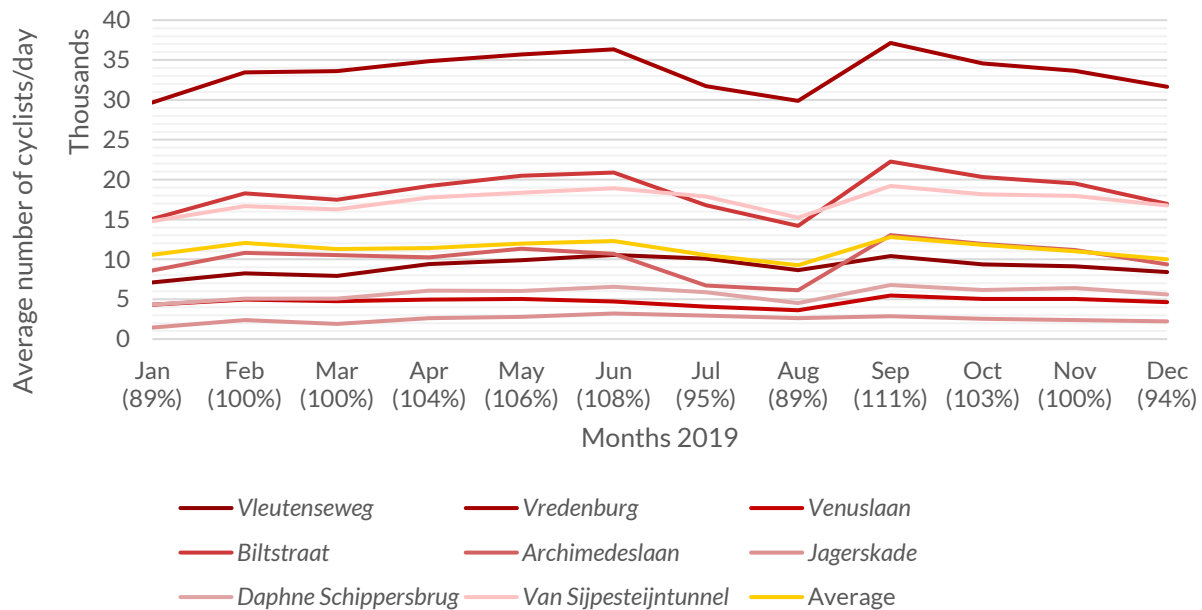


**Figure 4.14:** Average cycling traffic over the year for several counting locations (HIG, 2019)

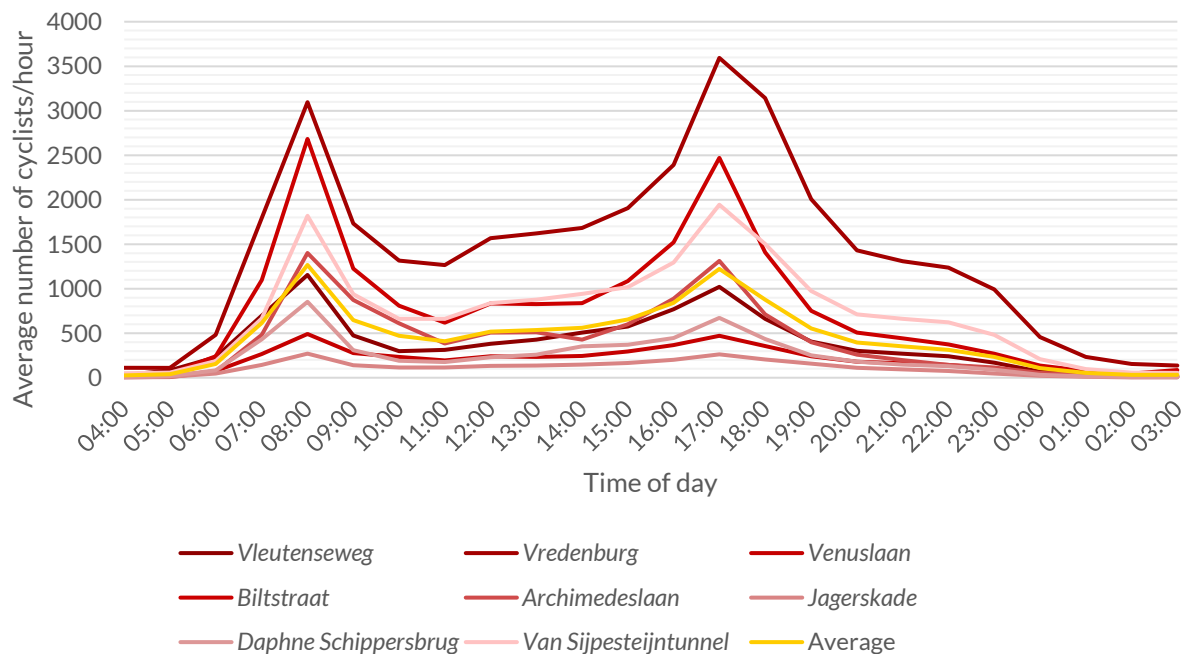


**Figure 4.15:** Cycling traffic over the day for several counting locations (HIG, 2019)

Besides the collected traffic data, additional estimations had to be made for the cyclists inputs. The input from both bicycle parking locations is estimated according to the capacity. The *Jaarbeursplein* facility has 4200 parking spaces of which half is estimated to change daily. By using the conclusions drawn from figure 4.15, 10% of the daily total is traveling during one peak hour. Corresponding to 210 cyclists per hour that exit and enter the bicycle parking. The same estimation for the *Knoop* bicycle parking, yields 150 cyclists/hour. Both people working in the area and commuters taking the train to another city arrive at the parking facilities in the morning. The network input from the bicycle parking (exiting) in the morning therefore is expected to be around one-third of the input value in the afternoon. For the MX inputs in the future network, input values around 50% higher than the AM and PM inputs are roughly estimated. Appendix C shows the enlarged version of the input and route flows overview in figure 4.16.

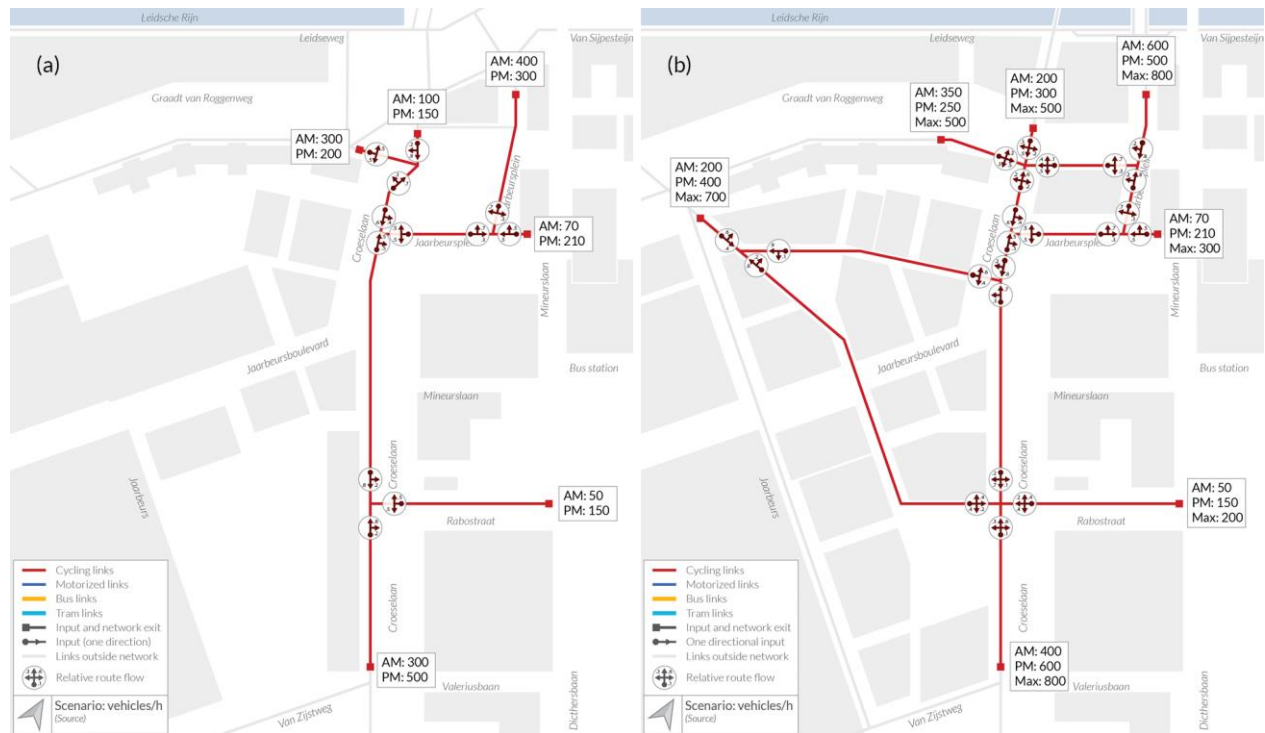


**Figure 4.16:** Input values and relative route flow for cycling traffic in: a) base and b) future network

#### 4.2.5. Pedestrian traffic

Pedestrian traffic is rare to find, since counting has to be done manually or with advanced camera technology. No traffic pedestrian traffic data from the area was found. In order to simulate the presence of pedestrians, a pedestrian OD matrix was created based on very rough estimations. Appendix D shows the complete pedestrian OD matrices for both networks. In the base network, ten areas are identified as areas to enter or exit the network. From and to these areas, 10 pedestrians/h were estimated. Among these ten areas are the waiting platform of the tram to Nieuwegein the entrance of *Utrecht Centraal*. Since many pedestrians in the area have their origin or destination at *Utrecht Centraal*, an input value of 50 pedestrians/h was estimated from *Utrecht Centraal* to the other nine areas and 50 pedestrians/h from the other nine areas to *Utrecht Centraal*. Resulting in an hourly input rate of 130 pedestrians per area. In addition, 16 buildings or building

blocks are included in the OD matrix with 20 pedestrians/hour from and to *Utrecht Centraal*. All 25 origin areas in the base network have a total input of 2130 pedestrians/hour. The arriving tram passengers are separately modeled (section 4.2.2) and are distributed among the exit areas. A similar estimation technique is applied to the future network, with 11 network entry/exit areas and 28 buildings or building blocks. Based on this, the future network sees a total input of 3170 pedestrians/hour. The pedestrian inputs are equal for all simulations, firstly because leaving these variables constant would more clearly show the influence of changing cyclist inputs. Also, the estimations are not data-based so it would be very fabricated to estimate different scenarios as well.

This section presented the results of the traffic demand estimation research phase. In this phase the case study area was analyzed and data sources were combined to estimate the traffic inputs and routes for the different scenarios. Appendix B and Appendix C visualize the locations of all inputs and the relative route flows for each intersection. An overview of the estimated hourly input values presented in this section (excluding the pedestrian OD matrices) is shown in table 4.7.

**Table 4.7:** Vehicle inputs per hour for all scenarios

	Input name	B-AM	B-PM	F-AM	F-PM	F-MX
Motorized	M-Croeselaan South	500	350	960	430	960
	M-Graadt van Roggenweg North*	90	100	100	100	100
	M-Westplein*	40	60	50	100	100
	M-Graadt van Roggenweg West**	0	0	100	50	100
	M-Rabostraat	90	320	90	320	320
	M-Hojel Center***	100	200	150	250	250
	M-Galaxy Tower	50	50	50	50	50
	M-Jaarbeurs P3 ***	20	100	50	30	50
	M-Parking Croeselaan	50	300	60	330	330
	M-Wonderwoods	80	30	80	50	80
	M-Parking Mineurslaan	30	150	50	200	200
	M-Jaarbeursplein Building**	0	0	20	100	100
Busses	B-Graad van Roggenweg North	22	22	22	22	22
	B-Busstation	88	88	88	88	88
	B-HOV Bridge	66	66	66	66	66
Cyclists	C-Croeselaan north	100	150	200	300	500
	C-Jaarbeursplein northeast	400	300	600	500	800
	C-Graadt van Roggenweg north	300	200	350	250	500
	C-Croeselaan south	300	500	400	600	800
	C-Graadt van Roggenweg west**	0	0	200	400	700
	C-Parking Jaarbeursplein	70	210	70	210	300
	C-Parking Knoop	50	150	50	150	200

\* Become same input link in future network

\*\* Only exists in future network

\*\*\* Becomes an input of Beurskwartier

### 4.3. Scenario simulation results

With the infrastructure network and input values specified for all scenarios, simulations are run. As stated before, all scenarios are run for two hours. Table 4.8 provides an overview of the scenarios.

**Table 4.8:** Overview of simulation scenarios

Scenario	Network	Input	Spatial variation
<i>B-AM</i>	Base network	Morning peak (AM)	-
<i>B-PM</i>		Afternoon peak (PM)	-
<i>F-AMa</i> <i>F-AMb</i> <i>F-AMc</i>	Future network	Morning peak (AM)	a: none b: Wider paths c: Shared space
<i>F-PMa</i> <i>F-PMb</i> <i>F-PMc</i>		Afternoon peak (PM)	a: none b: Wider paths c: Shared space
<i>F-MXa</i> <i>F-MXb</i> <i>F-MXc</i>		Event peak (Max)	a: none b: Wider paths c: Shared space

Vissim offers the possibility of turning on and off data collection for different attributes. The attributes that are evaluated are: link segments (1 m), pedestrian grid cells (1mx1m), nodes (with one node specified), vehicle travel times and pedestrian travel times. For all attribute measurements, a data collection time interval of 5 min (300 seconds) is chosen, this way the progression of the simulation can be tracked with some detail and the output data has a fairly high resolution. These additional evaluations have a large influence on the computation time as well.

A couple of measurement evaluations are conducted to compare the scenarios. Barceló et al. (2010) reports these evaluation units to be Measures Of Effectiveness (MOEs). They state some typical MOEs for network evaluation: delay, travel time, stops, queues, speed and density (Barceló et al., 2010). Wu et al. (2013) also mentions delay as a common method to evaluate a network. The units that will be used to evaluate the effectiveness of the network are travel time, relative delay and average speed. The relative delay is defined as the link delay time share of the total travel time, a delay percentage (PTV Group, 2020). For the highlighted analysis of the specific intersection, also queue length, stops, delay time and density are evaluated.

The data is extracted in two different forms, primarily by copying the data tables into MS Excel for further processing. But also by automatically extracting visual information for each time interval (5 min). To achieve this, a custom script was written to automatically take a screenshot at multiple locations, with two different graphic presentation layouts, being the average speed and relative delay during that time interval. By applying this method the relative delay and speed can be easily evaluated over the course of the simulation, since the data is directly visualized within the simulation environment. It can also be used to quickly check the behavioral performance of the



model, without constantly watching the simulation. Similar to the shared space transition script (introduced in [section 3.1.3](#)), a '.py' file is loaded into Vissim and executed every 300 seconds. [Appendix F](#) shows the script in full.

#### 4.3.1. General simulation performance

After labor-intensive troubleshooting in the network, the overall performance of the simulation is satisfactory. All input vehicles, cyclists and pedestrians were able to enter and exit the network. With the exception of the maximal (MX) scenarios, where the high traffic volumes at some point causes traffic jams that quickly spread around the entire network. Road users block each other and the whole network gradually reaches a standstill. When the traffic jams reach the network entry, the inputs could not be completed at these locations. After extensive efforts to prevent a total gridlock, the situation is accepted since this eventually only occurred near the end of the MX scenarios simulations. The blockage typically originates at the main intersection at *Jaarbeursplein*, when pedestrians were alighting from the arriving tram. Another small issue occurs at the Croeselaan input, occasionally vehicles that turn right at the *Rabostraat* slow down the incoming vehicles, if many cars in a row want to make this turn, the queue can extend to the network entry point. Then a small number of cars is unable to enter the network. Often this is quickly resolved at does not influence the overall performance of the network.



**Figure 4.17:** Pedestrian density (scenario F-PMa)

This research focusses primarily on cyclists and it is therefore logical to focus the analysis on the cyclists output data as well. Public transport, motorized traffic and pedestrians have an influence on the traffic situation, but the resulting outcomes are not evaluated. Concentrating on cyclists makes the results more clear and comparable for the goal of this research. The City of Utrecht also qualifies motorized traffic as a subordinate traffic flow in this area, where additional waiting times for cars are acceptable if traffic jams do not transfer to surrounding intersections ([City of Utrecht, 2020d](#)).



Since the pedestrian OD-matrix does not change for scenarios with the same network, the pedestrians will walk on roughly the same routes. Still it is possible to visualize the movement of pedestrians, to identify busy locations. [Figure 4.17](#) shows the key routes pedestrians choose to walk on, with the busiest area around *Utrecht Centraal*.

The locations where pedestrians have the most influence on the traffic flow in the network are the crossings around the tram station and the main route from *Utrecht Centraal* to the *Jaarbeurs*, where a zebra crossing indicates pedestrians have the right of way over cyclists. Also the shared space area in front of the *Jaarbeursplein* bicycle parking should receive extra attention. Since the entrance of the bicycle parking is so close to one of two escalators used by pedestrians to get onto the *Forum* from *Jaarbeursplein*, cyclists and pedestrians hinder each other at this location. Cyclists need to considerably decrease their speed to prevent accidents, which is acceptable since this is the start or end of their trip but could have been solved by having more distance between the parking entrance and escalator.

#### 4.3.2. Network evaluation

Valuable quantities to evaluate the overall performance of the network and compare the different scenarios are speed, density, flow and delay. The automatically extracted visualizations (by executing script in [Appendix F](#) during the simulation) contain the speed and relative delay (delay time as percentage of total travel time) of cyclists for each time interval. For three different viewpoints, this yields 144 images per scenario, [figure 4.18](#) shows one of these images. Being able to dynamically access visualizations like [figure 4.18](#) in an interactive platform, can be insightful to predict and identify bottlenecks at different times during the simulation.

07:40



**Figure 4.18:** Full network average speed in F-AMa scenario (07:35 to 07:40)

In this report it is not possible to show all images with the 5-minute time interval. To present the results in static images, [figure 4.19](#) shows the overall average speed during the simulations for future network main scenarios (without spatial variation).



**Figure 4.19:** Average speed during simulations in future network

Clearly visible in all scenarios are the lower average speeds around intersections, as well as straight cycling paths where the average speed is around the average desired speed of 19.43 km/h (see 3.4.3 for the validation of desired speed). The most interesting difference between the scenarios is a generally lower speed in the afternoon scenario than in the morning scenario. This can be explained by the higher input values in the afternoon scenario. Logically the maximum scenario therefore shows the lowest average speeds, especially at the northeast crossing at *Jaarbeursplein* and the southern intersection at *Croeselaan*. The average speed is lower when approaching the intersection, cyclists leaving the intersection are showing to quickly reach a higher average speed. Instead of visualizing the average speed, the relative delay can also distinguish problem areas in the network (see figure 4.20).



**Figure 4.20:** Jaarbeursplein average relative delay in F-PMa scenario (16:35 to 16:40)

Figure 4.21 shows an example of the relative delays for the future network, zoomed at *Jaarbeursplein*. To compare the complete simulation time among scenarios, figure 4.21 shows the average for the three main future network scenarios. Inspecting figure 4.21 across all three



scenarios makes it clearer that the most cycling delays occur when approaching the north intersection where also cars can enter *Jaarbeursplein*. The similar pattern in of link segments in the speed and delay images suggests a very strong relationship between these variables.

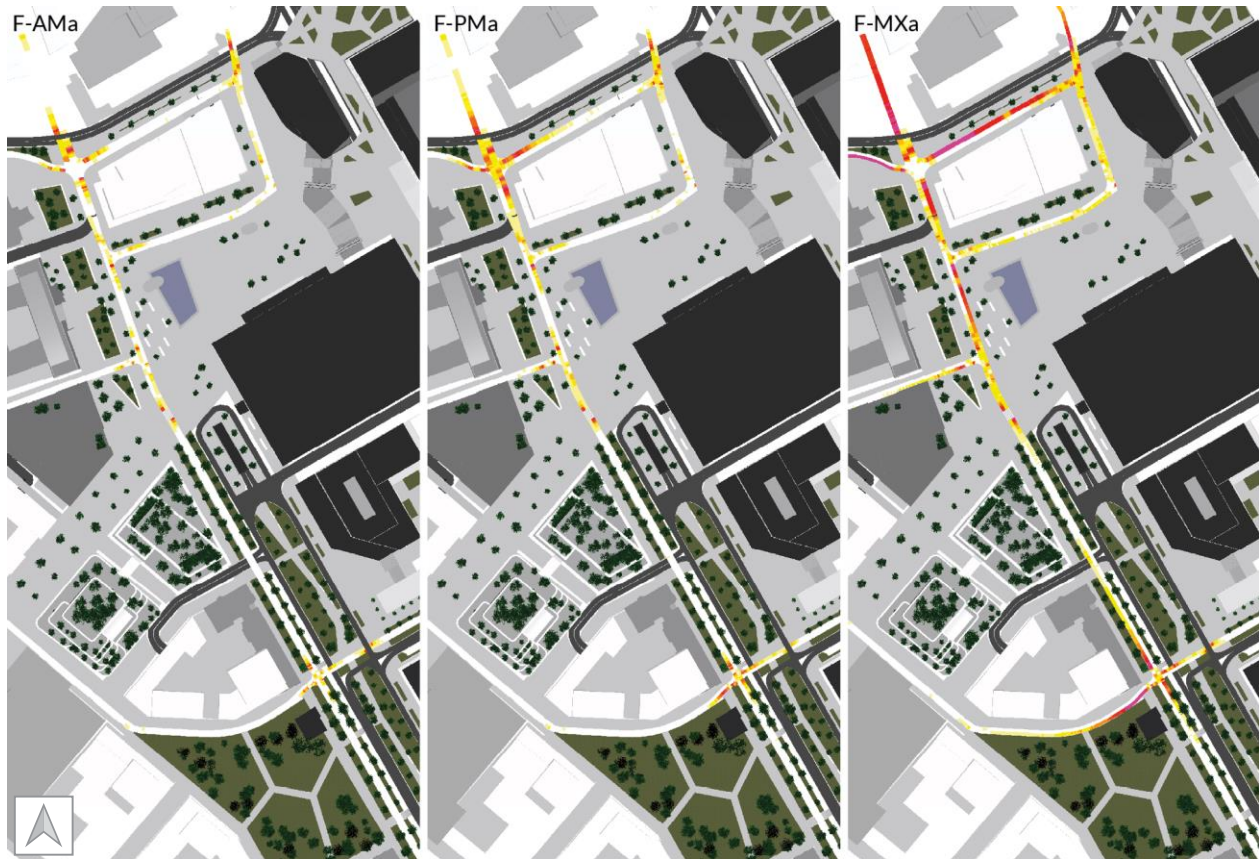


**Figure 4.21:** Average relative delays during simulations in future network

The data aggregated in segments of 1.0 m and time intervals of 300 s is further analyzed by extracting data from *Jaarbeursplein* (at the pedestrian zebra crossing) towards the south (leaving at *Croeselaan*), this link thus also crosses the intersection transformed in the variation scenarios. Data from this centrally located link is used to test statistical relationships between variables and compare among scenarios. For example the speed-density relationship is a common outcome to compare in behavioral models (Huang et al., 2017). From 9120 measurements per scenario, the speed, density, flow and relative delay are all included for testing statistical relations. To evaluate if the width of the path influences these relationships, scenarios with the 'wider paths' spatial variation are also considered (F-AMb, F-PMb and F-MXb). The strength of the linear relationship between two variables can be measured with Pearson's correlation coefficient. Pearson's correlation assumes a linear relationship. If no significant linear relation is found, the Spearman  $\rho$  correlation test is executed to account for non-linear relationships as well. The Spearman coefficient uses rank-ordered variables instead of the absolute data values used to determine the Pearson coefficient. This test assess how well the relationship can be described using a monotonic function (Ramzai, 2020). Table 4.9 provides an overview of statistical correlation tests for combinations of speed (km/h), density (cyclists/km), flow (cyclists/h) and relative delay (%). Values greater than 0.6 are considered strong positive relations and values below -0.6 strong negative relations. The

strongest linear relations across all scenarios are speed-density, speed-delay and density-delay. Flow does not show significant linear relations, however, the density-flow relationship proves to have a statistically significant non-linear relation, with high values of Spearman's  $\rho$ . The statistically strong relationships are visualized by scatterplots in [figure 4.22](#) till [figure 4.25](#) for the three main future scenarios (without variation).

**Table 4.9:** Pearson's and Spearman's correlations between variables over different scenarios

		F-AMa	F-AMb	F-PMa	F-PMb	F-MXa	F-MXb
<b>Speed-Density</b>	Pearson's r	-.655	-.641	-.636	-.584	-.804	-.649
	Spearman's $\rho$	-.894	-.887	-.845	-.850	-.771	-.922
<b>Speed-Delay</b>	Pearson's r	-.785	-.779	-.816	-.802	-.953	-.854
	Spearman's $\rho$	-.091	-.155	-.164	.017	-.194	-.148
<b>Speed-Flow</b>	Pearson's r	-.043	-.104	-.060	-.007	-.039	-.017
	Spearman's $\rho$	.353	.347	.248	.238	.144	.279
<b>Density-Delay</b>	Pearson's r	.747	.730	.737	.707	.858	.786
	Spearman's $\rho$	.894	.887	.845	.850	.771	.922
<b>Density-Flow</b>	Pearson's r	.137	.174	.084	.089	.073	.194
	Spearman's $\rho$	.326	.392	.313	.205	.211	.444

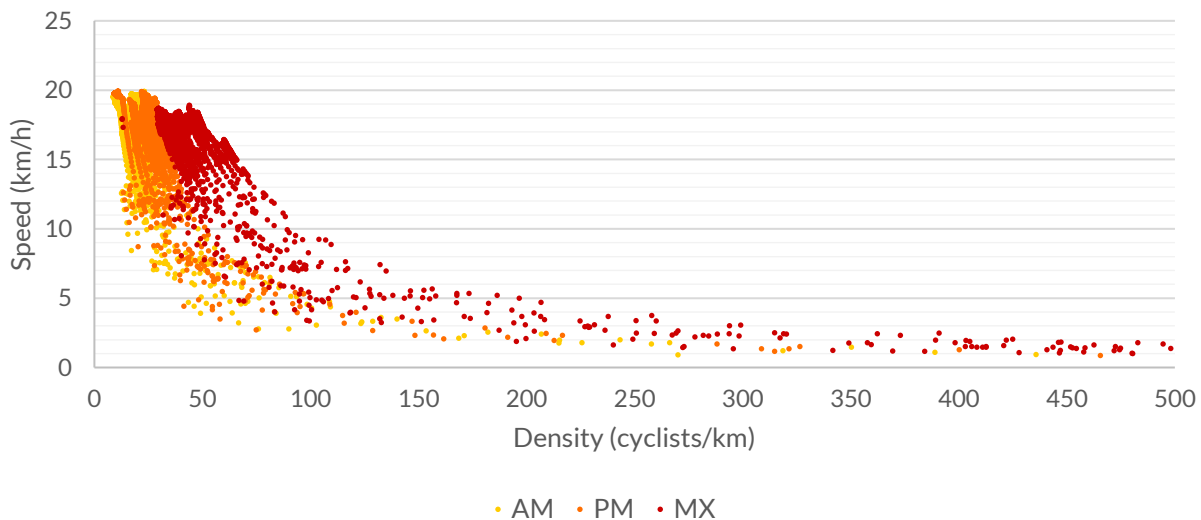


**Figure 4.22:** Speed-density relation for main future scenarios

[Figure 4.22](#) presents higher densities for scenarios with higher input values. Also the measured speeds are lower in the PM than AM scenario and even lower in the MX scenario, corresponding to the findings from [figure 4.19](#). What this figure also tells is that an increase in density causes a rapid drop in speed, until around 100 cyclists/km, then the average speed is stabilizing between 0 km/h to 5 km/h. Worth mentioning is that the density measurement does not consider the width of the cycling path, only the number of cyclists per km.

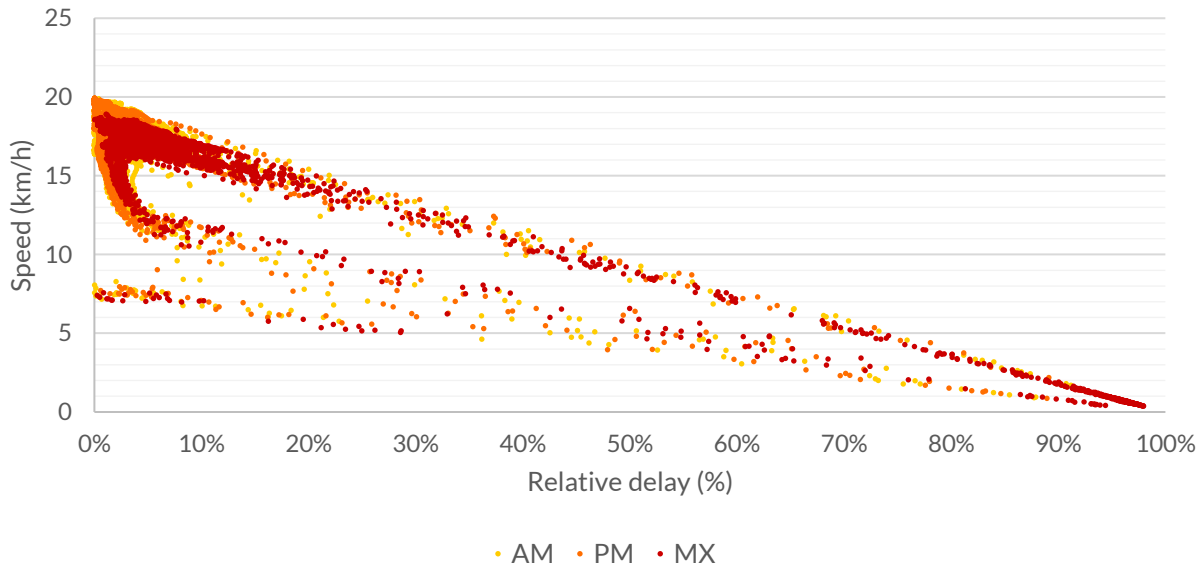


**Figure 4.23:** Speed-delay relation for main future scenarios

Figure 4.23 clearly shows the tested negative linear relation between speed and delay, with the main trend from the upper left corner towards the bottom right. A trend where the speed lowers but the delay does not increase immediately can also be observed, this might be due to cyclists leaving an intersection and still needing to speed up, with is not recognized as delay. The graph shows a very similar pattern for all scenarios, but Pearson's  $r$  in table 4.9 reveals that the relationship is stronger for higher input values. Meaning a low speed leads to more delays for the MX scenario, than a lower speed in the AM scenario. Contrarily, a delay in the MX scenario leads to slower speeds more quickly than in the AM scenario. The causality between the variables remains unclear, however it seems more logical that the delay is caused by a low speed.

The density is plotted against the delay in figure 4.24, were also a clear trend can be distinguished. At a density above 100 cyclists/km, the delay rapidly increases. The relatively low delay values all occur around a density of 50 cyclists/km, whereas large delays (>70%) see much higher density values. However, these high density values do not occur frequently.

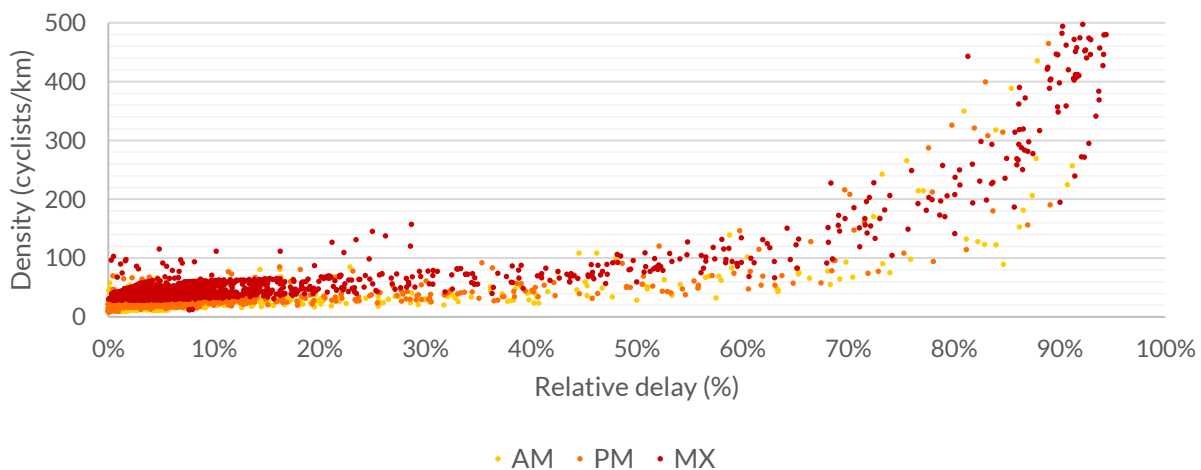


**Figure 4.24:** Density-delay relation for main future scenarios

The same can be said for [figure 4.25](#), where the density is visualized together with the flow (cyclists/h), that most density values lie between 10 to 60. In [figure 4.25](#), a clear positive relation between density and flow is observed for relatively low values of density. For high density values, this relation becomes unclear. This figure shows relatively small flow values can occur with high and low density, but large flow values can only occur with a high density. Which suggests the high flow can develop, until hindered by a high density.

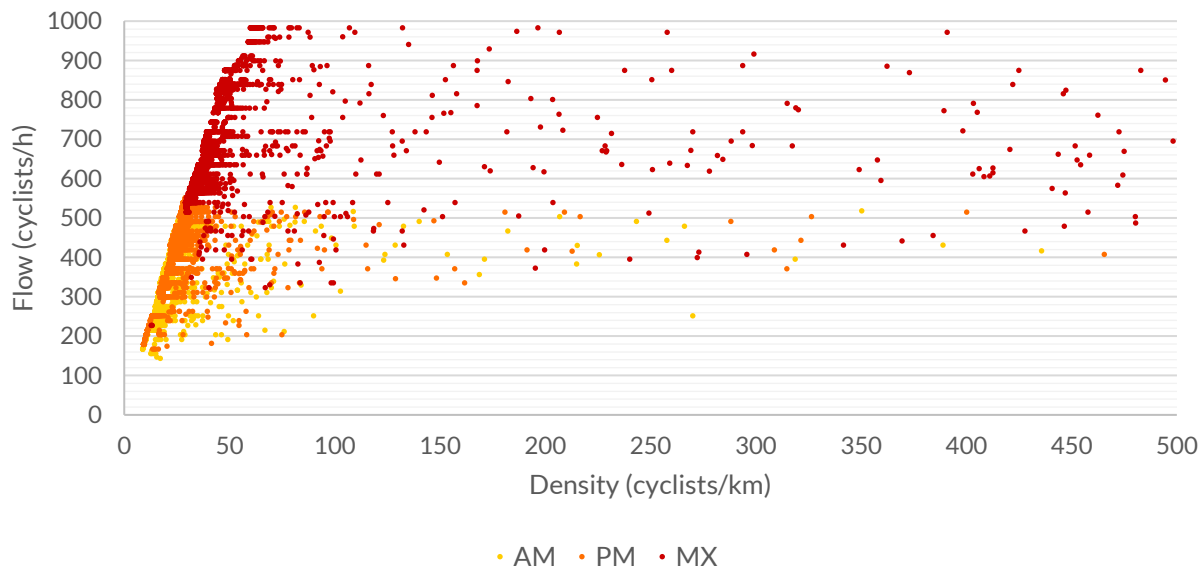


**Figure 4.25:** Flow-density relation for main future scenarios

Looking at the correlation differences ([table 4.9](#)) between the scenarios with the same input, it is noticeable that most relationships are stronger in the main scenarios than in the *wider paths* (b) scenarios. From this phenomenon, the general conclusion can be drawn that when cyclists have more space, changes in their behavior are less likely to lead to interruptions. Because cyclists can overtake more easily, the behavior of one cyclist is less influenced by other cyclists. All these variables are used to draw general conclusions on the different scenarios, but when extracting the data from a particular area of attention, in details analysis can be performed. In [section 4.3.4](#), the intersection in the south of the network will be subject to a more extensive analysis.



### 4.3.3. Route evaluation

Travel time from one location to another is a concrete measurement unit that is directly relevant to users of the area. It is one of the key factors for route choice and mode choice (Broach et al., 2012; Hardingham & Papantoniou, 2020). By measuring the travel time, a more straightforward comparison between scenarios can be made. The travel time is measured along three main connections in both directions, six routes. The routes cover all the main cycling paths that traverse through the area, [figure 4.26](#) shows a map of the measured routes. The travel time is measured as the time one cyclist needs to travel from one measurement point to another, the actual route can differ among cyclists. This is the reason [figure 4.26](#) shows multiple options to travel between the measurement points. The relative route flows for each intersection (see [figure 4.16](#)) remain identical, therefore the routes can be compared between scenarios. Note that in the base network, only the North-South/South-North routes exist. This connection sees the most traffic and often has the right of way over other routes.

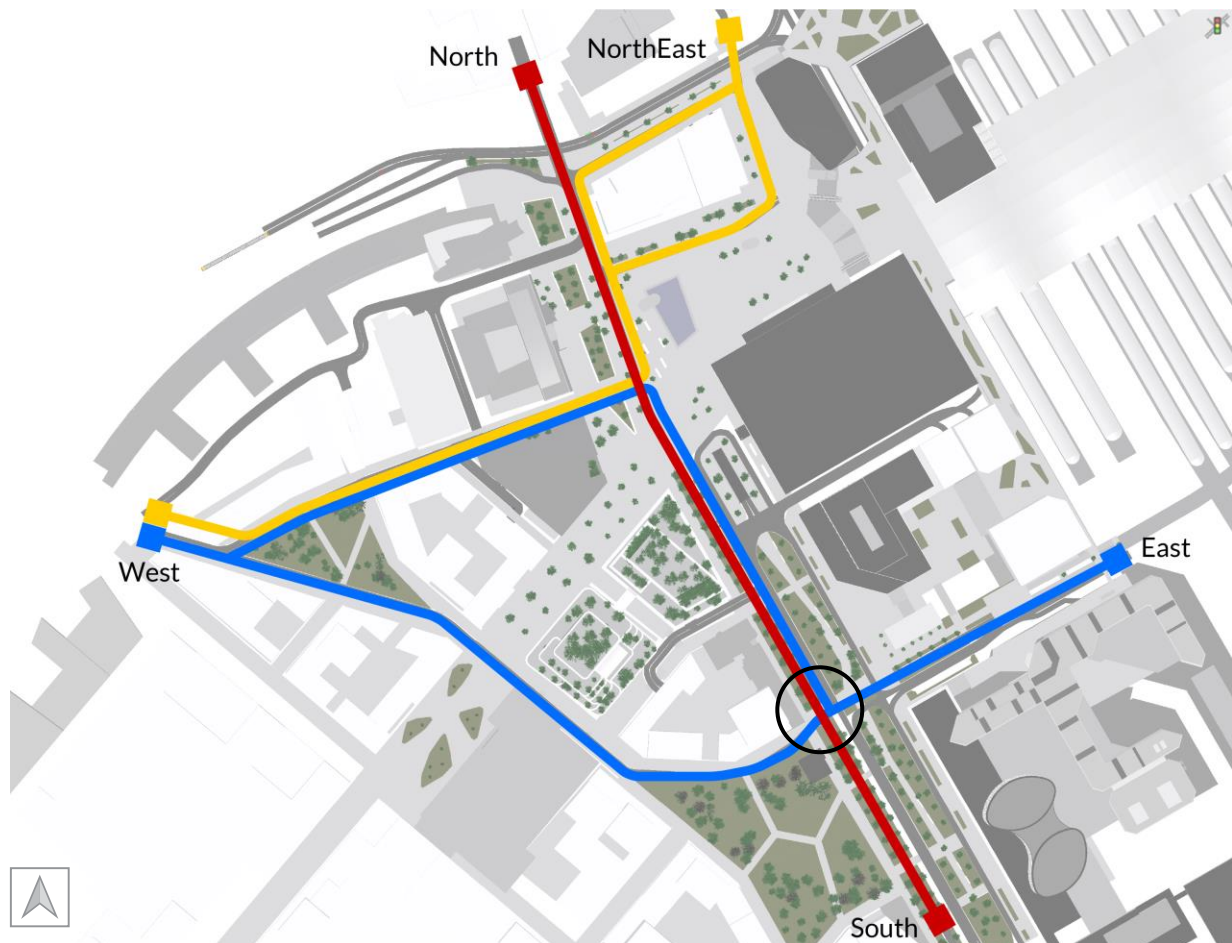


**Figure 4.26:** Routes measured for travel time evaluation

The average travel time of cyclists in a 5-minute interval is calculated for each route. The average travel time can be evaluated over the course of the simulations, [figure 4.27](#) shows the average travel time over all scenarios. While the graph shows a continuous line, in reality these are three separate simulation inputs (AM, PM, MX). The time of day for the maximal scenarios is not specified, but two hours are simulated to compare it to the other scenarios.

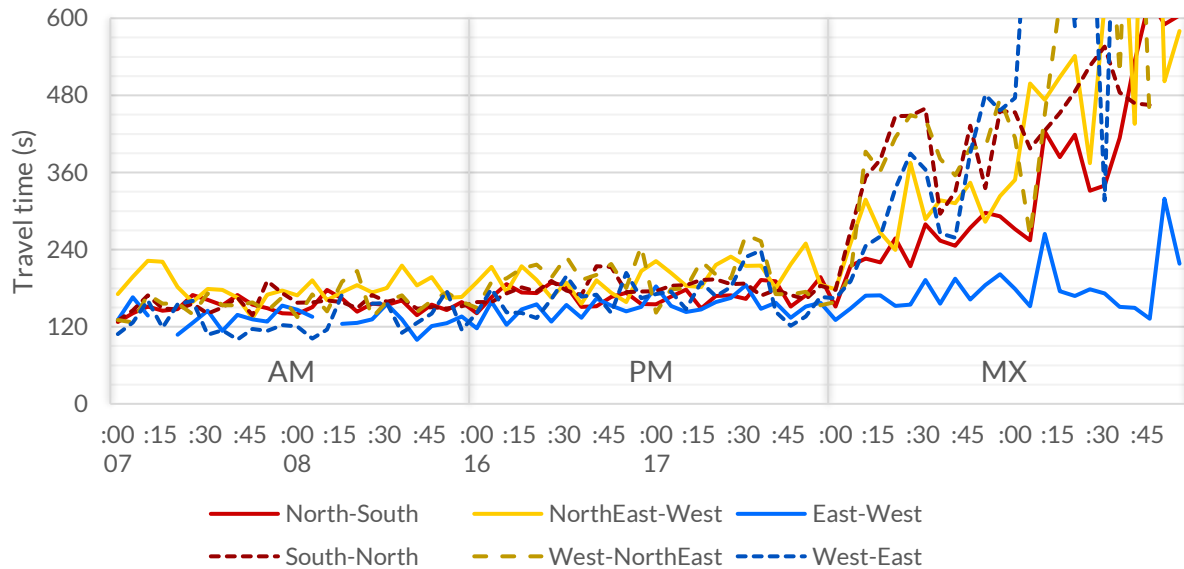


**Figure 4.27:** Average travel time for each route (average of all scenarios)

Aside from some fluctuations, the average travel time remains quite stable during the morning (AM) and afternoon (PM) scenarios. An increase in travel time is visible when comparing the AM and PM scenarios. Since the travel times are relatively stable across the AM and PM simulations, the averages are used to compare the routes and scenarios in figure 4.28. In the maximal (MX) scenario, the average travel time increases enormously due to the aforementioned traffic jams, especially after the first hour (section 4.3.1). This makes it irrelevant to compare to the overall average of the MX scenarios. Therefore, only the average of the first hour is used to determine the average travel time of the MX scenarios from this point onward, including figure 4.28.

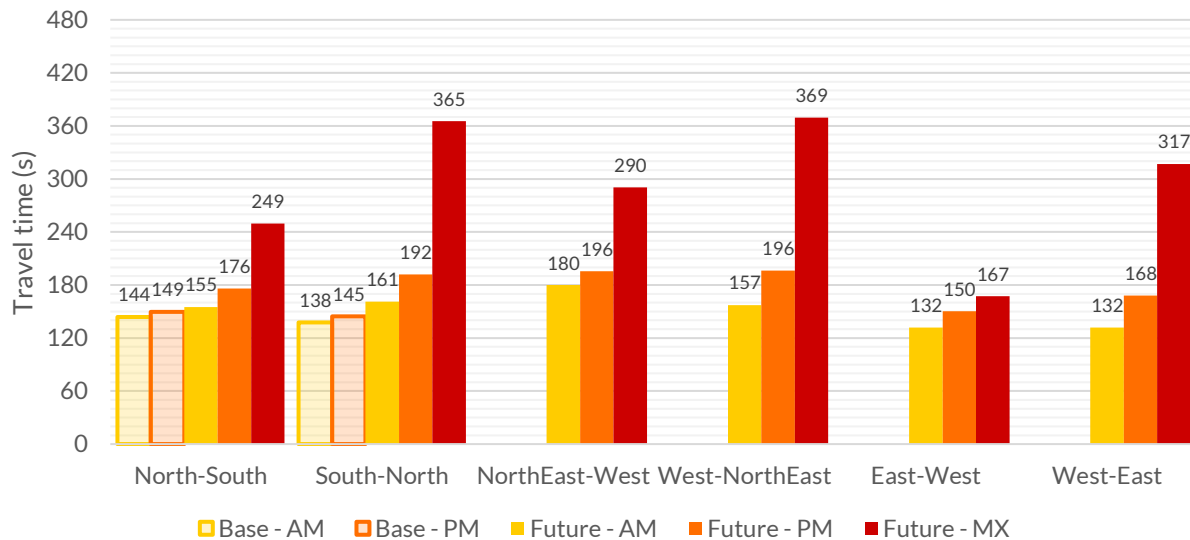


**Figure 4.28:** Average travel time per route and time of day (all scenarios)

The base network scenarios show expected average travel times, which are lower than for the future network. Curious is that for the base network, the South-North route is faster than the North-South route. Which is in contrast to the future network, where the southbound route is faster than

the northbound route. An exact reason for this observation is not found, but it is likely that this is a result of the links added in the future network.

Using the F-AM input scenarios as a reference, a similar pattern for all routes is observed when comparing to the afternoon scenarios. The PM input shows a 10% to 25% increase in travel time among all routes ( $M = 17.9\%$ ,  $SD = 7.2\%$ ). This corresponds to an average travel time increase of 26.8 s, due to the higher input values. In the F-MX scenario, relative increase differs much more between routes ( $M = 91.8\%$ ,  $SD = 48.0\%$ ). The West-East route sees an enormous 140% increase compared to the AM scenario, while the East-West route only has a 27% increase in travel time. This is probably due to the rough estimations on input values at the MX input. The input value from the West is increasing more than the input from the East at the MX scenarios compared to the PM scenarios (see [figure 4.16](#)).

Within the scenarios the differences between the spatial variations can also be analyzed. For all routes, [figure 4.29](#) shows the average travel time among all 11 simulated scenarios.

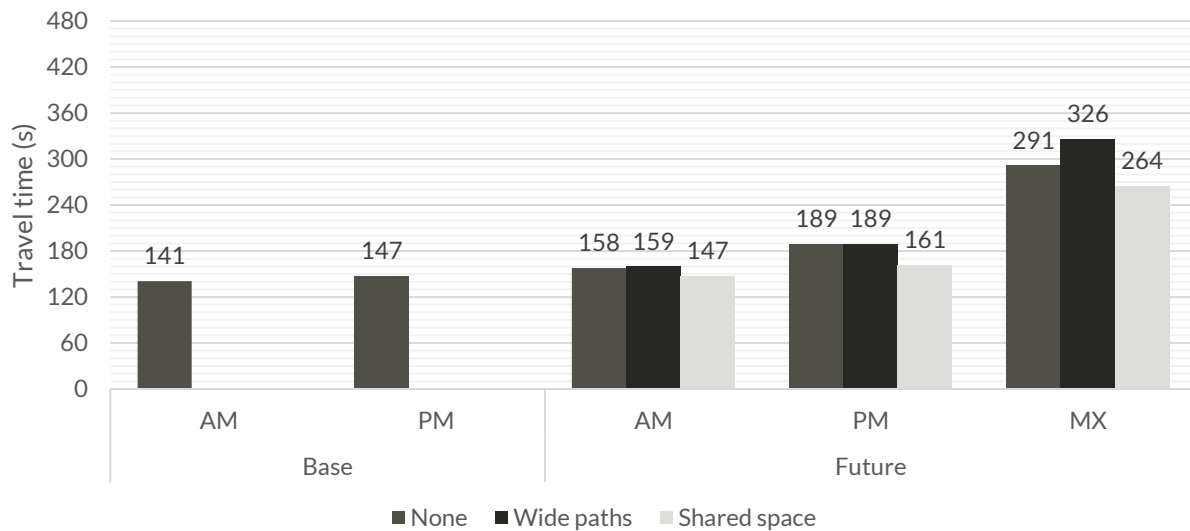


**Figure 4.29:** Average travel time for different scenarios (all routes)

Excluding the base network, the scenario with the *shared space* variation show the lowest average travel times. As a result of the large decrease in waiting time at the modified southern intersection. A surprising result is the *wide paths* scenarios having a longer average travel time then the scenarios without modification (more narrow paths). To further investigate this, the travel times are disaggregated for each route in [figure 4.30](#).

From [figure 4.30](#) it is noticeable that for the AM scenarios, the differences in travel time are minor. The travel time difference in the scenario without a spatial variation and the *wider paths* variation is very small for all routes. The *shared space* variation results in shorter travel times at all routes except the North-South route, possibly because the delay at the southern intersection was already low and the decreased desired speed at the shared space area causes a longer travel time than the small initial delay.

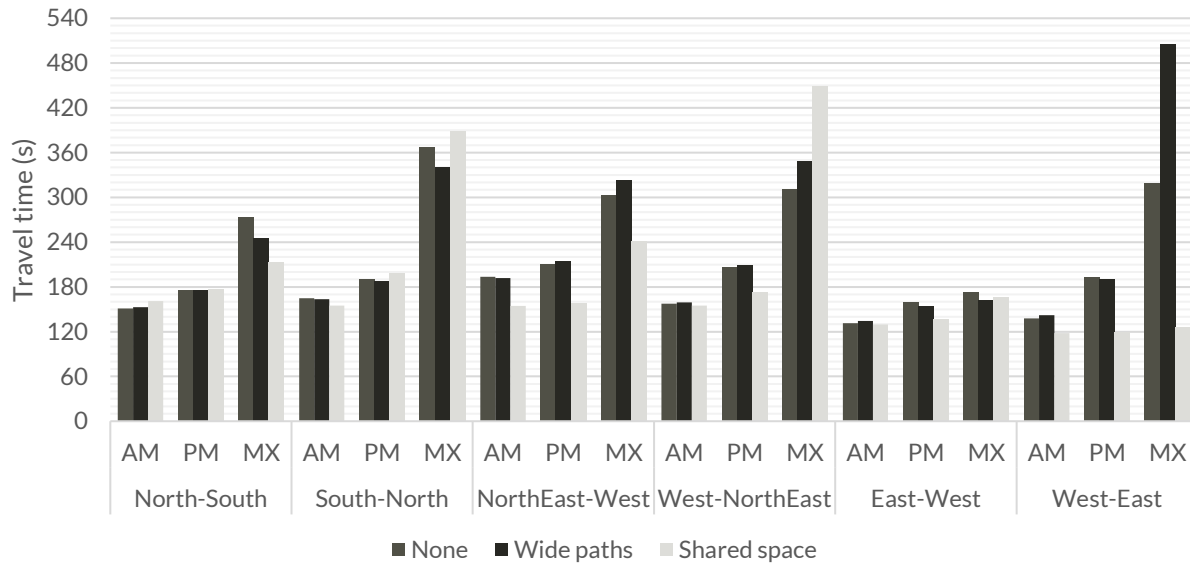


**Figure 4.30:** Average travel time all routes and scenarios in future network

The same can be said for the North-South and South-North routes in the PM scenarios. Here the shared space also results in longer travel times than without variation. The 'wider paths' variation has more impact on some routes than on others. The travel time becomes slightly shorter for the South-North, East-West and West-East route, while it becomes slightly longer for the North-South, NorthEast-West and West-NorthEast route. This suggests that because of an improved traffic flow at the intersection in the south, cyclists in other routes (e.g. NorthEast-West) are negatively affected by the improved flow of cyclists from the south. An interesting result since this is an indirect effect, not occurring at the modified intersection but elsewhere in the network.

At the MX traffic input, the travel time differences between routes from the three variations are much larger. The most outstanding result is the immense travel time increase at the West-East route in the F-MXb (wider paths) scenario. The travel time decrease at the busiest routes (North-South/South-North) seems to be accomplished by an increased travel time for the cyclists on the West-East route. This observation is further investigated in [section 4.3.4](#), where the modified intersection is closely evaluated.

The travel time values from [figure 4.30](#) are used to test if the difference between the overall travel times for different scenarios is significant. A two-way ANOVA test is performed to find if the traffic inputs (AM, PM or MX) and the spatial variations (none, wider paths and shared space) have an influence on the travel time at a significance level of .05. As expected, the traffic input has a significant effect on travel time  $F(2, 54) = 24.08, p < .001$ . The effect of the variation  $F(2, 54) = 1.21, p = 0.31$ , was found to be insignificant. Meaning the difference in average travel time between the variations is not significantly influenced by the spatial variation. Besides this outcome, the travel time differences between different routes result in some interesting conclusions.

#### 4.3.4. Intersection evaluation

For the spatial variation scenarios, the southern cycling intersection was modified to have wider paths and into a shared space with the pedestrians. The cycling paths are widened from 2.0 m/2.3 m to 2.5 m in all directions. To examine the differences in travel time more closely, additional



measurements are conducted at this unsignalized intersection. The intersection is situated where the main cycling path at *Croeselaan* intersects with the *Rabostraat* in the east. In the future network, an additional cycling path will be added going in the west direction. The simulated traffic flow of cyclists is shown in figure 4.31. Noticeable is that the flow at the *Croeselaan* is much higher than the flows from the east and west. The MX traffic input shows smaller flow values because of the traffic jams that occurred in the MX scenarios. Therefore again only data from the first simulation hour is used for the intersection evaluation. .

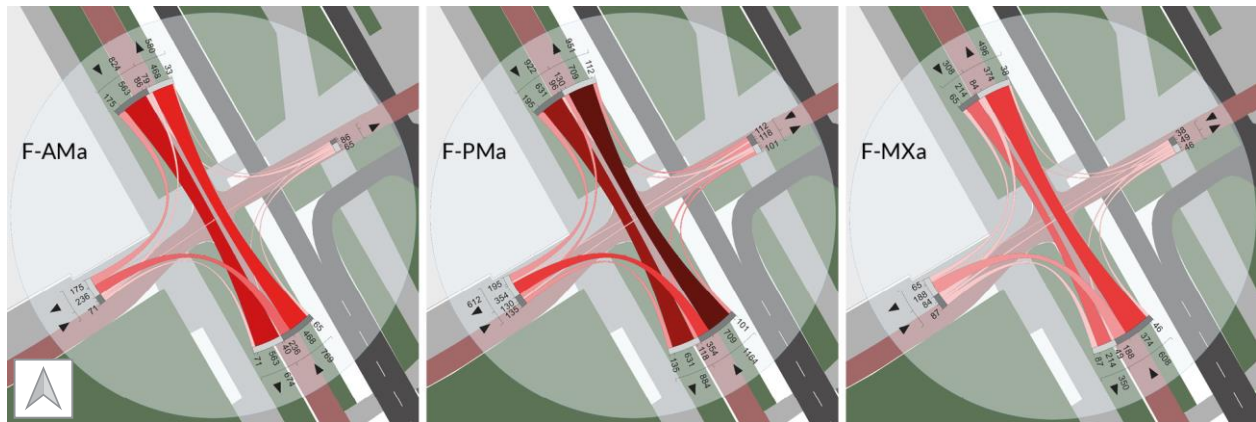


**Figure 4.31:** Cyclists' flows at intersection in future network (no spatial variation)

Just as for the entire network, automatic visualizations are generated from a perspective that concentrates on the intersection (figure 4.32). these visualizations are used to trace conflicts and examine differences between scenarios. Figure 4.32 already shows the delay might be bigger at the *Rabostraat* and its extension than at the *Croeselaan*.

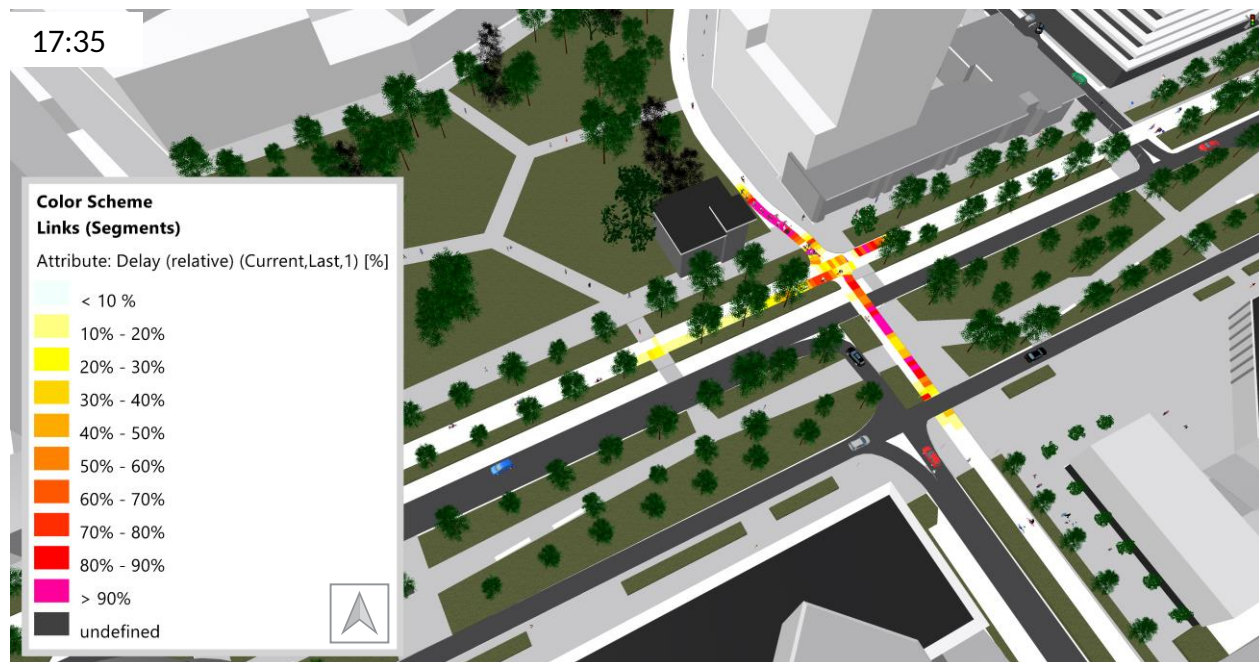


**Figure 4.32:** Highlighted intersection relative delay in F-PMa scenario (17:30-17:35)

Firstly the average delay per cyclist is evaluated for each direction of origin. This is defined as the direction from which a cyclist is approaching the intersection. Figure 4.33 shows the average delay over time in a stacked area chart, also displaying the total average delay per cyclist over time. In contrast to the earlier evaluated delay (section 4.3.2), here the absolute delay value is calculated in seconds, by subtracting the time it takes to use the intersection/node in free flow conditions from the actual time. Immediately standing out is the enormous increase of delay at the west direction, while the delay from the north, south, and to a lesser degree, the east remain stable.

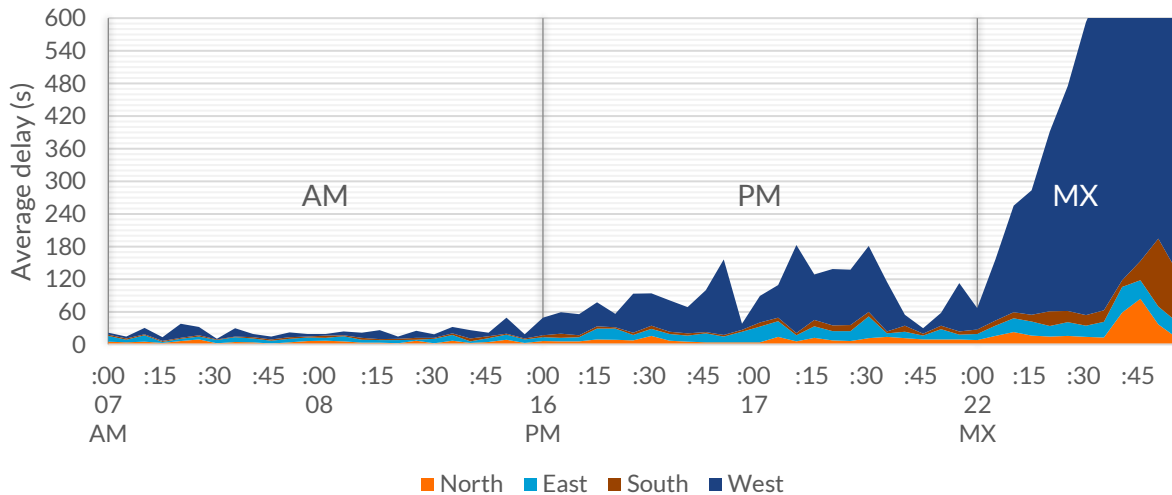


**Figure 4.33:** Average delay over time per approaching direction

To evaluate the delay at the west side more in depth, also the differences in spatial variations can be split. Because of the techniques used to model the 'shared space' variation (see section 3.1.3), these results cannot be included in the node evaluation. Therefore only the 'wider paths' variation can be compared to the standard network. In addition to looking at the delay, the maximal queue length for each time interval (5 min) is used to calculate the average maximal queue length in figure 4.34. Cyclists are considered to be part of the queue from slowing down to less than 5 km/h, to accelerating to more than 5 km/h again.

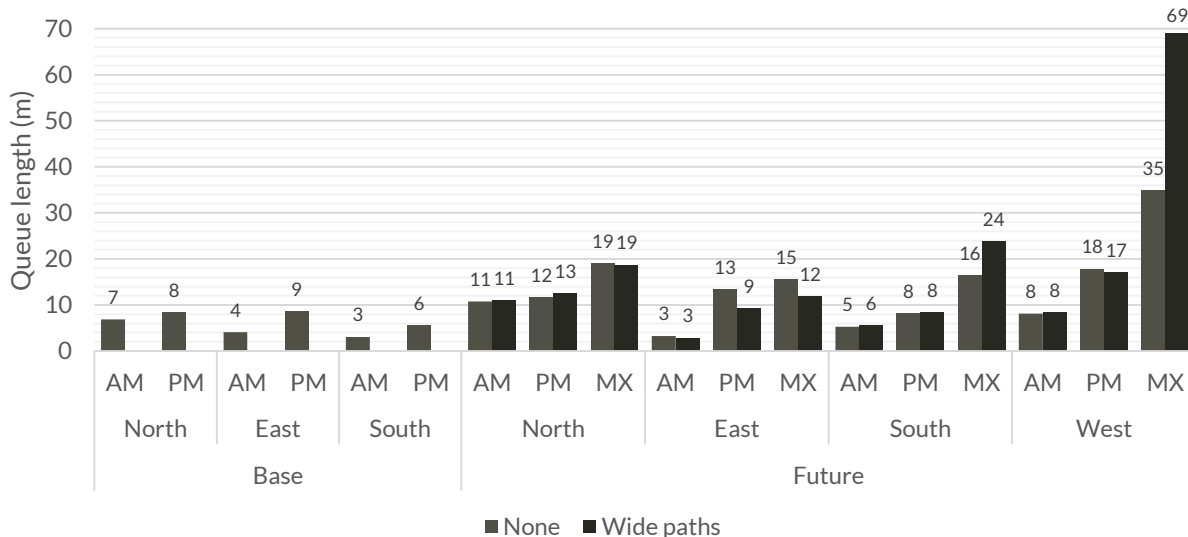


**Figure 4.34:** Average maximal queue length for time intervals per network, origin and variation



Comparing the AM and PM scenarios sees a queue length increase at all approaching directions of the intersection besides the north direction. The increased cyclists' flow from *Jaarbeursplein* seems to have more effect on queues of the east and west direction, than on the queue from the north. This agrees with the delay values visualized in [figure 4.33](#). For the AM and PM scenarios, the 'wider paths' variation seems to have little influence on the queues. Only the queue length from the east (*Moreelse* bridge) sees a noteworthy decrease. A two-way ANOVA test with significance level .05 proves the average maximal queue length is only influenced by the traffic input ( $F(2, 23) = 5.86, p = .011$ ), not by the 'wider paths' variation ( $F(2, 23) = 0.36, p = .556$ ). This is in line with the findings in [section 4.3.2](#). The MX scenarios experience some interesting changes, like the extreme queue of cyclists originating from the west in the 'wider paths' scenario. In both the scenario without spatial variation as in the 'wider paths' variation, an increase in queue length can be observed. The larger increase of queue length at the west than at the other directions is in line with the earlier findings from the PM scenarios. However, the most surprising result is the disproportional queue length increase at the F-MXb (wider paths) scenario (97% increase). Since the queue length is almost doubling, a large queue length decrease is expected at another origin direction. The east direction shows some queue length decline, but the north queue remains equally long and the south queue length is even increasing as well.

To go in depth on this issue, [figure 4.35](#) compares for spatial variations the average delay over time at four directions of the intersection, within the first hour of the simulation. Comparing to the scenario with smaller paths, [figure 4.35](#) shows as the delay at the west side is increasing, the delay at the three other routes declines. This behavior peaks at the 25 min mark in the simulation, then the delays at the north, south and east start rising again. This behavior confirms the hypothesis that an increased delay at the west causes a decreasing delay in another direction. Note that the scale of [figure 4.35](#) is logarithmic and the delay at the south also sees a huge increase after 40 min, this is the reason why calculating the average results in a higher delay for the south route as well.

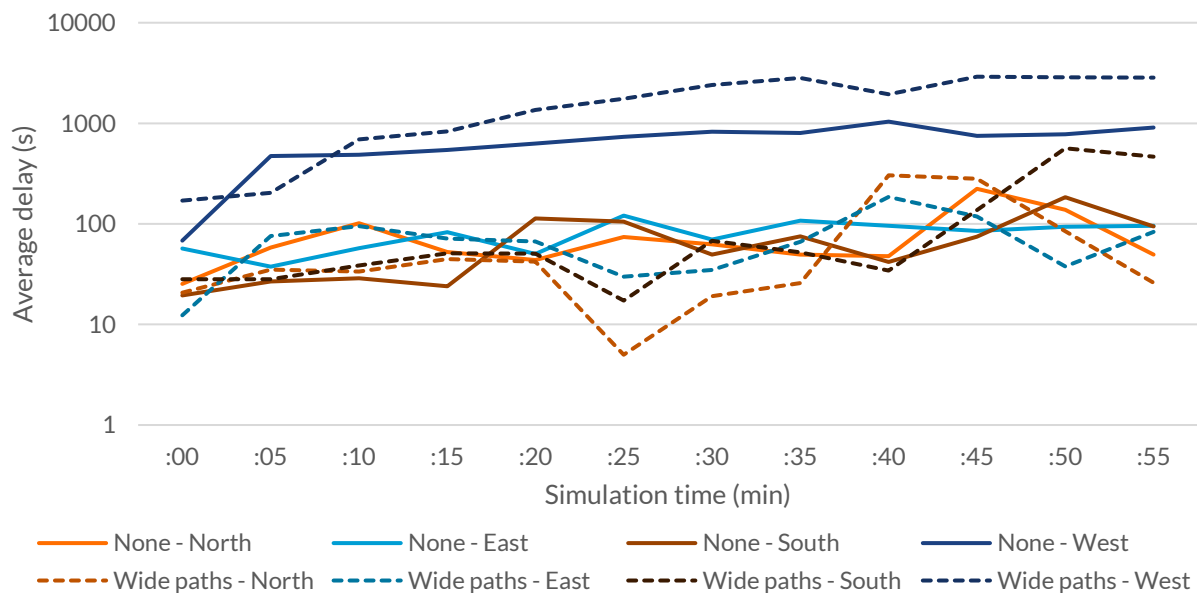


**Figure 4.35:** Average delay for different directions for F-MXa (none) and F-MXb (wider paths)

Constantly taking average values can give a distorted image in the overall performance. The seemingly strange result that having wider paths leads to higher delays is a result of this. When

taking the median instead of the mean of the delay values in the MX scenarios, the 'wider paths' variation (69 s) does show a shorter delay than the variation with narrower paths (84 s). Hence, it can be concluded that the 'wider paths' variation initially causes a better flow through the intersection. But this is mostly effecting the north, south and east directions, the improved flow from these directions causes additional waiting time in the west direction. The large cyclists' flow from the west direction in the MX input is delayed to a point where the average delay for the intersection is more in the F-MXb (wider paths) scenario than in the F-MXa scenario.

#### 4.3.5. Area-specific conclusions

Working with combinations of traffic input and network variations to form scenarios is an insightful way to compare the influence of changes. Whether these are changes in the traffic demand or the infrastructure. The microscopic scenario simulations showed some general outcomes for example that the effect of density on speed and delay is increasing in more dense traffic situations. This relation is not linear, in a higher density, cyclists are increasingly influenced by the environment and dimensions of the infrastructure.

But also more area specific observations were made. For future development of the area, main points of attention are found to be the crossings near the tram station at *Jaarbeursplein*, specially the unsignalized intersection where cyclists and cars share the road. By using various traffic demand estimations this location constantly caused the most delay. This intersection might not function properly as an unsignalized intersection because the traffic flow at the priority route (North-South/South-North) is causing large delays at the east and west direction. The simulation showed that also the shared space where the entrance of the *Jaarbeursplein* bicycle parking is located next to the escalators to enter the *Forum* and *Utrecht Centraal* proved to be an area of potential conflict. Even though there is no functional argument these two destinations have to be located next to each other. The entrance of the *Knoop* bicycle parking is also designed as a shared space between pedestrians and cyclists. Here this could also lead to accidents since this shared space does not provide much room for conflict avoidance.

Scenarios where a shared space was implemented to substitute a regular intersection showed promising results. Although two conditions are important for a shared space to be beneficial. Firstly, the area should be large enough so cyclists have enough space to avoid pedestrians and each other. Furthermore, the conclusion is drawn that at intersections that already experience little delays, a shared space only causes more delay. Because cyclists ride with a lower speed and possibly pay extra attention to the environment, even though they could have continued in their desired speed.

Constructing wider paths seems like it would benefit the traffic flow in all directions, but the simulation results showed that this can differ for each route. Improving the traffic flow in one direction, can have the side effect that another direction is more delayed. When modifying one intersection, also indirect effects were observed that increased delays in other intersections. Therefore it is important to include the surrounding network when conducting analysis on an intersection. Lastly it is important to not only look at the average values but disaggregate the data to investigate the impact from different scenarios, in different routes, at different times. Because an apparent drawback in one direction, might lead to improvement in another.



## 5. Conclusions

This research first explored the current practice in the field of microscopic traffic simulation with a focus on cyclists. Afterwards, new methods for the simulation of cyclists' behavior were developed and integrated in existing simulation tools. The behavioral model was calibrated by looking at data from other researchers. Additionally, a data collection experiment provided data to verify the speed and acceleration of cyclists in various situations.

A case study area was selected and investigated to apply the behavioral model in practice and test its performance in a digitally recreated environment. The developments in the area around *Jaarbeursplein* and *Beurskwartier* in Utrecht provided an interesting context to create different scenarios to simulate.

After analyzing the results of the simulated scenarios, conclusions can be drawn on the relevance of this research in a scientific and societal context. The research questions formulated at the beginning of the project will be answered by summarizing the findings from each research phase. A critical reflection on the results will identify limitations of the research, that function as recommendations for further research.

## 5.1. Conclusion

Six research phases were completed to answer the main research question. First, a literature review was conducted that strived to answer the sub-question: *How is cyclists' behavior modeled in existing microscopic models?* The review of past research and state-of-the-art developments in the field of microscopic behavioral models showed most research efforts are directed at modeling car and pedestrian traffic. Resulting in the conclusion that most cyclists' behavioral models are based on either typical car movement or pedestrian movement.

In the second research phase, the 'methods exploration', modeling methods were explored to establish: *Which attributes have been used to model cyclists' interaction with the built environment and other road users?* This sub-question pointed in the direction of traffic simulation program Vissim as the most promising software to develop the behavioral model for cyclists. Within Vissim, a unique approach was developed that combines the strengths of the car following model and SFM. Both models were calibrated using previous research data and a script was developed that models the transition between both models so they can be used interchangeably.

The behavioral model was validated in the third research phase, that aimed to answer the sub-question: *How can the cyclists' behavioral model be validated with naturalistic data?* Using GPS trackers, a data collection experiment was set up to retrieve data for the validation of the behavioral model. Naturalistic data was collected, used to validate unconstrained cycling parameters. This provided a solid base for the most important functions and parameters in both models.

After the behavioral model was developed and validated, the model was applied to a case study area. In research phase four, the area around *Jaarbeursplein* in Utrecht was modeled to find an answer to the fourth sub-question: *How to model the influence of built environment attributes on cyclists' behavior?* A base and future network were constructed and the formulation of spatial variations and traffic input configurations resulted in 11 scenarios that were evaluated in the final research phase.

Research phase five was devoted to answering the sub-question: *How to estimate traffic demand by using available data sources?* All available data from the area was used to estimate the traffic inputs at different times of the day. The predictions for the future traffic input were combined with the spatial variations to create the scenarios.

By evaluating the results of the simulations in phase six, the last sub-question was also answered: *What is the influence of traffic demand and infrastructure designs on travel time of cyclists?* The relative delay and speed across the entire network were compared across the scenarios. The travel time was evaluated for the most important routes in the area and a detailed analysis was performed on a specific intersection. Conclusions on the influence of traffic demand and infrastructure designs were drawn specifically for the case study area ([section 4.3.5](#)).

To formulate an answer to the main research question: *How can the impacts of traffic demand and urban infrastructure designs on cyclists' behavior be evaluated with the support of microscopic traffic simulation?* An innovative coupled cyclists' behavioral model was validated and applied to a case study network using scenarios comparison. The research process showed the steps needed to develop and apply a microscopic behavioral model for the evaluation of traffic in a specific area.

## 5.2. Scientific relevance

This research aimed to contribute to the identified research gap in cyclists' behavioral modeling by exploring innovative methods of cyclists microsimulation. To model motorized traffic, often (a version of) car following models is used. The most common behavioral model for pedestrian simulation is the Social Force Model (SFM). Because of the unique nature of cyclists' behavior, using one of these two models to simulate cyclists, generally leads to inaccuracies in reflecting cyclists' behavior. A literature review showed that currently, cyclists' behavior is regularly modeled using creative and not fully developed methods. This research developed an innovative method that shows the application of combining lane-based and area-based behavioral models. Cyclists riding on lane-based infrastructure were modeled by a car following model, also interacting with cars. When entering a two-dimensional area, their behavior was modeled by a SFM, making interaction with pedestrians possible.

A second contribution to the research field of cyclists' behavior is the collection of naturalistic data of cyclists and e-cyclists. The collected GPS data was processed to assess the distribution of desired speed and acceleration in unconstrained situations. Furthermore, the speed reduction in turns and in shared spaces was evaluated. The resulting distributions and functions were used to validate the behavioral models. The data from this experiment can be used in future models to quantify parameters.

The final contribution of this research is to reveal the potential of improving cyclists' behavioral models to evaluate traffic input and spatial scenarios. The case study provided valuable insights in how the developed model functions in a simulated environment. Using microsimulation opened up the possibility of disaggregating data to a single cyclist or the tiniest surface. In the future, cyclists will gain presence in the urban environment and their unique behavior should not be overlooked in future multimodal traffic models.



### 5.3. Societal relevance

This project was executed in collaboration with the City of Utrecht to provide insights on the future traffic situation in their high density urban projects. The societal relevance section mainly focuses on the relevance for the municipality. Since it is a governmental organization, it should be in their best interest to translate the projects' relevance into positive policy and environments for all people.

For the scenario simulations, not all needed data was available to accurately estimate all traffic inputs, but the presented results help to lay the foundation for more extensive data collection. When having all data available, the complete simulation model can provide an insightful overview of the area. Or when having concrete design or policy choices, governments can make investments collect the desired data. Because in the future, it will take less effort to collect data and compute complex simulations, the technology of microsimulation will become scalable for larger areas. A scalable model also increases the feasibility of developing a neighborhood or city-wide model. Which can be reused every time new policy decisions have to be made. A model that is kept up-to-date can also be used to interactively show the results of different designs or policies. An interactive platform would contain parameters to modify and instantly show the effects of modifications. In application, there are three main advantages of a simulation model of this type.

Firstly, the microscopic model is multimodal, so all road users and their effects on each other are included. Giving a more complete representation of actual traffic situations. The advantages for motorized, public or active transportation modes can be compared for different scenarios. This raises the opportunity to apply weighing factors for different modes to analyze how available space should be divided.

Furthermore, microscopic simulations generate data with a very high resolution, the exact desired details can be extracted from the simulation. Therefore models like these can be used to calculate all desired units of measurement. A large-scale model would also be able to account for different route choices. Variations can be chosen by directly comparing units relevant to the end users of the area. For example, by designing to improve travel time or decrease delay.

Lastly, traffic simulation models like these are powerful visualization tools. When developing new environments, the impact on the traffic situation is three-dimensionally visualized. Besides the visualizations created within Vissim presented in this project, the software can also be integrated with Unity3D. An exchange is then made between the Vissim engine and Unity gaming engine, static and dynamic data are fetched from Vissim and are used as input in Unity (Munigety et al., 2020). Then, operators can essentially drive around the digital environment while road users around them react to their behavior according to the behavioral models defined in Vissim, opening a whole opportunity area for serious gaming and virtual reality applications. Visualization not only makes the work of experts more intuitive, it is also an important element of citizen participation. Residents or other stakeholders can be included in the decision-making process for their future living environments. These main advantages generate additional data relevant for well-argued designs and policy making. Enabling municipalities and other stakeholders to better support investments on (cycling) infrastructure.



## 5.4. Limitations and recommendations

The case study simulations showed that when executing multiple scenarios, countless amounts of data can be collected from the simulations, even when only considering cyclists. In theory, numerous attribute values from every square meter, from every road user, for every second can be extracted, and presented for every imaginable scenario. Because of this abundance of data, the processing and presentation is vital to drawing the right conclusions. Data could be made dynamically accessible through an interactive platform, functioning as a dashboard to visualize all results. However, presenting an overview of essential data depends on more general graphs and images that show average values. The results of the simulations show that an average value often does not tell the entire story, an average value might result in non-significant influence, when a further disaggregation of data reveals different impacts at different locations. It was observed that often an exchange of travel times among different routes occurs when modifying intersections. Therefore it is recommended to look at the right aggregation level of scenarios, transportation modes or routes.

The outcomes of the project provided valuable insights for developments in the case study area and future research on cyclists' behavior modeling. However, many estimations were made to ensure a well-functioning model. In terms of verifying the behavioral model, only verification was executed for parameters in unconstrained situations. The data collection experiment resulted in valuable input for the (desired) speed and acceleration of cyclists, but did not consider interaction behavior of cyclists. For a more robust model, also validation on cyclists interaction should be performed. When modeling with priority rules, the parameters should be calibrated to prevent collisions, but not cause traffic jams. Since cyclists show the unique behavior characteristics between obeying traffic rules and completely ignoring them, validation on interaction is essential. The limited available time, expertise and the traffic situation during the COVID-19 pandemic prevented validation at intersections for this project, but this is strongly recommended for future research. Besides more insights in the interaction behavior between cyclists and other road users, also the influence of built environment characteristics on cyclists behavior would be an interesting topic for future research since (besides routes choice) little information on this is known. Being able to include built environment attributes into the model would result in a more representative reflection of reality. Another major limitation was imposed by the absence of traffic data. Even though the City of Utrecht collects a substantial amount of (cycling) traffic data, to accurately estimate all inputs, compositions and routes in a microsimulation model, more detailed traffic data is needed. Especially the number of pedestrians was very roughly estimated since practically no data in the region was available. As demonstrated in the results, the model is quite sensitive to different inputs, further emphasizing the importance of correct traffic volume measurements and estimations. For new construction projects, the traffic flows could have been predicted more accurately by, for example, predicting the number of trips per resident for each direction and transport mode. This was outside of the scope of this project but can be considered in future research.

The process of modeling the infrastructure network and 3D buildings is quite labor intensive. The network includes numerous objects and parameters to consider. This makes the modeling process rather error sensitive. Errors are easily overlooked and only discovered in at the simulation outcome

values or visualization. Many network objects, inputs and attributes were changed between the base network and future network, making it hard to compare the two. It became very complicated to identify what caused the differences between the outcome values. In order to minimize errors caused by the modeling process or inaccurate parameter/input estimations, a recommendation is to have minimal differences between scenarios to draw more confident conclusions. This project primarily focused on analyzing the impact of different scenarios on cyclists' travel time, but also other transportation modes should be considered in future research. Because of the absence of data, it is probable that pedestrians are underrepresented in the simulated scenarios. For the inclusion of all transportation modes, microsimulation is an appropriate method. Trade-offs for the travel times between different modes can be evaluated. However, certainly also less easily quantifiable aspects like safety and comfort should be incorporated in the decision-making process.

When selecting the most suitable behavioral model, initially the SFM showed the most promising capabilities of simulating cyclists' behavior. However, it soon became clear that this particular model was designed to reflect pedestrian behavior. Which was mainly expressed in the isotropy of social forces on cyclists, resulting in situations where either cyclists collided with each other or avoided each other so much they were unable to overtake or cycle abreast. In this project, this issue was resolved by assuming cyclists behave similar to pedestrians in pedestrian areas and using the car following model for lane-based infrastructure. But future models should be able to make more distinction between longitudinal and lateral forces on a cyclist. Using Vissim as simulation software offered many benefits for modeling because it has a pleasant balance of preprogrammed models and user modification options. Still some limitations were caused by the software, besides the earlier mentioned absence of cyclists-specific behavioral models. Although it was possible to model a custom transition between the lane-based and area-based models, the way this was achieved prevented the continuous evaluation of cyclists traveling over lanes and areas. Future models should be more capable of simulating behavior changes in different types of environments. The reason surrounding intersections were not included in the network model is attributed to a drastic increase in computation time when adding additional conflict areas, traffic signal programs and vehicle inputs. Simulations were run on a laptop with Intel Core i7 (1.30GHz) processor, 16 GB of Random Access Memory and a NVIDIA GeForce GTX 1050 Graphic Processing Unit. Simulating a more extensive network model might have been possible with advancements in the software or a more powerful device to run the simulations.

Altogether, this research provided valuable insights and innovative methods in cyclists' behavior modeling. Many estimations were made to reach the final results, but besides the quantitative results this research presented, the findings also demonstrate the future potential of microsimulation of cyclists' behavior. Traffic models should embrace the advancement of cycling, contributing to a more comfortable living environment and sustainable transportation system.

## References

- Aghabayk, K., Sarvi, M., Young, W. & Kautzsch, L. (2013). A novel methodology for evolutionary calibration of Vissim by multi-threading. *Australasian Transport Research Forum 2013 Proceedings* 1-15. [https://www.australasiantransportresearchforum.org.au/sites/default/files/2013\\_ghabayk\\_sarvi\\_young\\_kautzsch.pdf](https://www.australasiantransportresearchforum.org.au/sites/default/files/2013_ghabayk_sarvi_young_kautzsch.pdf)
- Alsaleh, R. & Sayed, T. (2020). Modeling pedestrian-cyclist interactions in shared space using inverse reinforcement learning. *Transportation Research Part F* 70 (2020) 37–57. <https://doi.org/10.1016/j.trf.2020.02.007>
- Anvari, B., Bell, M., Sivakumar, A. & Ochieng, W. (2015). Modelling shared space users via rule-based social force model. *Transportation Research Part C* 51 (2015) 83–103. <http://dx.doi.org/10.1016/j.trc.2014.10.012>
- ANWB (2020). Verkeer in de Stad, een nieuwe ontwerpaanpak voor de stedelijke openbare ruimte. Retrieved from: [https://www.anwb.nl/binaries/content/assets/anwb/pdf/belangenbehartiging/verkeer/verkeer-in-de-stad/200615-verkeer-in-de-stad\\_rapport\\_2020.pdf](https://www.anwb.nl/binaries/content/assets/anwb/pdf/belangenbehartiging/verkeer/verkeer-in-de-stad/200615-verkeer-in-de-stad_rapport_2020.pdf)
- ANWB (n.d.). Verkeersborden Nederland. Retrieved at 01-10-2020, from: <https://www.anwb.nl/verkeer/nederland/verkeersinformatie/verkeersborden-nederland>
- Architectenweb (2011) Rabobank-toren Utrecht in gebruik genomen. Retrieved from: <https://architectenweb.nl/nieuws/artikel.aspx?ID=27464#:~:text=Het%20interieur%20is%20volledig%20ingericht,bestaande%20gebouwen%20in%20de%20omgeving>.
- Barceló, J. (2010). Fundamentals of Traffic simulation. *Springer Science + Business Media*.
- Bernardi, S. & Rupl, F. (2015). An analysis of bicycle travel speed and disturbances on off-street and on-street facilities. *Transportation Research Procedia* 5, 82 – 94. <https://doi.org/10.1016/j.trpro.2015.01.004>
- Basyir, M., Nasir, M., Suryati, & Mellyssa, W. (2017). Determination of Nearest Emergency Service Office using Haversine Formula Based on Android Platform. *International journal of engineering and technology* 5, 270. <https://core.ac.uk/download/pdf/234937175.pdf>
- Boffey, D. (2020) Utrecht restores historic canal made into motorway in 1970s. *The Guardian*. Retrieved at 18-01-2021, from: <https://www.theguardian.com/world/2020/sep/14/utrecht-restores-historic-canal-made-into-motorway-in-1970s>
- Boggelen, O. & Ulshof, R. (2019). Fietsberaadnotitie aanbevelingen fietsstraten binnen de kom. *Fietsberaad CROW*. Retrieved from: [https://www.fietsberaad.nl/getmedia/c8a66983-9cbf-48c4-b0df-3d7f5550e6b0/Fietsberaadnotitie-Aanbevelingen-Fietsstraten-binnen-de-bebouwde-kom-2018-\(versie1-1\).pdf.aspx?ext=.pdf](https://www.fietsberaad.nl/getmedia/c8a66983-9cbf-48c4-b0df-3d7f5550e6b0/Fietsberaadnotitie-Aanbevelingen-Fietsstraten-binnen-de-bebouwde-kom-2018-(versie1-1).pdf.aspx?ext=.pdf)
- Boufous, S., Hatfield, J. & Grzebieta, R. (2018). The impact of environmental factors on cycling speed on shared paths. *Accident Analysis and Prevention* 110 (2018) 171-176. <http://dx.doi.org/10.1016/j.aap.2017.09.017>

- Bouwinvest (2021) Central Park. Retrieved at 17-01-2021, from: <https://www.bouwinvest.nl/beleggingen/dutch-office/portfolio-highlights/central-park/>
- Broach, J., Dill, J. & Gliebe, J. (2012). Where do cyclists ride? A route choice model developed with revealed preference GPS data. *Transportation Research Part A* 46 (2012) 1730–1740. <http://dx.doi.org/10.1016/j.tra.2012.07.005>
- BSA (2017). Verschil tussen fietsstrook en fietssuggestiestrook. Retrieved from: <https://www.bsabv.nl/verschil-fietsstrook-en-fietssuggestiestrook/>
- Bureau Nieuwe Gracht (2018). Living Lab Utrecht, Stadslogistiek in een duurzaam en bereikbaar Beurskwartier. Retrieved from: <https://www.slimmeengezondestad.nl/Kennisnetwerk/archief/HandlerDownloadFiles.ashx?idnv=1266171>
- C40 Cities (2019). C40 Cities Annual Report 2019. Retrieved from: [https://c40-production-images.s3.amazonaws.com/other\\_uploads/images/2574\\_C40\\_2019\\_Annual\\_Report.original.pdf?1587634742](https://c40-production-images.s3.amazonaws.com/other_uploads/images/2574_C40_2019_Annual_Report.original.pdf?1587634742)
- CAF (2020). Regio Utrecht Tram. Retrieved from: [https://regiotramutrecht.provincie-utrecht.nl/sites/regiotram/files/2020-05/factsheet\\_urbos\\_100\\_trams.pdf](https://regiotramutrecht.provincie-utrecht.nl/sites/regiotram/files/2020-05/factsheet_urbos_100_trams.pdf)
- CBS (2020). Onderweg in Nederland (ODiN) 2019. Retrieved from: <https://easy.dans.knaw.nl/ui/datasets/id/easy-dataset:178556/tab/2/rd/1>
- City of Utrecht (n.d.). Ruimtelijke plannen. Retrieved at 01-09-2020, from: <https://0344.ropubliceer.nl/>
- City of Utrecht (2003) Masterplan Stationsgebied Utrecht. *Projectorganisatie Stationsgebied (POS)*. Retrieved from: [https://www.cu2030.nl/images/1\\_10-masterplan-stationsgebied.pdf](https://www.cu2030.nl/images/1_10-masterplan-stationsgebied.pdf)
- City of Utrecht (2016). Mobiliteitsplan Utrecht 2025. Retrieved from: <https://omgevingsvisie.utrecht.nl/thematisch-beleid/verkeer-en-mobiliteit/>
- City of Utrecht (2017). Omgevingsvisie Beurskwartier Lombokplein. Retrieved from: <https://omgevingsvisie.utrecht.nl/fileadmin/uploads/documenten/zz-omgevingsvisie/gebiedsbeleid/beurskwartier-en-lombokplein/2018-02-omgevingsvisie-beurskwartier-lombokplein.pdf>
- City of Utrecht (2020a) Mobiliteitsplan 2040. Retrieved from: <https://ris2.ibabs.eu/Reports/ViewListEntry/Utrecht/f2e4c801-1d3d-4294-9479-258410450018>
- City of Utrecht (2020b) Verkeerstellingen Gemeente Utrecht. Retrieved from: <http://mobiliteitsdata-utrecht.nl/tellingen/>
- City of Utrecht (2020c) Lombokplein, Herstructurering Westplein, Leidse Rijn en Graadt van Roggenweg. Retrieved from: <https://www.utrecht.nl/wonen-en-leven/bouwen/bouwprojecten/beurskwartier-en-lombokplein/lombokplein-herinrichting/>
- City of Utrecht (2020d) Verkeersanalyse Wonderwoods. Retrieved from: [https://www.planviewer.nl/imro/files/NL.IMRO.0344.BPKOPBEURSKWARTIER-VA01/b\\_NL.IMRO.0344.BPKOPBEURSKWARTIER-VA01\\_tb4.pdf](https://www.planviewer.nl/imro/files/NL.IMRO.0344.BPKOPBEURSKWARTIER-VA01/b_NL.IMRO.0344.BPKOPBEURSKWARTIER-VA01_tb4.pdf)
- City of Utrecht (2021) Ruimtelijke Strategie Utrecht 2040. Retrieved from: <https://omgevingsvisie.utrecht.nl/de-koers/ruimtelijke-strategie-utrecht-2040/>

- Copenhagenize Design Co. (2019). The most bicycle-friendly cities of 2019. Retrieved from: <https://copenhagenizeindex.eu/the-index>
- COWI (2013) Micro simulation of cyclists in peak hour traffic. *City of Copenhagen*. Retrieved from: [https://your.vissim.ptvgroup.com/LP=3247?utm\\_source=ptvgroup.com&utm\\_medium=referral&utm\\_campaign=ptv-group-website&utm\\_content=succopenhagen#report](https://your.vissim.ptvgroup.com/LP=3247?utm_source=ptvgroup.com&utm_medium=referral&utm_campaign=ptv-group-website&utm_content=succopenhagen#report)
- Coya (2019). Global Bicycle Cities Index 2019. Coya. Retrieved from: <https://www.coya.com/bike/index-2019>
- CU2030 (2020) Projecten. Retrieved at 01-01-2021, from: <https://cu2030.nl/pagina/alle-projecten>
- Dahlberg, L. & Segernäs, M. (2017). Optimisation of the simulated interaction between pedestrians and vehicles, A comparative study between using conflict areas and priority rule in Vissim. *Master's thesis, Chalmers University of Technology*. Retrieved from: <http://publications.lib.chalmers.se/records/fulltext/250882/250882.pdf>
- Dane, G., Feng, T., Luub, F. & Arentze, T. (2020). Route Choice Decisions of E-bike Users: Analysis of GPS Tracking Data in the Netherlands. *Geospatial Technologies for Local and Regional Development - Proceedings of the 22nd AGILE Conference on Geographic Information Science*. 109-124. [https://doi.org/10.1007/978-3-030-14745-7\\_7](https://doi.org/10.1007/978-3-030-14745-7_7)
- Decisio (2016) Maatschappelijke Waarde en Investeringsagenda Fietsen, Verantwoordingsrapportage. Retrieved from: <https://www.fietsberaad.nl/Tour-de-Force/Documenten>
- Dias, C., Nishiuchi, H., Hyoudo, S. & Todoroki, T. (2018). Simulating Interactions between Pedestrians, Segway Riders and Cyclists in Shared Spaces Using Social Force Model. *Transportation Research Procedia* 34 (2018) 91-98. <https://doi.org/10.1016/j.trpro.2018.11.018>
- Dias, G. & Riberio, P. (2020). Cycle Highways: a new concept of infrastructure. *European Planning Studies*. <https://doi.org/10.1080/09654313.2020.1752154>
- Diepens, J., Weststrate, P., Egeter, B. & Tacq, R. (2020). Verkeer in de Stad, een nieuwe ontwerpaanpak voor de stedelijke openbare ruimte. ANWB, Mobycon, Ben Immers Advies, Bart Egeter Advies, Adviesbureau Awareness. Retrieved from: <https://www.anwb.nl/belangenbehartiging/verkeer/verkeer-in-de-stad>
- Dozza, M., Piccini, G. & Werneke, J. (2015). Using naturalistic data to assess e-cyclist behavior. *Transportation Research Part F Traffic Psychology and Behaviour* 55 <https://doi.org/10.1016/j.trf.2015.04.003>
- DTV Consultants (2016). Capaciteit fietspaden bij VRI's. CROW *fietsberaad*. Retrieved from: [https://fietsberaad.nl/CROWFietsberaad/media/Kennis/Bestanden/Eindrapport\\_Capaciteit\\_fietspaden\\_bij\\_VRI\\_s\\_18\\_okt\\_2016.pdf?ext=.pdf](https://fietsberaad.nl/CROWFietsberaad/media/Kennis/Bestanden/Eindrapport_Capaciteit_fietspaden_bij_VRI_s_18_okt_2016.pdf?ext=.pdf)
- Dutch Data Protection Authority (n.d.). Data protection impact assessment (DPIA). *Autoriteit Persoonsgegevens*. Retrieved at: 20-01-2021, from: <https://autoriteitpersoonsgegevens.nl/nl/zelf-doen/data-protection-impact-assessment-dpia#voor-welke-soorten-verwerkingen-is-het-uitvoeren-van-een-dpia-verplicht-6667>

- Ejercito, P., Fera, R., Nebrija, K. & Lara-Figueroa, L. (2017). Traffic simulation software review. *8th International Conference on Information, Intelligence, Systems & Applications (IISA)*.  
<https://doi.org/10.1109/IISA.2017.8316415>
- Eriksson, J., Forsman, A., Niska, A., Gustafsson, S. & Sörensen, G. (2019). An analysis of cyclists' speed at combined pedestrian and cycle paths. *Traffic Injury Prevention*.  
<https://doi.org/10.1080/15389588.2019.1658083>
- European commission (2016). A European Strategy for Low-Emission Mobility. Retrieved from:  
<https://eur-lex.europa.eu/legal-content/EN/TXT/HTML/?uri=CELEX:52016DC0501&from=en>
- European Parliament (2016). Data protection in the EU. *EUR-Lex*. Retrieved from: <https://eur-lex.europa.eu/legal-content/EN/TXT/?uri=CELEX%3A02016R0679-20160504&qid=1532348683434>
- Fietsenwinkel (2018) Wat is de snelheid van een elektrische fiets? Retrieved from:  
<https://www.fietsenwinkel.nl/blog/snelheid-elektrische-fiets>
- Fietzersbond (n.d.). Fietspaden. Retrieved at 01-10-2020, from: <https://www.fietzersbond.nl/ons-werk/infrastructuur/fietspaden/>
- Fiets Telweek (2016). Fietstelweek2016. Data provided by: Gemeente Utrecht.
- Figliozzi, M., Wheeler, N. & Monsere, C. (2013). Methodology for Estimating Bicyclist Acceleration and Speed Distributions at Intersections. *Transportation Research Record* 2387(1), 66-75.  
<https://doi.org/10.3141/2387-08>
- Fishman, E. & Cherry, C. (2016). E-bikes in the Mainstream: Reviewing a Decade of Research, *Transport Reviews*, 36:1, 72-91 <https://doi.org/10.1080/01441647.2015.1069907>
- Gao, Y. (2008). Calibration and Comparison of the VISSIM and INTEGRATION Microscopic Traffic Simulation Models. *Master's thesis: Virginia Polytechnic University*. Retrieved from:  
[https://vtechworks.lib.vt.edu/bitstream/handle/10919/35005/Yu\\_Gao\\_Thesis.pdf?sequence=1&isAllowed=y](https://vtechworks.lib.vt.edu/bitstream/handle/10919/35005/Yu_Gao_Thesis.pdf?sequence=1&isAllowed=y)
- Gavriilidou, A., Wierbos, M., Daamen, W., Yuan, Y., Knoop, V. & Hoogendoorn, S. (2019). Large-Scale Bicycle Flow Experiment: Setup and Implementation. *Transportation Research Record* (2019), Vol. 2673(5) 709-719. <https://doi.org/10.1177/0361198119839974>
- Gavriilidou, A., Daamen, W., Yuan, Y. & Hoogendoorn, S. (2019). Modelling cyclist queue formation using a two-layer framework for operational cycling behavior. *Transportation Research Part C* 105 (2019) 468-484. <https://doi.org/10.1016/j.trc.2019.06.012>
- Grigoropoulos, G., Lücken, L., Erdmann, J. & Kath, H. (2019). Modelling Bicycle Infrastructure in SUMO. *EPiC Series in Computing Volume 62*, 187-198. <https://doi.org/10.29007/6cs5>
- Group A (2014). Casco Ontwerp Forum Westflank, Stationsgebied Utrecht.  
[https://cu2030.nl/images/2014-11/2014-09-16\\_BOEK%20Casco%20Ontwerp%20lowres.pdf](https://cu2030.nl/images/2014-11/2014-09-16_BOEK%20Casco%20Ontwerp%20lowres.pdf)
- Group A (2020). Plankaart Fourm Noord en SPW. Retrieved from:  
[https://issuu.com/bouwput/docs/spw\\_forum\\_noord](https://issuu.com/bouwput/docs/spw_forum_noord)



- Hardinghaus, M. & Papantoniou, P. (2020). Evaluating Cyclists' Route Preferences with Respect to Infrastructure. *Sustainability* 12, 3375. <https://doi.org/10.3390/su12083375>
- Harms, L. & Kansen, M. (2018). Cycling Facts. Netherlands Institute for Transport Policy Analysis (KiM). Ministry of Infrastructure and Water Management. <https://english.kimnet.nl/publications/publications/2018/04/06/cycling-facts>
- Helbing, D. & Molnár, P. (1995). Social Force Model for Pedestrian Dynamics. *Physical review. E, Statistical physics, plasmas, fluids, and related interdisciplinary topics* 51(5). <https://doi.org/10.1103/PhysRevE.51.4282>
- Hendriksen, I. & van Gijlswijk, R. (2010). Fietsen is groen, gezond en voordelig. TNO Quality of Life group. Retrieved from [http://s3-eu-west-1.amazonaws.com/fietsersbond/app/uploads/2010/01/18104705/rapport%20lvDM%20fietsen\\_lage%20resolutie.pdf](http://s3-eu-west-1.amazonaws.com/fietsersbond/app/uploads/2010/01/18104705/rapport%20lvDM%20fietsen_lage%20resolutie.pdf)
- Het Verkeershuis (2014). Fietstellingen incidenteel. City of Utrecht. Retrieved from: <https://data.overheid.nl/dataset/fietstellingen-incidenteel>
- Hermans, L. (2003). Fietsen 5x zuiniger dan lopen. NEMO Kennislink. Retrieved from: <https://www.nemokennislink.nl/publicaties/fietsen-5x-zuiniger-dan-lopen/>
- HIG Traffic Systems (2015). Utrecht verkeerstellingen najaar 2015. *Utrecht Dataplatform*. Retrieved from: <https://utrecht.dataplatform.nl/#/data/0a1fb0e4-8520-4e94-9c9f-17e2cbdd2f5>
- HIG Traffic Systems (2019). Fietstellingen Utrecht 2019. Data provided by: City of Utrecht.
- HIG Traffic Systems (2020). Fietstellingen Utrecht 2020. Data provided by: City of Utrecht.
- Hoogendoorn, S., van Wageningen-Kessels, F., Daamen, W. & Duives, D. (2014). Continuum modelling of pedestrian flows: From microscopic principles to self-organised macroscopic phenomena. *Physica A* 416(2014) 684–694. <http://dx.doi.org/10.1016/j.physa.2014.07.050>
- Hoogendoorn, S. & Daamen, W. (2016). Bicycle headway modeling and its applications. *Transportation Research Record: Journal of the Transportation Research Board* 2587, 34–40. <https://doi.org/10.3141/2587-05>
- Horni, A., Nagel, K. & Axhausen, K. (2016). The Multi-Agent Transport Simulation MATSim. London: Ubiquity Press. <https://doi.org/10.5334/baw>
- Huang, L., Wu, J., You, F., Lv, Z. & Song, H. (2017). Cyclist Social Force Model at Unsignalized Intersections With Heterogeneous Traffic. *IEEE Transactions on Industrial Informatics* 13 (2). 782–792. <https://doi.org/10.1109/TII.2016.2597744>
- Huang, W., Fellendorf, M. & Schönauer, R. (2012). Social Force based Vehicle Model for 2-dimensional Spaces. *Transportation Research Board 91st Annual Meeting* 12, 1–16. <https://graz.pure.elsevier.com/en/publications/social-force-based-vehicle-model-for-two-dimensional-spaces>
- Huber, S., Lissner, S. & Francke, A. (2019). Utility of GPS data for urban bicycle traffic planning in Germany: Potentiality, limitations and prospects. *International Journal of Transport Development and Integration* 3(1). 1–14. <https://doi.org/10.2495/TDI-V3-N1-1-14>
- Hung, N. & Lim, O. (2020). A review of history, development, design and research of electric bicycles. *Applied Energy* 260, 114323. <https://doi.org/10.1016/j.apenergy.2019.114323>

- InControl (n.d.). Pedestrian Dynamics. *InControl*. Retrieved at 23-11-1020, from: <https://www.incontrolsim.com/software/pedestrian-dynamics/>
- Jaarbeurs (2019). Masterplan Jaarbeurs en Jaarbeursdistrict. Retrieved from: [https://issuu.com/bouwput/docs/masterplan\\_nieuwe\\_jaarbeurs\\_en\\_jaarbeursdistrict\\_d](https://issuu.com/bouwput/docs/masterplan_nieuwe_jaarbeurs_en_jaarbeursdistrict_d)
- Johansson, F., Duives, D., Daamen, W. & Hoogendoorn, S. (2014). The many roles of the relaxation time parameter in force based models of pedestrian dynamics. *Transportation Research Procedia* 2, 300 – 308. <https://doi.org/10.1016/j.trpro.2014.09.057>
- Jousma, A., Winkel, de, C., Weperen, van, S., Terlouw, D., Huisman, H., Kwant, A., Palsrok, C. & Kinzel, W. (2018). Verkeersmodel Regio Utrecht VRU3.4 Technische rapportage en verantwoording. Retrieved from: <https://www.utrecht.nl/fileadmin/uploads/documenten/bestuur-en-organisatie/publicaties/onderzoek-en-cijfers/verkeerscijfers/2018-10-rapport-verkeersmodelregio-utrecht-VRU3-4.pdf>
- Kadaster (2021). Basisregistratie Adressen en Gebouwen (BAG). Retrieved from: <https://bagviewer.kadaster.nl/lvbag/bag-viewer/index.html#?geometry.x=135784.53303612&geometry.y=455396.97960214&zoomlevel=4>
- Kalter, M. & Groenendijk, L. (2018). Onderzoek reistijdbeleving fietsers. *Goudappel Coffeng, NS, ThuisraadRO, Universiteit van Amsterdam*. Retrieved from: <https://www.goudappel.nl/download?path=%2Fmedia%2F678641%2Fonderzoek-reistijdbeleving-fietsers.pdf>
- Kawwa, N. (2020). When to Use the Kolmogorov-Smirnov Test. *Towards Data Science*. Retrieved from: <https://towardsdatascience.com/when-to-use-the-kolmogorov-smirnov-test-dd0b2c8a8f61>
- Khan, S. & Raksuntorn, W. (2001). Characteristics of Passing and Meeting Maneuvers on Exclusive Bicycle Paths. *Transportation Research Record* 1776 (1), 220-228. <https://doi.org/10.3141/1776-28>
- Krajzewicz, D., Erdmann, J., Härr, J. & Spyropoulos, T. (2014). Including Pedestrian and Bicycle Traffic in the Traffic Simulation SUMO. *10th ITS European Congress, Helsinki*. From: [https://www.researchgate.net/publication/314949965\\_An\\_Approach\\_for\\_Simulating\\_Bicycle\\_Traffic\\_using\\_Observed\\_Trajectory\\_Data](https://www.researchgate.net/publication/314949965_An_Approach_for_Simulating_Bicycle_Traffic_using_Observed_Trajectory_Data)
- Kretz, T., Lohmiller, J. & Sukennik, P. (2018). Some Indications on How to Calibrate the Social Force Model of Pedestrian Dynamics. *Transportation Research Record* 2672 (20) 228–238. <https://doi.org/10.1177/0361198118786641>
- Lagervall, M. & Samuelsson, S. (2014). Microscopic Simulation of pedestrian traffic in a station environment; a study of actual and desired walking speeds. <https://www.diva-portal.org/smash/get/diva2:763111/FULLTEXT01.pdf>
- Lee, K. & Sener, I. (2020). Emerging data for pedestrian and bicycle monitoring: Sources and applications. *Transportation Research Interdisciplinary Perspectives* 4 (2020) 100095. <http://dx.doi.org/10.1016/j.trip.2020.100095>
- Li, M., Shi, F. & Chen, D. (2011). Analyze bicycle-car mixed flow by social force model for collision risk evaluation. *3rd International Conference on Road Safety and Simulation*, 14-16. From: <https://www.semanticscholar.org/paper/ANALYZE-BICYCLE-CAR-MIXED-FLOW-BY-SOCIAL-FORCE-FOR-Li/d16b9d21e175443649db3d2745155c19fbd93dd3>

- Liang, X., Mao, B. & Xu, Q. (2012). Psychological-Physical Force Model for Bicycle Dynamics. *Journal of Transportation Systems Engineering and Information Technology*, Volume 12, Issue 2. (2012) 91-97. [https://doi.org/10.1016/S1570-6672\(11\)60197-9](https://doi.org/10.1016/S1570-6672(11)60197-9)
- Liang, X., Xie, M. & Jia, X. (2018). New microscopic dynamic model for bicyclists' riding strategies. *Journal of Transportation Engineering, Part A* 144 (8), 1-16. <https://doi.org/10.1061/JTEPBS.0000148>
- Lin, Z. & Fan W. (2020). Modeling bicycle volume using crowdsourced data from Strava smartphone application. *International Journal of Transportation Science and Technology*. <https://doi.org/10.1016/j.ijtst.2020.03.003>
- Liu, Q., Sun, J., Tian, Y. & Xiong, L. (2020). Modeling and Simulation of Overtaking Events by Heterogeneous Non-Motorized Vehicles on Shared Roadway Segments. *Simulation Modelling Practice and Theory* 103. <https://doi.org/10.1016/j.simpat.2020.102072>
- Liu, Y., Yang, D., Timmermans, H. & de Vries, B. (2020). Analysis of the impact of street-scale built environment design near metro stations on pedestrian and cyclist road segment choice: A stated choice experiment. *Journal of Transport Geography* 82 (2020) 102570 <https://doi.org/10.1016/j.jtrangeo.2019.102570>
- Livingston, M., McArthur, D., Hong, J. & English, K. (2020). Predicting cycling volumes using crowdsourced activity data. *Environment and Planning B: Urban Analytics and City Science* 0(0) 1-17. <https://doi.org/10.1177/2399808320925822>
- Lopez, M. (2019). Modelling Movements in Shared-Use Paths with PTV Viswalk. *Master's thesis, University of Stuttgart*. Retrieved from: [https://www.researchgate.net/publication/344877520\\_Modelling\\_Movements\\_in\\_Shared-Use\\_Paths\\_with\\_PTV\\_Viswalk](https://www.researchgate.net/publication/344877520_Modelling_Movements_in_Shared-Use_Paths_with_PTV_Viswalk)
- Ma, X. & Luo, D. (2016). Modeling cyclist acceleration process for bicycle traffic simulation using naturalistic data. *Transportation Research Part F* 40 (2016) 130-144. <https://doi.org/10.1016/j.trf.2016.04.009>
- Maptiler (n.d.). WGS 84 - World Geodetic System 1984, used in GPS. *EPSG.io*. Retrieved at 20-12-2020, from: <https://epsg.io/4326>
- Mathew, T., Munigety, C. & Bajpai, A. (2015). Strip-Based Approach for the Simulation of Mixed Traffic Conditions. *Journal of Computing in Civil Engineering*, 29(5). [https://doi.org/10.1061/\(ASCE\)CP.1943-5487.0000378](https://doi.org/10.1061/(ASCE)CP.1943-5487.0000378)
- Mauttone, A., Mercadante, G., Rabaza, M., & Toledo, F. (2017). Bicycle network design: model and solution algorithm. *Transportation Research Procedia* 27 (2017) 969-976. <https://doi.org/10.1016/j.trpro.2017.12.119>
- McArthur, D. & Hong, J. (2019). Visualising where commuting cyclists travel using crowdsourced data. *Journal of Transport Geography* 74 (2019) 233-241. <https://doi.org/10.1016/j.jtrangeo.2018.11.018>
- Meel, van der, E. (2013). Red light running by Cyclists: Which factors influence the red light running by cyclists? *Thesis TU Delft, Civil Engineering and Geosciences*. Retrieved from: <http://resolver.tudelft.nl/uuid:1242ee85-a041-44c5-b291-2b0dddc82ed0>

- Mohammed, H., Bigazzi, A. & Sayed, T. (2019). Characterization of bicycle following and overtaking maneuvers on cycling paths. *Transportation Research Part C* 98 (2019) 139–151. <https://doi.org/10.1016/j.trc.2018.11.012>
- Munigety, C., Sivkov, B., Dhandapani, P. & Al Jayyousi, M. (2020). Webinar: Integrating the PTV Vissim with Unity3D for carrying out driver behavioral studies. *PTV Group Channel*. Retrieved from: <https://www.youtube.com/watch?v=RP5B64dm-7g>
- Nagel, K. & Schreckenberg, M. (1992). A cellular automation model for freeway traffic. *Journal de Physique I*, vol. 2(12) 2221– 2229. <https://www.researchgate.net/publication/263504490>
- NDC (2018). Verkeerstellingen Westplein Utrecht. Data provided by: City of Utrecht.
- Netherlands Institute for Transport Policy Analysis [KiM] (2016). Mobiliteitsbeeld 2016. Kennisinstituut voor het Mobiliteitsbeleid, *Ministry of Infrastructure and Water Management*. Retrieved from: <https://www.kimnet.nl/actueel/nieuws/2016/10/24/mobiliteitsbeeld-2016>
- Netherlands Institute for Transport Policy Analysis [KiM] (2019). Mobiliteitsbeeld 2019. *Ministry of Infrastructure and Water Management*. Retrieved from: <https://www.kimnet.nl/publicaties/rapporten/2019/11/12/mobiliteitsbeeld-2019-vooral-het-gebruik-van-de-trein-neemt-toe>
- Nijland, H. (2017). Fietsen leidt tot langer en gezond leven. *Netherlands Environmental Assessment Agency (PBL)*. Retrieved from: <https://www.pbl.nl/publicaties/fietsen-leidt-tot-langer-en-gezond-leven>
- Nigam, V. (2018). Statistical Tests — When to use Which. *Towards Data Science*. Retrieved from: <https://towardsdatascience.com/statistical-tests-when-to-use-which-704557554740>
- NS (2019). Grootste, kleinste en snelst groeiende stations 2018. Retrieved from: <https://nieuws.ns.nl/download/731822/nsin-enuitstappers2018-409296.pdf>
- Olstam, J. & Tapani, A. (2004). Comparison of Car-following models. *Swedish National Road Administration*. <https://www.diva-portal.org/smash/get/diva2:673977/FULLTEXT01.pdf>
- Oostvogels, B. (2018). De populairste autokleuren van Nederland. *Autonieuws*. Retrieved from: <https://autorai.nl/de-populairste-autokleuren-van-nederland-2018/>
- OpenStreetMap (n.d.). OpenStreetMap. Retrieved at 03-11-2020, from: <https://www.openstreetmap.org/about>
- Ordinez, L., Savarro, M., Ascagorta, O., Cura, R., Buckle, C., Barry, D. & Stickar, R. (2018). A Cyclists Traffic Simulation and Analysis Tool. *Proceedings 2018*, 2(19), 1220. <https://doi.org/10.3390/proceedings2191220>
- OSGeo (n.d.). About OSGeo. Retrieved at 03-11-2020, from <https://www.osgeo.org/about/>
- Osowski, C. & Waterson, B. (2017). Establishing the validity of cycle path capacity assumptions in the Highway Capacity Manual. *International Journal of Sustainable Transportation* 11 (6), 422–432. <https://doi.org/10.1080/15568318.2016.1266424>
- Paulsen, M., Rasmussen, T. & Nielsen, O. (2019). Fast or forced to follow: A speed heterogeneous approach to congested multi-lane bicycle traffic simulation. *Transportation Research Part B* 127 (2019) 72–98. <https://doi.org/10.1016/j.trb.2019.07.002>

- Pogodzinska, S., Kiec, M., & D'Agostino, C. (2020). Bicycle Traffic Volume Estimation Based on GPS Data. *Transportation Research Procedia* 45 (2020) 874–881. <https://doi.org/10.1016/j.trpro.2020.02.081>
- Poll, van, R., Breugelmans, O., Houthuijs, D. & van den Broek, I. (2016). Beleving Woonomgeving in Nederland : Inventarisatie Verstoringen 2016. *National Institute for Public Health and the Environment (RIVM)*. <https://doi.org/10.21945/RIVM-2018-0084>
- Province of Utrecht (2020). Vernieuwde tramlijn 60 Utrecht-Nieuwegein/Zuid rijdt vanaf 3 januari. Retrieved from: <https://www.provincie-utrecht.nl/actueel/nieuws/vernieuwde-tramlijn-60-utrecht-nieuwegeinzuid-rijdt-vanaf-3-januari>
- PTV Group (2020). PTV Vissim 2020 User Manual. Retrieved as part of the installation from: <https://www.ptvgroup.com/en/ptv-group/ptv-academics/> Online version: [https://cgi.ptvgroup.com/vision-help/VISSIM\\_2020\\_ENG/Content/0\\_TitelCopyright/Index.htm](https://cgi.ptvgroup.com/vision-help/VISSIM_2020_ENG/Content/0_TitelCopyright/Index.htm)
- Qu, Z., Cao, N., Chen, Y., Zhao, L., Bai, Q. & Luo, R. (2017). Modeling electric bike–car mixed flow via social force model. *Advances in Mechanical Engineering* 2017, Vol. 9(9) 1–14. <https://doi.org/10.1177/1687814017719641>
- Ramzai, J. (2020). Clearly explained: Pearson V/S Spearman Correlation Coefficient. *Towards Data Science*. Retrieved from: <https://towardsdatascience.com/clearly-explained-pearson-v-s-spearman-correlation-coefficient-ada2f473b8>
- Richardson, M. & Caulfield, B. (2015). Investigating traffic light violations by cyclists in Dublin City Centre. *Accident Analysis & Prevention*, 84, 65–73. <http://www.tara.tcd.ie/handle/2262/74776>
- Rinke, N., Schiermeyer, C., Pascucci, F., Berkhahn, V. & Friedrich, B. (2017). A multi-layer social force approach to model interactions in shared spaces using collision prediction. *Transportation Research Procedia* 25 (2017) 1249–1267. <https://doi.org/10.1016/j.trpro.2017.05.144>
- Rosman, S. (2015). Path planning for cyclists. (Master's thesis). *Utrecht University*. Retrieved from: <https://dspace.library.uu.nl/bitstream/handle/1874/320194/path-planning-cyclists%20aug%2027.pdf?sequence=2&isAllowed=y>
- Roy, A., Nelson, T., Fotheringham, S. & Winters, M. (2019). Correcting Bias in Crowdsourced Data to Map Bicycle Ridership of All Bicyclists. *Urban Science* 3(62) <https://doi.org/10.3390/urbansci3020062>
- Royal HaskoningDHV (2018). Doorstroming Voorlopig Ontwerp Busbaan Dichterswijk. *Gemeente Utrecht*. Retrieved from: [https://www.planviewer.nl/imro/files/NL.IMRO.0344.BPKRUISVAARTKWARTI-VA02/b\\_NL.IMRO.0344.BPKRUISVAARTKWARTI-VA02\\_tb4.pdf](https://www.planviewer.nl/imro/files/NL.IMRO.0344.BPKRUISVAARTKWARTI-VA02/b_NL.IMRO.0344.BPKRUISVAARTKWARTI-VA02_tb4.pdf)
- Saidallah, M., El-Fergougui, A. & Elalaoui, E. (2016). A Comparative Study of Urban Road Traffic Simulators. *MATEC Web of Conferences* 81 05002 (2016) <https://doi.org/10.1051/matecconf/20168105002>
- Saifuzzaman, M. & Zheng, Z. (2014). Incorporating human-factors in car-following models: A review of recent developments and research needs. *Transportation Research Part C* 48 (2014) 379–403. <http://dx.doi.org/10.1016/j.trc.2014.09.008>
- Sallomi, P., Lee, P., Jarvis, D., Casey, M., Loucks, J., Arkenberg, C., Wigginton, C. & Stewart, D. (2020). Technology, Media, and Telecommunications predictions 2020. *Deloitte insights*. Retrieved



from: [https://www2.deloitte.com/content/dam/insights/us/articles/722835\\_tmt-predictions-2020/DI\\_TMT-Prediction-2020.pdf](https://www2.deloitte.com/content/dam/insights/us/articles/722835_tmt-predictions-2020/DI_TMT-Prediction-2020.pdf)

Schönauer, R., Stubenschrott, M., Huang, W., Fellendorf, M. & Rodloff, C. (2012). Modeling Concepts for Mixed Traffic Steps Toward a Microscopic Simulation Tool for Shared Space Zones. *Transportation Research Record Journal of the Transportation Research Board* 2316. 114-121. <https://doi.org/10.3141/2316-13>

Seer, S., Rudloff, C., Matyus, T. & Brändle, N. (2014). Validating social force based models with comprehensive real world motion data. *Transportation Research Procedia* 2 ( 2014 ) 724-732. <https://doi.org/10.1016/j.trpro.2014.09.080>

Su, V. (2019). In Cycle-Crazed Utrecht, the World's Largest Bike Parking Facility Opens. *Metropolis*. Retrieved from: <https://www.metropolismag.com/architecture/bicycle-garage-utrecht/>

Sun, Q., Feng, T., Kemperman, A. & Spahn, A. (2020). Modal shift implications of e-bike use in the Netherlands: Moving towards sustainability? *Transportation Research Part D* 78 (2020) 102202. <https://doi.org/10.1016/j.trd.2019.102202>

Toll, van, W., Triesscheijn, R., Kallmann, M., Oliva, R., Pelechano, N., Pettre, J. Geraerts, R. (2016). A comparative study of navigation meshes. *MIG '16: Proceedings of the 9th International Conference on Motion in Games* 91-100. <https://doi.org/10.1145/2994258.2994262>

Tour de Force (2017). Agenda fiets 2017-2020. *Ministry of Infrastructure and Water Management*. Retrieved from: <https://www.rijksoverheid.nl/binaries/rijksoverheid/documenten/rapporten/2017/02/16/agenda-fiets-2017-2020/agenda-fiets-2017-2020.pdf>

Tour de Force (2021). Nationaal Toekomstbeeld Fiets op hoofdlijnen. *CROW fietsberaad*. Retrieved from: <https://www.fietsberaad.nl/Kennisbank/Nationaal-Toekomstbeeld-Fiets-op-hoofdlijnen>

Transport for London (2017). Analysis of Cycling Potential. *Policy Analysis Report*. Retrieved from: <http://content.tfl.gov.uk/analysis-of-cycling-potential-2016.pdf>

Transystem (n.d.). GL-770. Retrieved at 10-11-2020, from: <http://www.transystem.com.tw/www/product.php?b=G&m=pe&cid=4&sid=14&id=150>

Trimble (n.d.). Sketchup Pro. Retrieved at 20-12-2020, from: <https://www.sketchup.com/products/sketchup-pro>

TU/e (2019). Data management and data storage for surveys. Retrieved from TU/e Intranet.

Twaddle, H. (2018). Analysis and Modelling of the Operational and Tactical Behaviour of Bicyclists. *UR:BAN Human Factors in Traffic*. [https://doi.org/10.1007/978-3-658-15418-9\\_18](https://doi.org/10.1007/978-3-658-15418-9_18)

Twaddle, H. & Grigoropoulos, G. (2016). Modeling the speed, acceleration and deceleration of bicyclists for microscopic traffic simulation. *Journal of the Transportation Research Board*, 2587. <https://doi.org/10.3141/2587-02>

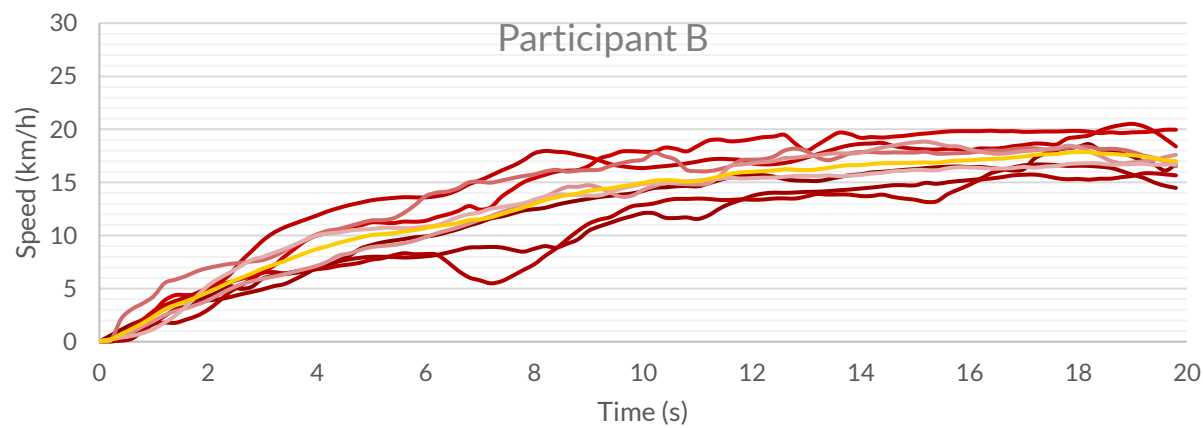
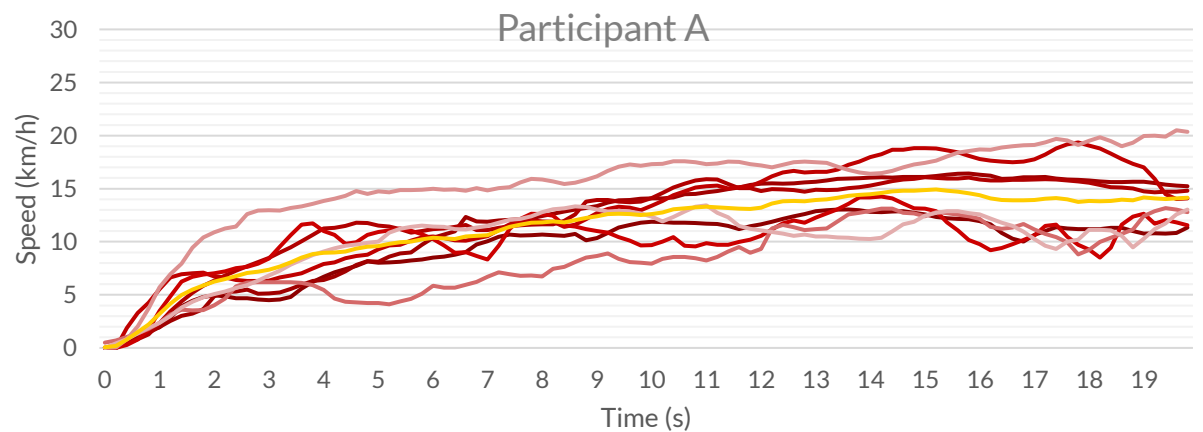
Twaddle, H., Grigoropoulos, G. & Busch, F. (2016). Integration of an External Bicycle Model in SUMO. *Conference: SUMO Conference 2016, Berlin*. From: [https://www.researchgate.net/publication/302909195\\_Integration\\_of\\_an\\_External\\_Bicycle\\_Model\\_in\\_SUMO](https://www.researchgate.net/publication/302909195_Integration_of_an_External_Bicycle_Model_in_SUMO)

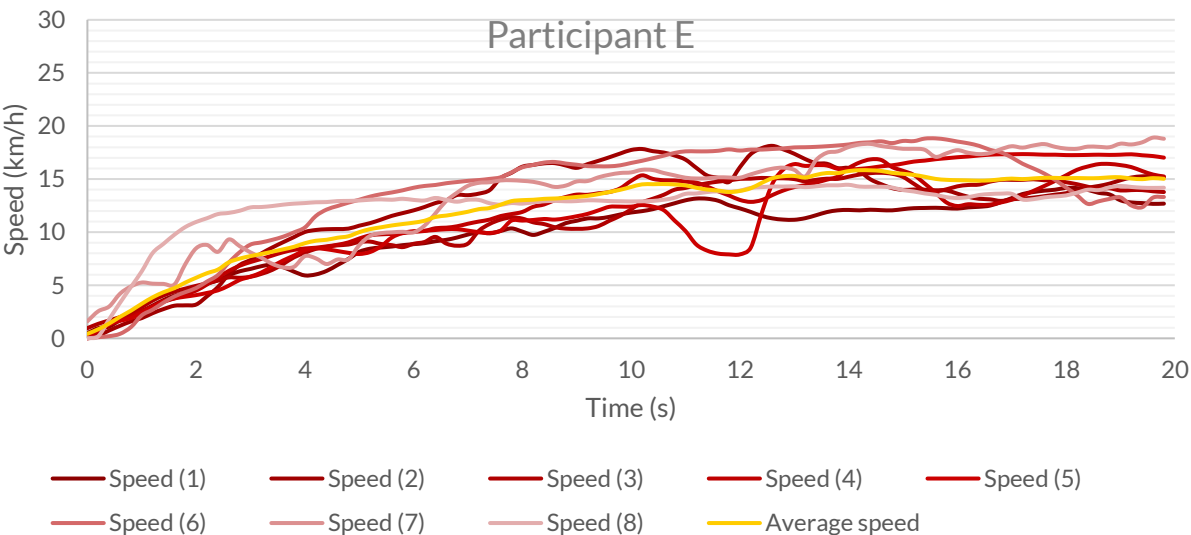
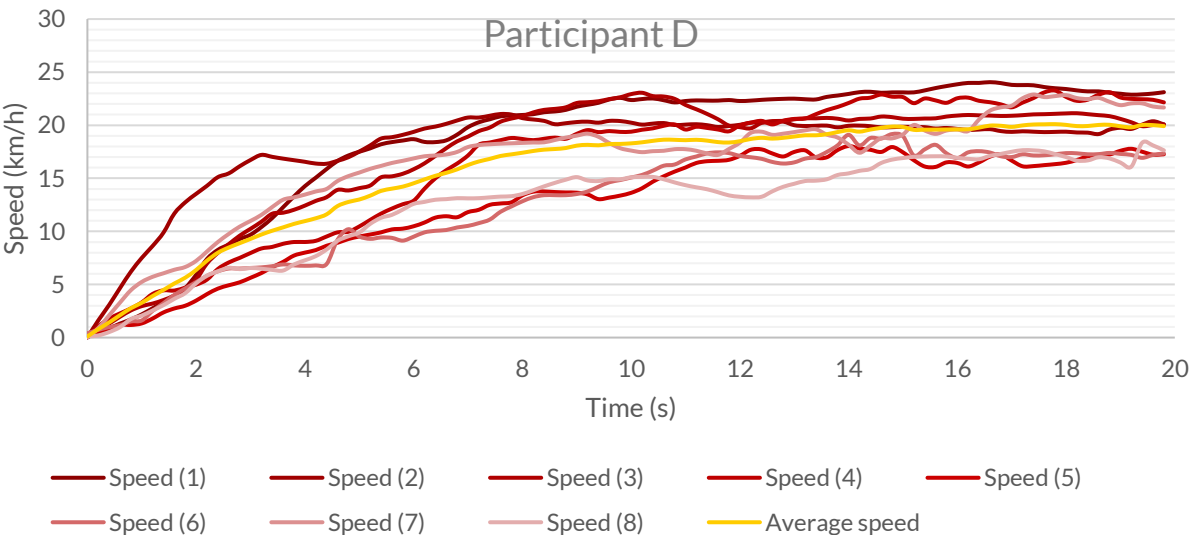
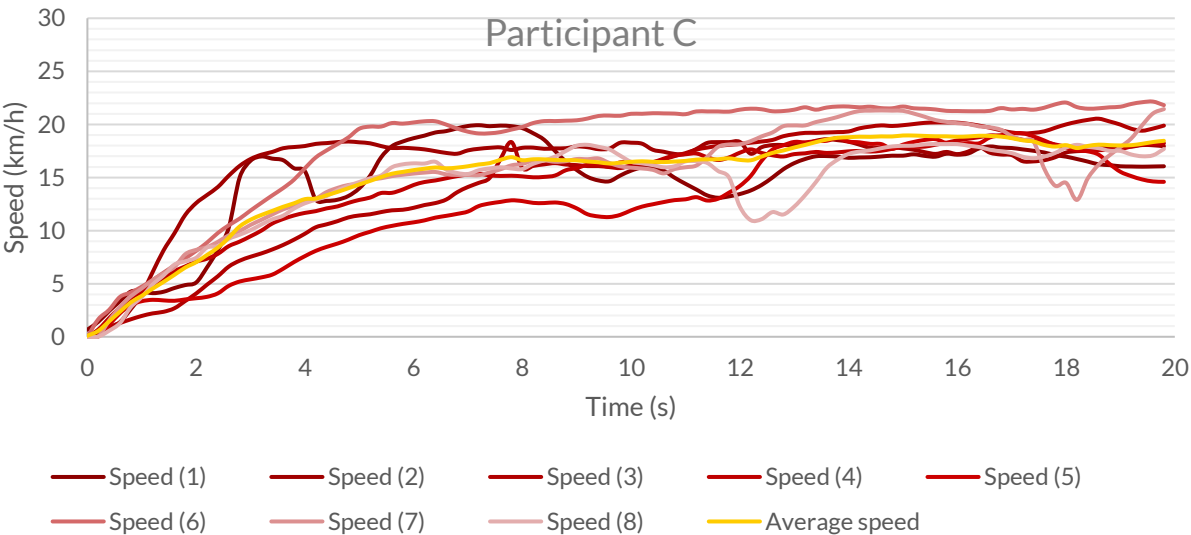
Twaddle, H., Schendzielorz, T. & Fakler, O. (2014). Bicycles in urban areas: Review of existing methods for modeling behavior. *Transportation Research Record Journal of the Transportation Research Board* 2434 140-146. <https://doi.org/10.3141/2434-17>

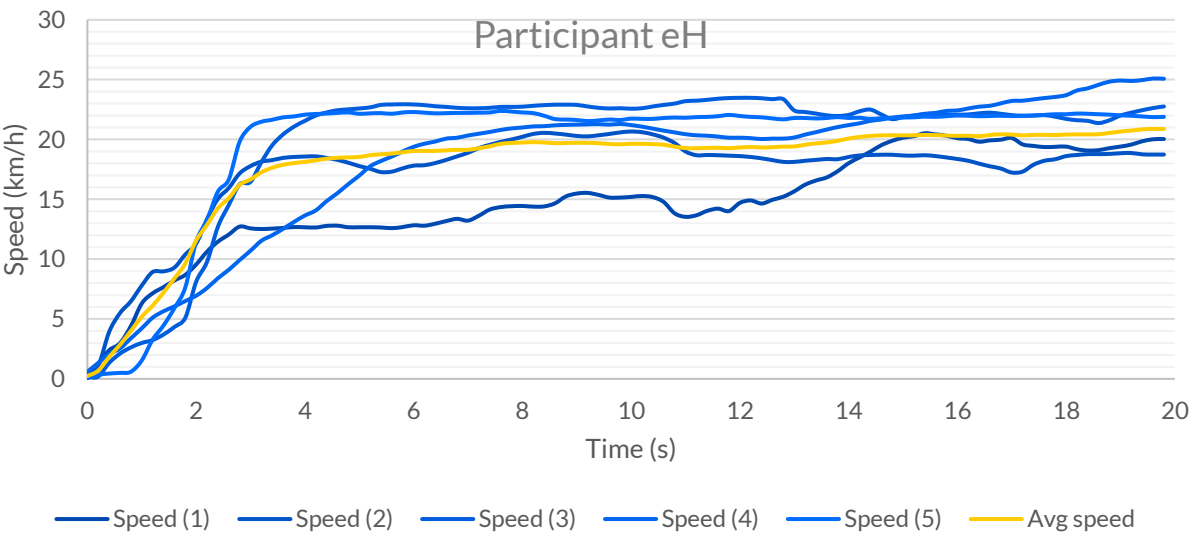
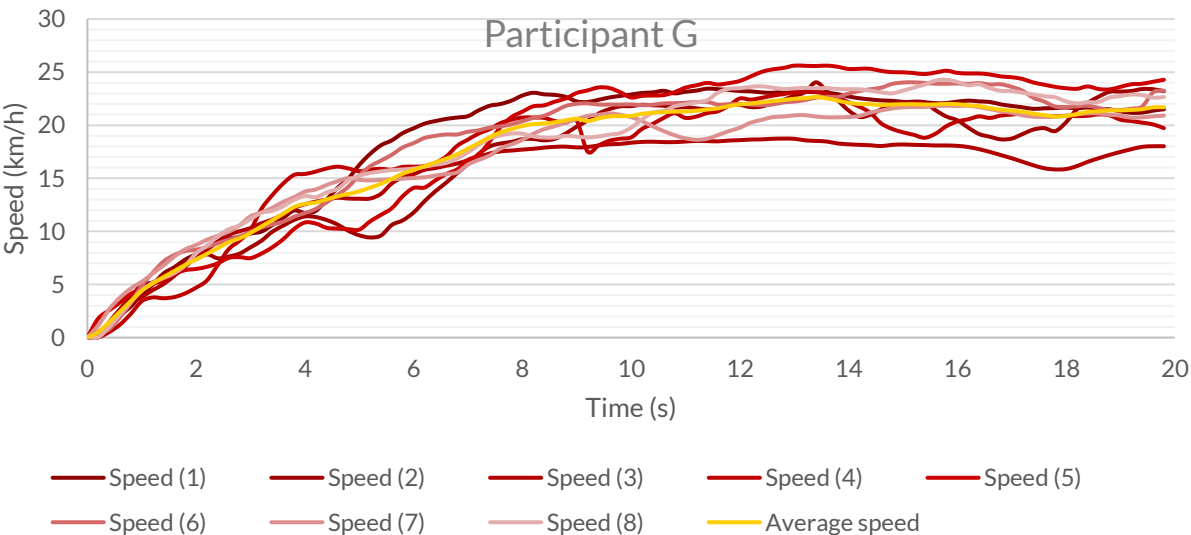
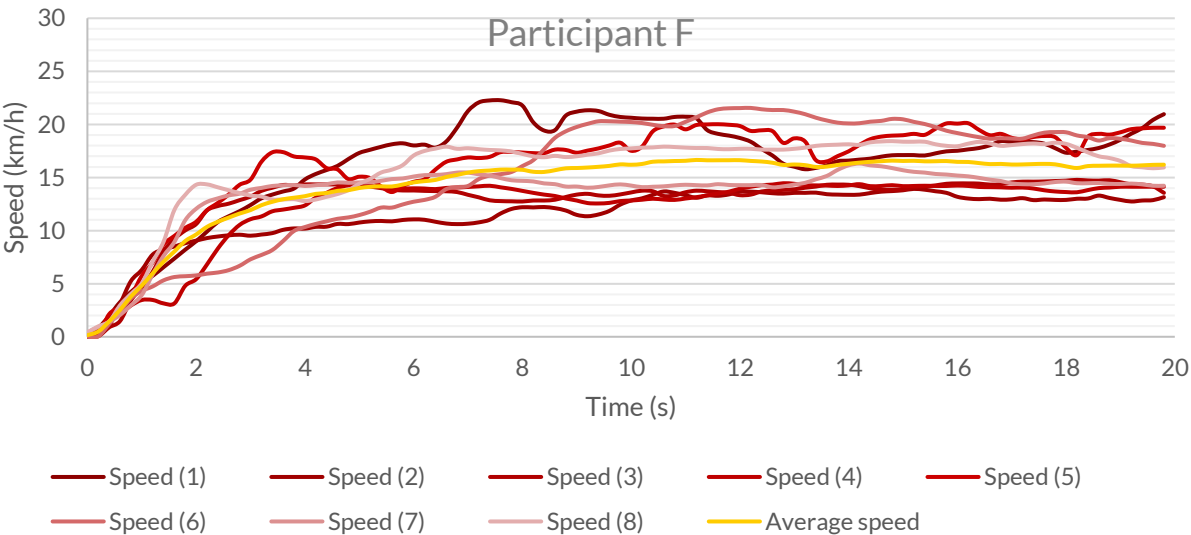
- UCrowds (n.d.). Crowd simulation. *UCrowds*. Retrieved at 02-09-2020, from: <https://www.ucrowds.com/>
- U-OV (n.d.). Dienstregeling lijn 60 van Utrecht CS naar Nieuwegein. Retrieved at 01-02-2021, from: <https://www.u-ov.info/lijn/QBUZZ/u060/1>
- U-OV (2021). Lijnenkaart. Retrieved from: [https://uov-prod.cdn.prismic.io/uov-prod/91ecaa3f-1077-4128-9cdd-1d5bf3f6fb0e\\_301+-+WEB+-+Netplan+BRU+-+012021.pdf](https://uov-prod.cdn.prismic.io/uov-prod/91ecaa3f-1077-4128-9cdd-1d5bf3f6fb0e_301+-+WEB+-+Netplan+BRU+-+012021.pdf)
- Waard, van, D., Schepers, P., Ormel, W. & Brookhuis, K. (2010). Mobile phone use while cycling: Incidence and effects on behaviour and safety. *Ergonomics*, 53:1, 30-42. <https://doi.org/10.1080/00140130903381180>
- Wiedemann, R. (1974). Simulation des Straßenverkehrsflusses. Schriftenreihe des Instituts für Verkehrswesen der Universität Karlsruhe.
- Wierbos, M., Knoop, V., Hänseler F. & Hoogendoorn, S. (2019). Capacity, Capacity Drop, and Relation of Capacity to the Path Width in Bicycle Traffic. *Transportation Research Record* (2019), Vol. 2673(5) 693–702. <https://doi.org/10.1177/0361198119840347>
- Wierbos, M., Knoop, V., Hänseler F. & Hoogendoorn, S. (2020). A macroscopic flow model for mixed bicycle–car traffic. *Transportmetrica A: Transport Science*. <https://doi.org/10.1080/23249935.2019.1708512>
- Winters, M. & Teschke, K. (2010). Route preferences among adults in the near market for bicycling: Findings of the cycling in cities study. *American Journal of Health Promotion*. 25(1) 40–47. <https://doi.org/10.4278/ajhp.081006-QUAN-236>
- Wolbertus, S. (2020). Personal communication, 21-12-2020. Advisor Urban Development, City of Utrecht
- Wu, A., Qi, L. & Yang, X. (2013). Mechanism Analysis and Optimization of Signalized Intersection Coordinated Control under Oversaturated Status. *Procedia - Social and Behavioral Sciences* 96 (2013) 1433–1442. <https://doi.org/10.1016/j.sbspro.2013.08.163>
- Yuan, Y., Goñi-Ros, B., Poppe, M., Daamen, W. & Hoogendoorn, S. (2019). Analysis of Bicycle Headway Distribution, Saturation Flow and Capacity at Signalized Intersection using Empirical Trajectory Data. *Transportation Research Record* 2019, Vol. 2673(6) 10–21. <https://doi.org/10.1177/0361198119839976>
- Zhou, D., Xu, C., Wang, D. & Jin, S. (2014). Estimating Capacity of Bicycle Path on Urban Roads in Hangzhou, China. *The 94th 43 Annual Meeting of the Transportation Research Board*. [https://nacto.org/wp-content/uploads/2016/04/5\\_Zhou-Xu-Wang-and-Sheng-Estimating-Capacity-of-Bicycle-Path-on-Urban-Roads-in-Hangzhou-China\\_2014.pdf](https://nacto.org/wp-content/uploads/2016/04/5_Zhou-Xu-Wang-and-Sheng-Estimating-Capacity-of-Bicycle-Path-on-Urban-Roads-in-Hangzhou-China_2014.pdf)
- Ziemke, D., Metzler, S. & Nagel, K. (2017). Modeling bicycle traffic in an agent-based transport simulation. *Procedia Computer Science* 109C (2017) 923–928. <https://doi.org/10.1016/j.procs.2017.05.424>

# Appendices

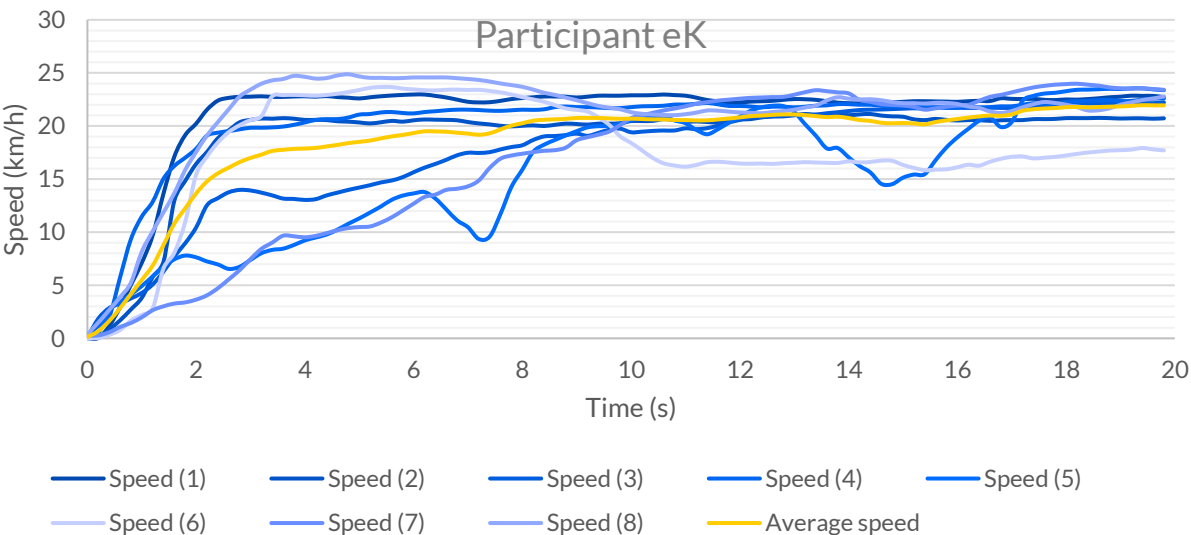
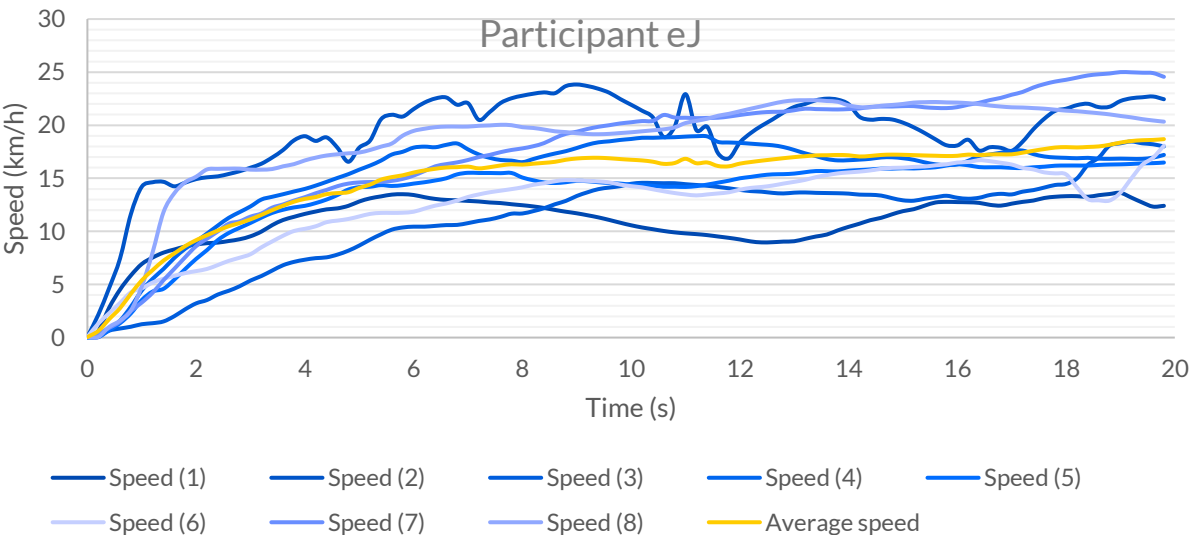
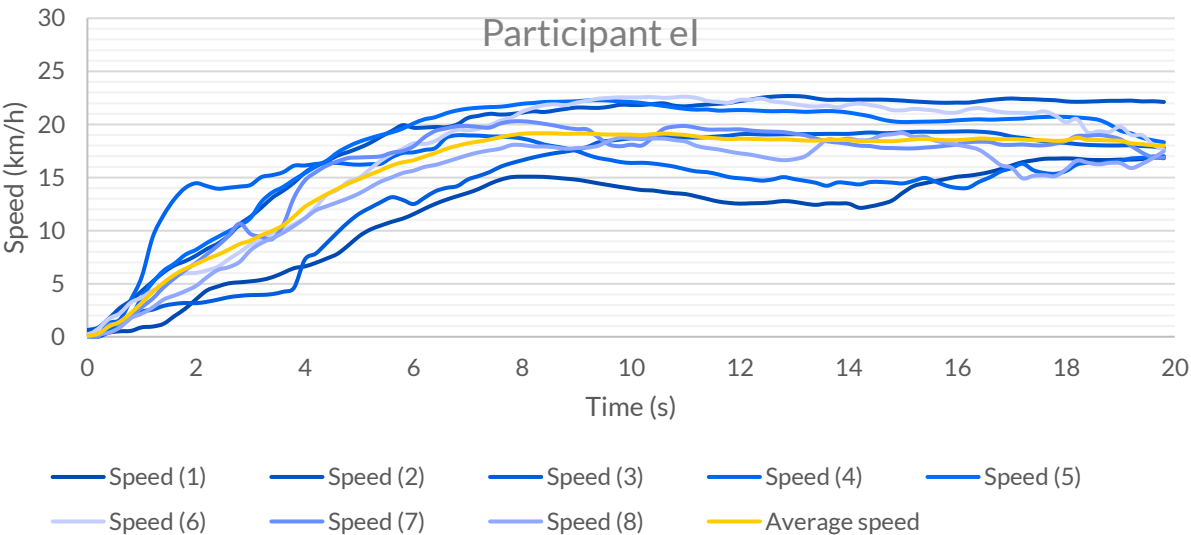
## Appendix A. Speed profiles





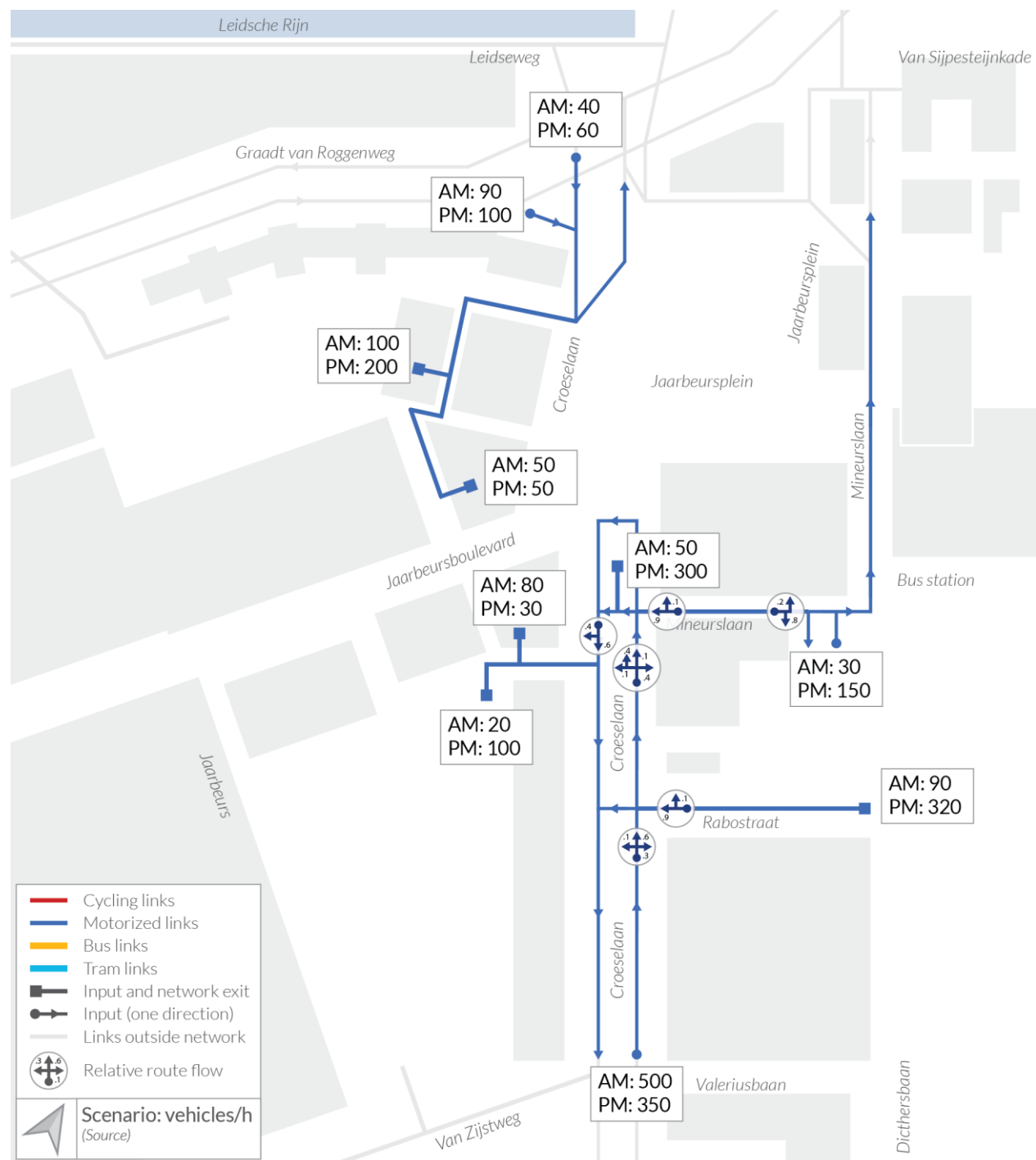




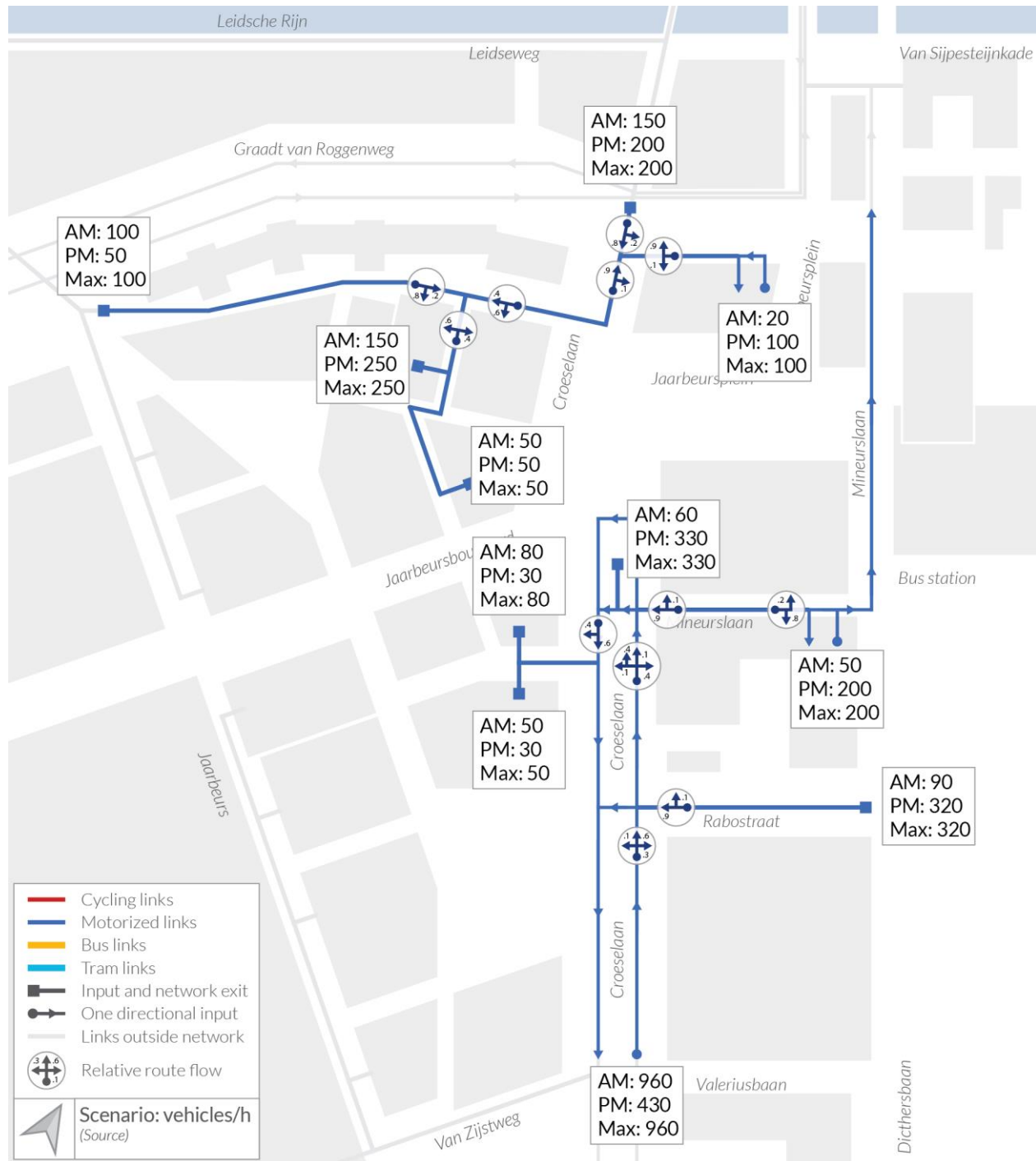


## Appendix B. Motorized traffic input and relative route flow

Base network:

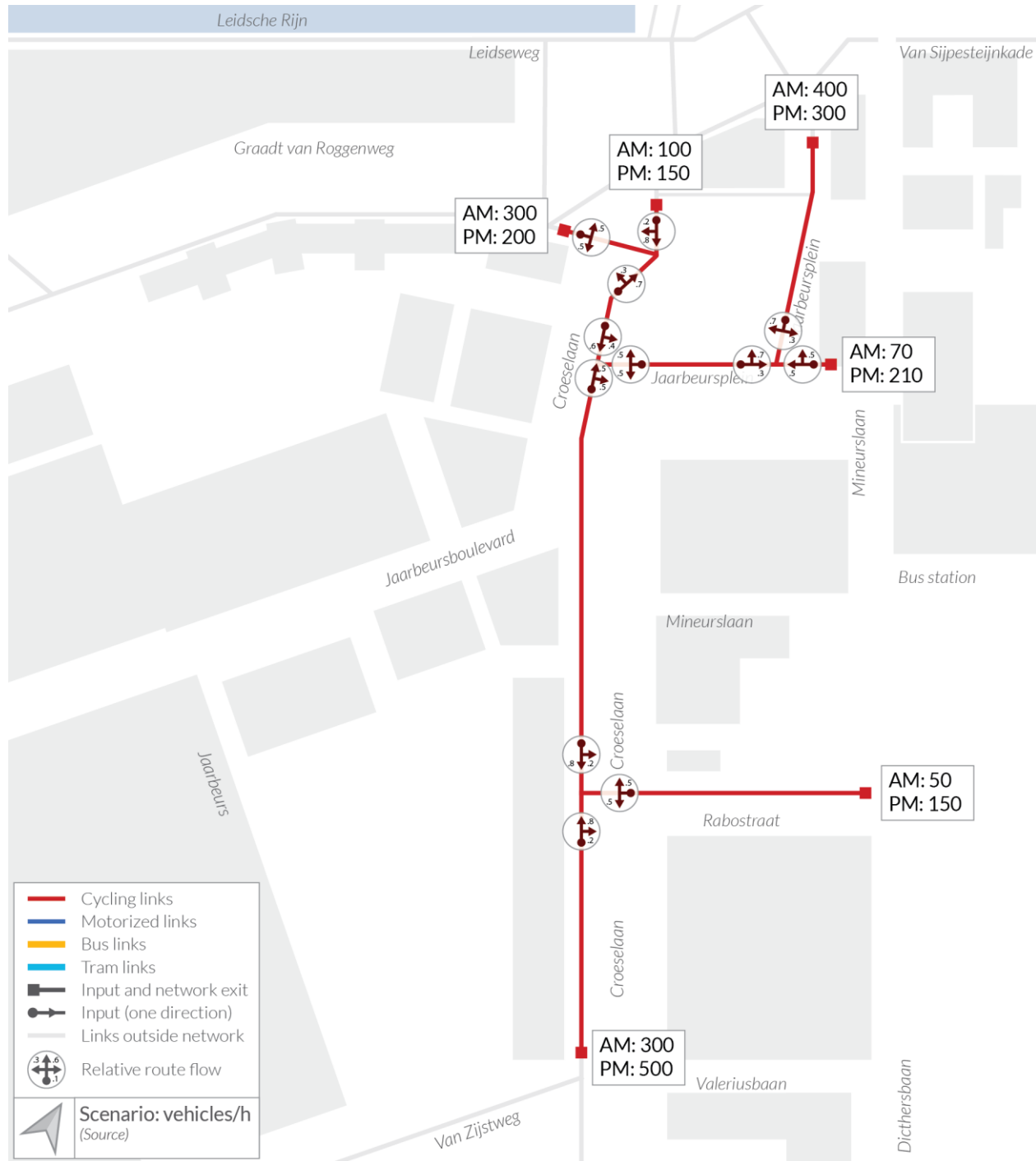


## Future network:

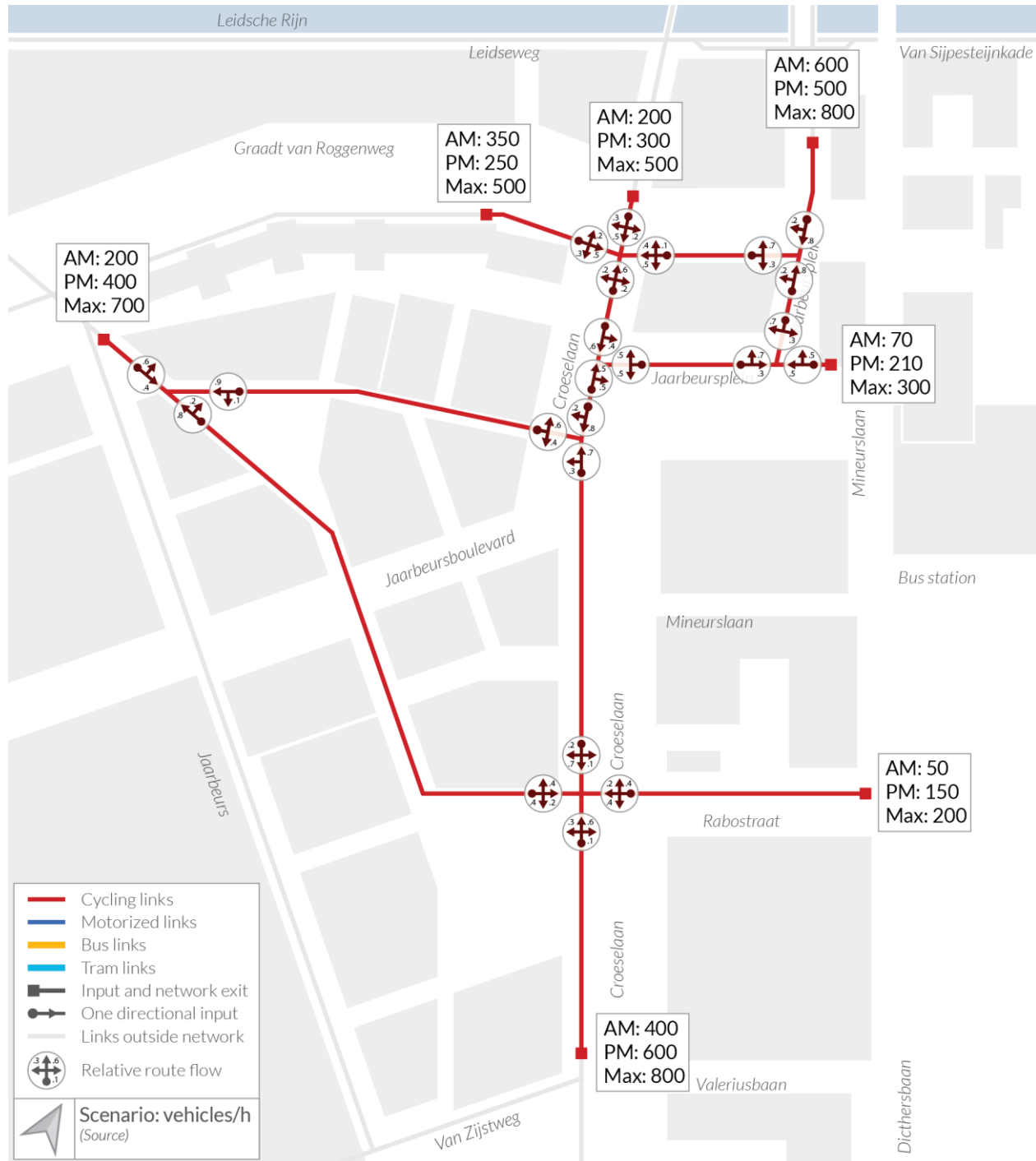


## Appendix C. Cycling traffic input and relative route flow

Base network:



## Future network:





Total	Origins \ Destinations	Destinations																										
		Croeslaan - SouthEast	Croeslaan - SouthWest	Moreelsbrug	Central Station	Forum North	Jaarbeursplein - NorthEast	Croeslaan North	Graadt van Groggeweg North	Jaarbeurs	Rabobank lower level	Rabobank upper level	Knoop Office	Beatrix theater	City Hall	WTC Forum level	WTC base level	Central Park	Parking Jaarbeursplein - East	Parking Jaarbeursplein - West	Hojel city center 1	Hojel city center 2	Galaxy Tower	Wondervoods west	Wondervoods east	Kinepolis	Tram Waiting to city center	Tram Waiting to Nieuwegein
130	Croeslaan - SouthEast		10	10	50	10	10	10	10	10	0	0	0	0	0	0	0	0	0	0	0	0	0	0	0	0	0	0
130	Croeslaan - SouthWest	10		10	50	10	10	10	10	10	0	0	0	0	0	0	0	0	0	0	0	0	0	0	0	0	0	0
130	Moreelsbrug	10	10		50	10	10	10	10	10	0	0	0	0	0	0	0	0	0	0	0	0	0	0	0	0	0	0
770	Central Station	50	50	50		50	50	50	50	50	20	20	20	20	20	20	20	20	20	20	20	20	20	20	20	20	20	20
130	Forum North	10	10	10	50		10	10	10	10	0	0	0	0	0	0	0	0	0	0	0	0	0	0	0	0	0	0
130	Jaarbeursplein - NorthEast	10	10	10	50	10		10	10	10	0	0	0	0	0	0	0	0	0	0	0	0	0	0	0	0	0	0
130	Croeslaan North	10	10	10	50	10	10		10	10	0	0	0	0	0	0	0	0	0	0	0	0	0	0	0	0	0	0
130	Graadt van Groggeweg North	10	10	10	50	10	10	10		10	0	0	0	0	0	0	0	0	0	0	0	0	0	0	0	0	0	0
130	Jaarbeurs	10	10	10	50	10	10	10	10		0	0	0	0	0	0	0	0	0	0	0	0	0	0	0	0	0	0
20	Rabobank lower level	0	0	0	20	0	0	0	0	0		0	0	0	0	0	0	0	0	0	0	0	0	0	0	0	0	0
20	Rabobank upper level	0	0	0	20	0	0	0	0	0	0		0	0	0	0	0	0	0	0	0	0	0	0	0	0	0	0
20	Knoop Office	0	0	0	20	0	0	0	0	0	0	0		0	0	0	0	0	0	0	0	0	0	0	0	0	0	0
20	Beatrix theater	0	0	0	20	0	0	0	0	0	0	0	0		0	0	0	0	0	0	0	0	0	0	0	0	0	0
20	City Hall	0	0	0	20	0	0	0	0	0	0	0	0	0		0	0	0	0	0	0	0	0	0	0	0	0	0
20	WTC Forum level	0	0	0	20	0	0	0	0	0	0	0	0	0	0		0	0	0	0	0	0	0	0	0	0	0	0
20	WTC base level	0	0	0	20	0	0	0	0	0	0	0	0	0	0	0		0	0	0	0	0	0	0	0	0	0	0
20	Central Park	0	0	0	20	0	0	0	0	0	0	0	0	0	0	0	0		0	0	0	0	0	0	0	0	0	0
20	Parking Jaarbeursplein - East	0	0	0	20	0	0	0	0	0	0	0	0	0	0	0	0	0		0	0	0	0	0	0	0	0	0
20	Parking Jaarbeursplein - West	0	0	0	20	0	0	0	0	0	0	0	0	0	0	0	0	0	0		0	0	0	0	0	0	0	0
20	Hojel city center 1	0	0	0	20	0	0	0	0	0	0	0	0	0	0	0	0	0	0	0		0	0	0	0	0	0	0
20	Hojel city center 2	0	0	0	20	0	0	0																				

3170 Total input / hour

## Appendix E. Shared space transition script

```

"""
=====
Two separate scripts to generate and remove cyclists in two situations:
1. From Vehicles to Pedestrians (link to area)
2. From Pedestrians to Vehicles (area to link)

Desired speed adjustment states the factor by which the desired speed of
each cyclist is multiplied when entering a pedestrian zone. When exiting
the pedestrian zone, their desired speed is again set to their original
desired speed.

=====
"""

DesSpeedAdjust = 0.8

# 1. From Vehicles to Pedestrians (link to area)
def GeneratePedCyclists():

    ExitLinkNum = 21          # Change link number where veh is removed
    EnterAreaNum = 98         # Change area Number where new Ped enters

    EnterX      = 0           # X-offset from center of EnterArea
    EnterY      = 0           # Y-offset from center of EnterArea
    OrientX     = 3           # Change X Orientation of Ped when entering
    OrientY     = 1           # Change Y Orientation of Ped when entering

    ExitLink = Vissim.Net.Links.ItemByKey(ExitLinkNum)      # Object exit link
    Length   = ExitLink.AttValue("Length2D")                # Length of exit link
    Width    = ExitLink.Lanes.ItemByKey(1).AttValue("Width") # Width of exit link

    for veh in ExitLink.Vehs:
        if veh.AttValue("Pos") > Length - 1:
            CyclType = veh.AttValue('VehType')
            #EnterY = (veh.AttValue("PosLat") * Width) - (Width / 2)
            DesiredSpeed = veh.AttValue("DesSpeed")
            ExitSpeed = veh.AttValue("Speed")
            EnterSpeed = ExitSpeed
            Vissim.Net.Pedestrians.AddPedestrianOnAreaAtCoordinate(CyclType,
                EnterAreaNum, EnterX, EnterY, OrientX, OrientY,
                (DesiredSpeed * DesSpeedAdjust), EnterSpeed)

            VehNum      = veh.AttValue('No')
            Vissim.Net.Vehicles.RemoveVehicle(VehNum)

```

```
# 2. From Pedestrians to Vehicles (area to link)
def GenerateVehCyclists():

    ExitAreaNum    = 300          # Change number of exit area
    EnterLinkNum   = 4            # Change link Number where new Veh enters

    EnterLane      = 1            # Number of Lane where new Veh enters
    EnterPosition  = 1            # Distance in meters from start of link

    ExitArea = Vissim.Net.Areas.ItemByKey(ExitAreaNum) # Object exit area

    for ped in ExitArea.Peds:
        if ped.AttValue("RemainDist") < 1:
            CyclType = ped.AttValue('PedType')
            DesiredSpeed = ped.AttValue("DesSpeed")
            Vissim.Net.Vehicles.AddVehicleAtLinkPosition(CyclType,
                EnterLinkNum, EnterLane, EnterPosition,
                DesiredSpeed * (1/DesSpeedAdjust))

            PedNum      = ped.AttValue('No')
            Vissim.Net.Pedestrians.RemovePedestrian(PedNum)
```

## Appendix F. Visual data extraction script

```

"""
=====
Takes screenshots from 3 different camera positions,
in 2 different layouts: Speed and delay average in the last interval.

The script temporarily turns off quick mode before taking the screenshots
in order to visualize vehicles, cyclists and pedestrians.
=====
"""

ResolutionFactor = 3

def ScreenshotsFull3D():

    # Turn off quick mode:
    Vissim.Graphics.CurrentNetworkWindow.SetAttValue("QuickMode", 0)

    # Apply 1st layout:
    Layout1 = "Delay3D"
    Vissim.Graphics.CurrentNetworkWindow.ApplyLayout(Layout1)

    # Set 3D Mode and camera position full:
    Vissim.Graphics.CurrentNetworkWindow.SetAttValue("3D", 1)
    xPos = -50
    yPos = -300
    zPos = 16000
    yawAngle = 90
    pitchAngle = 90
    rollAngle = 0
    fieldOfView = 2
    Vissim.Graphics.CurrentNetworkWindow.SetCameraPositionAndFieldOfView(xPos,
yPos, zPos, yawAngle, pitchAngle, rollAngle, fieldOfView)

    # Make a Screenshot:
    Time = Vissim.Simulation.AttValue('SimSec')
    FileLocation = "C:\\Users\\svent\\Documents\\Screenshots\\"
    Filename = 'Full Network_' + Layout1 + "_" + str(Time) + '.png'
    Vissim.Graphics.CurrentNetworkWindow.Screenshot(
FileLocation + Filename , ResolutionFactor)

    # Apply 2nd Layout:
    Layout2 = "Speed3D"
    Vissim.Graphics.CurrentNetworkWindow.ApplyLayout(Layout2)

    # Set 3D Mode and camera position full:
    Vissim.Graphics.CurrentNetworkWindow.SetAttValue("3D", 1)
    xPos = -50
    yPos = -300
    zPos = 16000
    yawAngle = 90
    pitchAngle = 90
    rollAngle = 0
    fieldOfView = 2
    Vissim.Graphics.CurrentNetworkWindow.SetCameraPositionAndFieldOfView(xPos,
yPos, zPos, yawAngle, pitchAngle, rollAngle, fieldOfView)

```

```

# Make a Screenshot:
Time = Vissim.Simulation.AttValue('SimSec')
FileLocation = "C:\\Users\\svent\\Documents\\Screenshots\\"
Filename = 'Full Network_' + Layout2 + "_" + str(Time) + '.png'
Vissim.Graphics.CurrentNetworkWindow.Screenshot(
FileLocation + Filename , ResolutionFactor)

```

### **def ScreenshotsIntersection3D():**

```

# Apply 1st layout:
Layout1 = "Delay3D"
Vissim.Graphics.CurrentNetworkWindow.ApplyLayout(Layout1)

# Set 3D Mode and camera position full:
Vissim.Graphics.CurrentNetworkWindow.SetAttValue("3D", 1)
xPos = 333.7
yPos = -471.9
zPos = 140.4
yawAngle = 183.157
pitchAngle = 61
rollAngle = 0
fieldOfView = 45
Vissim.Graphics.CurrentNetworkWindow.SetCameraPositionAndFieldOfView(xPos,
yPos, zPos, yawAngle, pitchAngle, rollAngle, fieldOfView)

# Make a Screenshot:
Time = Vissim.Simulation.AttValue('SimSec')
FileLocation = "C:\\Users\\svent\\Documents\\Screenshots\\"
Filename = 'Intersection_' + Layout1 + "_" + str(Time) + '.png'
Vissim.Graphics.CurrentNetworkWindow.Screenshot(
FileLocation + Filename , ResolutionFactor)

# Apply 2nd Layout:
Layout2 = "Speed3D"
Vissim.Graphics.CurrentNetworkWindow.ApplyLayout(Layout2)

# Set 3D Mode and camera position full:
Vissim.Graphics.CurrentNetworkWindow.SetAttValue("3D", 1)
xPos = 333.7
yPos = -471.9
zPos = 140.4
yawAngle = 183.157
pitchAngle = 61
rollAngle = 0
fieldOfView = 45
Vissim.Graphics.CurrentNetworkWindow.SetCameraPositionAndFieldOfView(xPos,
yPos, zPos, yawAngle, pitchAngle, rollAngle, fieldOfView)

# Make a Screenshot:
Time = Vissim.Simulation.AttValue('SimSec')
FileLocation = "C:\\Users\\svent\\Documents\\Screenshots\\"
Filename = 'Intersection_' + Layout2 + "_" + str(Time) + '.png'
Vissim.Graphics.CurrentNetworkWindow.Screenshot(
FileLocation + Filename , ResolutionFactor)

```

**def ScreenshotsJBP3D():**

```

    # Apply 1st layout:
    Layout1 = "Delay3D"
    Vissim.Graphics.CurrentNetworkWindow.ApplyLayout(Layout1)

    # Set 3D Mode and camera position full:
    Vissim.Graphics.CurrentNetworkWindow.SetAttValue("3D", 1)
    xPos = 115.6
    yPos = -174
    zPos = 500
    yawAngle = 115.6
    pitchAngle = 90
    rollAngle = 0
    fieldOfView = 25
    Vissim.Graphics.CurrentNetworkWindow.SetCameraPositionAndFieldOfView(xPos,
yPos, zPos, yawAngle, pitchAngle, rollAngle, fieldOfView)

    # Make a Screenshot:
    Time = Vissim.Simulation.AttValue('SimSec')
    FileLocation = "C:\\Users\\svent\\Documents\\Screenshots\\"
    Filename = 'JBP_' + Layout1 + "_" + str(Time) + '.png'
    Vissim.Graphics.CurrentNetworkWindow.Screenshot(
FileLocation + Filename, ResolutionFactor)

    # Apply 2nd Layout:
    Layout2 = "Speed3D"
    Vissim.Graphics.CurrentNetworkWindow.ApplyLayout(Layout2)

    # Set 3D Mode and camera position full:
    Vissim.Graphics.CurrentNetworkWindow.SetAttValue("3D", 1)
    xPos = 115.6
    yPos = -174
    zPos = 500
    yawAngle = 115.6
    pitchAngle = 90
    rollAngle = 0
    fieldOfView = 25
    Vissim.Graphics.CurrentNetworkWindow.SetCameraPositionAndFieldOfView(xPos,
yPos, zPos, yawAngle, pitchAngle, rollAngle, fieldOfView)

    # Make a Screenshot:
    Time = Vissim.Simulation.AttValue('SimSec')
    FileLocation = "C:\\Users\\svent\\Documents\\Screenshots\\"
    Filename = 'JBP_' + Layout2 + "_" + str(Time) + '.png'
    Vissim.Graphics.CurrentNetworkWindow.Screenshot(
FileLocation + Filename , ResolutionFactor)

    # Turn on quick mode
    Vissim.Graphics.CurrentNetworkWindow.SetAttValue("QuickMode", 1)

```